THE UNIVERSITY
of EDINBURGH

Dysfunctional Innate Immunity in Cystic Fibrosis Lung Disease

Sheonagh MacPhail Law

THE UNIVERSITY of EDINBURGH

Doctor of Philosophy

The University of Edinburgh

2019

Declaration

I declare that I have composed this thesis and the work is my own except where explicitly stated within the text. Material in this thesis has not been submitted for any other degree or professional qualification. Any included publications are my own work.

Chapter 3: Steven Mitchell performed sample dehydration, fixation and mounting prior to scanning/transmission electron microscopy.

Chapter 4: Lauren Melrose performed murine genotyping.

Chapter 4: [3H]-PK11195 radiotracer assay on murine lung sections was in collaboration with Dr Adriana Tavares.

Chapter 5: Samuel Stanfield performed nanosensor preparation and pH calibration curve experiments.

Chapter 5: Samuel Stanfield performed Raman data analysis using MATLAB software.

Sheonagh MacPhail Law

November 2019

Abstract

Cystic Fibrosis (CF) lung disease is characterised by dysfunctional innate immunity. Even before microbial colonisation is established, there is an accumulation of neutrophils within the airways. Neutrophil extracellular traps (NETs) are an evolutionarily conserved antimicrobial defence mechanism of neutrophils. However, NETs can also cause inflammation and damage when in excess and as such are implicated in the pathogenesis of CF lung disease. Within the airways, NETs are a source of proinflammatory proteins including myeloperoxidase, neutrophil elastase and calprotectin. Treatment of CF patients with DNase reduces airway inflammation and sputum viscosity, which may be due to the drug increasing clearance and/or decreasing the production of NETs. Our group has previously found that NETs are proinflammatory to monocyte-derived macrophages (MDM) in co-culture, and that this was more exaggerated in CF MDM, so it is likely that an interplay between the innate immune cells exacerbate airway damage. Several defects have been reported in CF MDM previously, which may exacerbate airway infection and inflammation. One such reported defect is failure of the macrophage phagolysosome to acidify, which impairs bacterial killing and may lead to more bacteria surviving in the airway as a driver of inflammation.

Throughout this PhD, sputum samples from both CF and healthy control (HC) participants were collected and lung function measured to investigate whether

NETs are associated with airways inflammation and increased severity of lung disease. Using ELISA quantification of NETs (by an in-house ELISA which measures histone-bound calprotectin) and proinflammatory cytokines, CF participants were found to produce higher levels of sputum NETs than HC. Those CF participants taking DNase had significantly decreased levels of sputum NETs relative to those not on the drug. Furthermore, positive associations were found between NETs and proinflammatory proteins, whilst negative correlations were demonstrated between these proteins and lung function. Furthermore, when forced expiratory volume in one second (FEV_1) was predicted by multi-variate linear regression, the level of sputum NETs was a significant independent indicator of FEV_1.

A murine model of lipopolysaccharide (LPS)-induced acute lung injury was used to characterise how CFTR alters NET formation and associated inflammation following a sterile inflammatory challenge and whether DNase affected this. It was demonstrated that $CFTR^{-/-}$ mice have an exaggerated inflammatory response to LPS-induced acute lung injury relative to wild type (WT) littermates in terms of airway proinflammatory cytokine concentrations and histopathological scoring of acute lung inflammation. This was despite no acute increase in airway neutrophil or macrophage numbers, suggesting intrinsic defects exist within these innate immune cells due to absence of CFTR. The receptor for advanced glycation end-products (RAGE) had higher gene expression in $CFTR^{-/-}$ vs WT littermates, which leads us to speculate that

up-regulation of NF-κB signalling could be responsible for increased inflammation in CF mice. Importantly, airway NETs were not significantly different between genotypes and DNase had no effect on inflammation, suggesting the CF murine model is imprecise in mimicking human disease. This is perhaps unsurprising given that people with CF have non-resolving airways inflammation, rather than an acute injury.

Final experiments investigated the role of CFTR in regulating macrophage phagolysosomal pH. Using MDM from both HC and CF donors, we developed a novel technique compatible with real-time analysis of phagocytosis, which showed that surface-enhanced Raman spectroscopy-based nanosensors exhibit superiority over conventional fluorescence spectroscopy in measuring macrophage phagolysosomal pH in terms of sensitivity, ratiometric quantification, and both spatial and temporal resolution. Human MDM phagolysosomal acidification was found to be CFTR-independent and may not be critical in the pathophysiology of CF lung disease, although further experiments using alveolar macrophages would strengthen these conclusions.

To summarise, NETs are associated with inflammation and disease severity in human CF lung disease. Our mouse work suggested that intrinsic defects of innate immune cells exist in $CFTR^{-/-}$ mice, manifest by an exaggerated response to sterile inflammation, possibly via RAGE-NFκB signalling pathways. We also demonstrated that macrophage phagolysosomal

acidification was not impaired in human CF MDM. Further research investigating the underlying mechanisms causing innate immune cell dysfunction will help identify therapeutic targets for the treatment of inflammation in CF lung disease

Lay Summary

Cystic Fibrosis (CF) is a genetic disease causing absence or malfunction of CFTR protein. This can adversely affect many body systems, including the lungs and white blood cells (such as neutrophils and macrophages, which deal with infection and inflammation). Neutrophil extracellular traps (NETs) are made by and released from neutrophils into the space surrounding these cells, and consist of DNA and inflammatory proteins. NETs help kill invading microorganisms such as bacteria. However, they may also be inflammatory and damaging to the airways. NETs may interact with macrophages in the airways of CF patients to worsen inflammation.

Sputum samples from CF and healthy control (HC) participants were processed and lung function measured. We found higher levels of NETs in CF airway samples compared to HC samples and this was associated with increased levels of damaging inflammatory mediators and decline in lung function. Sputum NET levels, alongside other factors such as age and sex, could help predict lung function in CF participants. We also studied CF mice and found they had more inflammation in their lungs compared to non-CF mice. Airway NETs were not significantly different between CF and non-CF mice. This does not match the human data but all of our CF participants were adults with established lung damage and so this might explain the difference in results.

I also assessed the effects of NETs on macrophages and showed them to increase inflammatory signals released by these cells. In addition, I studied whether CF macrophages were able to acidify their phagolysosomes (their "stomachs", within which invading bacteria are digested). Contrary to what has been suggested in published literature, CF macrophage phagolysosomal acidification was normal. This suggests the faulty bacterial killing by CF macrophages is due to some other abnormality in function.

These findings have important implications for CF patients. Further research will help to develop targeted anti-inflammatory therapies against NET proinflammatory proteins. Ultimately, we aim to help discover new treatments that preserve lung function and improve survival rates of CF patients.

Acknowledgements

I would like to thank my supervisors Dr Robert Gray, Professor Ian Dransfield and Professor Moira Whyte for their help and guidance throughout this Ph.D. I am incredibly grateful for the supervision, guidance and support from my post-doctoral colleague, Dr Gareth Hardisty. I would also like to thank my fellow group member Jonathan Gillan for his help during this Ph.D. I am grateful for the technical assistance provided by Stephen Mitchell for scanning/transmission electron microscopy experiments and Professor James Ross for his insights into macrophage structure and function. I acknowledge and thank Dr Colin Campbell and Samuel Stanfield for their collaborative work on the SERS-based nanosensor work. I thank Dr Adriana Tavares for her collaborative work on the [3H]-PK11195 radiotracer assay. I thank Dr Alastair Rushworth, for his assistance in using R software. I am grateful for the help of the CF Clinic team members at the Western General Hospital, Edinburgh, especially the CF Clinical Nurse Specialists Catriona McMullan, Lynne McIntosh and Julie Robertson. Lastly, I would like to thank the healthy volunteers and CF participants who gave up their time and provided samples for this research.

List of Abbreviations

Ab	antibody
AB	assay buffer
ABPA	allergic bronchopulmonary aspergillosis
AEC	airway epithelial cell
A.fumigatus	*Aspergillus fumigatus*
ASL	airway surface liquid
ATP	adenosine triphosphate
BAL	bronchoalveolar lavage
BALF	bronchoalveolar lavage fluid
BCA	bicinchoninic acid
B.cepacia	*Burkholderia cepacia*
BMI	body mass index
CAC	sodium cacodylate
cDNA	complementary DNA
CF	Cystic Fibrosis
CFTR	Cystic Fibrosis transmembrane conductance regulator
CI	confidence interval
DAMPs	damage-associated molecular patterns
DNA	deoxyribose nucleic acid
DPBS	Dulbecco's phosphate buffered saline
DPI	Diphenyleneiodonium chloride
DTT	dithiothreitol
EDTA	ethylenediaminetetraacetic acid
ELISA	enzyme-linked immunosorbant assay

FEV_1	forced expiratory volume in one second
FVC	forced vital capacity
GIMP	GNU Image Manipulation Program
HC	healthy controls
H&E	haematoxylin & eosin
HNE	human neutrophil elastase
IHC	immunohistochemistry
LAMP	lysosomal-associated membrane protein
LIMP	lysosomal integral membrane protein
LPS	lipopolysaccharide
MBA-NP	*para*-mercaptobenzoic acid functionalised nanoparticles
MDM	monocyte-derived macrophages
MMP-8	matrix metalloproteinase 8
MMP-9	matrix metalloproteinase 9
MPO	myeloperoxidase
mRNA	messenger ribonucleic acid
NADPH	nicotinamide adenine dinucleotide phosphate
NE	neutrophil elastase
NETs	neutrophil extracellular traps
NSAIDs	non-steroidal anti-inflammatory drugs
NOX2	NADPH oxidase 2
PAD4	peptidyl arginine deiminase 4
P.aeruginosa	*Pseudomonas aeruginosa*
PAMPs	pathogen-associated molecular patterns
PFA	paraformaldehyde
PI3K	phosphatidylinositol 3-kinase

PMA	Phorbol 12-myristate 13-acetate
p-MBA	*para*-mercaptobenzoic acid
PRP	platelet-rich plasma
PRR	pattern recognition receptor
PSGL-1	P-selectin glycoprotein ligand-1
rhDNase	recombinant human DNase
RNA	ribonucleic acid
ROS	reactive oxygen species
rpm	revolutions per minute
RT-PCR	reverse transcriptase-polymerase chain reaction
S.aureus	*Staphylococcus aureus*
SD	standard deviation
SEM	standard error of the mean
SERS	surface-enhanced Raman spectroscopy
S-HRP	Streptavidin-horseradish peroxidase
SuRF	shared university research facilities
TEM	transmission electron microscopy
TLR	toll-like receptor
TSPO	translocator protein
WT	wild type

List of Figures

Chapter 1

Chapter 2

Chapter 3

Chapter 4

Chapter 5

List of Tables

Chapter 1

Chapter 2

Chapter 3

Chapter 4

Chapter 5

Contents

Chapter 1: Introduction

1.1 Epidemiology of Cystic Fibrosis

Cystic Fibrosis (CF) is an autosomal recessive genetic disease occurring in people of all racial and ethnic backgrounds but is most common in Caucasians of northern European ancestry. In *2017,* there were 10469 people with CF in the UK(1). The reported incidence in the UK is one in 2500 live births(1). Worldwide, there are approximately 70,000-100,000 people living with the disease(2). Due to advances in therapy over the past 50 years, the UK's median predicted survival has increased from five to 47 years of age and the median age of people with CF is now 20 years of age(1). It is therefore becoming more common to have CF patients within adult Respiratory Medicine services.

1.2 Medical History of Cystic Fibrosis

The medical history of CF, and the professionals responsible for its characterisation, is a fascinating topic in its own right and is reviewed more fully by Paul M. Quinton(3). A disease thought most likely to be CF was first alluded to in European folklore from the Middle Ages: *"woe is the child who tastes salty from a kiss on the brow, for he is cursed, and soon must die"*(4). Indeed, such children were believed to be "hexed"(3). It was not until 1595 that Pieter Pauw, professor of botany and anatomy in Leiden, The

Netherlands, performed an autopsy on an 11-year-old girl and described her *"swollen, hardened, gleaming white pancreas"*(3). Later case reports throughout the 19th and early 20th century described the gastrointestinal complications of the disease but it was not until the 1936 that Fanconi *et al.* published a brief report of two children who were thought to have Coeliac syndrome associated with congenital "cystic pancreatic fibromatosis and bronchiectasis"(5). However, it was Dr. Dorothy Hansine Andersen (see Figure 1.1), an American physician, who first described CF as a disease.

(6)

***Figure 1.1: Dr. Dorothy Hansine Andersen (1901-1963)**, of Columbia University College of Physicians and Surgeons, first described Cystic Fibrosis as a disease.*

Dr. Andersen graduated from John Hopkins University School of Medicine in 1926 then completed a surgical internship at Strong Memorial Hospital in Rochester, New York. However, she was denied entry to the hospital's surgical residency programme because she was a woman. She therefore took up a post at Columbia University College of Physicians and Surgeons as an instructor of Pathology. In her seminal paper, Andersen described a series of 49 paediatric autopsies, all of which revealed extensive lesions of the acinar tissue of the pancreas – which she termed "cystic fibrosis of the pancreas" - despite the neonates/children having presented with different clinical syndromes(7). Her careful review of the case notes determined that subdivisions in clinical phenotypes existed, with some children presenting with nutritional disturbances whilst others had mainly infections of the respiratory tract. In the paper's closing discussion, Andersen stated: "*I do not know the cause of this disease…all the 44 patients had pulmonary lesions which were primary in the bronchi, and many had bronchiectasis"*(7). Her concluding hypothesis was that the pancreatic pathology prevented fat absorption and hence children developed vitamin A deficiency (since it is a fat-soluble vitamin), which was responsible for the bronchiectasis and bronchopneumonia(7). It was interesting to note a quote from one of the children's mothers: *""Whatever my first baby had, this baby has too"*(7).

It took Andersen and her colleague Dr. Richard G. Hodges another eight years to publish evidence that supported this mother's intuition. In their paper of

1946, Andersen and Hodges concluded: *"Cystic fibrosis of the pancreas occurs among siblings, twins and more distant relatives with a distribution which is compatible with the hypothesis that it is carried as a relatively infrequent hereditary trait"*(8). In August 1948, a heat wave struck New York and several of Andersen's patients developed vomiting as a result. Those with cystic fibrosis of the pancreas had a quick response to medical treatment but the return of plasma chlorides to normal levels was more gradual compared to children with other conditions(9). This observation prompted one of Andersen's colleagues – Dr. Paul di Sant'Agnese – to discover the abnormal electrolyte composition of sweat in patients with cystic fibrosis of the pancreas(10). This ultimately led to the development of the chloride sweat test, which remains to this day a key diagnostic test for CF(11).

1.3 The genetic mutations responsible for Cystic Fibrosis

Another 36 years of scientific endeavour resulted in the gene responsible for CF being successfully cloned and located to the long arm of chromosome 7. In 1989, Kerem *et al.* published their findings in Science, followed shortly after by confirmatory studies by other groups(3,12). The gene within which mutations reside was named the Cystic Fibrosis Transmembrane conductance Regulator gene (*CFTR*). Whilst there are now over 2000 known *CFTR* mutations known to cause CF, approximately 70% of those in Northern European CF patients are caused by the F508del mutation(1). This is characterised by the specific deletion of three base pairs, with resultant loss of

a phenylalanine residue at amino acid position 508 of the resultant CFTR protein. Indeed, this mutation accounts for 84.5-89.8% mutations in the UK CF cohort(1).

CFTR Mutation	Percentage of total mutations in the UK CF cohort (range indicating the different percentages by devolved nations)
G542x	3.1 -7.2
G551D	4.7 – 10.6
R117H	3.0 – 13.8
621+1G->T	1.4 – 11.2

Table 1.1: The most common* CFTR *mutations in the UK Cystic Fibrosis population. *Modified from* (1).

Genotypes vary in frequency by devolved nation within the UK (see Table 1.1) and indeed vary geographically throughout Europe. Looking at the wider CF population, Farrell *et al.* performed genetic analysis of 190 European CF patients and their parents to determine the age and origin of the F508del mutation. Their age estimates put the mutation at 4600-4725 years old in northwestern populations and 1000 years old in southeastern populations(13). The authors propose that the ancient migrations of the early Bronze age people, known as the Bell Beaker folk (who were characterised by their

production and use of ceramic bell-shaped beakers, innovative metallurgy and great migrations(14)) were responsible for the mutation's dissemination from northwest to southeast in prehistoric Europe(13).

1.4 CFTR mutation classifications and the CFTR protein

The *CFTR* genotype – whilst not necessarily predicting disease phenotype - has become clinically very important due to the development of drug therapies, such as Orkambi, which is indicated only in CF patients ≥ two years of age who are homozygous for the F508del mutation. Mutations in the *CFTR* gene result in abnormalities in the CFTR protein. This protein is an adenosine triphosphate (ATP)-binding cassette (ABC) transporter(15) (see Figure 1.2). Such ABC proteins hydrolyse ATP to generate energy, which drives the transport of substrates against a concentration gradient. In the case of CFTR, it is a transmembrane ion channel responsible for the transport of chloride and bicarbonate ions across membranes. It is expressed on the apical surface of airway, intestinal and exocrine epithelial cells where it functions to secrete chloride and bicarbonate into the lumens(16) and may regulate reabsorption of sodium ions and water molecules by the epithelial sodium channel (ENaC), although the latter point is contested within existing literature(17,18).

More recently, immune cells have been shown to express CFTR messenger RNA (mRNA) at low levels(19) and express functional CFTR protein both

intracellularly(20) and at the cell membrane(21). The protein's expression varies between cell types, e.g. there is increased expression of CFTR on airway epithelial cells (AEC) compared to neutrophils. With regard to CFTR activity, Plasschaert *et al.* described a novel cell type – the pulmonary ionocyte – as a major source of CFTR activity in the human airway(22). They used single cell RNA sequencing to profile subpopulations of both human bronchial epithelial cells and mouse tracheal epithelial cells. In doing so, they described the ionocyte, which accounted for 1-2% of airway epithelial cells. These cells strongly co-expressed FOXI1, multiple subunits of vacuolar ATPase (see Chapter 5, section 5.9 for a description of this enzyme) and CFTR(22). They conducted Ussing chamber experiments and cell-type quantification in human bronchial epithelial cell cultures derived from seven human donors to demonstrate that CFTR activity had a significant positive correlation with ionocyte but not ciliated cell number. The authors suggested that ionocytes may have a role in airway luminal pH regulation, which could be of importance in the context of CF lung disease(22).

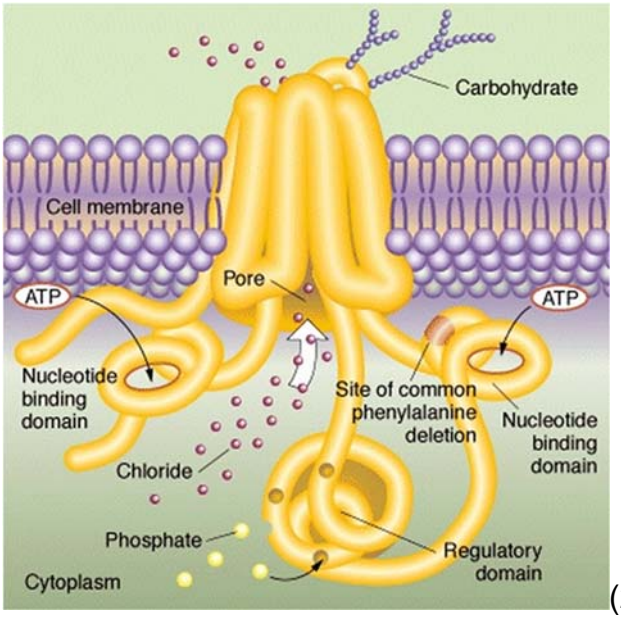

(23)

Figure 1.2: Schematic representation of the structure of the Cystic fibrosis Transmembrane Conductance Regulator (CFTR) protein. *CFTR is a transmembrane protein, generating energy via the hydrolysis of adenosine triphosphate to transport chloride and bicarbonate ions via a membrane channel against concentration gradients.*

The CFTR protein has varying dysfunctions, depending upon the type of mutation affecting the gene. Classification of these mutations in the *CFTR* gene results in six broad groups (see Table 1.2). However, this is an over-simplification of a complex process. For example, some F508del mutations result in misfolded CFTR proteins, which are not degraded by the cells and so do reach the membrane. However, once within the membrane, their misfolding causes a gating defect.

CFTR Mutation Class	Example Mutation	Effect on CFTR Protein
I: Often introduce premature stop codons, which are non-sense mutations	G542x	Resultant mRNA is truncated and unstable and usually results in non-functional CFTR.
II: Base pair deletions	F508del	Results in abnormal folding of the CFTR protein, preventing efficient trafficking to the apical membrane because the cell recognises it as faulty and so degrades it.
III: Gating mutations, the main target of ivacaftor drug treatment	G551D	CFTR protein is structurally normal but fails to open effectively such that ions do not have time to pass through.
IV: As per III and include conductance and (some) gating defects	R117H	CFTR is structurally normal but inefficient ion transport occurs.
V: Intron mutations affecting splicing	A445E	Reduced amount of CFTR is present on the cell membrane, although those that are present function normally.
VI: Missense mutations	432delTC	CFTR is unstable with a decreased half-life and so there is a reduction in functional protein present at the membrane.

Table 1.2: Classification of* CFTR *genotypes, example mutations and their effects on CFTR protein function. *Modified from* (16).

1.5 The Clinical Manifestations of Cystic Fibrosis

Mutations described in the last section result in CFTR protein dysfunction, reduction or absence, which underpin the pathophysiology of CF. Due to the protein's expression on epithelial cells and immune cells, CF is a multi-organ disease with varying phenotypes noted between patients, as was illustrated in Andersen's original paper(7). The morbidity and mortality related to CF principally relates to the chronic airway inflammation and infection, which causes respiratory failure, and will be the focus of this thesis. However, other systems (e.g. the gastrointestinal, endocrine and reproductive systems) are also affected and this causes several modes of presentation that have important clinical implications (although precise pathophysiological mechanisms are out with the scope of this thesis). Paediatric and adult CF patients have different modes of presentation. Data in the UK CF Registry Annual report 2017 demonstrates that only 26.7% patients were diagnosed via the newborn screening programme; this is likely to be an historical anomaly, since newborn screening was only rolled out throughout the UK in 2007. Of the remaining patients, 6308 were diagnosed with CF under the age of 16 (i.e. 87%) whilst 848 were diagnosed once over the age of 16 (i.e. 11.7%)(1). The most common mode of presentation in both adults and children is persistent or acute respiratory infection. Thereafter, in the paediatric population, patients often present with features of pancreatic exocrine insufficiency such as failure to thrive/malnutrition and steatorrhea/malabsorption. Neonates often present with meconium ileus (i.e. small bowel obstruction caused by thicker-than-normal meconium). In the adult cohort, the gastrointestinal manifestations are

not as common in the modes of presentation. Instead, patients may present with a positive family history, genotyping, nasal polyps, bronchiectasis and infertility, as illustrated in Figure 1.3. Other clinical manifestations of CF include cirrhosis of the liver and portal hypertension and pancreatic endocrine insufficiency causing CF-related diabetes (CFRD).

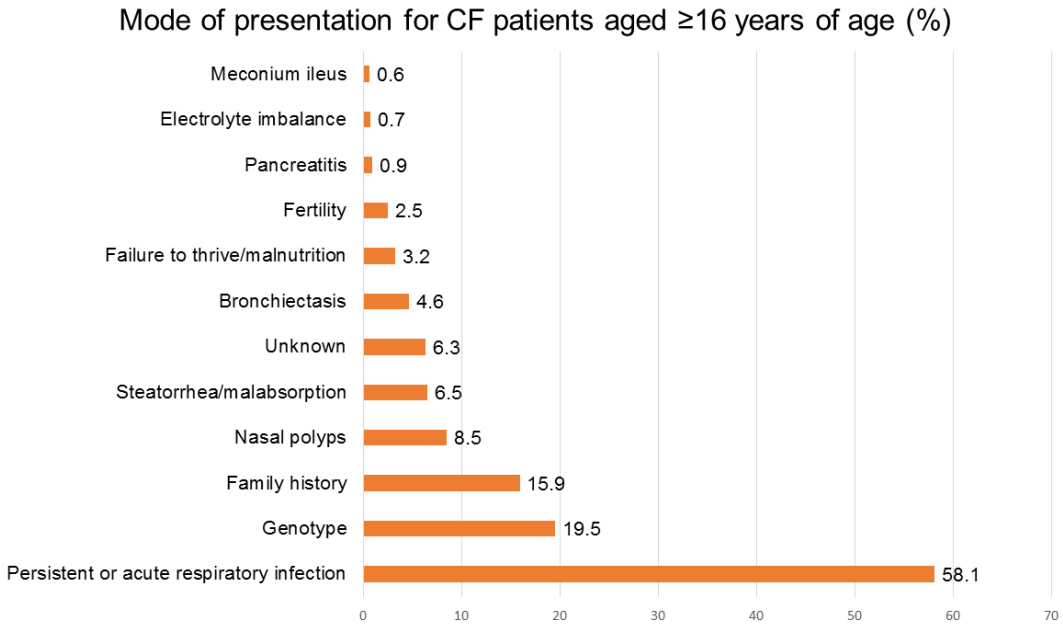

Figure 1.3: Mode of presentation of Cystic Fibrosis patients ≥ 16 years of age, *adapted from the UK CF Registry's Annual Report 2017*(1). *Adult patients most commonly present with persistent or acute respiratory infection (58.1%), followed by genotyping (19.5%), family history (15.9%), nasal polyps (8.5%), steatorrhea/malabsorption (6.5%), unknown (6.3%), bronchiectasis (4.6%), malnutrition (3.2%), infertility (2.5%), pancreatitis (0.9%), electrolyte imbalance (0.7%) and meconium ileus (0.6%). Patients may present with one or more of these manifestations of CF. These data illustrate that CF is a multi-organ disease and due to the rarity of the disease, clinicians need to have a high index of suspicion when reviewing a patient presenting with such features.*

1.6 Cystic Fibrosis Lung Disease

Not only is lung disease the most commonly occurring mode of presentation of CF but it also causes the most morbidity and mortality, with 85% of deaths being attributable to respiratory complications(24). Chronic inflammation and infection ultimately leads to respiratory failure and one third of CF patients on the transplant list die whilst awaiting transplantation(25). The CF lung has dysfunctional immunity exacerbated by chronic bacterial infection. In infants with CF, *Staphylococcus aureus (S.aureus)* and *Haemophilus influenzae (H.influenzae)* are the most common infections(1). Patients then accrue further chronic microbial infections with increasing age (e.g. with *Pseudomonas aeruginosa (P.aeruginosa), Burkholderia cepacia (B.cepacia)* and *Aspergillus fumigatus (A.fumigatus)).* Failure to resolve these microbial infections is due to multiple abnormalities within the CF lung environment caused by absence, reduction or dysfunction of CFTR protein.

The pathophysiology of CF lung disease is therefore multi-factorial. In recent years, the CF pig model has been used to study CF lung disease because unlike CF mice, CF pigs develop spontaneous post-natal lung disease, mimicking human disease. Studies have shown that foetal lung development is abnormal in CF pigs(26). CFTR is thought to be responsible for anion transport/liquid secretion during branching morphogenesis of the proximal airways and so CF airways have smaller, hypo-distended lumens compared to non-CF airways(26). Furthermore, submucosal gland functioning is impaired

(they do not release the mucous strands effectively in the CF pig model(27)) which may contribute to the mucous burden seen in paediatric patients' airways, evident even before infection has occurred(28).

The AEC are also dysfunctional in CF lung disease. AEC provide a physical barrier against pathogens, regulate transport of ions that maintain airway hydration and are central in the innate immune response to pathogens(29). The cell membranes of AEC contain pattern recognition receptors (PRR), including the toll-like receptors (TLR), which recognise microbial pathogen-associated molecular patterns (PAMPs, e.g. LPS) and "self" damage-associated molecular patterns (DAMPs), which include nucleic acids. Through these constitutively expressed PRR, AEC can respond to numerous pathogens by producing proinflammatory cytokines including IL-6, IL-8 and IFN-β(29). In CF, AEC produce excessive amounts of these cytokines, especially IL-8, which is a neutrophil chemokine(30). This contributes to the excessive accumulation of neutrophils within the CF airways (see section 1.9).

In addition to their key role in innate immunity, AEC together with submucosal glands produce the airway surface liquid (ASL). ASL comprises an upper mucous layer – within which microorganisms, cellular debris and foreign materials are trapped – and a lower periciliary liquid layer, which bathes the AEC cilia and lubricates their beating movements(25,29). The cilia beat to move the mucous layer upwards and out of the airways – this is termed the mucociliary clearance escalator - ultimately moving unwanted material towards

the pharynx for elimination from the airway via either expectoration or swallowing into the gastrointestinal system. In addition to this physical removal of pathogens, the ASL also contains antimicrobial peptides (e.g. lactoferrin, LL-37 and the human β-defensins) and antiproteases (e.g. alpha 1 anti-trypsin and secretory leucoprotease inhibitor) which function to sequester and degrade microorganisms(29). However, in the CF lung, degranulation of neutrophils releases excessive amounts of the serine protease neutrophil elastase (NE), which cleaves and inactivates these antimicrobial peptides and antiproteases, contributing to the dysfunctional immune response. Furthermore, in CF lung disease, the ASL is dehydrated and acidic, which impairs bacterial killing and clearance and contributes to mucopurulent secretions(31). The reduced pH of the ASL is thought to be due to loss of CFTR, which reduces bicarbonate secretion and hence hydrogen ions secreted by the non-gastric hydrogen/potassium ATP12A are not buffered(32). The fact that ATP12A is expressed at low levels in the mouse airways may be why they do not develop spontaneous, post-natal lung disease(32). Indeed, ATP12A expression in CF mouse airways acidified the ASL, impaired host defenses and increased bacteria within the airways, conversely inhibition of ATP12A in the CF pig model abrogated host defence abnormalities(32). The acidic ASL has been demonstrated *in vitro* in cultured human CF airway epithelial cells(33), in the CF pig model(34), and in a study measuring the nasal ASL pH in infants with CF(35). Moreover, the recently described pulmonary ionocyte (described in section 1.4) may play an important role in ASL pH regulation(22).

Finally, inflammation is present in the CF airways shortly after birth and before microbial infection occurs(21,36,37). Sly *et al.* reported a study of 127 infants diagnosed with CF by newborn screening in which they used chest computed tomography and bronchoalveolar lavage (BAL) assays to monitor clinically stable children up until 3 years of age(38). In doing so, they found that BAL NE activity at 3 months of age was associated with persistent bronchiectasis at both 12 months and 3 years of age(38). This suggests that a dysfunctional innate immune response involving neutrophils is key to the inflammation seen in CF lung disease. The roles of neutrophils and macrophages within the context of both health and CF lung disease will be discussed in detail in sections 1.7-1.15.

Whilst neutrophils predominate within the airway lumens of CF patients, there is evidence to show that the adaptive immune system also plays a role in CF lung disease. Endobronchial biopsies performed on children with CF and healthy controls show that subepithelial bronchial mucosa has a lymphocytic infiltration (comprising mainly CD3+ T lymphocytes) in CF patients, the numbers of which were increased in patients with *P.aeruginosa* colonisation and during exacerbations(39). There is also cross talk between the innate and adaptive immune systems. For example, Th17 lymphocytes are CD4+ T cells that secrete IL-17 cytokines(40) in response to stimulation by IL-23, IL-6 and TGF-β from innate immune cells. IL-17 is elevated in BAL and sputum of CF patients(40), especially when colonised with *P.aeruginosa.* This cytokine

activates innate immune cells, stimulates antimicrobial peptide production by epithelial cells, and recruits neutrophils and so exacerbates CF lung pathology(41).

1.7 The role of the neutrophil in health

Despite there being emerging evidence that the adaptive immune system plays an important role in CF, it remains a disease characterised by neutrophil-dominant airways inflammation. Neutrophils account for 80% of the total cells present in CF sputum, even when patients are clinically stable(42). In order to understand this phenomenon, exploration of physiological neutrophil function and homeostasis mechanisms is first required.

Neutrophils form in the bone marrow from granulocyte/macrophage precursor cells and are released into the circulation once terminally differentiated, accounting for 40-60% peripheral blood leucocytes in humans(43). In health, they have a relatively short half-life, on average six to eight hours(44). Recruitment of neutrophils from the bloodstream into the lungs increases in response to inflammation/infection. Neutrophil recruitment consists of three stages: 1) adherence to activated endothelial cells and subsequent rolling under vascular flow; 2) neutrophils arrest and firm attachment to the endothelial cells; and 3) migration across the endothelium to the inflamed/infected airways(45). The first step relies upon the interaction between the glycoprotein P-selectin glycoprotein ligand-1 (PSGL-1) and P-

selectin/E-selectin expressed on the plasma membrane of activated endothelial cells(46). Firm attachment is then achieved by the interaction between *β*2-integrins and up-regulated endothelial cell-surface adhesion molecules such as intercellular adhesion molecule 1 (ICAM-1)(47). The final migratory stage is dependent upon several factors including cytokine production (i.e. cell signalling proteins such as IL-8 and TNF-α) and the production of chemokines (i.e. cell signalling proteins released by cytokine-activated endothelial, epithelial and immune cells to stimulate directed cellular chemotaxis). The release of such cytokines, chemokines, and presence of microbial products such as lipopolysaccharide (LPS, present on the outer membrane of gram-negative bacteria) primes recruited neutrophils. That is, they have an enhanced response to activating stimuli due to an upregulation in enzymatic and transcriptional processes that results in activation and production of proinflammatory mediators and enzymes that regulate downstream phenotypic and functional alterations(48). Primed neutrophils have altered shape and a more rigid cytoskeleton, which serve to trap them in the capillary microvasculature of the inflamed lung tissue (49).

Once at a site of inflammation and/or infection, such as the CF lung environment, a neutrophil is a key effector cell in the innate immune response. Neutrophils express PRR, including the TLR, which recognise PAMPs and DAMPs. Through these constitutively expressed PRR, neutrophils can respond to numerous pathogens by employing their antimicrobial defence mechanisms.

Neutrophils' antimicrobial defence repertoire consists of phagocytosis, degranulation, generation of reactive oxygen species (ROS), and NET formation(50). Phagocytosis is the process whereby the neutrophils uptake microbes, foreign material and cellular debris to degrade them safely within designated organelles called phagolysosomes. Neutrophils contain nicotinamide adenine dinucleotide phosphate (NADPH) oxidase, an enzyme that generates superoxide (O_2^-), which acts as a precursor of hydrogen peroxide (H_2O_2). This hydrogen peroxide is used by myeloperoxidase (MPO) to produce other oxidants such as hypochlorous acid, which are highly microbiocidal(51). Most of these reactions occur within phagosomes/phagolysosomes containing microbes, but ROS can also be released by neutrophils and act as signalling molecules, which drive inflammation. Degranulation results in release of granule contents including NE, which alongside degrading microbial structures, also damages lung parenchyma if not held in check by protease inhibitors such as alpha-1 anti-trypsin. NET formation, the final antimicrobial defence mechanism of neutrophils, will be discussed independent of the others in section 1.8.

To maintain appropriate neutrophil numbers in tissues, they undergo cell death once they have deployed their antimicrobial defence mechanisms. After neutrophils have died, they are cleared from sites of inflammation and infection by phagocytes, or are lost from the body after trans-epithelial migration into fluids such as sputum(43). Neutrophil death occurs via the processes of apoptosis, necrosis, necroptosis, autophagy and NETosis. Apoptosis, derived

from the Greek “apo” for separation and “ptosis” for falling off, was a term used to describe leaves falling from a tree(52). It is a term adopted by the field of cell biology to describe programmed cell death and reminds us that death is an essential part of healthy life. Apoptosis is tightly regulated and neutrophils “shut down” their cytotoxic machinery but maintain cell membrane integrity to avoid release of harmful contents into the tissues. Such apoptotic neutrophils have altered morphology(53), including cytoplasmic vacuolation, retention of membrane integrity (particularly plasma membrane), changes in membrane phospholipid (i.e. exposure of phosphatidylserine), nuclear degradation, especially due to the activation of endonucleases, which catalyse intranucleasomal DNA cleavage. The nuclear changes also include condensation of chromatin, which results in the characteristic appearance of nuclei of apoptotic cells. Activation of caspases (especially caspase 3) is also a feature of apoptosis, which performs proteolysis of cell proteins such as actin. Apoptotic bodies may occasionally form, i.e. small membrane-bound vesicles released by the dying cell(52). These apoptotic bodies are taken up by nearby phagocytes including macrophages, and this is protective and is a critical step in resolution of inflammation and infection(54). Necrosis, on the other hand, is an unprogrammed and chaotic form of cell death resulting from inflammatory insults including infection, which can release the cells’ toxic contents, which act as DAMPs, into the site of infection. It is characterised by cytoplasmic swelling, disorganisation of organelles, ruptured plasma membrane, and nuclear lysis(55). Necroptosis is a programmed form of necrosis characterised by rapid plasma membrane permeabilisation and

release of DAMPs into the extracellular environment(56). It is therefore a proinflammatory form of cell death. Autophagy is a cell death process employed by cells under excessive stress(57). Autophagic neutrophils display vacuolation of their cytoplasm (autophagosome formation), degradation of organelles within autophagosomes, and lack the chromatin condensation step that is typical for apoptotic cells. Autophagic neutrophils are phagocytosed by neighbouring innate immune cells and so autophagy is a non-inflammatory form of cell death(58).

1.8 NET formation

NETosis, first described by Brinkmann *et al.* in 2004, is a distinct form of cell death, which results in the production of neutrophil extracellular traps (NETs). NETs are extracellular, web-like structures composed of decondensed deoxyribonucleic acid (DNA), histones and an array of proinflammatory cytosolic and granule proteins including NE, MPO, LL-37 and calprotectin(59,60). Once within the extracellular space, NETs function to ensnare and degrade microbes. Due to these key antimicrobial effects, NETs have been conserved throughout evolution. For example, extracellular trap formation has been shown to be critical for encapsulation of microbes by haemocytes of the invertebrate shore crab *Carcinus maenas*(61), the extracellular traps of which contain histone 2A and peroxinectin, the crustacean homologue of MPO(61), and NETs (or equivalent) have been described in fish(62), chickens(63), dogs(64) and pigs(25). Studies in humans have also demonstrated NETs to be antimicrobial(65).

The cellular mechanisms understood to be involved in PMA- or bacteria-induced NET formation are summarised in Figure 1.4 and involve NADPH oxidase 2 (NOX2)-dependent mechanisms.

Figure 1.4

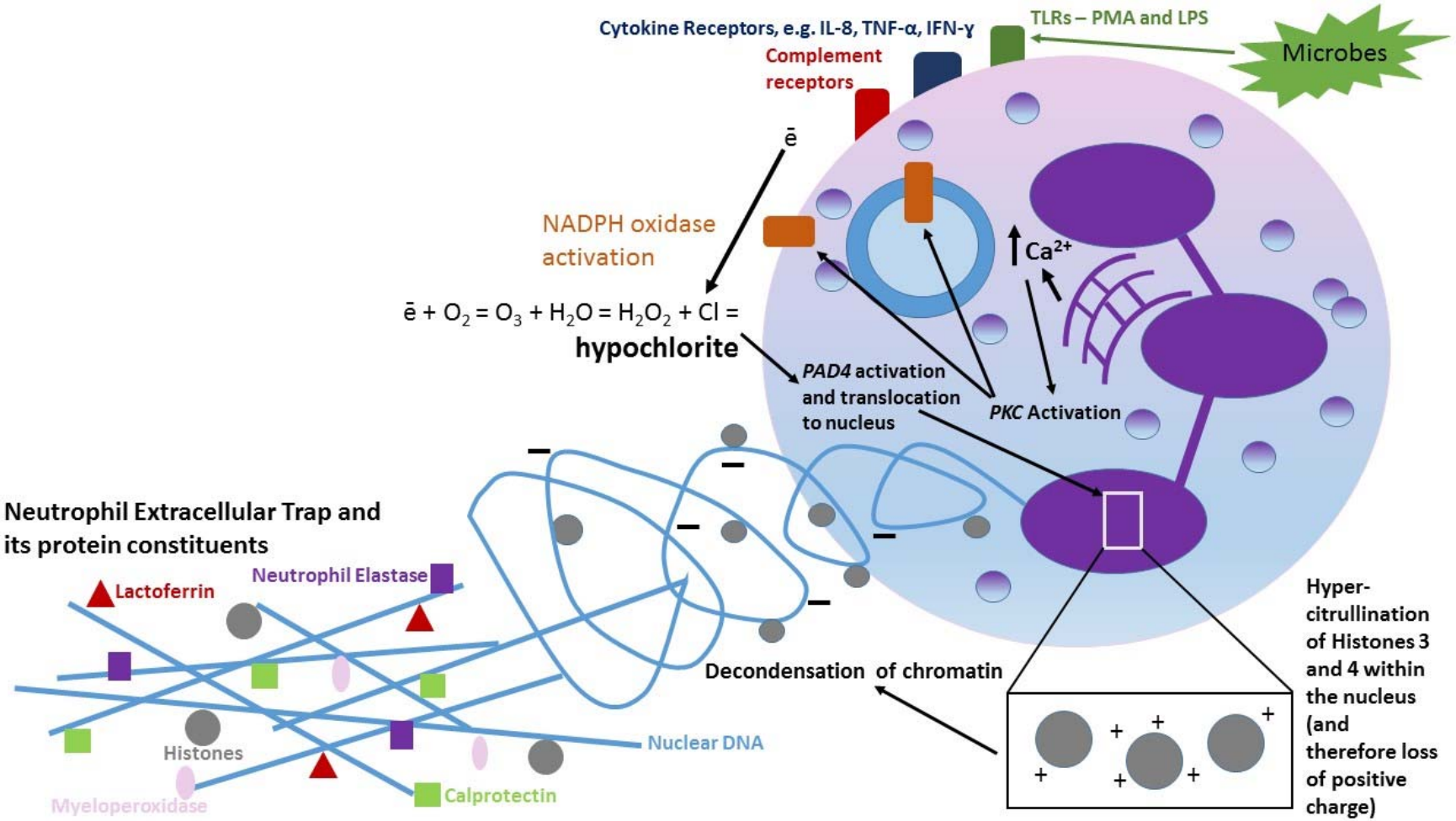
Cytokine Receptors, e.g. IL-8, TNF-α, IFN-γ
Complement receptors
TLRs – PMA and LPS
Microbes
ē
NADPH oxidase activation
Ca^{2+}
ē + O_2 = O_3 + H_2O = H_2O_2 + Cl =
hypochlorite
PAD4 activation and translocation to nucleus
PKC Activation
Neutrophil Extracellular Trap and its protein constituents
Lactoferrin
Neutrophil Elastase
Histones
Myeloperoxidase
Nuclear DNA
Calprotectin
Decondensation of chromatin
Hyper-citrullination of Histones 3 and 4 within the nucleus (and therefore loss of positive charge)

Figure 1.4: Neutrophil extracellular trap (NET) production via the NADPH oxidase 2 (NOX2)-dependent mechanisms(66)***.*** *Neutrophils undergo NET formation when triggered by microbial (bacterial, viral and fungal), inflammatory (e.g. IL-8, TNF-α) and sterile endogenous triggers (e.g. platelets and monosodium urate crystals)*(66)*. When these ligands bind their respective receptors on neutrophils, it triggers increased calcium release from the endoplasmic reticulum, which activates Protein Kinase C (PKC). This leads to activation of NAPDH oxidase on both the cell membrane and lysosomes, forming* O_2^-*, which reacts with chloride and water to form hypochlorite. This activates peptidyl arginine deiminase 4 (PAD4) which translocates to the nucleus where it catalyses hypercitrullination of histones 3 and 4*(67)*. This causes the histones to lose their positive charge, weakening their binding to negatively charged DNA, leading to decondensation of chromatin. NOX-2-mediates release of neutrophil elastase (NE) and myeloperoxidase (MPO) from azurophilic granules, which function as co-factors for decondensation of chromatin. The neutrophil's plasma membrane loses integrity then decondensed chromatin and histones are expelled into the extracellular space where they form complexes with granule and cytoplasmic proteins such as MPO (= pink ovals), NE (= purple squares), lactoferrin (= red triangles) and calprotectin (=green squares). Recent research suggests that NETs are an end product of numerous, independent cell signalling pathways, not all of which require all of the above steps*(68)*.*

However, since the original description of NETosis, mounting evidence suggests that neutrophils may also release NETS *in vivo* without cell death in a process called “vital” NETosis, which may involves the release of mitochondrial DNA(69) and this does not require the presence of citrullinated histones on the DNA backbone(70). Indeed, authors of a recently published consensus document advise that the term “NETosis” only be used in situations where death of the neutrophil is obvious and “NET formation” should otherwise be the preferred terminology(71).

NET formation is triggered by bacterial, fungal and viral infections, inflammatory mediators including IL-8 and TNF-α, and sterile endogenous triggers such as sodium urate crystals and platelets(66). In NOX-2-dependent NET formation, NE and MPO were shown to be essential co-factors for the decondensation of chromatin but evidence now shows that NET formation can be independent of NOX-2 and MPO(68). Furthermore, there now exists a debate about whether peptidyl arginine deiminase 4 (PAD4) is essential for NET formation. PAD4 is an enzyme that translocates to the nucleus and catalyses hypercitrullination of histones, which results in the loss of positive charge of histones and consequently decondensation of chromatin. Pharmacological PAD4 inhibition and PAD4 knock-out mouse model experiments have suggested that this enzyme is critical for NET formation(72–74). Conversely, more recent investigations reveal that NET formation can occur independent of PAD4 in response to microbes such as *Candida albicans*

and *Group B streptococcus*(68). We can conclude that a diverse range of cell signalling pathways ultimately result in NET formation.

Moreover, there are emerging links between autophagy and NET formation(75,76). Remijsen *et al*. used wortmannin (a phosphatidylinositol 3-kinase (PI3K) inhibitor often used to inhibit autophagy) to inhibit PMA-induced NET formation in human neutrophils(75). Similarly, synovial fluid neutrophils from gout patients did not produce NETs *ex vivo* when phagolysosomal fusion was inhibited, implicating autophagy in NET formation(77). However, treatment with late-autophagy inhibitors such as Bafilomycin A1 and chloroquine had no impact on NET formation(78) and so whether a relationship exists between the two pathways remains equivocal.

1.9 Neutrophil homeostasis is dysregulated in CF lung disease

In CF lung disease, neutrophils accumulate within the airways from an early stage, before infection has occurred. Impaired apoptosis may contribute to neutrophil accumulation(79,80) and our group has recently shown that CF neutrophils survive longer due to delayed apoptosis and this is associated with the absence of CFTR function and results in enhanced NET formation(70). Furthermore, this apoptosis delay is reversed in patients treated with ivacaftor (a CFTR potentiator drug), which alludes to CFTR's key role in apoptosis pathways(70). Our group's previous *in vitro* studies demonstrated that NETs are proinflammatory to macrophages, causing the release of proinflammatory

cytokines and chemokines including IL-8 and TNF-α(70). Within the CF airways, chemokine release would recruit more neutrophils and so a cycle of inflammation ensues, summarised in Figure 1.5. Indeed, infants diagnosed with CF at newborn screening or with early modes of presentation such as meconium ileus have increasing levels of IL-8 in their BAL fluid with increasing age, despite there being no bacterial infection or impairment in their lung function(81). The inflammatory response heightens once bacterial infection occurs. For reasons that will be discussed in sections 1.10, 1.11 and 1.15, the host inflammatory response is unable to eradicate such infections and this leads to persistent release of proinflammatory mediators, chemoattractants and recruitment of more neutrophils and macrophages(82).

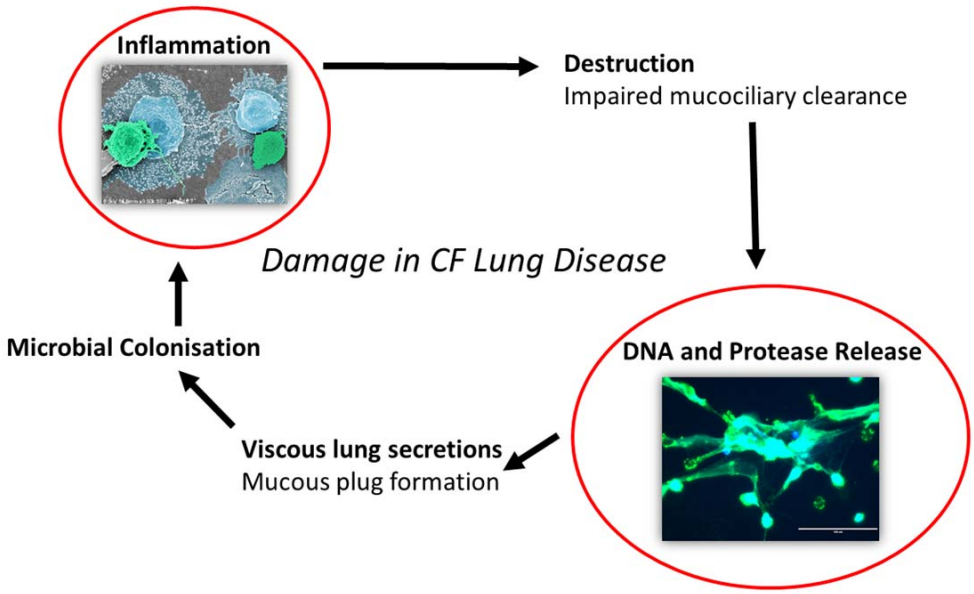

Figure 1.5: Cystic Fibrosis (CF) lung disease is characterised by a cycle of inflammation, in which innate immune cells play a key role. *Inflammation occurs in CF infants before bacterial infection has occurred. Neutrophils and macrophages release proinflammatory mediators, which cause destruction of lung tissue and impaired mucociliary clearance within the airways. This leads to accumulation of DNA – much of which is NET-derived – and protease release. This contributes to the viscosity of lung secretions and so mucous plugs form. These are ineffectively cleared, contributing to microbial colonisation/infection, which further drives this vicious cycle of inflammation.*

1.10 Intrinsic defects exist within CF neutrophils

Not only do neutrophils excessively accumulate in the CF airway environment but also their function is abnormal due to CFTR dysfunction. The aforementioned antimicrobial defence mechanisms of degranulation, phagocytosis, ROS generation and NET formation are all abnormal in the context of CFTR dysfunction. Previous studies have confirmed CFTR expression within neutrophils. For example, Painter *et al.* used reverse transcriptase-polymerase chain reaction (RT-PCR), immunofluorescence staining, and immunoblotting to demonstrate low level expression of CFTR in neutrophils at both mRNA and protein levels, with CFTR protein expression on secretory vesicles and phagolysosomes(83). This suggests CFTR could have multiple roles in neutrophil function. For example, CFTR is responsible for ion exchange between the cytoplasm and phagolysosome. CF neutrophils have impaired transport of chloride into the phagolysosome from the cytoplasm and accordingly have increased cytosolic concentrations of sodium and chloride ions and reduced chloride concentrations in their phagolysosome(83). This has two detrimental effects to neutrophil function. Firstly, the formation of hypochlorite (a potent microbiocidal ROS formed from hydrogen peroxide and chloride) within the phagolysosome is impaired due to a reduction in chloride availability(84). Secondly, the increased cytosolic sodium and chloride concentrations decreases cytosolic pH, which leads to excessive degranulation of azurophilic granules, thus increasing the release of antimicrobial enzymes such as peroxidases (e.g. MPO), proteases (e.g. NE) and antimicrobial peptides (e.g. calprotectin)(85). The resulting high

extracellular levels of NE overwhelms the binding capacity of the anti-protease alpha-1 antitrypsin(86), and degradation of elastin within lung parenchyma contributes to lung destruction and bronchiectasis seen in CF(38). Pohl *et al.* also demonstrated that human CF peripheral blood neutrophils have abnormal cytosolic ion concentrations that result in the inactivation of Rab27a, an intracellular protein involved in granule trafficking. This led to impaired degranulation of secondary and tertiary neutrophil granules with resultant impaired bacterial killing(87). Treatment of CF patients with the G551D *CFTR* mutation with the ion channel potentiator Ivacaftor abrogated these defects in CF neutrophils(87).

Whether CFTR dysfunction directly causes abnormalities in NET formation remains to be determined. Gray *et al.* showed that aged CF neutrophils have higher levels of NET formation compared to HC neutrophils(70). Whilst this observation does not implicate CFTR directly in regulation of NET formation pathways, it demonstrates that CF neutrophils form more NETs compared to HC neutrophils, which was abrogated by blocking apoptosis(70), suggesting an indirect mechanism linking CFTR to NET formation. Akong-Moore *et al.* performed *in vitro* experiments stimulating neutrophils with PMA to induce NET formation in the presence and absence of chloride in the culture media. They found NET formation was significantly decreased in the absence of extracellular chloride(88), which may be of relevance in the context of CF. The potential role of CFTR in NET formation certainly merits further investigation.

1.11 NETs are an ineffective antimicrobial defence mechanism within CF airways

Within the context of CF, non-resolving neutrophilic inflammation has negative consequences for patients' respiratory systems. In spite of there being high numbers of neutrophils present in their airways, patients suffer recurrent lower respiratory tract infections and colonisation with organisms such as *S.aureus, P.aeruginosa* and *A.fumigatus* as defence mechanisms are overwhelmed. It has been demonstrated that NETs are an ineffective defence against bacteria in CF airways. For example, laboratory strains and CF clinical isolates of *P.aeruginosa* strongly trigger NET release(89), however *P.aeruginosa* isolates from patients with established airways colonisation acquire resistance against NETs(90,91). Furthermore, Fuchs *et al.* showed that only 25% of neutrophils form NETs to kill *S.aureus in vitro;* the majority of bacterial killing was by phagocytosis(92). NET formation appears better suited to tackling large microbes, such as fungal hyphae, which are too large to be phagocytosed(93). In line with this suggestion, Marcos *et al.* found NETs in airway samples of CF patients were associated with fungal colonisation with *A.fumigatus* but not with bacterial infection(94). Furthermore, a recent study elegantly showed that NETs are crucial in preventing central nervous system dissemination of *P.aeruginosa* bacterial keratitis in a mouse model of acute keratitis(95). Thus, NETs are likely to be bacteriostatic rather than bactericidal. With these studies in mind, we hypothesise that in the context of CF, NETs play only a minor antimicrobial role, as despite the presence of large numbers of activated

neutrophils and extracellular DNA in their airways, patients suffer microbial colonisation and recurrent infections.

This introduces the concept of NETs acting as the Jekyll and Hyde of immunity(66). In lower order species, NETs ensnare and kill microbes(61) but in higher order species, due to the presence of an adaptive immune system, NET constituents may function as auto-antigens and so drive autoimmune disease.

1.12 NETs contribute to autoimmune disease and sterile inflammation

There are a number of diseases characterised by NET-mediated sterile inflammation including Systemic Lupus Erythematosus (SLE), psoriasis, small vessel vasculitis, rheumatoid arthritis, gout, venous thrombosis and cardiovascular disease(96–100). The autoantibodies present in autoimmune diseases target NET-bound proteins, which act as auto-antigens, e.g. anti-MPO, anti-Proteinase 3, extractable nuclear antibodies (ENA), anti-nuclear antibodies (ANA) and anti-dsDNA antibodies. The autoantibodies bind to their respective auto-antigen and form immune complexes that are pathogenic. Hakkim *et al.* demonstrated that serum endonuclease DNase1 is critical for degradation of NETs in the sera of SLE patients(97). A sub-set of their patient cohort had impaired NET degradation, due to either the presence of DNase1 inhibitors in their sera or anti-NET antibodies, which prevented the enzyme's access to the NETs. These patients suffered renal impairment secondary to resultant lupus nephritis(97). Similarly, during the pathophysiology of

atherosclerosis, NETs activate macrophages to release proinflammatory cytokines which interact with the adaptive innate immune system by activating T helper 17 cells, driving further immune cell recruitment and exacerbating inflammation(100). In the context of venous thrombosis, NETs act as a third scaffold of the blood clot, alongside fibrin and von Willebrand Factor(99). In psoriasis, an autoimmune skin condition, NET formation is increased in peripheral blood and the skin plaques and correlates with disease severity(98). Intact NETs were shown to induce human β-defensin-2 production by plaque keratinocytes, partly explaining the decreased susceptibility of psoriasis plaques to microbial infections. However, the fact that NET levels correlate with disease severity suggests that they are also a driver of inflammation.

1.13 The pathophysiological role of NETs in Cystic Fibrosis

In view of this evidence that NETs are involved in the pathophysiology of autoimmune and sterile inflammatory diseases, it is likely that NETs are an important proinflammatory component in the CF airway, where inflammation is driven by chronic infection. Higher levels of free DNA are present in BAL samples of CF patients compared to healthy controls(101). Originally, it was thought this DNA was derived from apoptotic and necrotic cell debris. However, more recent studies have suggested most DNA present in the airways arises from NETs, levels of which are increased in airway samples from CF patients compared to healthy controls and are associated with poorer lung function(94,102). However, these studies used the PicoGreen® assay as a measure of NETs, which only measures dsDNA and so may not be specific

for NETs(103). In order to quantify NETs *in vitro,* a recent expert review article recommended that assays demonstrate co-localisation between the DNA backbone alongside constituent proteins(103). Numerous studies have previously focussed only on NET proteins in isolation and although indirect, these studies still add to the evidence that NETs are proinflammatory.

1.14 NET constituent proteins are associated with lung injury and inflammation

Histones

Chromatin is a complex of negatively charged DNA wound around positively charged histones that functions to efficiently package DNA within the nuclei of eukaryotic cells. This means that when the chromatin unravels in the process of NET formation (see Figure 1.4) histones are extruded into the extracellular space along with the nuclear DNA. Indeed, histones are the most abundant NET protein. In a study where neutrophils were stimulated to form NETs using PMA, resultant NETs were digested then analysed by nano-scale liquid chromatography coupled matrix-assisted laser desorption/ionization mass spectrometry (nano LC-MALDI-MS); histones H2A, H2B and H3 together accounted for ~ 64% total NET protein content(104). Histones have been studied extensively in the context of acute lung injury in mice(105–108) in which their positive charge binds to and disrupts the phosphodiester bonds within cell membranes, thus causing toxic calcium influx(105). They also bind TLR-2 and TLR-4 and induce proinflammatory cytokine production in macrophages(107). Histone sub-types - H1, H2A, H2B, H3 - have defined

effects upon murine and human phagocytes; they can lead to cell swelling, lactate dehydrogenase release, cytokine and chemokine release to varying degrees(107). Interestingly, the treatment of mice with DNase has been shown to reduce citrullinated H3 levels in BAL fluid and protect from LPS-induced acute lung injury, suggesting NETs are a source of these damaging histones(108).

Neutrophil Elastase

NE is another key NET constituent, accounting for 5.8% total NET protein content(104) in PMA-induced NETs, and implicated in the pathophysiology of CF. It is an azurophilic granule protein, which functions in an antimicrobial capacity to degrade phagocytosed proteins. It can also be released into the extracellular space in the process of degranulation and as an adverse effect within the airways, NE degrades protein structures including elastin and collagen(109). It is found in high concentrations in CF sputum and BAL samples and levels correlate with lung function decline in CF(38,85). Dubois and co-workers demonstrated that *in vitro* DNase treatment of NETs significantly increased NE activity(102). They concluded that negatively charged DNA binds to cationic NE and protects it from inhibition by anti-proteases in the lungs. This interaction likely contributes to the protease-anti-protease imbalance seen in CF lung disease, which leads to parenchymal destruction. These findings suggest that combining protease inhibitors with DNA-degrading treatments may represent an effective therapeutic strategy for preventing lung damage.

Myeloperoxidase

MPO, a peroxidase enzyme involved in innate immune responses, is another NET constituent protein used as a biomarker in CF. MPO helps degrade phagocytosed material within lysosomes and is released from azurophilic granules into the extracellular space during neutrophil degranulation. This enzyme is also an essential mediator of PMA- and some bacterial-induced NET formation(110). Serum MPO levels decrease significantly during antibiotic treatment of a CF lung exacerbation(111). Elevated sputum MPO levels are associated with increased mortality in CF patients infected with *B.cepacia* complex(112) and are associated with albumin/g sputum (a measure of protein leakage into the airways) and radiographic evidence of lung damage, as well as reduced lung function in CF patients(113). However, this has not been a consistent finding in all studies. Gray *et al.* did not find a significant reduction in sputum MPO levels following antibiotic treatment of a CF exacerbation(114), possibly because baseline levels are high due to the chronic airway neutrophilia. Calprotectin may be a more sensitive biomarker of CF lung disease, because its levels did significantly fall in sputum following treatment of an exacerbation(114).

Calprotectin

Calprotectin is a neutrophil cytosolic protein (accounting for 40-60% of the cytoplasmic protein load(115) and 5% total protein load(116)), incorporated onto NETs during NET formation. It is a heterodimer formed from S100A8 and S100A9, which account for 4% and 1.41% total NET protein content,

respectively(104). S100A8 was identified as a protein abnormally elevated in the serum from CF homozygotes and obligate heterozygotes in 1982 by Bullock *et al.* using quantitative immunoprecipitation and immunoradiometric assays(117). Following on from this discovery of the "CF antigen", its gene was cloned and located to chromosome 1 by Dorin *et al.* in 1987(118), although its involvement in the pathophysiology of CF was unknown. Since then, calprotectin has been studied extensively and is associated with inflammatory and infectious diseases, including inflammatory bowel disease and arthritis. It has numerous functions including chelation of micronutrient metals like zinc and manganese, which limits their availability to microbes in a process called nutritional immunity(119). Calprotectin on NETs has been shown to be crucial as an anti-fungal defence in mice(104). It also induces apoptosis(120) and promotes chemotaxis of neutrophils and macrophages to sites of inflammation(121). In addition, calprotectin acts as a TLR-4 agonist, contributing to proinflammatory cytokine production through NF-κB activation(122). Our group has also studied calprotectin in the context of CF lung disease. Gray *et al.* previously demonstrated that it could be used as a biomarker for CF(114). Both sputum and serum calprotectin levels significantly decrease following treatment of an exacerbation, and serum calprotectin levels were negatively correlated with forced expiratory volume in one second (FEV_1) (a measure of patient lung function) and predicted time to next exacerbation(114,123).

In summary, histones, NE, MPO and calprotectin are all found to be associated with NETs, cause inflammation and correlate with lung function decline in CF. Free DNA has similarly been shown to correlate with airflow obstruction in CF(94). The available evidence therefore suggests that NETs are critically involved in the pathophysiology of CF, although the precise mechanisms require further elucidation. Mutation of the *CFTR* causes abnormal function of innate immune system cells, including decreased apoptosis that may contribute to excessive production and/or impaired clearance of NETs.

1.15 Intrinsic defects also exist within CF macrophages

NETotic and apoptotic neutrophils are cleared from the airways partly by phagocytosis by macrophages - the professional phagocytes of the innate immune system, integral to an effective antimicrobial response. Macrophages clear dead cells, microorganisms and foreign material from the airways. In common with neutrophils, macrophages express PRR that recognise microbial PAMPs and self-DAMPs (e.g. NETs). In addition, macrophages initiate the inflammatory response through production of cytokines, ROS and antimicrobial peptides, to target microbes and resolve inflammation(124). Hence, exposure of macrophages to NETs may amplify proinflammatory responses and tissue damage caused directly by the accumulated neutrophils.

Macrophages specialise in the phagocytosis of pathogens and dead cell debris. The ultrastructure of these cells is beautifully adapted to such a role, with a cytoskeleton that rapidly alters its structure to permit efficient

chemotaxis. Macrophages express PRR, complement Fc, and scavenger receptors, which aid phagocytosis of target material(124). Ligation and activation of these receptors results in intracellular signalling cascades involving PI3Ks and phospholipase C(125), which lead to actin cytoskeletal reorganisation and alteration of the plasma membrane to permit engulfment of the target material into assembled phagosomes. These membrane-bound organelles in turn fuse with lysosomes (i.e. another type of membrane bound organelle containing degradative enzymes) to form a phagolysosome which has an acidic environment, with a pH of around 4.5-5.0 at full maturity(126,127). The phagolysosome functions to break down ingested substances via the activity of lysosomal enzymes together with proton-pump acidification. The mechanisms by which phagolysosomes are acidified are described more fully in Chapter 5.

Numerous intrinsic abnormalities of the CF macrophage have been reported in the literature. Recent work by our group demonstrated that when human monocyte-derived macrophages (MDM) were co-cultured with NETs and control neutrophils, NETs induced an exaggerated proinflammatory response from the MDM and this effect was enhanced in CF MDM(70). Associations between human alveolar macrophage numbers and airway proinflammatory cytokine levels have been shown to exist, adding support to the hypothesis that CF macrophages have an exaggerated response to inflammatory stimuli(128). Indeed, the macrolide antibiotic Azithromycin functions in an immunomodulatory capacity to reduce proinflammatory cytokine production

from alveolar macrophages and is known to reduce pulmonary exacerbation rates and promote weight gain in CF(129,130). In the context of atherosclerosis, circulating CD14-purified monocytes have been shown to increase IL-1β and IL-6 production when pre-treated with NETs prior to culture with cholesterol crystals(100). This effect was abrogated with DNase treatment, suggesting DNA is crucial for the proinflammatory response(100). In newborn CF pigs, CF macrophages also have a hyper-responsive phenotype, which is independent of the inflammatory milieu of the CF lung (since lung inflammation is not present in the newborn animals)(131). *Ex vivo* experiments using MDM from newborn CF pigs demonstrate that CF MDM produce more IL-8 and TNF-α compared to WT MDM in response to LPS(21).

The MDM hyper-responsiveness to LPS seen in the CF pig model may be due to aberrant trafficking of its PRR, TLR-4. Bruscia *et al.* demonstrated that CF murine macrophages have prolonged TLR-4 retention in the early endosome and reduced translocation into the lysosomal compartment. Consequently, TLR-4 had reduced degradation and so more remained available on the plasma membrane. When stimulated with LPS, murine CF macrophages had increased activation of the NF-κB, MAPK, and IFN regulatory factor-3 pathways and hence increased proinflammatory cytokine production(132), including IL-8, which acts as potent chemokine for neutrophils. CFTR inhibition of murine WT macrophages resulted in similar hyper-responsive phenotype. This demonstrates that CFTR plays a key role in spatial and temporal resolution of TLR-4.

As well as this exaggerated response to PAMPs and DAMPs, CFTR dysfunction may adversely affect macrophage phagocytosis. This is both in terms of the cells' ability to uptake bacteria(124,133) and in the degradation of internalised microbes. In a recent *ex vivo* study, Barnaby *et al.* demonstrated that the CFTR modulator Lumacaftor (which increases export of F508del CFTR from the endoplasmic reticulum to the plasma membrane) restored the ability of CF MDM to phagocytose and kill *P. aeruginosa* to levels seen in non-CF MDM(134). This suggests CFTR plays a key role in macrophage phagocytosis pathways, although precise mechanisms of action are unknown. Furthermore, CFTR function may contribute to the regulation of macrophage organelle acidification. The debate surrounding this topic is described more fully in Chapter 5. Some groups have reported failure of phagolysosomal acidification in CF macrophages which led to impaired bacterial killing of the pathogenic organism *P.aeruginosa,* although this was contended by others(20,135). Discrepancies in reported results may relate to potential insensitivity of fluorescence microscopy techniques used to quantify phagolysosomal pH.

Lastly, recruitment of monocytes into the inflamed lung environment may be compromised in CF due to intrinsic defects in mononuclear cells. The chemoattractant-induced activation of β1 and β2-integrins and subsequent chemotaxis (via Rho family GTPases) is defective in human CF mononuclear cells(136). This abnormality was reproduced when healthy mononuclear cells were treated a pharmacological inhibitor of CFTR (CFTR-$_{inh}$172). Moreover,

when CF monocytes were treated with CFTR-correcting drugs, integrin functionality was restored(136). Hisert *et al.* studied peripheral blood monocytes from CF patients commencing treatment with the CFTR potentiator ivacaftor. They measured the plasma membrane proteome and found that proteins involved in the inflammatory response and monocyte migration were altered significantly by 7 days' ivacaftor treatment, perhaps due to decreased IFN-ɣ responses(137). These studies suggest that the non-resolving neutrophilia of CF lung disease may be in part due to failure of mononuclear cell recruitment, which would help resolve the inflammation.

1.15 Anti-inflammatory treatments for Cystic Fibrosis lung disease

Despite the unrelenting neutrophilic inflammation of the airways in CF lung disease, there remains no effective, targeted anti-inflammatory treatment for CF. The drugs that do have anti-inflammatory actions such as Azithromycin exert these as additional, off-target effects or with unknown mechanisms of action. Non-resolving inflammation, including NET formation represents a key response to chronic microbial infection, preventing microbial dissemination. Treating inflammation in CF lung disease is therefore likely to require a balance between maintaining host defence and preventing excessive inflammation. For example, a randomised double-blind, placebo-controlled phase 2 trial of an LTB_4 receptor antagonist in adults and children with CF had to be terminated early after interim analysis revealed significant increases in pulmonary related serious adverse events in the adult cohort(138). LTB_4 is produced by macrophages and neutrophils and is a potent chemoattractant

and activator of neutrophils(139). In the group receiving the LTB_4 antagonist drug, there were significant increases in respiratory symptoms necessitating intravenous antibiotics and hospitalisation, as well as impaired lung function and increased peripheral blood neutrophil counts(139). These data suggest that reducing neutrophil recruitment and activation actually worsened inflammation and so any inhibition of host defence mechanisms must be measured to avoid unintentional harm to patients. Given the evidence that an excessive innate immune response is key to the pathophysiology of CF, it is likely that *moderated* immunomodulation would be of benefit to most patients.

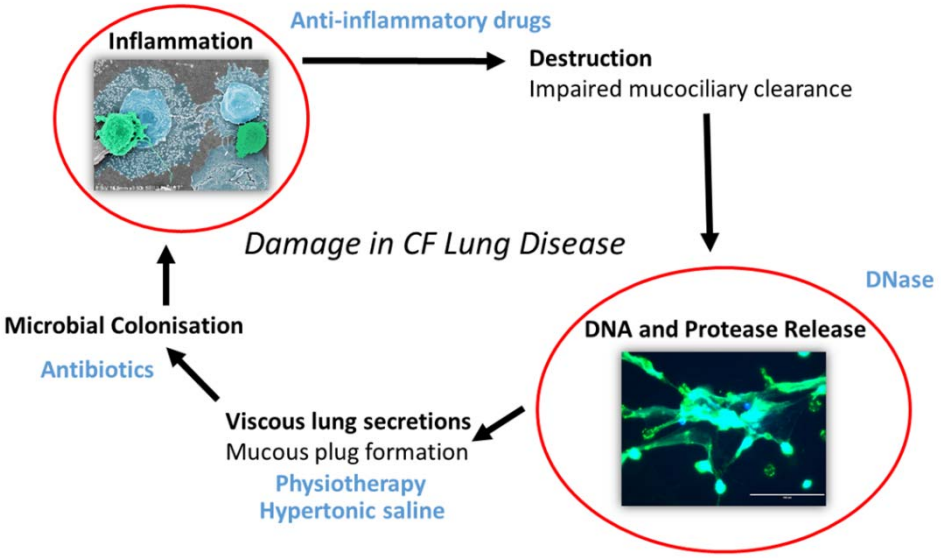

Figure 1.6: Anti-inflammatory treatments targeting the causes of inflammation that lead to damage in Cystic Fibrosis lung disease. *Clinicians prescribe only a handful of anti-inflammatory medications in CF, shown in blue text. Anti-inflammatory drugs include ibuprofen and Azithromycin, which modulate innate immune cell functions. Nebulised recombinant human DNase targets the excessive DNA within the airways to reduce sputum viscosity. Hypertonic saline similarly reduces sputum viscosity. Antibiotics are prescribed to target colonisation and recurrent infections. CFTR potentiators and correctors are also emerging as modulators of immune cell function.*

Anti-inflammatory Medications

With regard to anti-inflammatory medications, inhaled and oral corticosteroids are indicated in CF patients only if they suffer from asthma or Allergic Bronchopulmonary Aspergillosis (ABPA)(140). Non-steroidal anti-

inflammatory drugs (NSAIDs) have also been evaluated in the context of CF. A Cochrane review reports three trials studying the effects of ibuprofen in CF(141). One of those, by Konstan *et al.,* demonstrated that patients assigned to four years' treatment with high-dose ibuprofen had a slower annual rate of change in FEV_1 and weight(142). These effects were greatest when ibuprofen was started in paediatric patients(141). It is therefore recommended that in patients with CF six years of age and older, and with FEV_1 > 60% predicted, oral ibuprofen is used to slow lung function decline. However, the bleeding diathesis may limit ibuprofen's use.

Recombinant Human DNase

DNase I is a human enzyme present in the blood, saliva, pancreatic secretions and urine, which functions to digest extracellular DNA(143). Recombinant human DNase (Pulmozyme®, known generically as dornase alfa) is classed as a mucoactive agent and as such, is offered to patients with evidence of lung disease(144). It functions to degrade the excessive DNA that accumulates in CF sputum, reducing sputum viscosity and aiding clearance(140). It improves lung function in both paediatric and adult CF patients(145–147). In a randomised placebo-controlled trial, Fuchs *et al.* demonstrated that the administration of once or twice daily rhDNase improved FEV_1 over the 24 weeks' follow up by an average of 5.8% and 5.6%, respectively(146). This was a statistically significant improvement in lung function as compared to the placebo group, whose FEV_1 remained static. Furthermore, rhDNase improved quality of life in terms of reduced dyspnoea and improved overall well-

being(146). In addition to slowing the rate of lung function decline(148), the BEAT study demonstrated that rhDNase has direct anti-inflammatory effects. In this placebo-controlled study, which followed patients over three years after initiation of treatment, those untreated had significant increases in BAL median neutrophil percentage, IL-8 and elastase levels, whereas those treated with DNase did not(149). Furthermore, a sub-study showed that the matrix metalloproteinases 8 and 9 (MMP-8 and -9), enzymes implicated in lung tissue destruction in CF, had increased levels in the untreated group but decreased levels in the rhDNase treated group(150). With these anti-inflammatory actions in mind, we hypothesise that DNase may reduce inflammation in CF through decreased NET formation or increased degradation of NETs. If this were to be the case, there could be an argument for commencing DNase treatment at an earlier stage of disease.

Nebulised Hypertonic Saline

Nebulised hypertonic saline is another mucoactive drug treatment indicated in CF lung disease. It improves hydration of the ASL to improve airway clearance(151). Studies have shown that hypertonic saline treatment improves lung function and reduce exacerbation rates, but not to the same extent as rhDNase(140). If patients cannot tolerate rhDNase due to side effects, hypertonic saline can be prescribed as a monotherapy. Similarly, these two mucoactive drugs can be given in combination in patients who have an inadequate response to rhDNase alone. Antibiotics

When CF patients experience lower respiratory tract infections, treatment is with antibiotics as per local formulary guidelines. However, there is also a role in prescribing antibiotics for the prevention of infection. In some regions, paediatric patients receive prophylactic Flucloxacillin to protect against *S.aureus* infection from the point of diagnosis up to the age of 3 or 6(144). In patients newly infected with *P.aeruginosa,* eradication is attempted by treatment with at least two oral/IV antibiotics coupled with an inhaled antibiotic, followed by a prolonged course of oral an inhaled antibiotics(144). However, if patients are chronically infected with *P.aeruginosa,* the first-line inhaled antibiotic is Colistimethate sodium, a polymyxin antibiotic, which degrades the bacterial cell membrane(144) (polymyxin is also used *in vitro* as an LPS blocker because it binds LPS). If this is ineffective, inhaled Tobramycin is indicated in patients over the age of 6 years who are symptomatic or with mild lung disease(140). Tobramycin is an aminoglycoside antibiotic, which inhibits bacterial protein synthesis through binding their cytoplasmic ribosomes(152). This treatment reduces exacerbation rates and improves pulmonary function(140,153–155).

Azithromycin

Another antibiotic used in CF is Azithromycin, a macrolide antibiotic which has been shown to improve lung function and reduce exacerbation rates in patients(140). It is indicated in patients with deteriorating lung function or repeated pulmonary exacerbations who are chronically infected with *P.aeruginosa*(144). It reduces mucin secretion and biofilm formation by

P.aeruginosa and increases the bacterium's susceptibility to other antibiotics(156). Of relevance to this PhD, Azithromycin also has marked immunomodulatory mechanisms of action. It works to inhibit the acute phase of the innate immune response, by reducing proinflammatory cytokine production from neutrophils, macrophages and AEC, thereby reducing recruitment of immune cells to the inflamed lung environment(129,157–159). It also acts upon the resolution stages of the immune response, by increasing neutrophil apoptosis and reducing neutrophil oxidative burst(160). Azithromycin might decrease NET formation in CF airways, perhaps indirectly by increasing apoptosis rates, a question that will be addressed in Chapter 3, section 3.3.

CFTR Modulators

Finally, we will review the role of the recently introduced CFTR modulators because abnormalities in immune cell function are reversed with ivacaftor treatment (see sections 1.8, 1.9 and 1.10). Ivacaftor (trade name, Kalydeco) was the first precision medicine available on the NHS for CF patients. It is indicated in those with at least one gating mutation in the *CFTR* gene (e.g. G551D), which accounts for ~ 5% UK CF patients(1). Ivacaftor is a CFTR potentiator because it increases the open probability of the CFTR channel (i.e. the fraction of time the channel is open, to aid ion transport)(161). Treatment with this drug significantly improves lung function, with median FEV_1pp increasing from 55.4 to 64.1%(1). Ivacaftor was shown to decrease significantly CF patient sputum inflammatory measures from the first week of

treatment and this effect is maintained over two years' follow up(162). Furthermore, chest CT scan studies before and one year after commencement of ivacaftor revealed that the drug decreased airway mucous plugging(162). Taken together, these findings suggest CFTR function is indeed related to airways inflammation.

Orkambi was the second precision medicine available in the UK and it is a combination therapy made up of ivacaftor and lumacaftor. Lumacaftor is a CFTR corrector, which increases export of F508del CFTR from the endoplasmic reticulum to the plasma membrane(134). It is indicated in patients with at least one F508del mutation, accounting for half of the UK's CF population(1), but the cost of the drug currently precludes its prescription, asides apart from on compassionate use. The TRAFFIC and TRANSPORT studies report that lumacaftor/ivacaftor improved FEV_1 and reduced exacerbation rates in patients with CF homozygous for the F508del *CFTR* mutation(163).

Moreover, Symkevi is another combination therapy consisting of ivacaftor and tezacaftor (the latter functioning like lumacaftor to move CFTR to the cell membrane) but is only licensed in patients ≥12 years of age. This combination drug has been evaluated in the recently published EVOLVE and EXPAND studies. The EVOLVE study, was a phase 3, randomised, double-blind, multicenter, placebo-controlled, parallel-group trial which studied tezacaftor and ivacaftor combination therapy for CF patients ≥ 12 years of age and

homozygous for F508del mutation. It demonstrated a statistically significant absolute change in the FEV_1pp of 4 percentage points in favour of the tezacaftor-ivacaftor over placebo and exacerbation rates were 35% lower in the treatment group(164). The EXPAND study evaluated tezacaftor-ivacaftor in CF patients with one F508del and one (out of a possible 14) residual function mutation. It found a significant absolute improvement in FEV_1pp of 6.8% in the treatment group compared with the placebo(165). This drug was given marketing authorisation by the European Medicines Agency in November 2018 and is now available in Scotland and soon to be available in England.

Finally, several next generation correctors have been trialed(166,167). One such corrector, VX-659 combined with tezacaftor and ivacaftor (VX-659-tezacaftor-ivacaftor) was shown to improve CF508del protein processing and trafficking and restore chloride transport in human bronchial epithelial cells *in vitro*(166). When trialed in CF patients with one or two F508del alleles, VX-659-tezacaftor-ivacaftor resulted in a significant mean increases in the percentage predicted FEV_1 at 29 days' follow up of up to 13.3% in patients with F508del-minimal function genotypes(166). In patients homozygous for F508del already on tezacaftor-ivacaftor, adding VX-659 resulted in a further 9.7% increase in percentage predicted FEV_1(166). VX-445-tezacaftor-ivacaftor treatment resulted in an 11-point increase in the percentage of predicted FEV_1 and improved quality of life in CF patients(167). These studies' conclusions are immensely exciting finding because triple combination correction-potentiation regimens could be indicated in 90% CF patients.

To summarise, CFTR modulators offer an exciting new group of drugs, which are likely to revolutionise the treatment of patients with CF. Emerging evidence highlights positive effects on neutrophil, macrophage and monocyte functioning and suggest that these drugs have important anti-inflammatory actions. For example, Pohl *et al.* demonstrated that human CF peripheral blood neutrophils have inactivation of Rab27a, a granule trafficking protein. This inactivation led to impaired degranulation with resultant impaired bacterial killing(87). Treatment of CF patients with the G551D *CFTR* mutation with ivacaftor corrected this defect in CF neutrophils(87). Furthermore, our group found that ivacaftor treatment corrected the propensity for human CF neutrophils to live longer due to delayed apoptosis(70). Abnormalities in CF peripheral blood monocyte protein expression are also restored by ivacaftor treatment, e.g. proteins affecting cell migration were increased and those involved in inflammation, including S100A9, were decreased(137). Future studies should focus on underlying mechanisms by which correction and potentiation of CFTR abrogates dysfunctional innate immune cells.

1.16 Summary

Innate immune cells play a vital role in the regulation of inflammation and infection. If unregulated, the functions of neutrophils and macrophages may become pathogenic, particularly in the context of the CF lung. The underlying mechanisms through which CFTR function affects NET formation and macrophage function require further investigation. Despite there being advances in CF therapy over the past 50 years, the median age of death of

UK CF patients is still only 31 years of age. Therefore, there is a real clinical need to design new anti-inflammatory drugs for CF to prevent the respiratory failure that causes premature death. A better understanding of the intrinsic defects of the CF innate immune cells and their interactions with one another will contribute towards this ultimate goal.

1.18 Hypotheses and Aims

The overarching hypothesis for the project was that NETs are central to inflammation and play only a minor antimicrobial role in CF lung disease. We also hypothesise that DNase therapy may reduce inflammation in CF through decreased production and/or increased clearance of airway NETs. We predict that CF macrophages will have a hyper-responsive phenotype in response to NETs *in vitro* and that CF NETs are hyper-inflammatory. We also set out to study a NET-independent defect in CF macrophages; we hypothesised that there would be a difference in macrophage phagolysosomal pH between CF and non-CF cells.

The principal aim of this PhD is to understand better the innate immune cell dysfunction in the context of Cystic Fibrosis airways disease. Specifically, the project aims:

1) To establish whether the presence of NETs in the sputum of CF participants was associated with more severe lung disease and inflammation.
2) To investigate responses of macrophages to NETs in culture, comparing macrophages from HC to those from CF participants.
3) To determine whether NET formation and associated inflammation are increased in a CF mouse model in comparison to WT mice following a sterile inflammatory challenge.

4) To investigate whether clearing NETs using DNase can reduce inflammation in a CF mouse model.
5) To develop a new, sensitive *in vitro* experimental technique using optical nanosensors to quantify phagolysosomal pH within living systems - comparing this method to conventional fluorescence spectroscopy – to address the hypothesis that there is a difference in pH between CF and non-CF cells.

Chapter 2: Materials and Methods

2.1 Common Buffer Solutions and Reagents

Buffer Solution	Description and Source
DPBS	Dulbecco's phosphate buffered saline without Mg^{2+}/Ca^{2+} (DPBS) (Gibco, UK)
HBSS	Hank's Balanced Salt Solution, without Mg^{2+}/Ca^{2+} (Gibco, UK).
1X TAE	1X Tris-acetate-EDTA (TAE), 0.05% PBS-Tween® (Sigma)
10% NBF	Neutral-buffered formalin (Thermo Fisher Scientific)
TBST	Tris-buffered Saline and 0.05% Tween 20
MACS buffer for Monocyte negative isolation	PBS without Mg^{2+}/Ca^{2+}, Bovine Serum Albumin (BSA) at 0.5g per 100 mL (Sigma) and 2mM EDTA.

Table 2.1.1: Common Buffer Solutions

Reagent	Description and Source
Phorbol 12-myristate 13-acetate (PMA)	10 nM, 50 nM and 100 nM. Phorbol 12-myristate 13-acetate (PMA) (Sigma)
Ionomycin	1 µM, 5 µM and 10 µM (Sigma)
Diphenyleneiodonium chloride (DPI)	2µM DPI (Sigma)
Ro-31-8220	1 µM Ro-31-8220 (3-[1-[3-(Amidinothio) propyl-1H-indol-3-yl]-3-(1-methyl-1H-indol-3-yl)maleimide) (Sigma)
DNase	100 U/mL DNase (Roche, UK)
SYTOX® green	Invitrogen, Thermo Fisher Scientific, UK
Cytochalasin D	5 µg/mL (Sigma, UK)
$CFTR_{inh}$-172	10 µM (R&D Systems, UK)
Bafilomycin A1	100 nM (Abcam, UK)

Table 2.1.2: Reagents

2.2 Human Participants

Experiments were performed on blood and/or sputum from CF adult patients attending the Edinburgh Adult CF Service at the Western General Hospital, Edinburgh. Age- and sex-matched HC were recruited from the Centre for Inflammation Research Blood Resource.

2.2.1 Inclusion and Exclusion Criteria

Participants included were over the age of 16, without any respiratory tract infection within two weeks' prior to donation, no immunosuppressant use, no past medical history of lung transplant, and were non-smokers by reporting (including the use of electronic cigarettes and vaporisers). HC participants included had no past medical history of respiratory disease whilst CF participants had a formal diagnosis of CF by clinical and genetic parameters.

2.2.2 Ethics Approval

The West of Scotland Research Ethics Committee 3 granted approval for this study (REC reference number: 16/WS/0239). HC participants were recruited from the Centre for Inflammation Research Blood Resource, ethical approval for which was granted by the Centre for Inflammation Research Blood Resource Management Committee (AMREC), 15/HV/013. All participants provided informed written informed consent.

2.2.3 Statistical analysis

Statistical analysis was performed using GraphPad Prism software (Version 8.0.2, USA). To verify that data were normally distributed, Shapiro Wilk normality tests were performed. Data were assumed to follow a non-parametric distribution where sample sizes were insufficient to test for normality. Summary data were expressed as the mean ± SD or median ± 95% confidence intervals (CI), with the number of experiments in parentheses. Significance testing was performed using an unpaired, two-tailed Student's *t*-test or Mann Whitney test when comparing two groups, or one-way/two-way ANOVA or Kruskal Wallis test when comparing three or more experimental groups with appropriate post-hoc tests. Multi-variate linear regression modelling to predict FEV_1 was performed using R software with the help of Dr Alastair Rushworth. Results were considered significantly different when $p<0.05$. Correlations were determined using Pearson Rank or Spearman Correlation Co-efficient, depending on the normality of data distribution.

2.2.4 Spirometry

FEV_1 and forced vital capacity (FVC) were measured according to ERS/ATS guidelines(169) using an EasyOne® Spirometer (New Diagnostic Design, Zurich, Switzerland) which was calibrated twice weekly.

2.2.5 Sputum Induction for Healthy Control Participants

All sputum and blood samples from HC participants were obtained at the Wellcome Clinical Research Facility at the Royal Infirmary of Edinburgh. HC participants had baseline FEV_1 measured in triplicate, after which they were treated with 2.5 mg nebulised Salbutamol then post-bronchodilator FEV_1 was measured after 10 min. Participants were subsequently given hypertonic saline nebulisers, the concentration of which increased incrementally at 10 min intervals (3%, 4%, 5%; 3% sourced from Tayside Pharmaceuticals and 4% and 5% from Stockport NHS Foundation Trust), similar to a method previously described(170). After each hypertonic saline nebulisation, participants were asked to blow their nose and rinse their mouth out with water (to avoid contamination of sputum with saliva) then were asked to cough and expectorate sputum into a sterile container. If FEV_1 fell by > 10% from the post-bronchodilator value, the hypertonic saline concentration was not increased. If FEV_1 fell by >20% or distressing symptoms occurred, the nebulisation was stopped. These complications did not occur in any participants.

2.2.6 Sputum collection from CF participants

All sputum and blood samples from CF participants were obtained at the Edinburgh Adult CF Service at the Western General Hospital, Edinburgh. CF participants were all able to expectorate sputum spontaneously so did not undergo the above induced sputum protocol.

2.2.7 Sputum Processing

Sputum was collected in sterile polypropylene tubes, which were transported on ice then samples processed within two hours of collection as described previously(170). In brief, sputum was transferred to a sterile petri dish then plugs (i.e. dense portions of sputum) were harvested from the expectorated sample using forceps and transferred to a petri dish. Forceps were used to gather plugs together using circular motions, to expel residual saliva. The resultant plug was transferred to a 15 mL BD Falcon tube. Sputum was homogenised using 0.1% dithiothreitol (DTT) (Sputolysin; Calbiochem Corp., San Diego, CA, USA), added to the sputum in equal volume to weight of sputum (e.g. 1mL DTT to 1g sputum). The sputum/DTT mixture was rotated at room temperature for 15 min. DPBS was subsequently added (in equal volume to that of the DTT) to stop further digestion. Samples were filtered through 48 µm nylon mesh (pre-soaked in DPBS) set in a funnel into a 50 mL BD Falcon tube, then centrifuged at 300g for 10 min at 4°C. The resulting cell pellet was re-suspended in DPBS. Cell-free supernatant was aliquoted and stored at -80°C until analysis.

2.2.8 Sputum Cell Pellet Cytocentrifuge Preparation and analysis

Sputum cell pellets were re-suspended in DBPS supplemented with BSA at 1g per 100 mL, and then 150 µL cell suspension was used per cytocentrifuge preparation, which permit visual assessment of cell morphology. Two

cytocentrifuge preparations were made per sample. Cell suspensions were pipetted into reusable Shandon™ Single Cytofunnel™ cell concentrators, apposed to disposable filter cards (Shandon™, Thermo Fisher, UK) in turn apposed to glass slides, all fixed together with metallic slide holders. Samples were centrifuged for three min in Thermo Scientific™ Cytospin™ 4 Cytocentrifuge (Thermo Fisher Scientific), at 300 revolutions per minute (rpm), on medium acceleration. All slides were air-dried, fixed with 100% methanol then stained with Shandon™ Kwik-Diff™ (Thermo Fisher Scientific, UK) to visualise acidic and nuclear structures. Lastly, slides were mounted with DPX Mountant (Sigma, MO 63146, USA) and glass coverslips.

Light microscopy of the above cytocentrifuge preparations was performed on EVOS™ XL Core light microscope at 20X magnification. Images were saved as TIF files and differential cell counts were performed using a cell counter function of ImageJ software (National Institutes of Health, USA, http://imagej.nih.gov/ij/download.html); 300 consecutive nucleated cells were counted and assessed for cell morphology. Sputum samples were adequate for further analysis if there were <40% squamous epithelial cells, indicating samples were from the lower airway.

2.2.9 Collection and Preparation of Serum Samples

Whole blood was obtained from participants by venepuncture and collected into 3mL tubes containing sodium citrate (Coagulation 9 NC/3mL tubes, Sarstedt monovette, Sarstedt AG and Co., Germany) to prevent clotting, then gently inverted. Samples were centrifuged at 350g for 20 min at 20°C. Platelet-rich plasma (PRP) was aspirated and transferred to a glass vial, to which 1M $CaCl_2$ was added (22µL per 1mL PRP). The vial was gently inverted then incubated in a 37°C waterbath for one hour. Resultant autologous re-calcified "serum" was aliquoted and stored at -80°C until analysis.

2.2.10 Sputum Supernatant and Serum Analysis by Enzyme-linked Immunosorbent Assays (ELISAs)

PBS containing 1% BSA (i.e.1g in 100mL (Sigma)) was used to dilute sputum samples for all ELISA experiments, unless otherwise stated. All samples were plated in duplicate. The sputum cytokines measured were IL-8, IL-6 and TNF-α. The optimal dilution of samples was elucidated for each analyte in a series of preliminary experiments. Details of dilutions and ELISA kit sources can be found in Table 2.2.1.

Sputum Constituent	ELISA Kit	HC Sputum Dilution	CF Sputum Dilution
IL-6	Human IL-6 ELISA Max™ Deluxe Kit, BioLegend®, UK	1:5	1:5
IL-8	Human IL-8 DuoSet, R&D Systems	1:10	1:100
TNF-α	Human TNF-α DuoSet, R&D Systems	1:5	1:5
Calprotectin	Human Calprotectin, Hycult Biotech	1:5000	1:25000 – 1:50000
NETs	Cell Death Detection ELISA (Roche) and Human Calprotectin ELISA (Hycult Biotech)	1:10	1:10

Table 2.2.1: ELISA kits used for sputum ELISAs *and dilution of sputum samples in PBS with 1% BSA.*

ELISAs were performed according to the manufacturers' protocols, summarised below for R&D Systems DuoSet. Plates (96-well EIA/RIA plate (Corning™ Costar™, NY, USA)) were coated with 100 µL capture antibody (Ab) per well that was diluted in DPBS without carrier protein and incubated at room temperature overnight. All antibodies and cytokine standards were prepared in reagent diluent (RD, i.e. PBS with BSA at 1g per 100mL). Wells were then washed 3x with 0.05% Tween-20 in PBS then blocked with 300 µL per well of RD at room temperature for one hour. After washing 3x, 100 µL sample and standards were added per well. Serial two-fold dilutions of cytokine standards were prepared to yield a standard curve to determine cytokine concentrations in unknown samples. Plates containing samples and standards were incubated at room temperature for two hours. Plates were washed 3x then 100 µL per well of the biotinylated detection Ab was added per well and incubated at room temperature for two hours. The plates were washed 3x before addition of 100 µL 1:40 Streptavidin-horseradish peroxidase (S-HRP) at room temperature in the dark for 20 min. Plates were washed 3x and then 100 µL of substrate solution (1:1 ratio of colour reagents A and B) was added per well and incubated at room temperature in the dark for 20 min. The reaction as stopped by adding 50 µL per well of Stop solution. Absorbance was read at 450 nm – 630 nm using a BioTek Synergy™ HT plate reader (BioTek Instruments Inc., VT, USA). Data were analysed using software available at elisaanalysis.com.

2.2.11 Sputum NET ELISA

An in-house, double-sandwich ELISA was developed to measure histone-bound calprotectin, as an estimate of NET formation. This ELISA is illustrated in Figure 2.2.1.

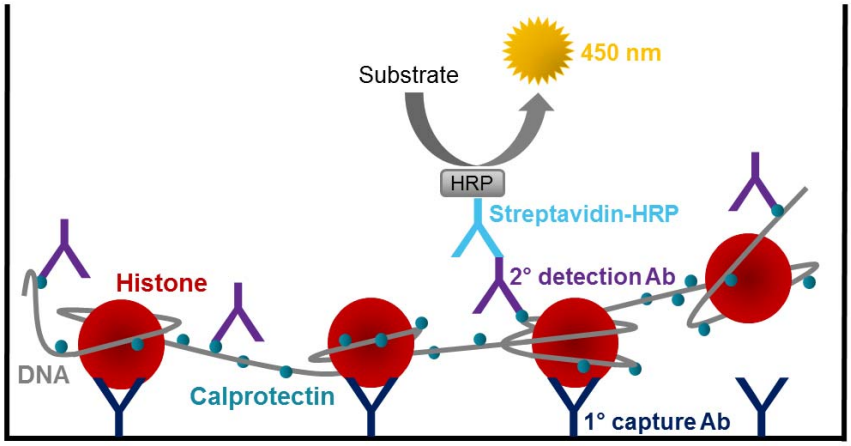

Figure 2.2.1: A schematic of the in-house NET ELISA *in which the primary antibody captures histones, ensuring eukaryotic DNA is specifically targeted and the secondary antibody binds calprotectin. The ELISA therefore specifically measures calprotectin associated with DNA as an estimate of the presence of NETs.*

The in-house NET ELISA used antibodies from two different ELISA kits, the anti-histone capture antibody from the Cell Death Detection ELISA (Roche) and S100A9/calprotectin detection antibody from Hycult Biotech. A modified

protocol was developed based on the respective protocols from each manufacturer. Briefly, the primary anti-histone Ab was diluted 1:10 using the kit's coating buffer, then added to the plate at 100µL/well. The plates were sealed then incubated in a fridge overnight. The following day, the anti-histone Ab was removed from plate by inversion and tapping then the plates were blocked with incubation buffer at 200µL/well for one hour. The plates were then washed three times. Sputum samples were diluted 1:10 with incubation buffer then 100 µL/well added and incubated at room temperature for 90 min. At this point, the Hycult Biotech's kit was used. The reconstituted S100A9/calprotectin detection Ab was diluted 1:12. The plates were washed four times, after which diluted detection antibody at 100 µL/well was added to the plates, incubated at room temperature for one hour. Plates were then washed four times after which S-HRP (diluted 1:200) was added to the plates at 100 µL/well. The plates were incubated at room temperature for one hour, after which plates were washed four times. TMB 100 µL/well was added to the plates, which were incubated under aluminium foil for 30 min. Finally, 100 µL/well Stop solution was added before the plates were read on 450 nm – 630 nm on the digital kinetic plate reader as before. Although it was not possible to generate a standard curve to quantify NET formation directly, fluorescence optical density (OD) (excitation 450 nm, emission 630 nm) was measured then fold-change in OD from mean HC values calculated.

2.2.12 Sputum and Serum Calprotectin ELISA

See Table 2.2.1 for sputum dilutions. HC serum samples diluted 1:200 whilst CF serum samples diluted 1:10000 for the Calprotectin ELISA, performed using the Human Calprotectin ELISA kit (Hycult Biotech), performed following manufacturer's instructions and absorption measured at 450 nm.

2.2.13 Sputum MPO Assay

All assays were performed in duplicate in flat-bottomed, 96-well EIA/RIA plates (Corning™ Costar™, NY, USA). Sputum samples were combined with 0.3 mM H_2O_2 (Sigma) and 1X TMB solution (Thermo Fisher Scientific). Plates were incubated at 37°C, 5% CO_2 for 5 min. The reaction was stopped by adding Stop solution and absorption was measured at 450 nm to estimate MPO activity.

2.2.14 Sputum Human Neutrophil Elastase Assay

Human Neutrophil Elastase (HNE) was measured using a NE Assay Kit (Cayman Chemical, MI, USA) following manufacturer's instructions. Briefly, the cell-based assay buffer (AB) was diluted: one tablet in 100 mL dH_2O. Two-fold dilutions of the HNE assay reagent were prepared in diluted AB to determine HNE using a standard curve. Sputum samples were diluted - 1:10 for HC sputum and 1:1000 for CF sputum - in AB then 100 µL per well of

samples and HNE standards (range 0 – 10 u/mL) were added to flat-bottomed, 96-well, black-sided plates (Thermo Fisher Scientific) in duplicate. 10 µL per well of the (Z-Ala-Ala-Ala-Ala)2Rh110 substrate solution was added then plates were incubated in the dark at 37°C, 5% CO_2 for 1.5 hours. Fluorescence (excitation 485 nm/emission 525 nm) was recorded and data analysed using software available at elisaanalysis.com for standard curve acquisition and corrected fluorescence calculation. The HNE activity was then calculated using the formula:

$$\text{HNE (mU/mL)} = \left(\frac{Fluorescence - (y - intercept)}{Slope}\right) x10$$

2.2.15 Sputum PicoGreen® Assay

The Quant-iT™ PicoGreen® dsDNA Reagent Kit (Thermo Fisher Scientific) was used to quantify dsDNA in sputum samples according to the manufacturer's protocol. Briefly, 1X TE assay buffer was prepared by diluting the concentrated buffer 20-fold in sterile, distilled DNase-free water. 100 µL Quant-iT™ PicoGreen® dsDNA reagent was added to 19.9mL assay buffer in a polypropylene tube then protected from light using aluminium foil. Double-stranded DNA standard curves were made ranging 25 pg/mL - 1µg/mL by dilution of calf thymus DNA (Thermo Fisher Scientific) in AB. In the wells of flat-bottomed, 96-well black-sided plates, 150 µL of DNA standards/samples

and 150 µL diluted Quant-iT™ PicoGreen® dsDNA reagent were mixed. The plates were incubated at room temperature in the dark for five min then fluorescence at 480 excitation/520 emission was measured. Standard curves were made then sample fluorescence readings multiplied by the line formulae to obtain DNA concentrations.

2.3 Cell Isolation and Co-culture

2.3.1 Isolation of PMN and PBMC from whole blood

Blood collected by venepuncture from HC and CF participants was anti-coagulated with 0.38% sodium citrate and centrifuged at 350g for 20 min to separate PRP and cells. Autologous re-calcified serum was generated as described in section 2.2.9. Erythrocytes were separated from leucocytes by differential sedimentation in 0.9% sodium chloride (NaCl) containing 0.72% Dextran-500 for 30 min at 37°C. Thereafter, the leucocyte-rich upper layer was aspirated and diluted in 0.9% NaCl then centrifuged at 350g for 6 min to pellet the leucocytes. PMN and PBMC were separated by discontinuous Percoll® (81%, 70% and 55%) gradient, centrifuged at 720g for 20 min (acceleration 1, deceleration 0). PBMC were removed from the 55%/70% interface and the PMN removed from the 70%/81% interface. Isolated cells were washed twice in DPBS, within which they were subsequently re-suspended to permit a cell count performed using a C-chip haemocytometer (NanoEnTek, SK).

2.3.2 Culture of Monocyte-derived Macrophages from adherent Monocytes

Monocytes were isolated from PBMC using a negative selection pan-monocyte isolation kit (Miltenyi Biotec Ltd., UK) according to the manufacturer's protocol. In brief, PBMC were re-suspended in MACS buffer (see Table 2.1.1) (40 µL per 10^7 cells) and FcR were blocked (10 µL of FcR Blocking Reagent per 10^7 cells). Cells were incubated with Biotin-Antibody cocktail (10µL per 10^7 cells) on ice for 5 min prior to adding MACS buffer (30 µL per 10^7 cells) and Anti-Biotin MicroBeads (20 µL per 10^7 cells) and incubation on ice for 10 min. A washed (3 mL of MACS buffer) LS column (Miltenyi Biotec Ltd., UK) was mounted in the magnetic field of a MidiMACS™ Separator (Miltenyi Biotec Ltd., UK) and the cell suspension was then applied, collecting the flow-through and 3 x 3mL washes of enriched monocytes in a polypropylene tube. Monocytes were centrifuged at 300g for 5 min at 20°C, re-suspended in DPBS and counted using a C-chip haemocytometer. The cell suspension was centrifuged as before and finally re-suspended in IMDM supplemented with 2mM L-Glutamine and 25 mM HEPES, 10% Autologous Serum, 1% Penicillin/Streptomycin (i.e. 10,000 U/mL of penicillin and 10,000 µg/mL streptomycin) and plated at $2.5x10^5$ per well in 48-well plates (Corning™ Costar™, Life Sciences, UK). Adherent monocytes were cultured at 37°C, 5% CO_2 for seven days to generate MDM, with media changes on days one and five.

2.3.3 NET formation from Neutrophils in Rolling Culture with PMA

Isolated neutrophils were re-suspended in HBSS to $1x10^6$/mL in a 15 mL BD Falcon tube. Neutrophils were stimulated with 100 nM PMA (Sigma) or HBSS-only control for 15 min at room temperature on a rolling platform set at 35 rotations/minute (Scientific Laboratory Supplies Lab Basics Hexiroll, UK). Neutrophils treated with PMA were deemed “NETs”, whilst non-PMA-treated neutrophils represented “control” neutrophils. *In vitro* experiments described in section 2.3.5 were employed to elucidate that PMA and DNase were the most efficient stimulator and inhibitor of NETosis, respectively.

2.3.4 Cytocentrifuge Preparations of blood cells

As per section 2.2.8. Samples with ≥ 95% PMN were deemed satisfactory for use in neutrophil assays. Cytocentrifuge preparation analysis was used to confirm that the negative isolation technique had effectively isolated monocytes from PBMCs. See Figures 2.3.1 and 2.3.2 for representative images of cytocentrifuge preparations.

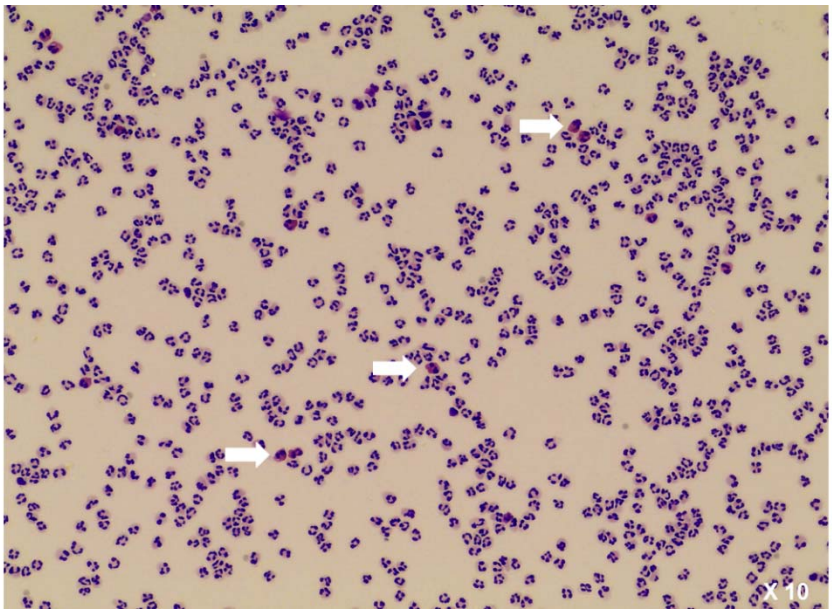

Figure 2.3.1: Cytocentrifuge preparation of polymorphonuclear leukocytes *following isolation from whole blood using dextran sedimentation and Percoll® gradient centrifugation. Contaminating eosinophils highlighted (white arrows).*

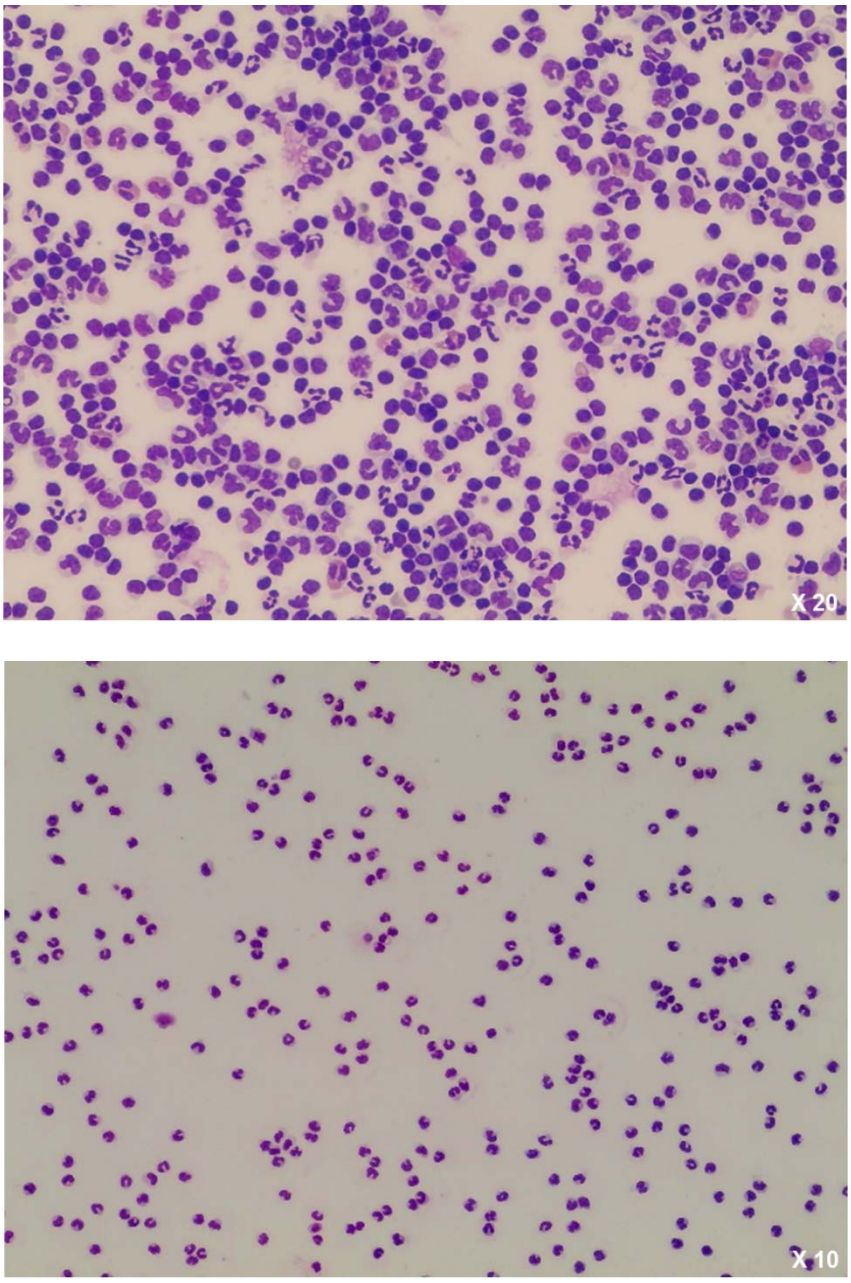

Figure 2.3.2: Cytocentrifuge preparation of peripheral blood mononuclear cells (top) and monocytes (bottom) following negative magnetic isolation *using Miltenyi Biotech Pan-Monocyte Isolation Kit (Human). Top image at 20X, bottom image at 10X magnification.*

2.3.5 *In Vitro* NET Formation and Inhibition

Preliminary experiments were performed prior to the co-culture experiment to optimise *in vitro* NET formation and inhibition. Two techniques were performed – microscopic detection of NETs and NET DNA release kinetic assay – based on published methodology (61,70,171). Immunofluorescence was also used to provide detailed images of the morphological appearances of NETs.

2.3.6 Microscopic Detection of NETS

Following isolation of PMN, neutrophils were plated at $5x10^4$ per well in RPMI supplemented with 10% FCS, 1% L-Glutamine (Gibco, UK), 1% Penicillin/Streptomycin into 24-well flat-bottomed plates (Corning™ Costar™, Life Sciences, UK) in duplicate. PMA was added at 10 nM, 50 nM and 100 nM whilst ionomycin was added at 1 μM, 5 μM and 10 μM, to allow fine-tuning of optimal concentration. Adherent neutrophils were incubated for four hours at 37°C, 5% CO_2 to permit NET formation prior to addition of 0.15 μM SYTOX® green (Invitrogen, Thermo Fisher Scientific). Plates were then imaged using bright field and fluorescent (470/22 nm excitation; 510/42 nm emission) microscopy using an EVOS™ FL cell imaging system (Thermo Fisher Scientific). Images were saved as TIF files and NET formation was quantified as a percentage of total cells by counting a minimum of 300 cells from a minimum of two 10X fields-of-view from duplicate wells using a cell counter function of ImageJ software, then averages calculated(61). Neutrophils were

classified as NETed if they had diffuse or spreading characteristics (see Figure 3.20). In some experiments, cells were incubated with 2 μM DPI, 1 μM Ro-31-8220 or 100U/mL DNase (see Table 2.1.2) to inhibit NET formation.

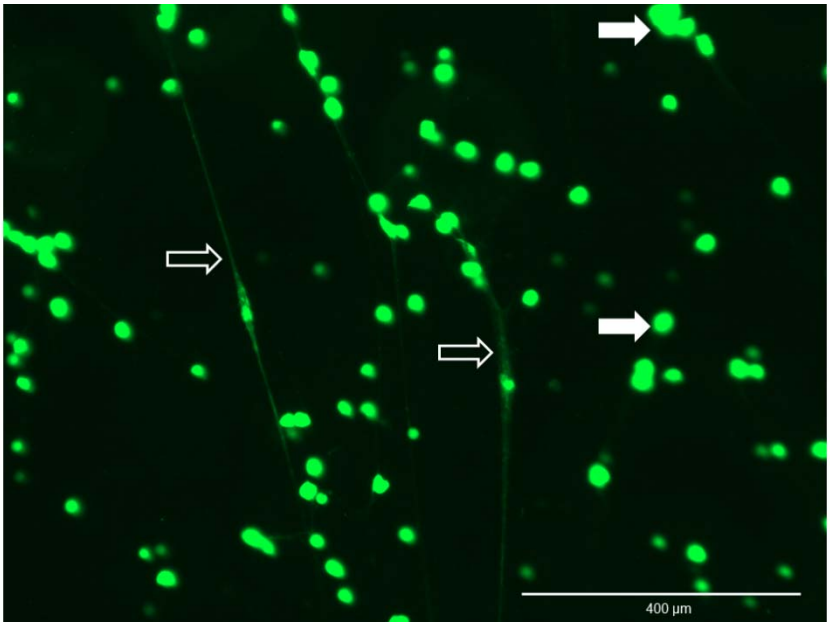

Figure 2.3.3: Fluorescence microscopy image of NETs* in vitro *stained with SYTOX® Green. *"Diffuse" NETs, which have a characteristic fluffy outline, are shown by solid white arrows. "Spreading" NETs, with strands of DNA seen to be spreading between individual cells, are shown by clear white arrows.*

2.3.7 Immunocytochemistry of NETs

Immunofluorescence was used to obtain detailed images of *in vitro* NETs. Isolated neutrophils were re-suspended $1x10^6$/mL in RPMI and seeded onto sterile, glass coverslips placed in flat-bottomed 12-well plates. Neutrophils were incubated for 30 min at 37°C, 5% CO_2 to allow cells to adhere to the coverslips. Cells were then incubated with 100 nM PMA for four hours to permit NET formation. Thereafter, the RPMI was gently aspirated and replaced with 1mL 2% paraformaldehyde (PFA) overnight at 4-8˚C to fix cells. After aspiration of PFA, cells were permeabilised using 1% Triton™-X-100 (Thermo Fisher Scientific). Cells were washed 3x with DPBS then blocked with 3% BSA in DPBS for 30 min at room temperature. The blocking solution was aspirated then cells were stained with primary rabbit anti-human MPO (Abcam, 1:200) for one hour. Cells were washed 3x with DPBS then incubated with the fluorochrome-tagged secondary antibody (goat anti- rabbit IgG Cy2® (Abcam, 1: 300) for one hour at room temperature under aluminium foil. Hoechst (Invitrogen™, Thermo Fisher Scientific, 1:10000 dilution) was used for DNA counterstaining. All antibodies/Hoechst were diluted in DPBS. Cells were washed 3x in DPBS then ProLong™ Diamond Antifade Mountant (Thermo Fisher Scientific) was used to mount coverslips onto microscope slides. Slides were imaged on the EVOS™ FL cell imaging system (470/22 nm excitation; 510/42 nm emission).

2.3.8 NET DNA release Kinetic Assay

Following isolation of PMN, neutrophils were plated at $5x10^4$ per well in RPMI into 96-well flat-bottomed plates (Corning™ Costar™, Life Sciences) in triplicate. NET formation was induced by addition of PMA added at 10 nM, 50 nM and 100 nM or ionomycin added at 1 μM, 5 μM and 10 then 0.15 μM SYTOX® green was added. The plate was inserted into a digital kinetic plate reader (BioTek® Synergy™ HT) with the set up: excitation 485/20 nm, emission 530/25 nm, bottom optics, sensitivity 35 and 50 nm, and temperature 37°C. Measurements were taken at 30 min intervals for six hours. Data were exported to Microsoft Excel and averages of each time point calculated to permit dose-response curve formulation. In some experiments, cells were incubated with 2 μM Diphenyleneiodonium chloride (DPI), 1 μM Ro-31-8220 or 100U/mL DNase (see Table 2.1.2) to inhibit NET formation.

2.3.9 Co-culture between MDM and NETed/control Neutrophils

A co-culture experiment was performed between MDM and neutrophils – either control or NETing – from different participants. There were four combinations of cells in the co-culture experiment, as shown in Figure 2.3.4:

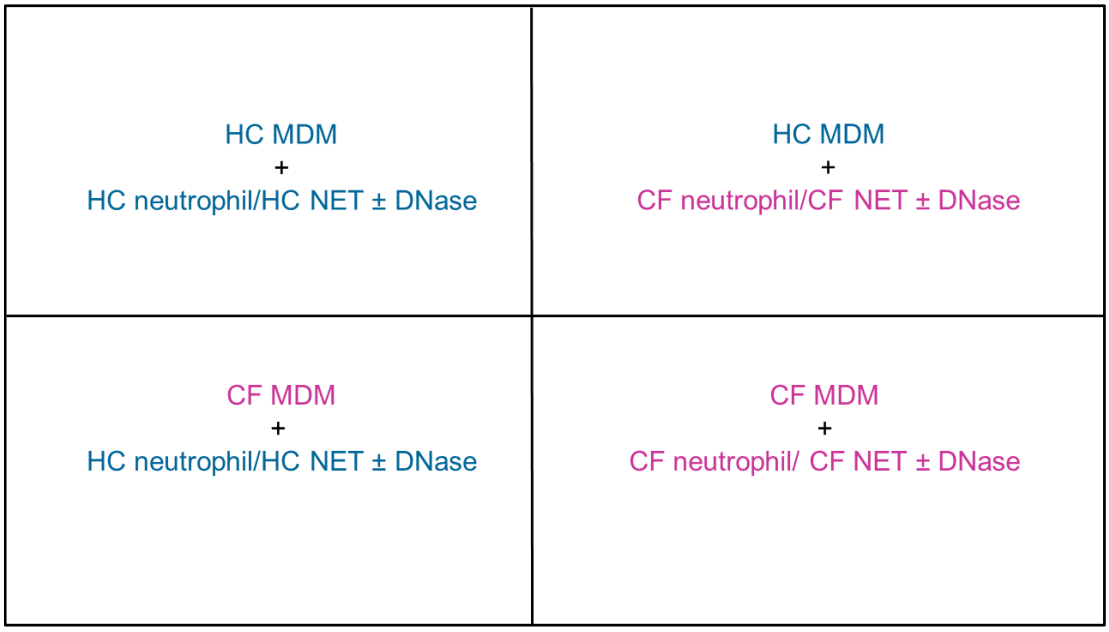

***Figure 2.3.4: Schematic of co-culture experiment**, illustrating the four combinations of cells. Neutrophils were either control or NETing ("NETs") and in some experiments in which NETs were present, DNase was added to determine if it affected parameters measured.*

On day seven of MDM culture (section 2.3.2), whole blood was obtained from a different participant (either HC or CF) then PMN were isolated and half were made to NET, as described in section 2.3.3. Neutrophils were then washed 3x in HBSS to remove any residual PMA before seeding $5x10^5$/well onto MDM (2:1 neutrophil to MDM ratio)(70) in 500 µL IMDM supplemented with 2mM L-Glutamine and 25 mM HEPES, 5% foetal calf serum (FCS) (Gibco, UK) and 1% Penicillin/Streptomycin. Plates were incubated at 37°C, 5% CO_2 for 24 hours. Negative control wells were also plated – a co-culture between MDM and NETs with the addition of 100U/mL DNase (Roche, UK) - to inhibit NET formation.

2.3.10 Co-culture Supernatant Harvest and ELISAs

Cells were co-cultured for 24 hours, after which supernatants were collected, centrifuged at 300g for 5 min at 20°C to remove cell debris, and then frozen at -80°C. Following collection of all samples, quantification of the cytokines IL-6, IL-8, TNF-α and IL-10 in the co-culture supernatants was carried out using commercially available ELISAs (R&D Systems, UK) as per section 2.2.10 with supernatants diluted as per Table 2.3.1.

Co-culture Supernatant Cytokine	ELISA Kit	Supernatant Dilution
IL-6	Human IL-6 DuoSet, R&D Systems	neat
IL-8	Human IL-8 DuoSet, R&D Systems	1:50
TNF-α	Human TNF-α DuoSet, R&D Systems	1:5
IL-10	Human IL-10 DuoSet, R&D Systems	neat

Table 2.3.1: ELISA kits used for co-culture supernatant ELISAs *and dilution of samples in PBS with 1% BSA.*

2.3.11 Scanning Electron Microscopy of Co-Culture Experiment

Scanning electron microscopy was performed to provide detailed microscopic evaluation of the morphological features of co-cultured cells. The experiments

were performed as described in section 2.3.9 but before monocyte adherence, Nunc™ Thermanox™ Coverslips (Thermo Fisher Scientific) were placed in the wells, onto which monocytes then adhered. After the seven days culture to permit differentiation of monocytes to MDM and subsequent 24 hours' MDM/NET or control neutrophil co-culture, cell samples were fixed in a solution of 3% glutaraldehyde (Sigma) in 0.1 M sodium cacodylate (CAC) buffer (pH 7.3) for two hours. They were then washed in 3x 10 min changes of 0.1 M CAC. Samples were then transported to Steven Mitchell at the King's Buildings, The University of Edinburgh, who performed the remainder of the steps in the protocol. Briefly, samples were post-fixed in 1% osmium tetroxide in 0.1 M CAC for 45 min then washed three times as before. Dehydration in graded concentrations of acetone (50%, 70%, 90% and 3 x 100%) for 10 min each was followed by critical point drying using liquid carbon dioxide. Samples were mounted on aluminium stubs with carbon tabs attached, then sputter-coated with 20 nm gold palladium, viewed and imaged using a Hitachi S-4700 scanning electron microscope with assistance from Steven Mitchell. Images were false-coloured using GNU Image Manipulation Program (GIMP) Version 2.8 software.

2.4 Cystic Fibrosis Mouse Model of Acute, Sterile Lung Inflammation

2.4.1 Use of Animals and Animal Facilities

All experiments were approved under a Project License (license number 70-8884) granted by the Home Office (UK) and conducted in accordance with local ethics approval from the Veterinary Scientific Services of The University of Edinburgh.

2.4.2 Strains of Animals Used

C57/BL6 littermate mice (Charles River Laboratories Ltd., UK) were used for the preliminary DPBS/LPS time course experiment.

The LPS and DNase nebulisation experiments were carried out using *Cftr*^{tm1Unc}Tg(FABPCFTR)1Jaw/J mice (Charles River Laboratories Ltd., UK) (referred to as CFTR$^{-/-}$ mice henceforth), which have been described previously(172). See Chapter 4 for a description of the genotype. CFTR$^{-/-}$ mice were bred with C57BL/6 mice to create a mixed background under specific pathogen-free conditions at the University of Edinburgh Animal Facilities. *CFTR*$^{-/-}$ mice were genotyped using qPCR by Lauren Melrose (see Appendix 1). The DNase activity assay experiments were carried out using CFTR$^{-/+}$ mice.

Mice had free access to chow and water. Mice were age- and sex-matched within experiments and used at 9-16 weeks of age. WT and heterozygote mice were from the same mixed background as the *CFTR*$^{-/-}$ mice because they were littermate controls. Experiments were designed to use the minimum number of animals possible, whilst attaining statistically meaningful results.

2.4.3 *In vivo* manipulations

Administration of PBS

Where indicated, mice received 3mL oxygen-driven nebulised DPBS on day zero.

Administration of LPS

Where indicated, mice received 3 mL oxygen-driven nebulised LPS 1mg/mL in DPBS (*P. aeruginosa 10,* Sigma) on day zero.

Administration of DNase

Where indicated, mice received oxygen-driven nebulised DNase (Pulmozyme®) 2500U in 2.5 mL (Roche, UK) at 12, 36 and 60 h post-LPS.

Administration of Euthatal

All mice were culled by intraperitoneal (i.p.) injection of 300 µL Euthatal (Pentobarbital Sodium, Henry Schein, UK).

2.4.4 Time course experiment to determine Peak and Resolution of Inflammation post-LPS Lung Injury

A nebuliser system was developed with local expertise (Figure 2.4.1).

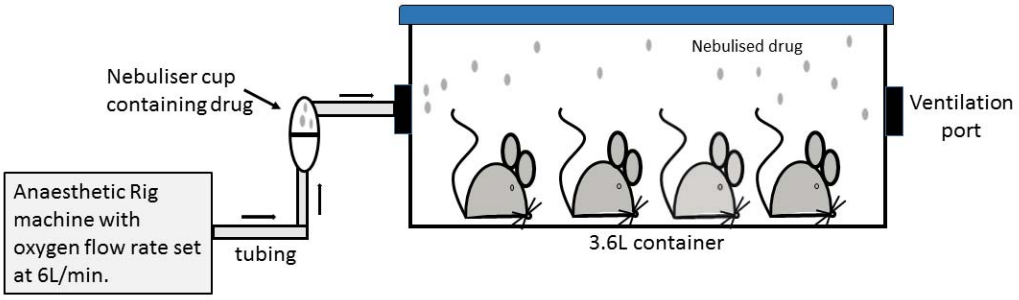

Figure 2.4.1: Mouse nebuliser system. *For all the animal experiments, compounds were administered to the mice via nebulisation using a sealed system in a fume hood – one sealed system per compound. Upon completion of nebulisation, animals were placed in standard cages – separated depending upon whether they received LPS only or LPS and DNase.*

With regard to the time course experiment, there were 48 female, 10-week old C57BL/6 mice. Half of the group received nebulised control DPBS whilst the other half received nebulised LPS (see Figure 2.4.1) on day zero. Groups were culled at 0, 24, 48 and 72 h by overdose of i.p. Euthatal. Mice were observed each day to ensure well-being using an established scoring system.

No mice became unwell to warrant euthanasia throughout any of the experiments.

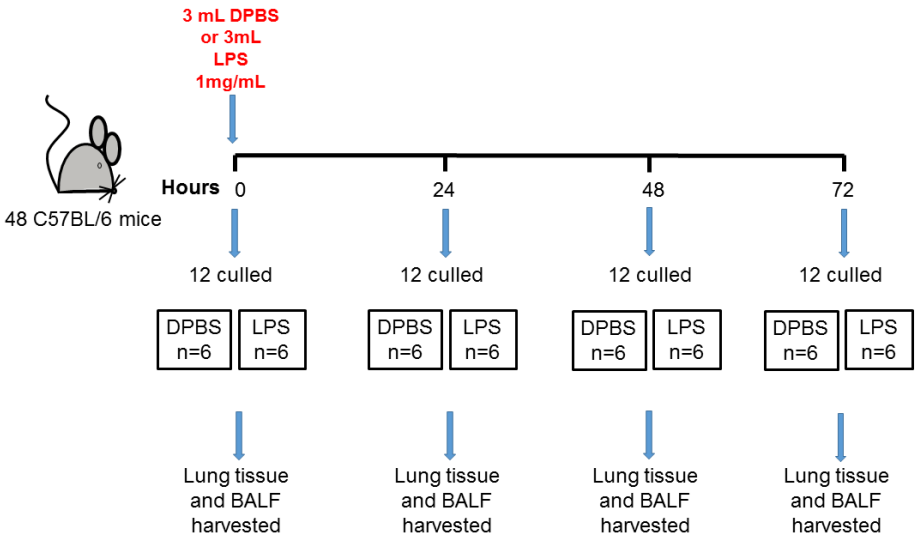

Figure 2.4.2: Overview of the mouse time course experiment *to determine the time of peak and subsequent resolution of inflammation following LPS-mediated lung injury. There were 48 C57BL/6 mice, half of which received 3mL DPBS, the other half received 1mg/mL LPS (P.aeruginosa 10 (Sigma)). Groups were culled at 0, 24, 48, and 72 hours and bronchoalveolar lavage and lung tissue harvest was subsequently performed. Samples frozen at -80°C for later analysis.*

2.4.5 Bronchoalveolar Lavage and Excision of Lung Tissue

Following i.p. Euthatal, death was confirmed by exsanguination: the axillary artery was severed by an incision at the axilla. Following an incision across

the abdominal wall and thoracic area, the diaphragm was dissected and anterior chest wall removed to gain access to the thoracic cavity. An elasticated string was tied around the left hilum then a left pneumonectomy was performed. Half of the tissue was placed in 250 µL RNAlater (Qiagen, Netherlands) for RNA extraction (for 24 hours, then RNAlater was removed and lungs were frozen at -80°C) and half was snap frozen on dry ice. Thereafter, the trachea was exposed by dissection through the anterior neck tissues then cannulated with Jelco® IV catheter Radiopaque (Smith Medical International Ltd, UK). This permitted bronchoalveolar lavage (BAL) of the right lung using HBSS supplemented with 3 mM Ethylenediaminetetraacetic acid (EDTA), which functioned to preserve cell morphology. An initial 500 µL was lavaged, providing a cytokine-rich sample used for later assays to measure cytokines. A further 1.5 mL was lavaged, which was for cytocentrifuge preparation.

Resultant BAL fluid (BALF) was stored on ice until centrifugation at 350g for 5 min at 4°C, and then supernatant from the cytokine-rich samples were aspirated and frozen at -80°C until analysis. BALF cell pellets from both the cytokine-rich lavage and cytocentrifuge preparation samples were re-suspended in DPBS and combined. Cells were counted using NucleoCounter® NC-200™ (Chemometec, USA), centrifuged as before then re-suspended at $1x10^6$/mL for cytocentrifuge preparation, as per section 2.2.8.

2.4.6 Lung Excision for Histological Examination

Some animals from each group were reserved for histological examination of lung tissue. In such cases, the right lung was not lavaged with HBSS; rather it was lavaged with 10% NBF, the trachea tied off with elasticated string, then the lung was dissected and placed in a sterile universal container containing 10% NBF for 24 hours. After this, the 10% NBF was replaced with 70% ethanol. These samples were paraffin-embedded, sectioned in the coronal plane and stained with Haematoxylin and Eosin (H&E) by the Histology Department of the Shared University Research Facilities (SuRF) at the Centre for Inflammation Research, Edinburgh.

2.4.7 Light Microscopy of BALF Cytocentrifuge Preparations for Differential Cell Counts

As per section 2.2.8.

2.4.8 Determination of Peak and Resolution of Inflammation post-LPS

In order to determine when peak and resolution of inflammation occurred following LPS administration, two parameters were used. Firstly, BALF differential cell counts were analysed and secondly, an IL-6 ELISA was carried out using the DuoSet ELISA Mouse IL-6 (R&D Systems). BALF supernatants

were diluted 1:5 in PBS with 1% BSA and ELISA methodology is described in section 2.2.10.

2.4.9 LPS-mediated Acute Lung Inflammation experiments

The time course experiment established that peak inflammation occurred 24 hours' post-LPS administration and resolution had occurred within 72 hours (Chapter 4, section 4.1). The experiment modelling acute lung inflammation in $CFTR^{-/-}$ and WT littermate mice was therefore conducted with culls at 24 and 72 hours post-LPS administration (see Figure 2.4.3). Mice were nebulised with 3 mL 1mg/mL LPS, then half the group received nebulised Pulmozyme® 12 hours post-LPS administration in a separate sealed system. All mice were culled and BALF and lung tissue harvested, as described in sections 2.4.5 and 2.4.6. The 24- and 72-hour time point experiments were performed over n=3 and n=4 separate experiments, respectively.

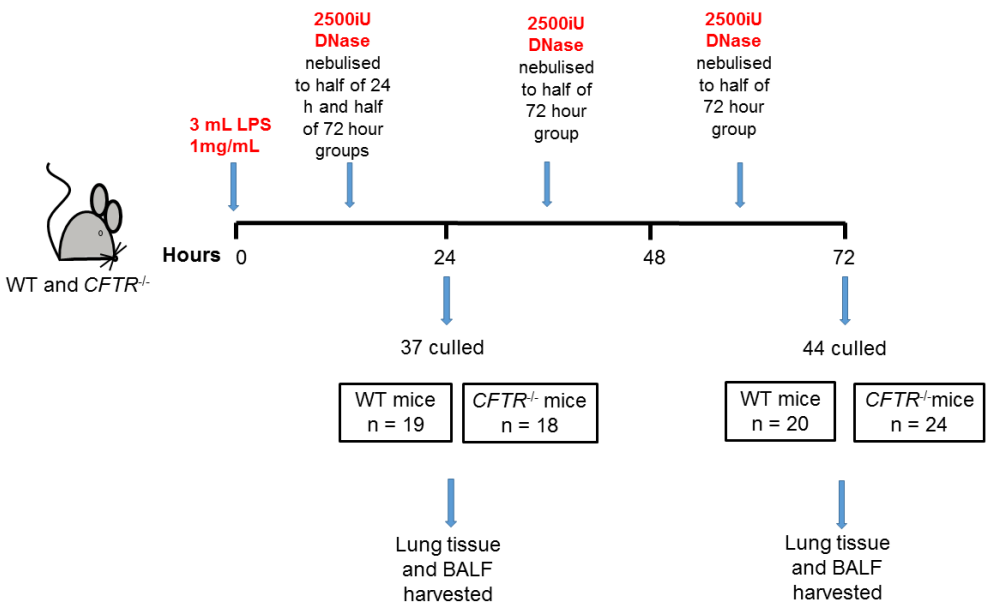

Figure 2.4.3: Overview of the mouse model of LPS-mediated acute lung inflammation. *CFTR$^{-/-}$ and WT littermate mice were received 3 mL 1mg/mL LPS (P. aeruginosa 10 (Sigma) in DPBS), then half the group received nebulised 2.5 mL 2500iU Pulmozyme® (Roche, UK) 12 hours' post-LPS administration in a separate sealed system. Thirty-seven animals were culled at the 24-hour time point (n=3 separate experiments). Forty-four animals were culled at the 72-hour time point (n=4 separate experiments) and these received 2.5 mL 2500iU Pulmozyme® treatment once daily.*

2.4.10 Cytokine U-PLEX® Biomarker Group 1 (Mouse) Assay

The commercially available U-PLEX® Biomarker Group 1 (Mouse) Assays (Meso Scale Diagnostics (MSD®), Maryland, USA) was used to measure the concentrations of 10 cytokines in murine BALF supernatant samples: IL-6, IL-10, IL-17A, IL-23, IL-1β, IFN-ɣ, KC, MCP-1, MIP-2 and TNF-α. This assay is

similar to an ELISA but biotinylated capture antibodies are coupled to U-PLEX Linkers, which self-assemble onto unique positions ("spots") on the U-PLEX plate, permitting up to ten cytokines to be quantified concomitantly in one assay. In the assay described here, there was cross-reactivity between some of the analytes and so the assay was performed over two U-PLEX plates, see Figure 2.4.4 according to the manufacturer's protocol.

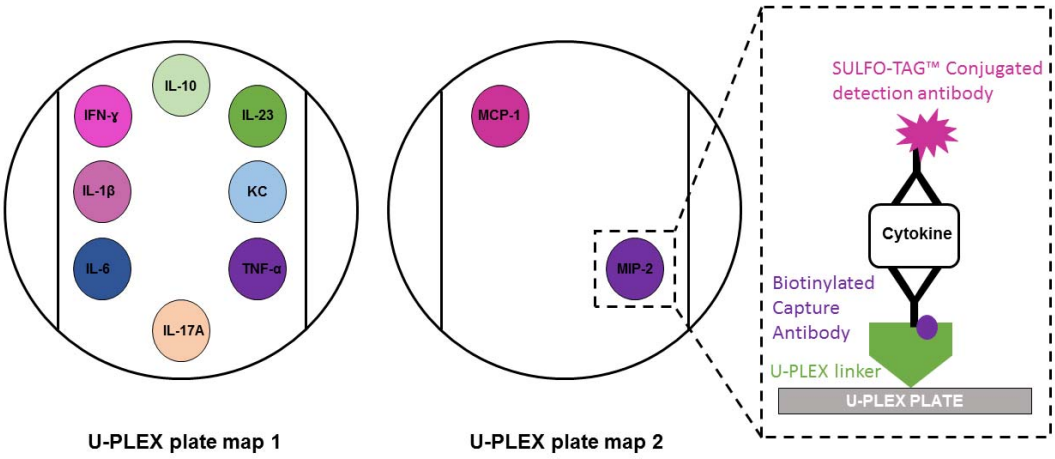

Figure 2.4.4: *U-PLEX immunoassay on U-PLEX 8-assay and 2-assay plates from Meso Scale Diagnostics (MSD®) was used to quantify proinflammatory cytokines in murine BALF. Quantification of numerous cytokines is possible in one assay because the biotinylated capture antibodies are coupled to U-PLEX linkers, which attach onto the designated positions on the U-PLEX plate. Figure adapted from page 5 of MSD® U-PLEX Platform U-PLEX® Biomarker Group 1 (Mouse) Multiplex Assays product insert (18164-v3-2016Nov) (https://www.mesoscale.com/en/products/u-plex-biomarker-group-1-mouse-assays-k15069l/).*

Briefly, 200 µL of each biotinylated capture antibody was coupled to 300 µL of a unique linker, identified on a spot map, and then incubated for 30 min at room temperature. The reaction was stopped by adding 200 µL Stop Solution, incubated for 30 min at room temperature. All of the U-PLEX®-coupled antibodies were combined – two solutions were made such that none of them shared the same linker – and the volume brought up to 6 mL with Stop Solution. The two black-sided 96-well plates were coated with 50 µL per well multiplex coating solution then incubated for one hour at room temperature on a plate shaker set at 500 rpm with a 1.5 mm stroke (Heidolph, Titramax 1000, Germany). Meanwhile, calibrator standard solutions were prepared from a 5X concentrated stock diluted five-fold to generate the highest point on the standard curve. BALF supernatants were diluted 1:2 in Diluent 41. The assay's detection antibodies are conjugated with electrochemiluminescent labels (MSD GOLD™ SULFO-TAG). These detection antibodies were diluted 1:100 with Diluent 45 and combined. Plates were washed 3x with wash buffer then incubated with samples and calibrators 25 µL per well for one hour at room temperature. The plates were washed 3x with 150 µL per well wash buffer after which 50 µL per well of detection antibody solution was added and incubated for one hour at room temperature on the plate shaker. Plates were washed 3x as above then 150 µL per well 2X Read Butter T was added before plates were analysed on a Mesoscale Quickplex sq120 instrument (MSD®). For details of analytes and calibrators, please see Appendix 2.

2.4.11 Quantification of Murine NETs by NET, Histone and S100A9 ELISAs

NET ELISAs were performed with BALF diluted 1:10 as described 2.2.11. The histone ELISA was performed using the Cell Death Detection ELISA (Roche) with BALF samples diluted 1:50. The S100A9 ELISA was performed using the Mouse S100A9 ELISA (Hycult Biotech) with BALF samples diluted 1:50. Manufacturer's protocols were followed in each case, with ELISA methodology described fully in section 2.2.10.

2.4.12 Pierce™ Bicinchoninic Acid (BCA) Assay

A protein analysis kit (Pierce™ Microplate BCA Protein Assay Kit, Thermo Fisher Scientific) was used to measure the total protein content of murine BALF. Two-fold dilutions of 2 mg/mL albumin standard was prepared in HBSS to determine protein concentration using a standard curve. BCA reagent was made by mixing BCA Reagent A with BCA Reagent B in a 1:1 ratio. Ten µL standard/sample and 200 µL of the BCA reagent was mixed in wells of a 96-well, round-bottomed plate (Corning™ Costar™) in duplicate and incubated at 37 °C for 30 min. Absorbance was read on the plate reader 450 nm – 630 nm using the BioTek Synergy™ HT plate reader.

2.4.13 Quantification of NETs by Immunohistochemistry on Murine Lung Tissue

De-paraffinisation and rehydration of paraffin-embedded murine lung sections was performed by moving them through the following wash steps:

Solutions	Number and Duration of Washes
Xylene	2 x 3 min
Xylene: 100% Ethanol at 1:1 ratio	2 x 3 min
100% Ethanol	2 x 3 min
95% Ethanol	1 x 3 min
70% Ethanol	1 x 3 min
50% Ethanol	1 x 3 min
Rinse in running tap water	Until antigen retrieval step

Antigen retrieval was then performed by heating slides to 110°C for 5 min in sodium citrate buffer (see Appendix 3) in a pressure cooker. Slides were then washed twice in DPBS and loaded onto a Sequenza® Slide Rack (Thermo Fisher Scientific) then 150 µL DPBS applied to each slide. Slides were blocked with 150 µL 25% goat serum in DPBS for one hour at room temperature. Primary antibodies were then applied and incubated at 37°C for one hour. Slides were washed twice in DPBS then secondary antibodies were applied and incubated at room temperature for one hour. Details of primary and secondary antibodies used can be found in Appendix 3. Slides were washed twice in DPBS then Hoechst (1:10000 dilution) was applied and incubated for

5 min at room temperature. Slides were lastly washed in tap water before being air-dried then ProLong™ Diamond Antifade Mountant (Thermo Fisher Scientific) was used to mount coverslips onto slides. Slides were covered in aluminium foil and left to dry for at least 24 hours. Confocal microscopy images were acquired using a Leica SP5 confocal laser scanning microscope with Leica Application Suite Software. Six images at 40X magnification were obtained per animal and images were saved as TIF files. These were analysed on ImageJ software by opening merged RBG channels and using the cell counter and grid functions. Cells positive for all three colours were counted first (i.e. suggestive of neutrophils due to morphology and the presence of DNA, MPO and S100A9) then cells positive for yellow pixilation were counted (i.e. suggestive of NETs due to co-localisation of S100A9 and MPO, see Introduction). The percentage of NETed neutrophils was subsequently calculated.

2.4.14 Murine Bronchoalveolar Lavage DNase Activity Assays

In order to confirm that the DNase being administered to the mice was active in its DNA-cleaving activity, two assays were used. The first was an *in vitro* DNA gel electrophoresis, in which the Pulmozyme® drug was mixed with calf thymus DNA. The second assay involved administering heterozygote mice ($CFTR^{-/+}$) with nebulised control DPBS or DNase, then immediately culling the animals and performing BAL, after which the Quant-iT™ PicoGreen® dsDNA Reagent Kit was used to quantify BALF dsDNA.

2.4.15 DNA Gel Electrophoresis using Pulmozyme® and Calf Thymus DNA

DNA was resolved using 1% agarose gels (containing GelRed® (Cambridge Bioscience, UK) at 1:10000 dilution) in 1X TAE buffer using a horizontal gel electrophoresis tank. Calf thymus DNA was diluted in DPBS to 1 µg/mL. This DNA was mixed in equal volumes with graded concentrations of Pulmozyme® (100%, 75%, 50%, 25% - diluted in DPBS), then incubated at 37°C, 5% CO_2 for 30 min to permit DNA digestion. A 6X DNA Loading Dye (Thermo Fisher Scientific) was added to each sample. The gel was then loaded with a 1kb Plus DNA ladder (Invitrogen, Thermo Fisher Scientific), a positive control well containing DNA at 1mg/mL, then samples. The gel was run at 70V for 70 min then imaged on Analytikjena UVP GelDoc-Ite Imaging System with VisionWorks® Software.

2.4.16 Murine Bronchoalveolar Lavage PicoGreen® Assay to quantify DNase activity

$CFTR^{-/+}$ mice received either nebulised 2.5mL DPBS or 2500iU Pulmozyme®, as per section 2.4.3. Animals were immediately culled then BAL performed as in section 2.4.5. BALF was stored on ice and transported immediately to the laboratory, where it was used in the Quant-iT™ PicoGreen® dsDNA Reagent Kit, being mixed with the PicoGreen® reagent with the assay performed as per section 2.2.15.

2.4.17 Semi-quantitative scoring of Acute Lung Inflammation on H&E stained lung sections

Two methodologies for assessment of acute inflammation following LPS administration were employed: a semi-quantitative score of lung histology and a quantitative translocator protein (TSPO) radiotracer assay. Taking the former method, following paraffin-embedding, sectioning and H&E staining, sections were imaged on the EVOS™ XL Core Imaging System: two images per animal were taken at 20X and 40X magnification (to permit mean calculations). Images were saved as TIF files then analysed on ImageJ software using the grid tool and cell counter function. Images were analysed using a semi-quantitative score of acute lung inflammation, modified from published, validated scores(173,174). The investigator was blinded to genotype and treatment group during analysis and parameters assessed were vascular congestion, thickness of the interalveolar septa (indicative of oedema), inflammatory cell infiltration, and haemorrhage (see Figure 2.4.5). The score is between zero and 16; zero suggested no inflammation whilst 16 indicated maximal acute inflammation.

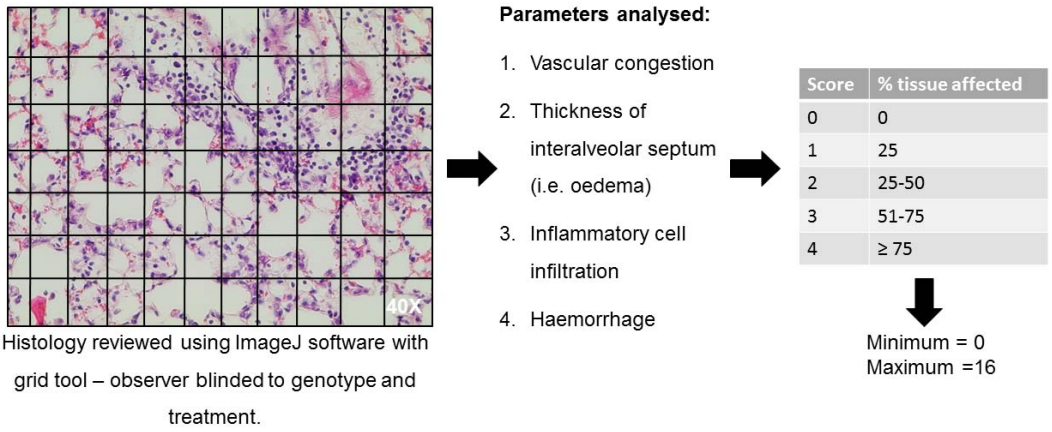

Figure 2.4.5: Semi-quantitative scoring *method employed for H&E stained sections of murine lung tissue to assess acute lung inflammation. Each animal had two sections analysed and mean scores were calculated based on the extent of any vascular congestion, oedema, inflammatory cell infiltration and haemorrhage.*

2.4.18 [3H]-PK11195 Autoradiography on 24 hour Murine Lung Sections

To provide a quantitative method for scoring lung inflammation, a [3H]-PK 11195 radiotracer, which binds TSPO (a protein demonstrating increased expression in immune cells during inflammatory responses(175) was used together with autoradiography. Performed in collaboration with Dr. Adriana Tavares of the Centre for Cardiovascular Science, University of Edinburgh.

For details of reagents used, please see Appendix 4. Two consecutive paraffin-embedded sections per animal were de-paraffinised and rehydrated as per section 2.4.13. Slides were pre-washed in 50mM Tris-Base buffer (pH 7.4) for 3x 5 min then incubated in 1.87nM [3H]-PK11195 for one hour at room temperature. The reaction was terminated by two 5 min washes in buffer and one immersion in dH_2O. Slides for non-specific binding were pre-washed as before then incubated in 1.87 nM [3H]-PK11195 and 10μM PK11195 for one hour at room temperature. The reaction terminated as before. Both the total and non-specific binding slides and ART0123A [3H]-microscales (American Radiolabelled Chemicals) were placed into the autoradiography cassettes, apposed to autoradiographic films (Fuji imaging plates), and incubated for five weeks. Films were exposed using a Fujifilm FLA-S100 phosphorimager with Image Reader FIA 5000 software. Images were saved as TIF files then analysed using ImageJ software. Calibration curves were generated from regions of interest (ROI) of standards of known tritium ([3H]) concentrations. ROI were then drawn around lung sections for both total binding and non-specific binding, then mean ROI pixel intensities were extracted. Non-specific binding was subtracted from total binding to obtain specific binding in nCi/mg and data was also expressed as % specific binding.

2.4.19 RT-PCR for Toll-like Receptors and Receptor for Advanced Glycation End Products (RAGE) on murine cDNA

Frozen lung sections were thawed, then homogenised in 600 µL TRIzol® (Life Technologies) in Precellys Lysing Kit tubes (CK28), shaken using the Precellys 24, Lysis and Homogenisation Machine (PeqLab, Bertin Technologies) for 1 x 20 s at 5000 rpm, then transferred to 1.5 mL Eppendorf tubes and centrifuged at 4000 rpm for 5 min to remove particulate debris.

The Direct-zol™ RNA MiniPrep kit (Zymo Research) was used to extract RNA. Supernatants were transferred to new tubes, to which ethanol was added, which functions to separate RNA. The samples were transferred into a Zymo-Spin™ IIC Column in a collection tube and centrifuged at 14000g for 30 sec. Flow-through was discarded then the column re-filled with remaining sample and centrifuged as before. Flow-through was once again discarded then a DNase I treatment was performed to guarantee removal of any contaminating genomic DNA: RNA wash buffer was added to the column, which was centrifuged as before, then DNase I and DNA digestion buffer were mixed in an RNase-free tube. This mix was added to each column and incubated at room temperature for 15 min. Samples were thoroughly washed by sequential centrifugation then columns were transferred to an RNase-free tube. To elute RNA, DNase/RNase-free water was added directly to the column matrix then centrifuged as before. The quantity and purity of RNA was analysed using a Nanodrop 100 spectrophotometer. Samples were stored at -80°C until use.

Complementary DNA (cDNA) was made using a Multiscribe™ cDNA/RT Kit (Applied Biosciences), details of the master mix and primers used are in Appendix 5. Samples were run on a C1000 Touch Thermal Cycler as follows:

- 25°C for 10 min;
- 42°C for 120 min;
- 85°C for 5 min;
- then 4°C until samples removed and samples stored at -20°C until use.

Gene expression was analysed using commercially available RT-PCR primer/probe assays (see Appendix 5) and PrimeTime® Gene Expression Master Mix 2X (Integrated DNA Technologies, Leuven). Samples were run in duplicate and the gene of interest expressed relative to expression of a house-keeping gene (β-actin). Negative controls included no RT and no cDNA. Assays were run on a StepOne™ machine with the cycling protocol as follows:

Step	Cycles	Temperature (°C)	Standard Cycling (min:sec)
Polymerase activation	1	95	3:0
Amplification:	35-45		
Denaturation		95	0:15
Annealing/Extension		60	1:0
Hold, if needed	1	4	Up to 24 hours

Data was analysed using SDS 2.0 software (Thermo Fisher Scientific).

2.4.20 Murine Lung Homogenisation for immunoblot lysates

Details of buffers used are in Appendix 7. The left lung segments snap frozen following the dissection in section 2.4.6 had been stored at -80°C. These samples were thawed then homogenised in Laemmli Buffer (see Appendix 7) using the Precellys Lysing Kit tubes (CD14), shaken using the Precellys 24, Lysis and Homogenisation Machine for 1 x 25 s at 5500 rpm, then centrifuged at 12000 g for 10 min at 4°C. Pierce® BCA Protein Assay Kit was used to quantify protein concentrations of resultant lysates, as described in section 2.4.12. Subsequent dilutions in Laemmli buffer and 2xSDS in a 1:1 ratio ensured all lysates had a protein concentration of 1 µg/µL. Lysates were then boiled at 95°C for 5 min then stored at -80°C until use.

2.4.21 Immunoblot for RAGE Protein Expression in Murine Lung Lysates

Murine lung lysates were analysed for RAGE protein expression by western blot. Details of the gels and buffers used are in Appendix 7. Proteins were separated by SDS-polyacrylamide gel electrophoresis using the BioRad mini-protean system (run at 70-150V until the dye front runs off the end of the gel) prior to electrophoretic transfer to polyvinylidene difluoride (PVDF) membranes (Merck Millipore), run at 100V for 90 min. Membranes were blocked with 5% skimmed milk powder in Tris-buffered saline and 0.05% Tween 20 (TBST) solution for a minimum of one hour. Membranes were incubated with primary antibodies (prepared in 5% skimmed milk in TBST) at 4°C overnight on a rolling

platform. Details of the primary antibodies are found in Appendix 7. Membranes were washed 3x in TBST for 10 min per wash. This was followed by incubation with anti-rabbit IgG horseradish peroxidase-conjugated secondary antibody (1:2000) (Dako) for one hour at room temperature on a rotating platform. Membranes washed 3x in TBST for 10 min per wash then developed in enhanced chemiluminescence (ECL) detection reagent as per manufacturer's instructions (ECL Select™ Western Blotting Detection Reagent, GE Healthcare, Buckinghamshire, UK). Chemiluminescence was assessed using the Odyssey® Fc Imaging System (LI-COR® Bio-sciences, NE, USA) and quantified using ImageStudioLite software. To allow semi-quantitative analysis of protein expression, membranes were stripped using Restore Western Blot stripping buffer (Thermo Fisher Scientific) for 15 min, washed in dH_2O and then re-probed for GAPDH as described above.

2.5 *Surface-enhanced Raman Spectroscopy-based Nanosensors Quantify Phagolysosomal pH in Healthy Control and Cystic Fibrosis Macrophages*

2.5.1 MDM Culture

For Raman spectroscopy experiments, PBMC were differentiated into MDM by plating at $1x10^6$/mL onto MgF_2 discs (Crystran, UK) in 12-well plates (Corning™ Costar™, Life Sciences, UK) in IMDM supplemented with 10% autologous serum, 1% Penicillin and Streptomycin, 1% L-glutamine and 25 mM HEPES at 37°C, 5% CO_2. Adherent monocytes were cultured for seven days with media changes on days one and five. For fluorescence spectroscopy experiments, PBMC were differentiated as above in six-well UpCell™ plates (Nunc™, SLS, UK). MDM differentiated in this manner have previously been shown to express CD14 and CD64, which are macrophage markers(176,177).

2.5.2 Optical nanosensor preparation and incubation with MDM

The Raman spectroscopy experiments were a collaborative study with Samuel J. Stanfield (studying for a PhD in Chemistry, supervised by Dr Colin J. Campbell of the Department of Chemistry, the University of Edinburgh) and myself.

Gold nanoparticles (~150nm diameter, Sigma, UK) were functionalised with *p*-MBA (termed MBA-NP) by S.J. Stanfield as previously described(178). On day seven of MDM culture, IMDM was removed and MBA-NP at $5x10^6$/mL in fresh IMDM were added (in a 5:1 ratio between MBA-NP and MDM) and incubated at 37ºC/5% CO_2 for one hour to permit phagocytosis of the MBA-NP by MDM. In some experiments, cells were treated with inhibitors as one-hour pre-treatments and throughout MBA-NP/Zymosan Bioparticles™' incubation with MDM.

2.5.3 Calibrating the pH response of MBA-NP

IMDM solutions with pH values ranging from 4.0 - 9.5 (increments of 0.5 pH units) were made by adding either sodium hydroxide or hydrochloric acid (0.1 M, aqueous) accordingly. The pH of these solutions were measured firstly using a Mettler-Toledo InLab Ultra-Micro-ISM pH electrode and secondly using our pH-responsive MBA-NP. For each pH, spectra from the MBA-NP were collected using the Renishaw inVia™ Raman microscope as described in the next section.

2.5.4 Measurement of phagolysosomal pH using Raman spectroscopy

Following incubation of MBA-NP with MDM, the MgF_2 discs, upon which MDM had adhered, were transferred to a petri dish containing IMDM pre-warmed to 37ºC. MDM were then imaged on the Renishaw inVia™ Raman microscope

using a 60X immersion objective (Olympus). To permit mean calculations, spectral acquisition was performed on MBA-NP within three individual MDM per sample and three spectra were collected from each of the MBA-NP. Spectral acquisition times were 30 sec with a laser power of 0.875 mW.

2.5.5 Acquisition of Raman Maps

Raman maps were also collected with a Renishaw streamline 785 nm laser at 0.0875 mW and a 30 sec acquisition time. Data were processed using WIRE™ 2.0, producing heat maps of Raman intensity based on the spectral peak at 1580cm^{-1}.

2.5.6 Raman Data Analysis using MATLAB® Software

Using MATLAB® software, the spectra were baseline corrected and normalised to a reference Raman-shift position (1580 cm^{-1}), the intensity of which was invariant to pH. The 1420 cm^{-1} peak intensity was used as the spectral metric for change in H^+ concentration, and its value was calculated and plotted against the pH of the IMDM solutions. The resultant scatter plot had a Boltzmann curve, the equation of which was:

$$y = A2 + \frac{A1-A2}{\left(1+e^{\frac{x-x_0}{dx}}\right)},$$

where y is pH, x is the intensity of the peak at 1420 cm^{-1}, and A1, A2, x_0, and dx are coefficients with values 0.003551, 0.224, 6.669 and 0.8053, respectively. The calibration curve $R^2 = 0.9895$ (see Chapter 5, section 5.4).

2.5.7 Temporal measurement of pH as the MBA-NP progresses through MDM Phagocytosis Compartments

In some experiments, single MBA-NP that looked to be adhered to the outside of an MDM (but not yet phagocytosed) on microscopy were imaged, as previously described, from 10 min to two hours' post-incubation with MDM at least every 5 min, to assess the acidification rate of the MDM phagocytosis compartments.

2.5.8 MDM MBA-NP phagocytosis quantification

To determine whether MBA-NP uptake differed between genotypes, light microscopy on the Renishaw inVia™ Raman microscope at X60 magnification was used to quantify the percentage of MDM performing MBA-NP phagocytosis, counting at least 100 consecutive cells from at least three fields-of-view and noting the presence of intracellular MBA-NP. Representative images were taken using a digital camera focussed down the eyepiece.

2.5.9 Quantification of Phagocytosis of pHrodo™ Green Zymosan Bioparticles™ by MDM

Fluorescent pHrodo™ Green Zymosan BioParticles® conjugates were re-suspended to 0.5 mg/mL in Live Cell imaging Solution (Thermo Fisher Scientific, UK) then sonicated for 5 min. MDM differentiated in UpCell™ 6 well plates, see section 2.3.2, were detached with cold DPBS supplemented with 0.5% BSA and 0.5 M EDTA and resuspended in IMDM at $1x10^6$/mL and 10^5 cells plated per well of a 96-well plate. After allowing the MDM to adhere for one hour (37ºC/5% CO_2), the culture medium was aspirated and replaced with BioParticles® suspension at 0.5mg/mL, incubated at 37ºC, 5% CO_2 for one hour. In some experiments, MDM were pre-treated with the inhibitors cytochalasin D or bafilomycin A1 for one hour. The no-cell and BioParticles® suspension-free controls were also plated (to determine cellular auto-fluorescence and reagent background fluorescence, respectively). Each sample was plated in triplicate. Plates were read on a BioTek Synergy™ HT microplate reader (excitation 509 nm and emission 533 nm).

2.5.10 Transmission Electron Microscopy to confirm MBA-NP Localisation to Phagolysosomes

In some experiments, following incubation with MBA-NP (one cell: eight MBA-NP), MDM samples were fixed, dehydrated, and washed, as described in section 2.3.11. Steven Mitchell performed the next steps in this protocol.

Samples were embedded in TAAB 812 resin. Sections, 1µm thick, were cut on a Leica Ultracut UCT Ultramicrotome, stained with Toluidine Blue, and viewed in a light microscope to select suitable areas for investigation. Ultrathin sections, 60 nm thick, were cut from selected areas, stained in Uranyl Acetate and Lead Citrate then viewed in a JEOL JEM-1400 Plus TEM. Representative images were collected on a GATAN OneView camera with assistance from Steven Mitchell.

These TEM experiments were repeated with the addition of an LPS pre-treatment of MDM in order to prime the MDM to increase the chances of finding MBA-NP within the phagolysosomes. In these experiments, MDM were treated with 10 ng/mL LPS (from *P.aeruginosa* 10) (Sigma) for one hour, after which wells were washed twice with DPBS, followed by MBA-NP incubation as before.

Chapter 3: Neutrophil Extracellular Traps are Associated with Airways Inflammation

Background

NETs were initially described as an anti-bacterial defence mechanism(65) and subsequent studies have revealed that NETs have been conserved throughout evolution(25,61–64), intimating the importance of their antimicrobial function. However, NETs have also been described as the "*double-edged swords of innate immunity*"(96) because they have been associated with numerous diseases characterised by sterile inflammation, including autoimmune disease, venous thrombosis and cardiovascular disease(97,99,100), described more fully in Chapter 1, section 1.12.

Within the context of CF lung disease, mounting evidence suggests that NETs are the principal source of the free DNA within the airways, which is found at higher levels in CF patients compared to HC(101). Marcos *et al.* quantified NETs using the Quant-iT PicoGreen® assay, based on a green fluorescent dye that binds DNA, and visualised sputum NETs using confocal laser scanning microscopy (CLSM) and electron microscopy(94). They concluded that the presence of NETs was associated with a decline in lung function in CF patients(94). Dwyer *et al.* also used the PicoGreen® assay to quantify NETs

then measured the NET-protein contents by liquid chromatography-mass spectroscopy (LC-MS/MS) and western blot analysis(180). However, a recent review article by Nauseef and Kubes highlighted the importance of confirming co-localisation between NET-DNA, histones and constituent proteins such as NE in assays which quantify NETs, to avoid false-positive results(103). Hence, during my PhD, a novel ELISA was used to quantify histone-bound calprotectin, as a measure of NET abundance.

Several of the aforementioned NET-associated proteins, such as NE, MPO and calprotectin, have been used as biomarkers for CF lung disease. For example, release of NE, an azurophilic granule protease, is known to degrade proteins including elastin and collagen in the airways(109). NE is also found in high concentrations in CF sputum and BAL samples and levels correlate with lung function decline in CF(38,181,182). Similarly, both sputum and serum calprotectin levels significantly decrease following treatment of CF exacerbations, and serum calprotectin is negatively correlated with FEV_1 and can predict time to next exacerbation in adult CF patients(114). Likewise, sputum MPO levels increase during CF exacerbations and have been associated with poorer outcomes(111–113). Given these NET constituent proteins are associated with lung function decline in CF, this strengthens the emerging favoured hypothesis that NETs contribute to lung damage in CF. Furthermore, recombinant human DNase (rhDNase, also referred to generically as dornase alfa, trade name Pulmozyme®) is a medication given to

CF patients, which may function through degradation of NETs. This medication contains DNase – an enzyme that cleaves extracellular DNA. It is administered to patients as a nebulised treatment, usually once daily. It decreases sputum viscosity(183) but also reduces airway inflammation, improves patients' lung function and reduces exacerbation rates in both children and adults with CF(146,147,184). DNase I is known to block G-actin polymerisation to F-actin(185), which could function to reduce sputum viscosity in the context of CF lung disease. It may be that the drug's main mechanism of action is through the inhibition of NET formation and/or clearance of NET-DNA and this is a hypothesis that was explored during my PhD.

Airway inflammation is usually quantified through measurement of sputum or BAL proinflammatory cytokines, such as IL-6, TNF-α and IL-8. IL-6 is an acute phase response protein released from immune cells in response to pathogen-associated molecular patterns (PAMPs). IL-6 regulates almost all aspects of the innate immune system but has been noted to be both pro- and anti-inflammatory(186). TNF-α is mainly produced by activated macrophages and is a potent chemoattractant for neutrophils. Once bound to its receptors on immune cells, TNF-α induces activation of NF-κB, MAPK and Caspase 8 pathways, which mediate apoptosis(187,188). Lastly, macrophages and monocytes are the main source of IL-8 production(189). This cytokine can also be released by other innate immune cells and epithelial cells, the latter of which may be a major source of IL-8 in CF lung disease(190). Once released, IL-8 induces chemotaxis of neutrophils and other granulocytes towards the site

of infection and stimulates phagocytosis. This is particularly relevant within the context of CF lung disease, where there is an excess of neutrophils within the airways(191), as described more fully in Chapter One, Section 1.9.

Hypotheses

1. NETs are proinflammatory in CF and their presence in patients' sputum is associated with increased severity of lung disease.
2. Macrophages produce proinflammatory cytokines when exposed to NETs and these effects are more pronounced in CF myeloid cells.

Aims

1. To quantify sputum NETs (using an ELISA that measures histone-bound calprotectin) and proinflammatory cytokine levels in CF and HC participants, in order to determine if the level of NETs is associated with more severe lung disease and inflammation.

2. To investigate the response of human HC and CF macrophages to NETs in culture, using microscopy to investigate cell morphology and ELISA quantification of the cytokines IL-8, TNF-α, IL-6 and IL-10 present within culture supernatants.

Results

3.1 Participant Demographics

Sputum was collected from HC and CF participants, following an induced sputum protocol in the former and spontaneous sputum from the latter, as described in Chapter 2, sections 2.2.5 and 2.2.6. Analysis of participant demographics showed that there were no significant differences in the sex, age or body mass index (BMI) between genotype groups (Table 3.1). As expected, CF participants had significantly lower FEV_1 and $ppFEV_1$ than HC participants (Table 3.1).

Demographic	HC (n=15) (median ± 95% CI)	CF (n=45) (median ± 95% CI)	Group comparisons: p-value for Mann-Whitney Test
Female	8 (53.3%)	18 (40%)	n/a
Male	7 (46.7%)	27 (60%)	n/a
Age, years	27 (25-32)	30 (27-35)	p = 0.404
BMI (kg/m^2)	23.6 (21-26.9)	22.5 (21.4-23.6), Male: 23.2 Female: 21.4	p = 0.110
FEV_1 (L)	3.84 (3.48-4.5)	2.04 (1.75-2.56)	p < 0.0001
$ppFEV_1$	98 (91-102)	61.1 (48.1-68.3)	p < 0.0001

Table 3.1: Participant demographics including sex, age, body mass index (BMI (kg/m^2)) and lung function. *There was no significant difference in the groups' median age. BMI was similar between both groups. CF participants had significantly reduced median forced expiratory volume in one second (FEV_1) compared to HC participants and median percentage predicted FEV_1 ($ppFEV_1$) was similarly significantly reduced. Data represents median ± 95% confidence intervals (CI) for continuous variables. Data analysed using Mann-Whitney test, where $p<0.05$ is deemed statistically significant.*

3.2 Neutrophils represent the predominant cell type in CF sputum and contain cytoplasmic vacuolations containing bacteria

Sputum cytology revealed differences between HC and CF sputum. Firstly, CF sputum samples had significantly higher total cell counts per gram of sputum compared to HC sputum, CF $2.9x10^7$ ($7x10^6$ – $7.7x10^7$/g) and HC $6.88x10^5$ ($2.32x10^5$ – $1.26x10^6$/g) (median ± 95% CI) (Figure 3.1). Secondly, macrophages were the predominant cell type within induced sputum from HC participants whilst neutrophils were the principal cell type within spontaneous sputum from CF participants (Figure 3.1). CF sputum contained significantly higher numbers of neutrophils per gram of sputum compared to HC sputum (Figure 3.2) and this negatively correlated with $ppFEV_1$ in CF participants (Figure 3.3).

The neutrophils from CF sputum samples were morphologically different from HC neutrophils, manifested by higher numbers of cytoplasmic vacuoles, many of which appeared to contain bacteria (Figures 3.4 and 3.5). It is important to note that HC sputum was collected using an induced sputum protocol whilst CF participants were able to spontaneously expectorate sputum. Previous studies specifically designed to contrast the two techniques in the context of CF show that cell differential counts (excluding squamous cells) from both collection methods were similar(192) but induced sputum gives rise to improved cell viability(170). It is unknown whether vacuolation and autophagy are affected by the sampling method employed. Future work could examine

this phenomenon (see Chapter 6, section 6.2). The percentage of neutrophils containing these cytoplasmic vacuolations was quantified. This demonstrated that the number of cells containing vacuolations was significantly higher in CF sputum neutrophils when compared to HC sputum neutrophils (Figure 3.6). These data support the hypothesis that an association exists between NET formation and autophagy and this should be investigated in future research (see Chapter 6, section 6.2).

Figure 3.1

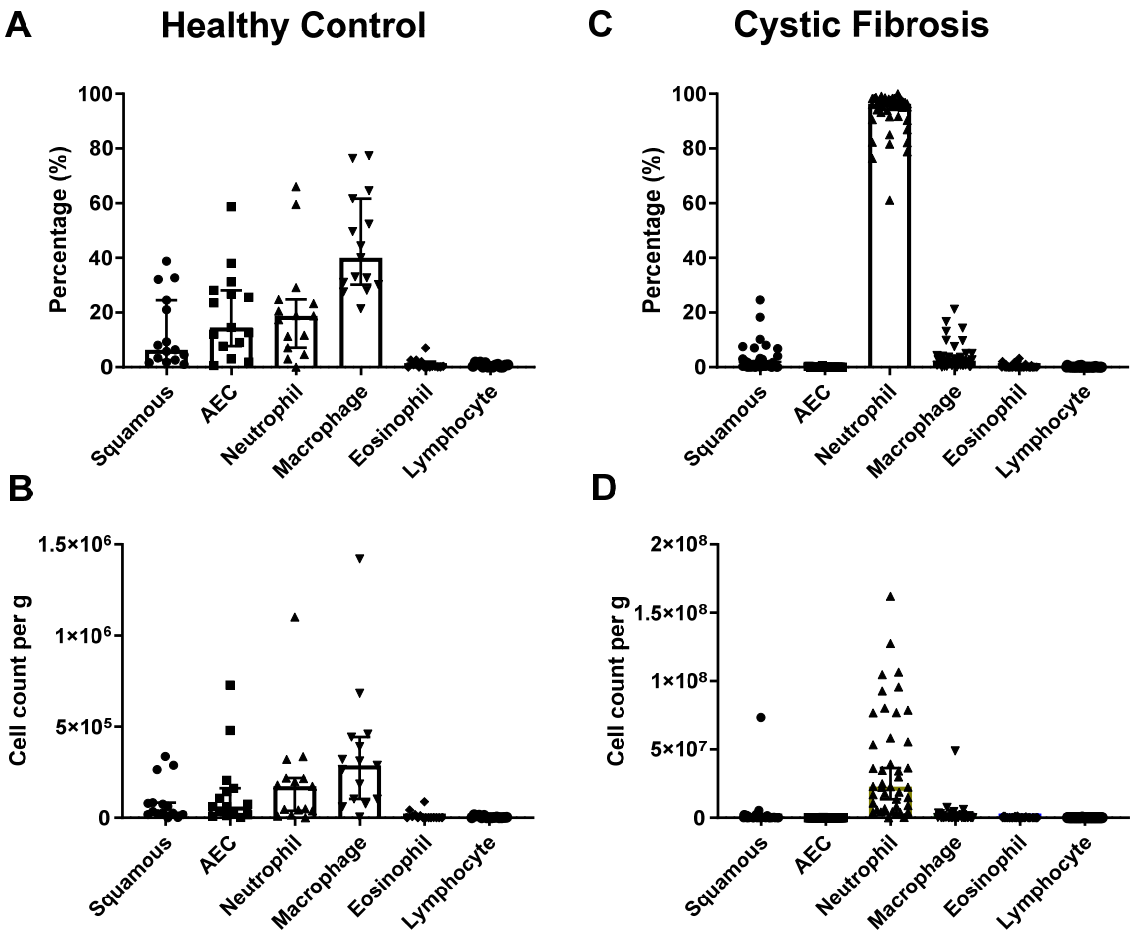
A
Healthy Control
C
Cystic Fibrosis
Percentage (%)
100
80
60
40
20
0
Squamous
AEC
Neutrophil
Macrophage
Eosinophil
Lymphocyte
B
D
Cell count per g
1.5×10⁶
1×10⁶
5×10⁵
0
2×10⁸
1.5×10⁸
1×10⁸
5×10⁷

Figure 3.1: Differential cell counts from healthy control (HC) (A&B) and Cystic Fibrosis (CF) (C&D) sputum. ***(A)*** *Within HC induced sputum, macrophages are the predominant cell type (40% (34.6 – 54.8%)), followed by neutrophils (18.8% (10.6 - 31.6%)), airway epithelial cells (AEC) (14.5% (10.8 - 28.3%)), squamous epithelial cells (squamous) (6.4% (5.6 - 20.2%)), lymphocytes (0.7% (0.3 - 1.1%)), then eosinophils (0.3% (0.01 - 2.1%)).* ***(B)*** *Differential cell count of HC induced sputum expressed as cell count per gram of sputum.* ***(C)*** *Neutrophils are the principal cell type in spontaneous sputum from CF participants (94.6% (90.8 - 95.6%)), followed by macrophages (2.4% (2.6 - 5.2%)), squamous (0.9% (1.2 - 4.3%)), eosinophils (0% (0.09 -0.5%)), lymphocytes (0% (0.01 - 0.13%)).* ***(D)*** *Differential cell count of CF spontaneous sputum expressed as cell count per gram of sputum. Note HC induced sputum contains significantly fewer total cells per g compared to CF spontaneous sputum: $6.88x10^5$ ($2.32x10^5$ - $1.26x10^6$) vs. $29x10^6$ ($7x10^6$ - $77x10^6$). HC induced sputum has more variation in cell type* ***(B)*** *compared to CF spontaneous sputum* ***(D),*** *in which neutrophils dominate. Data represents individual points and median with 95% confidence intervals.*

Figure 3.2

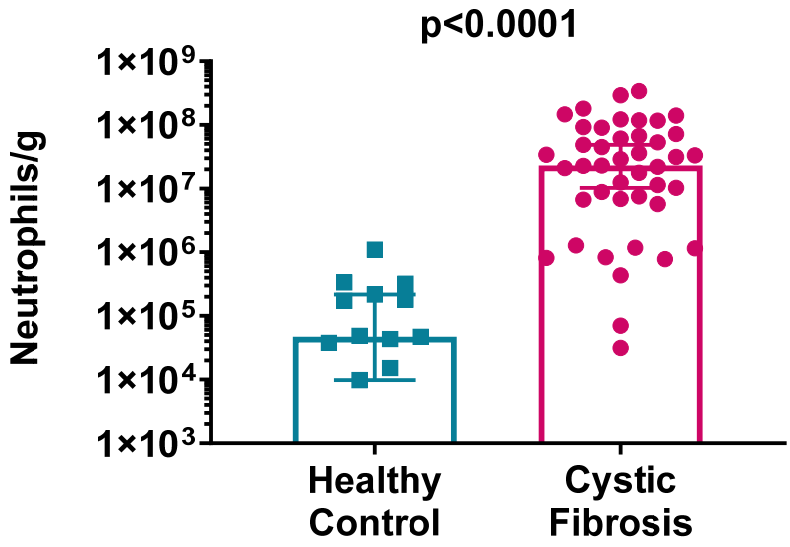

Figure 3.2: Cell counts of neutrophils per gram of sputum in Healthy Control (HC) and Cystic Fibrosis (CF) sputum. *HC induced sputum (shown in blue) contains significantly fewer neutrophils per gram compared to CF induced sputum (shown in pink). Data represents individual points and median ± 95% confidence intervals and was analysed by Mann-Whitney test. HC n=15, CF n=45. Note the logarithmic scale of the y-axis.*

Figure 3.3

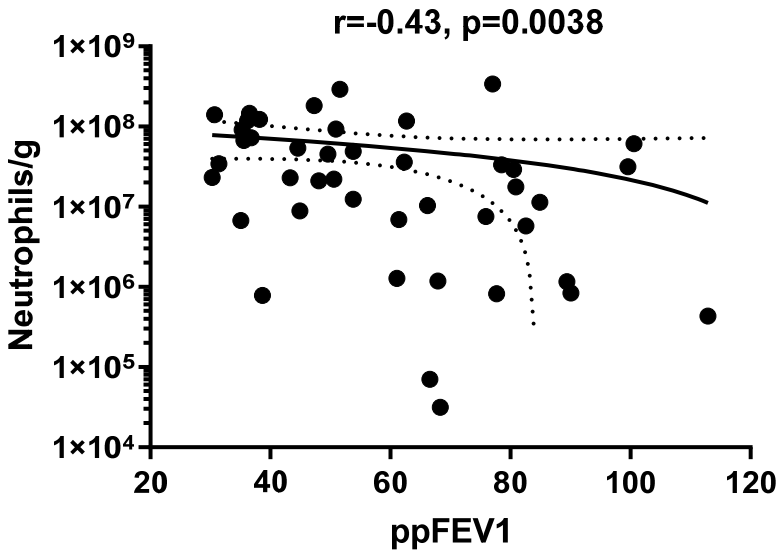

Figure 3.3: Neutrophils per gram of sputum correlated with lung function in Cystic Fibrosis participants. *The number of neutrophils per gram within CF spontaneous sputum (neutrophils/g) was correlated with the percentage predicted forced expiratory volume in one second (ppFEV1). This shows that a significant negative correlation exists between the two parameters, i.e. with increasing neutrophil numbers, lung function deteriorates, r = -0.43, p=0.0038. Data represents individual points with linear regression and 95% confidence bands. Data analysed using Spearman rank correlation coefficient.*

Figure 3.4

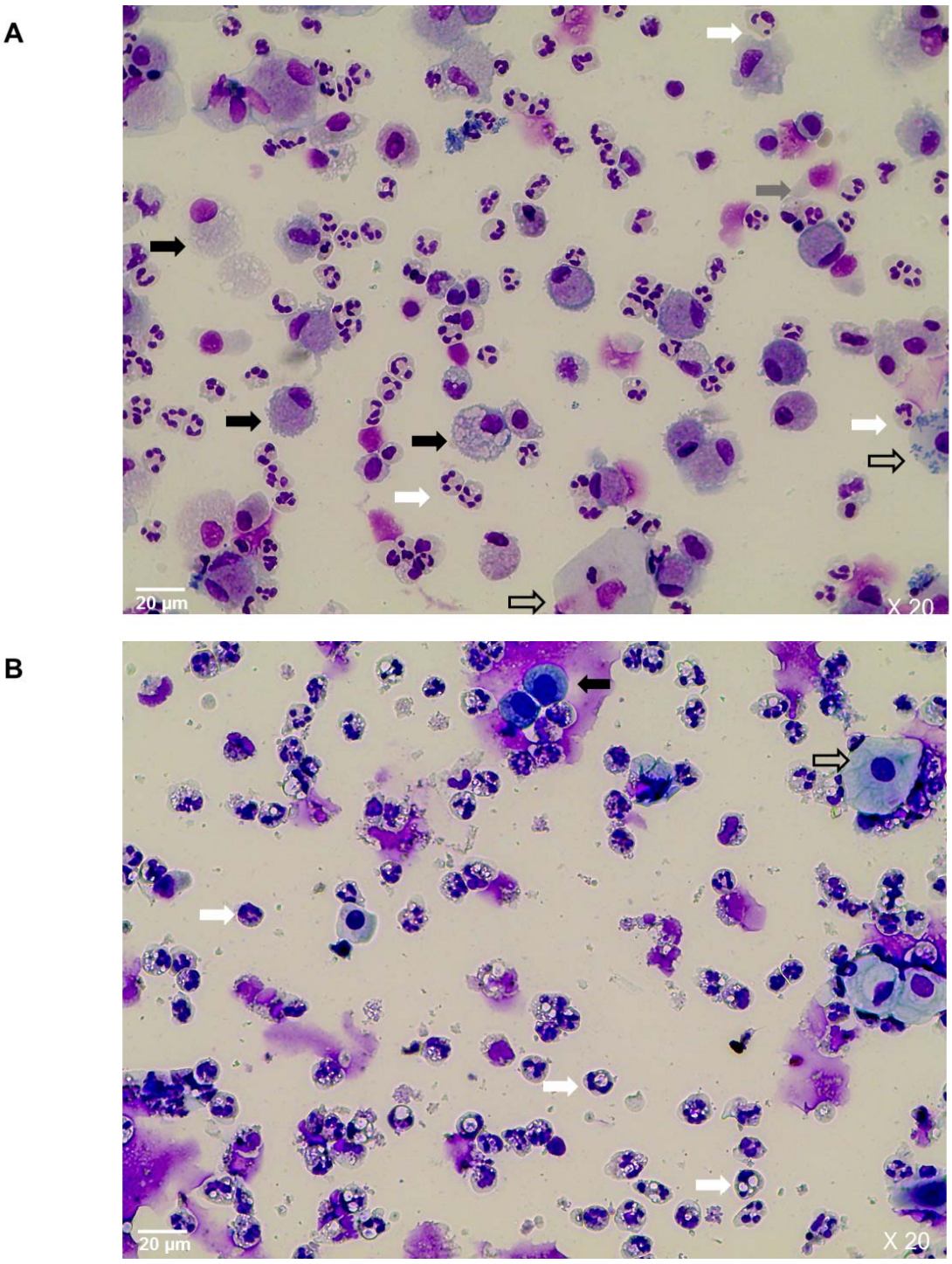

Figure 3.4: Morphological appearance of cells present in Healthy Control (HC) and Cystic Fibrosis (CF) sputum. *Representative photomicrograph images of cytocentrifuge preparations of cells present in HC induced* ***(A)*** *and CF spontaneous* ***(B)*** *sputum (taken using a x20 objective lens) to illustrate morphological appearance of cells that were present and quantified. Scale bar 20 µm. Neutrophils exhibit a distinctive multi-lobed nucleus (white arrows) with evidence of vacuolation in the cytoplasm of those within spontaneous sputum from CF participants* ***(B)*** *(see Figure 3.5 for further demonstration of this finding). Macrophages (black arrows) are identified by their characteristic features: they are large, irregular cells with an eccentrically placed nuclei, numerous vesicles and vacuoles, and ruffled surface*(193)*. Squamous epithelial cells (clear black arrows) are wide, flat cells with relatively featureless cytoplasms and contrast nicely to the airway epithelial cell (grey arrow of* ***(A)****), which has a distinctive columnar shape (with height 2-3 times greater than its width) and a basal nucleus*(194)*.*

Figure 3.5

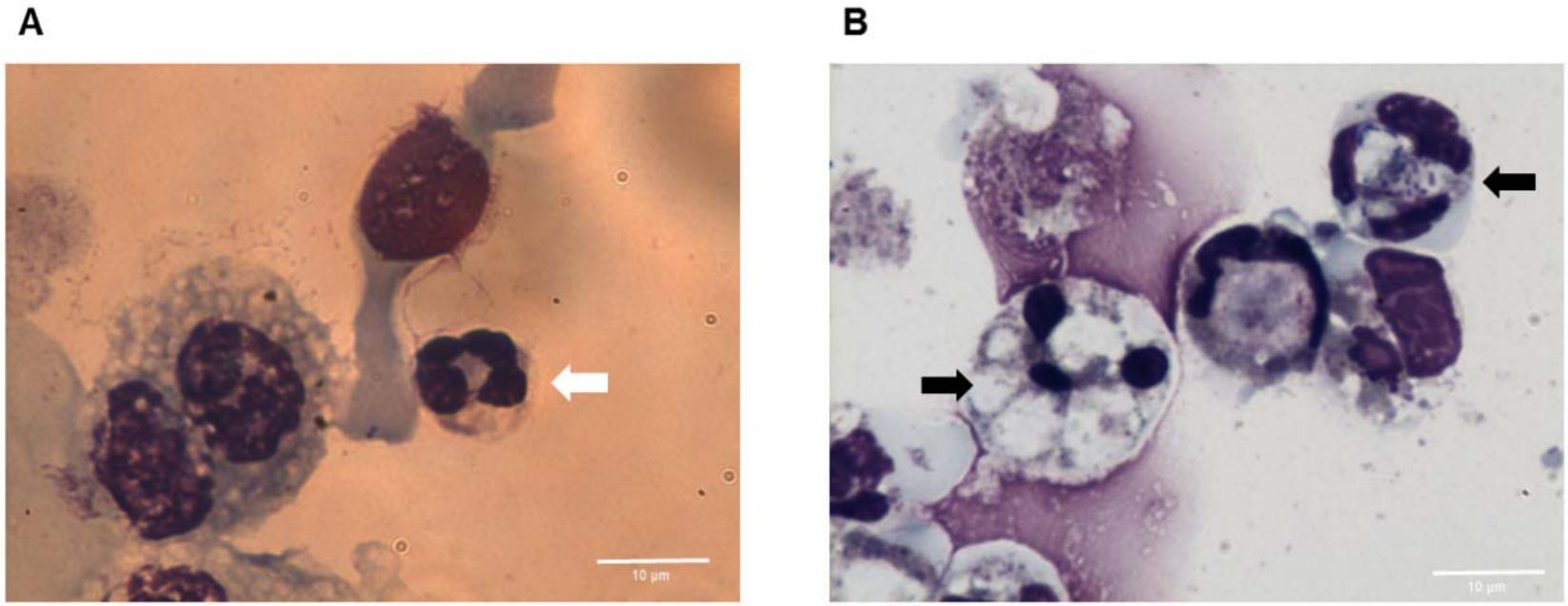

Figure 3.5: Comparison of morphological appearance of neutrophils in Healthy Control (HC) and Cystic Fibrosis (CF) sputum. *Representative photomicrograph images of cytocentrifuge preparations of cells present in HC induced* ***(A)*** *and CF spontaneous* ***(B)*** *sputum (taken using a x100 objective lens) to illustrate morphological appearance of cells that were present. Scale bar 10 μm. HC sputum neutrophils had few, if any, vacuoles present in their cytoplasm (white arrow,* ***(A)****). This image (from left to right) shows a macrophage, an airway epithelial cell and a neutrophil. In contrast, the cytoplasm of CF sputum neutrophils contains numerous vacuolations (black arrows, B) some of which appear to contain bacteria, suggesting these are phagosomes/phagolysosomes.*

Figure 3.6

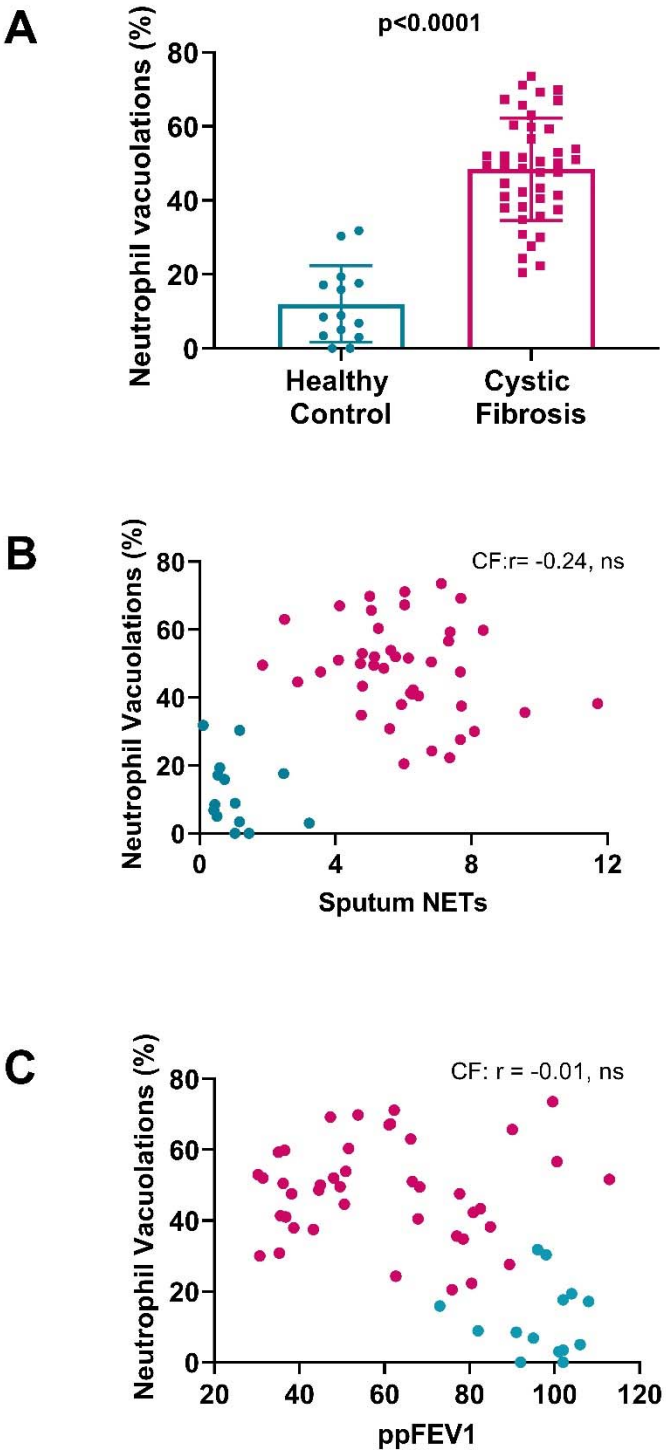
A
p<0.0001
Neutrophil vacuolations (%)
80
60
40
20
0
Healthy Control
Cystic Fibrosis
B
CF:r= -0.24, ns
Neutrophil Vacuolations (%)
80
60
40
20
0
0
4
8
12
Sputum NETs
C
CF: r = -0.01, ns
Neutrophil Vacuolations (%)
80
60
40
20
0
20
40
60
80
100
120
ppFEV1

Figure 3.6: Quantification of sputum neutrophil cytoplasmic vacuolation in Healthy Control (HC) and Cystic Fibrosis (CF) sputum. *HC data shown in blue, CF in pink. Sputum NETs were quantified in terms of fold-change in optical density (OD) compared to the mean OD of healthy control samples.* ***A)*** *Photomicrograph images of sputum cytocentrifuge preparations (taken using a x40 objective lens) were analysed to quantify the percentage of neutrophils containing cytoplasmic vacuolations. CF spontaneous sputum had significantly increased neutrophil vacuolation percentages relative to HC induced sputum, p<0.0001.* ***B)*** *Within the CF samples, there was no significant correlation between the percentage of vacuolated and sputum NETs, r= -0.24.* ***C)*** *With regard to CF samples, there was no significant correlation between the percentage of vacuolated neutrophils and the percentage predicted forced expiratory volume in one second ($ppFEV_1$), r= -0.01.* ***A)*** *Data represents individual points, and mean ± SD.* ***B&C)*** *Data represents individual points. Data analysed a two-tailed, unpaired Student's* t-*test (**A**) and Pearson's correlation coefficient (**B&C**). HC n=14, CF n=43.*

3.3 CF sputum contains significantly higher levels of NETs than HC sputum

Having established that the cohort of CF participants had excessive airway neutrophils, I next quantified the presence of NETs within the soluble phase of sputum samples using an in-house ELISA. CF sputum contained significantly increased levels of NETs when compared to HC sputum (Figure 3.7). Furthermore, sub-analysis of the CF participant data revealed that those on once daily nebulised Pulmozyme® (rhDNase) treatment had significantly reduced levels of NETs relative to CF participants who were not treated with rhDNase (Figure 3.8). Patients were not on rhDNase either because it was not indicated (i.e. their lung disease was not severe enough) or because they had not tolerated or were non-concordant with the treatment. These factors may have contributed to confounding of the data.

Sub-analysis was also performed to determine whether those CF participants with *P.aeruginosa* or *A.fumigatus* colonisation had higher levels of NETs in their sputum but this was found not to be the case (Figure 3.9). Similarly, Azithromycin treatment did not affect NET levels in the CF cohort (Figure 3.9).

CF sputum NET levels did not have a significant positive correlation with the number of neutrophils per gram of sputum – suggesting that an intrinsic abnormality in CF neutrophils accounts for enhanced NET formation, rather than there simply being more neutrophils present (Figure 3.10). NET levels in

CF sputum did not significantly correlate with lung function when analysed in isolation (Figure 3.11). However, when multi-variate linear regression modelling was used to predict FEV_1, it revealed that sputum NETs, the number of respiratory exacerbations in 12 months experienced by the participant prior to sputum sampling, sputum neutrophils per gram, age and sex were all significant predictors of FEV_1, whereas DNase treatment was not (Table 3.2).

In order to validate the results obtained using the in-house NET ELISA, they were compared to those from established indirect measures of NETs, namely MPO activity, PicoGreen® and HNE assays. We hypothesised that the in-house ELISA would be superior to these assays because it depends upon co-localisation of calprotectin and histones (the latter of which are associated with NET-DNA). This co-localisation of NET constituents is a key requirement of any NET quantification assay; it is no longer sufficient to measure only one constituent because they can occur independently of NETs(103). Sputum MPO activity, dsDNA and NE were found to be significantly increased in CF compared to HC sputum (Figures 3.12A, 3.13A and 3.14A). These parameters also all had significant positive correlations with NETs (Figure 3.12B, 3.13B and 3.14B) and significant negative correlations with $ppFEV_1$ (Figures 3.12C, 3.13C and 3.14C). Interestingly, with regard to the multi-variate linear regression model used to predict FEV_1, when sputum NETs was replaced with MPO, NE and dsDNA, the model was weaker overall in terms of adjusted r^2=0.6 (versus 0.64 when modelled with sputum NETs) and none of those

parameters were shown to be significant independent predictors of FEV_1. This suggests that sputum NETs, as measured by co-localisation of NET proteins and histones, could be an important biomarker for CF lung disease research.

3.4 Proinflammatory cytokines are elevated in CF sputum

Commercially available ELISA kits quantified the concentrations of key inflammatory cytokines present in sputum samples. IL-6 concentrations were significantly lower in CF sputum compared to HC sputum (Figure 3.15A). Conversely, TNF-α, IL-8 and calprotectin concentrations were all significantly higher in CF sputum compared to HC sputum (Figure 3.15B-D).

3.5 CF sputum proinflammatory cytokines are positively correlated with sputum NETs and negatively correlated with lung function

To determine whether there were any associations between these inflammatory cytokines and decline in lung function in CF participants, correlations were performed (Figure 3.16 A-D). Interestingly, only sputum calprotectin concentrations were negatively correlated with $ppFEV_1$ (Figure 3.16D). We next tested for correlations between the levels of inflammatory cytokines and sputum NETS. Positive correlations existed between sputum NETs and IL-8 and calprotectin but not between NETs and IL-6 or TNF-α (Figure 3.17).

3.6 Calprotectin levels were significantly increased in the serum of CF participants compared to HC serum.

A commercially available ELISA kit was used to measure serum calprotectin. Calprotectin was found to be significantly higher in the serum of CF participants compared to HC participants (Figure 3.18A). Serum calprotectin levels were demonstrated to have no significant correlation with the levels of sputum NETs (Figure 3.18B). However, serum calprotectin was shown to significantly negatively correlate with lung function. This was the case when HC and CF data were combined and when CF data were analysed in isolation (Figure 3.19).

Figure 3.7

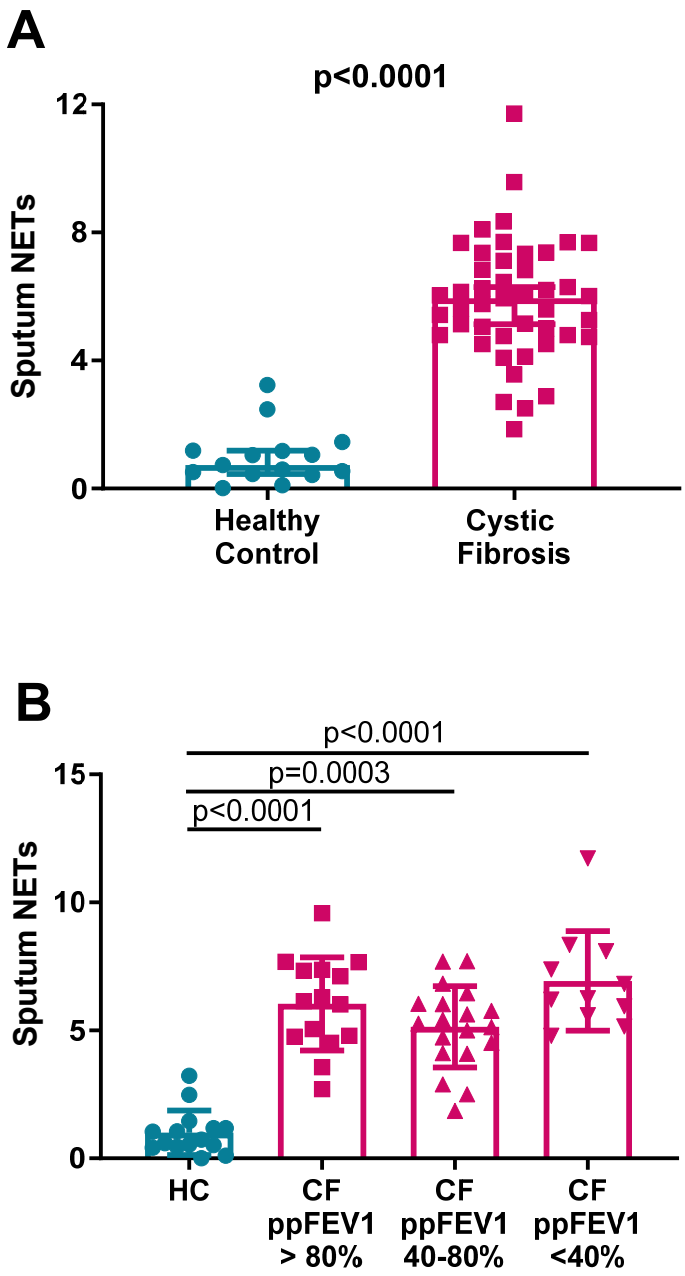

Figure 3.7: Quantification of NETs in the soluble phase of Healthy Control (HC) and Cystic Fibrosis (CF) sputum. *An in-house ELISA measured histone-bound calprotectin. Sputum NETs = fold-change in mean optical density (OD) from mean HC OD.* ***A)*** *CF sputum contains significantly more*

NETs than HC sputum. Median HC sputum NETs was 0.74 (0.45-1.18) and CF sputum NETs 5.94 (5.1-6.29). Data represents individual points and median ± 95% confidence intervals. Data analysed by Mann-Whitney test. HC n=15, CF n=44. ***B)*** *Differences in sputum NETs analysed by Kruskal-Wallis test with Dunn's multiple comparisons test for CF data divided into three groups based on percentage predicted forced expiratory volume in one second ($ppFEV_1$), i.e. into mild (i.e. > 80%), moderate (40% - 80%) and severe (< 40%). Analysis showed no statistically significant difference in sputum NET levels between the CF severity groups.*

Figure 3.8

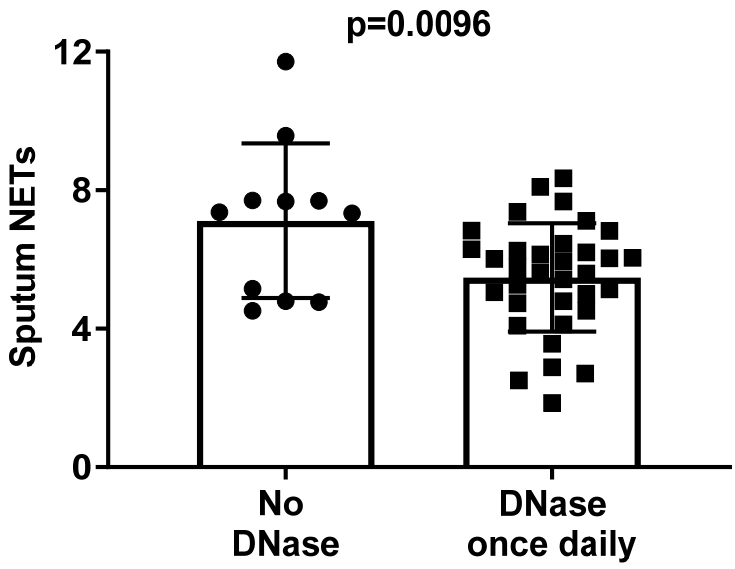

Figure 3.8: The impact of nebulised Pulmozyme® (recombinant human DNase) treatment on the levels of NETs present in sputum was measured by ELISA. *Data shown are determinations of NET levels from different individuals. Our CF cohort were divided into two groups based on whether or not they received nebulised rhDNase, a mucolytic therapy that functions to fragment DNA. Analysis of sputum NETs present in untreated versus once daily by unpaired two-tailed Student's* t*-test revealed significantly lower NETs in those treated with DNase (untreated 5.48 ± 1.56 vs. treated 7.12 ± 2.23, p=0.0096). Data represents individual points and mean ± standard deviation. DNase treatment: none n=10, once daily n=33. Sputum NETs = fold-change in mean optical density (OD) from mean HC OD.*

Figure 3.9

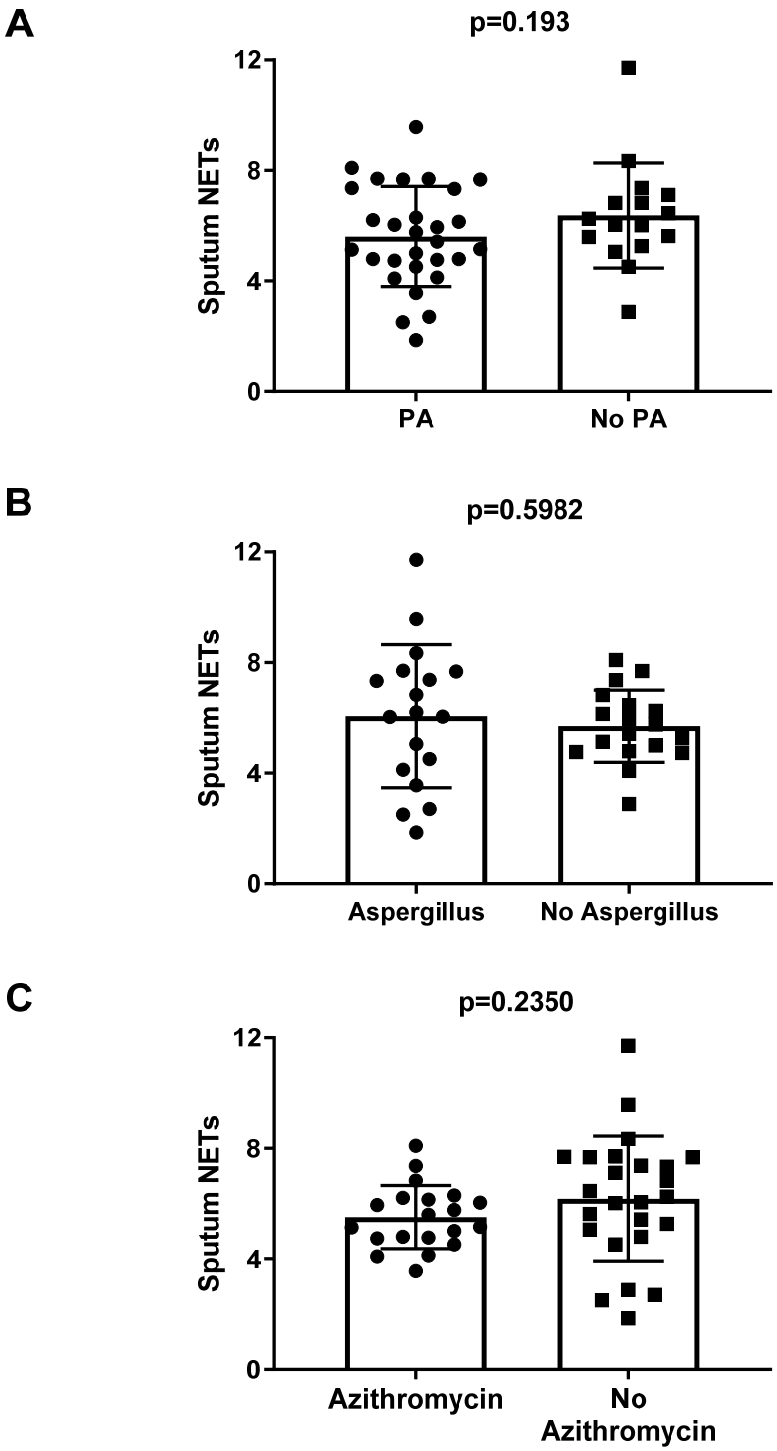
A
p=0.193
Sputum NETs
12
8
4
0
PA
No PA
B
p=0.5982
Sputum NETs
12
8
4
0
Aspergillus
No Aspergillus
C
p=0.2350
Sputum NETs
12
8
4
0
Azithromycin
No Azithromycin

Figure 3.9: Sputum NET levels in CF participants with or without* Pseudomonas aeruginosa (PA) *and* Aspergillus fumigatus (Aspergillus) *colonisation and Azithromycin treatment. ***A)*** *Analysis of sputum NET levels by an unpaired, two-tailed Student's* t*-test revealed no significant difference between those CF participants colonised with PA (n=29) versus those without PA (n=16)(p=0.193).* ***B)*** *Analysis of sputum NET levels by an unpaired, two-tailed Student's* t*-test revealed no significant difference between those CF participants colonised with* Aspergillus (n=18) v*ersus those without* Aspergillus (n=27) *(p=0.5982).* ***C)*** *Analysis of sputum NET levels by an unpaired, two-tailed Student's* t*-test revealed no significant difference between those CF participants taking azithromycin (n=20) versus those not on the drug (n=25) (p=0.235). All data represents mean ± SD. Sputum NETs = fold-change in mean optical density (OD) from mean HC OD.*

Figure 3.10

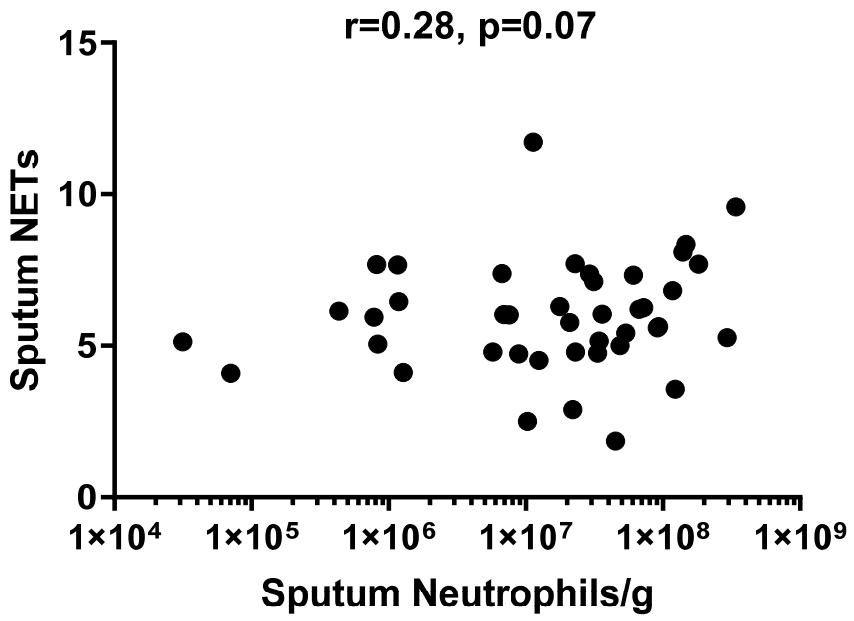

Figure 3.10: Correlation between neutrophils per gram of sputum and sputum NETs in CF participants. *Analysis of the correlation between neutrophils per gram of sputum and the level of sputum NETs by Pearson rank correlation coefficient revealed no significant correlation between these two parameters (r=0.28, p=0.07). Sputum NETs = fold-change in mean optical density (OD) from mean HC OD.*

Figure 3.11

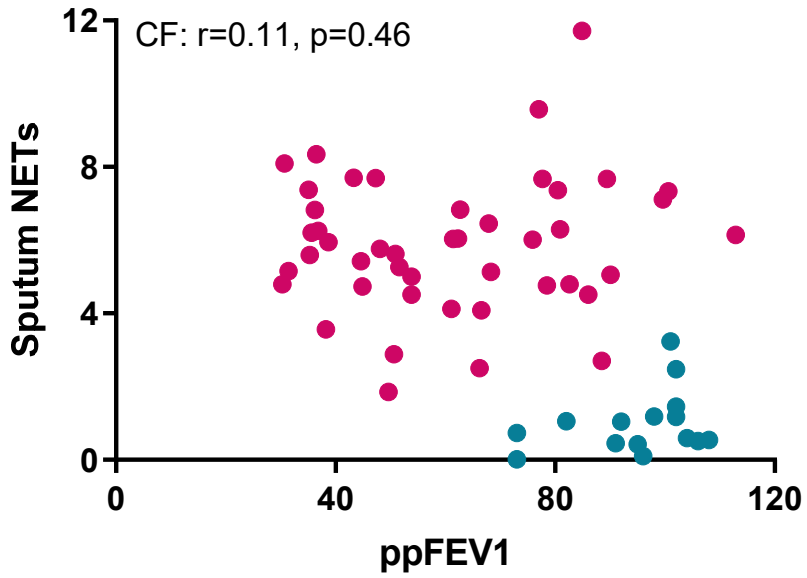

Figure 3.11: Healthy Control (HC) and Cystic Fibrosis (CF) sputum NETs correlated with lung function. *HC data represented by blue data points, CF data represented by pink data points. With regard to the CF data, analysis of the correlation between sputum NETs and percentage predicted forced expiratory volume in one second ($ppFEV_1$) by Spearman rank correlation coefficient revealed no significant correlation (r^2=0.11, p=0.46). Sputum NETs = fold change in optical density (OD) from mean healthy control OD.*

Variable	β	SE	t value	Significance
Sputum NETs	1.23E-01	5.72E-02	2.151	0.038*
DNase	-9.24E-02	2.57E-01	-0.359	0.722
Number of exacerbations in 12 months	-3.37E-01	5.87E-02	-5.737	0.0001***
Sputum neutrophil count per gram	-2.79E-09	1.32E-09	-2.112	0.042*
Age	-2.39E-02	9.14E-03	-2.616	0.013*
Sex	3.868E-0.1	1.739E-0.1	2.224	0.032*

Table 3.2: Predicting forced expiratory volume in one second (FEV_1) using a multi-variate linear regression model. *When FEV1 was predicted using multi-variate linear regression modelling, it was found that sputum NETs, the number of respiratory exacerbations experienced by the participant in 12 months prior to sputum sampling, sputum neutrophils per gram, age and sex were all independent significant predictors whereas DNase treatment was not. The overall model fit was $r^2 = 0.6927$. Specifically, CF sputum NETs remains independently associated with FEV_1, p=0.038. Residual standard error: 0.5553 on 36 degrees of freedom. Adjusted $r^2 = 0.6415$. F-statistic: 13.53 on 6 and 36 DF, p-value = 5.702e-08.*

Figure 3.12

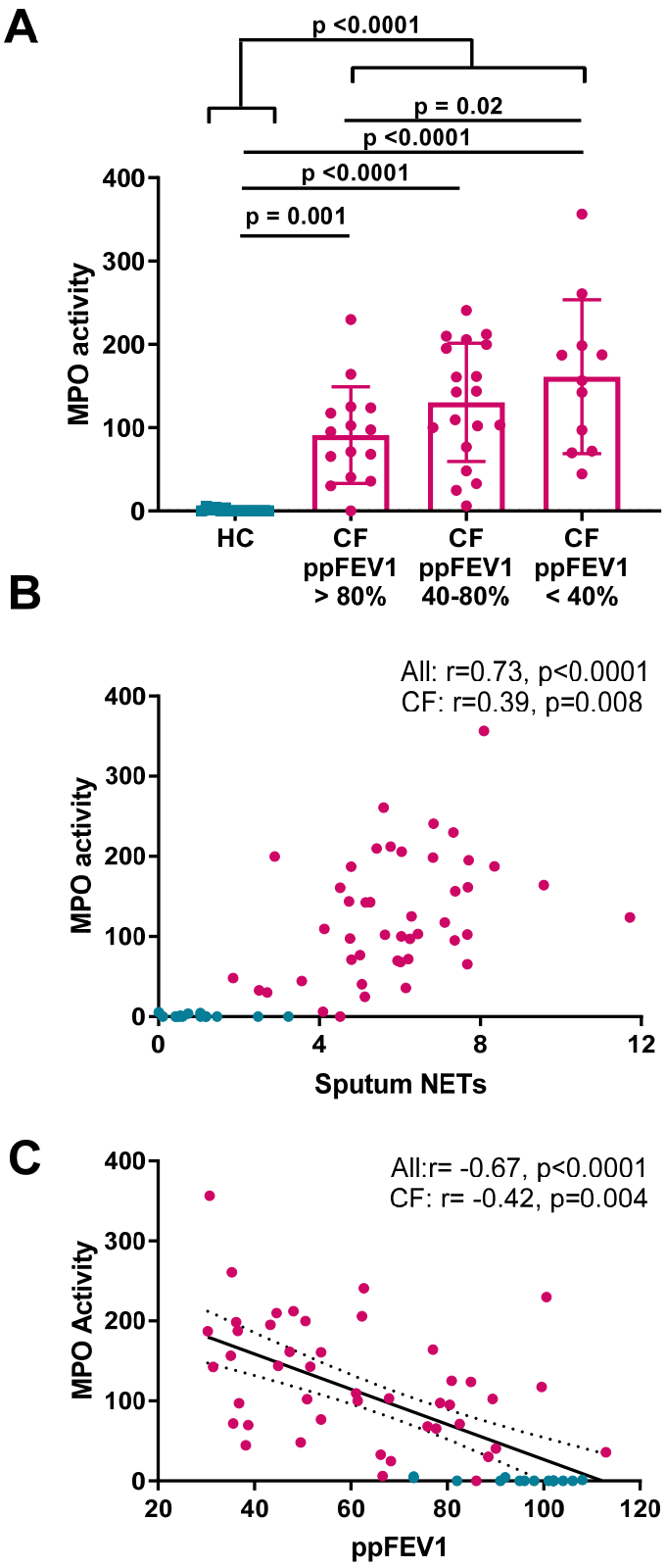
A
p <0.0001
p = 0.02
p <0.0001
p <0.0001
p = 0.001
MPO activity
400
300
200
100
0
HC
CF ppFEV1 > 80%
CF ppFEV1 40-80%
CF ppFEV1 < 40%
B
All: r=0.73, p<0.0001
CF: r=0.39, p=0.008
MPO activity
400
300
200
100
0
0
4
8
12
Sputum NETs
C
All:r= -0.67, p<0.0001
CF: r= -0.42, p=0.004
MPO Activity
400
300
200
100
0
20
40
60
80
100
120
ppFEV1

Figure 3.12: Sputum MPO activity correlated with sputum NETs and lung function. *Healthy Control (HC) data represented in blue data points. Cystic fibrosis (CF) data represented in by pink data points.* ***A)*** *Differences in sputum MPO activity analysed by Kruskal-Wallis test with Dunn's multiple comparisons test revealed a significant increase in MPO activity in CF sputum relative to HC sputum ($p<0.0001$). CF data were divided into three groups based on percentage predicted forced expiratory volume in one second ($ppFEV_1$), i.e. into mild (i.e. > 80%), moderate (40% - 80%) and severe (< 40%). Analysis of differences in MPO activity between these groups showed a statistically significant increase in MPO activity in the severe group compared to the mild group ($p=0.02$).* ***B)*** *Analysis of sputum MPO activity correlated with sputum NETs by Spearman rank correlation coefficient revealed a significant positive correlation ($r=0.73$, $p<0.0001$).* ***C)*** *Analysis of sputum MPO activity correlated with $ppFEV_1$ by Spearman rank correlation coefficient showed a significant negative correlation ($r= -0.67$, $p<0.0001$). Data represents individual points and linear regression (solid black line) with 95% confidence bands (dotted lines). MPO activity = fold change in optical density (OD) from mean HC OD.*

Figure 3.13

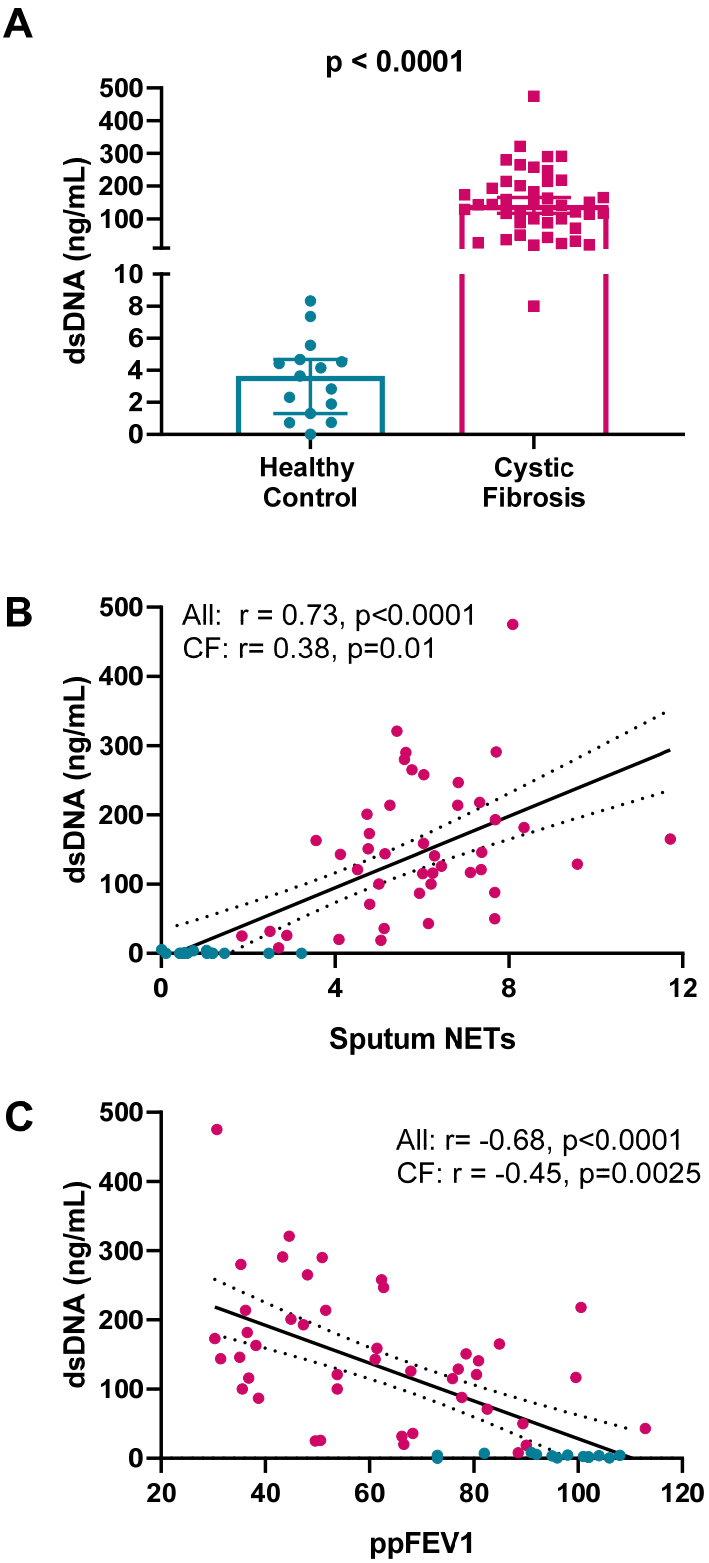
A
p < 0.0001
dsDNA (ng/mL)
500
400
300
200
100
10
8
6
4
2
0
Healthy Control
Cystic Fibrosis
B
All: r = 0.73, p<0.0001
CF: r= 0.38, p=0.01
dsDNA (ng/mL)
0
4
8
12
Sputum NETs
C
All: r= -0.68, p<0.0001
CF: r = -0.45, p=0.0025
dsDNA (ng/mL)
20
40
60
80
100
120
ppFEV1

Figure 3.13: Sputum dsDNA correlated with sputum NETs and lung function. *Healthy Control (HC) data represented in blue data points. Cystic fibrosis (CF) data represented in by pink data points.* ***A)*** *Differences in sputum dsDNA (ng/mL) analysed by two-tailed Mann-Whitney test revealed a significant increase in dsDNA concentrations in CF sputum relative to HC sputum ($p<0.0001$).* ***B)*** *Analysis of sputum dsDNA levels correlated with sputum NETs by Pearson correlation coefficient revealed a significant positive correlation when HC and CF data were analysed together ($r=0.73$, $p<0.0001$) and when CF data were analysed alone ($r=0.38$, $p=0.01$).* ***C)*** *Analysis of sputum dsDNA levels correlated with percentage predicted forced expiratory volume in one second ($ppFEV_1$) by Pearson correlation coefficient showed a significant negative correlation when HC and CF data were analysed together ($r= -0.68$, $p<0.0001$) and when CF data were analysed alone ($r= -0.45$, $p=0.0025$). Data represents individual points and linear regression (solid black line) with 95% confidence bands (dotted lines). Sputum NETs = fold-change in optical density (OD) from mean HC OD.*

Figure 3.14

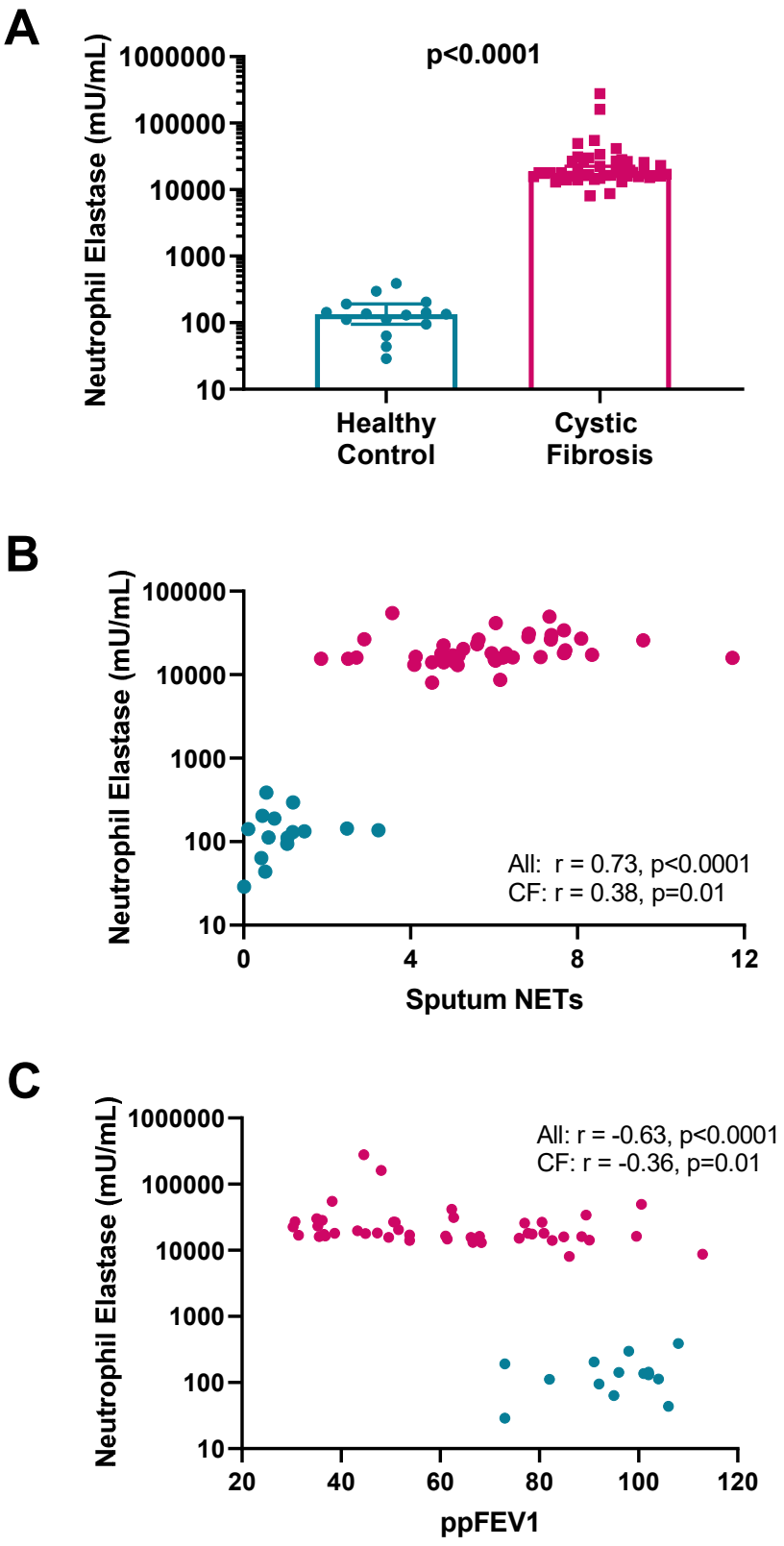
A
Neutrophil Elastase (mU/mL)
1000000
100000
10000
1000
100
10
p<0.0001
Healthy Control
Cystic Fibrosis
B
Neutrophil Elastase (mU/mL)
100000
10000
1000
100
10
All: r = 0.73, p<0.0001
CF: r = 0.38, p=0.01
0
4
8
12
Sputum NETs
C
Neutrophil Elastase (mU/mL)
1000000
100000
10000
1000
100
10
All: r = -0.63, p<0.0001
CF: r = -0.36, p=0.01
20
40
60
80
100
120
ppFEV1

Figure 3.14: Sputum Neutrophil Elastase (NE) protein level correlated with sputum NETs and lung function. *Healthy Control (HC) data represented in blue data points. Cystic fibrosis (CF) data represented in by pink data points.* ***A)*** *Differences in sputum NE concentrations (mU/mL) analysed by two-tailed Mann-Whitney test revealed a significant increase in NE concentrations in CF sputum relative to HC sputum ($p<0.0001$).* ***B)*** *Analysis of sputum NE levels correlated with sputum NETs by Spearman rank correlation coefficient revealed a significant positive correlation when HC and CF data were analysed together ($r=0.73$, $p<0.0001$) and when CF data were analysed alone ($r=0.38$, $p=0.01$).* ***C****) Analysis of sputum NE levels correlated with percentage predicted forced expiratory volume in one second ($ppFEV_1$) by Spearman rank correlation coefficient showed a significant negative correlation when HC and CF data were analysed together ($r= -0.68$, $p<0.0001$) and when CF data were analysed alone ($r= -0.36$, $p=0.01$). Sputum NETs = fold-change in optical density (OD) from mean HC OD.*

Figure 3.15

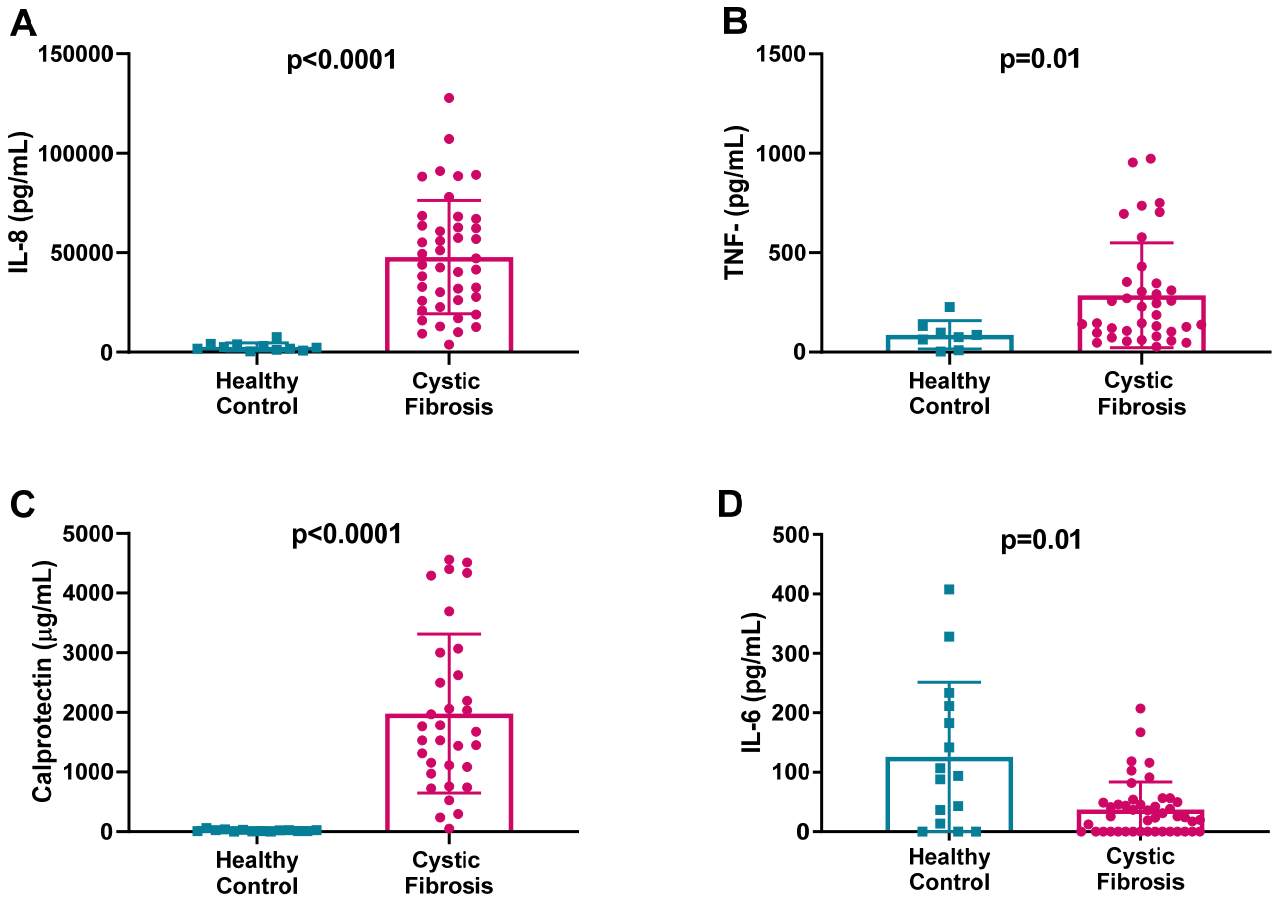
A
p<0.0001
IL-8 (pg/mL)
150000
100000
50000
0
Healthy Control
Cystic Fibrosis
B
p=0.01
TNF- (pg/mL)
1500
1000
500
0
Healthy Control
Cystic Fibrosis
C
p<0.0001
Calprotectin (µg/mL)
5000
4000
3000
2000
1000
0
Healthy Control
Cystic Fibrosis
D
p=0.01
IL-6 (pg/mL)
500
400
300
200
100
0
Healthy Control
Cystic Fibrosis

Figure 3.15: ELISA quantification of sputum inflammatory markers in healthy control (HC) and Cystic Fibrosis (CF) sputum. A) *Analysis of sputum IL-8 concentrations in CF vs. HC sputum revealed a statistically significant increase ($p<0.0001$).* ***B)*** *Analysis of sputum TNF-α concentrations in CF vs. HC sputum showed a statistically significant ($p=0.01$).* ***C)*** *Analysis of sputum calprotectin concentrations in CF vs. HC sputum demonstrated a statistically significant increase ($p<0.0001$).* ***D)*** *Analysis of sputum IL-6 concentrations in CF vs. HC sputum revealed a statistically significant decrease ($p=0.01$). Data represents individual points and median ± 95% confidence intervals. All data analysed using two-tailed Mann-Whitney test. HC n=8-15, CF n=32-45.*

Figure 3.16

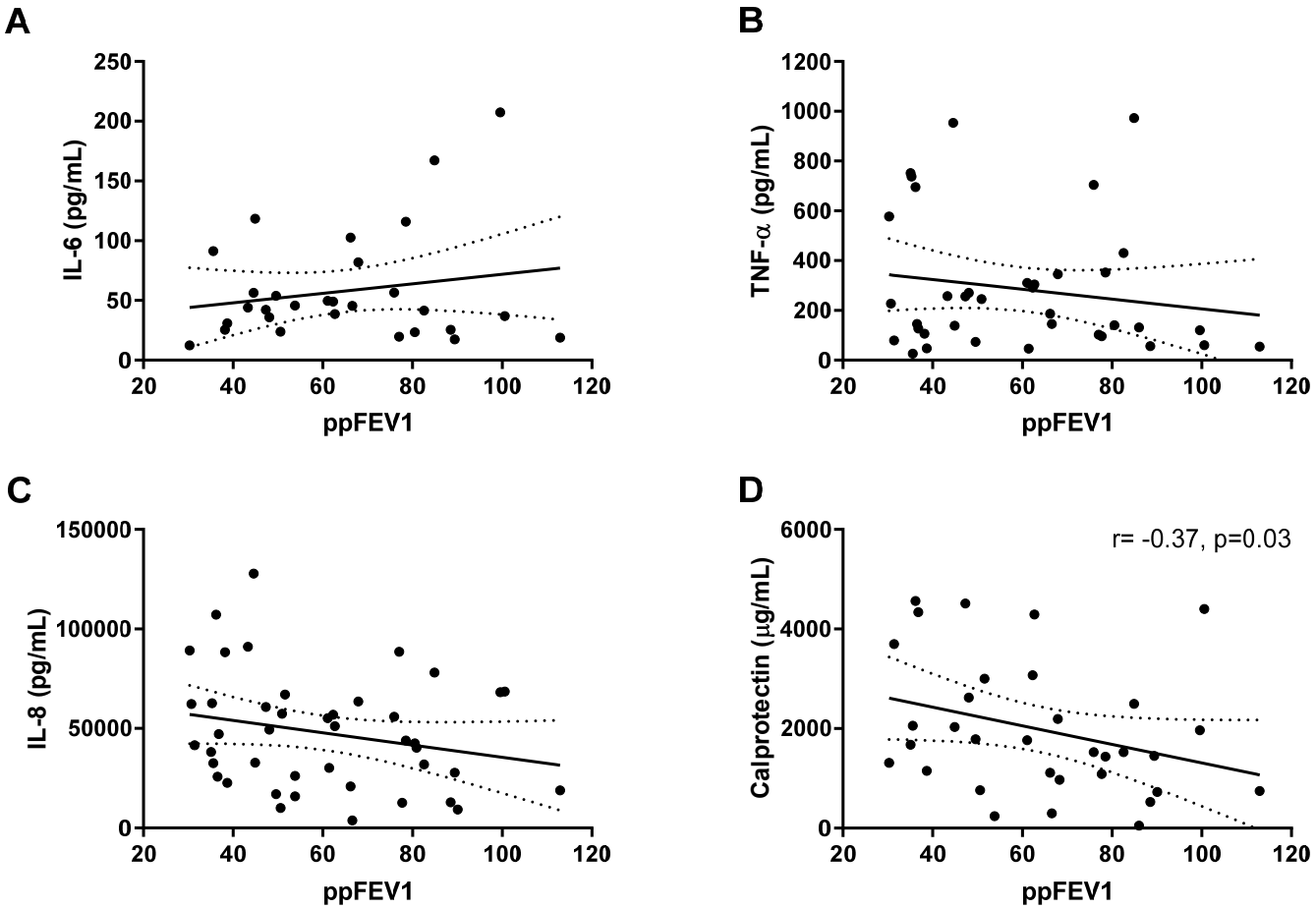
A
IL-6 (pg/mL)
250
200
150
100
50
0
20
40
60
80
100
120
ppFEV1
B
TNF-α (pg/mL)
1200
1000
800
600
400
200
0
20
40
60
80
100
120
ppFEV1
C
IL-8 (pg/mL)
150000
100000
50000
0
20
40
60
80
100
120
ppFEV1
D
Calprotectin (μg/mL)
6000
4000
2000
0
r= -0.37, p=0.03
20
40
60
80
100
120
ppFEV1

Figure 3.16: Cystic Fibrosis (CF) sputum inflammatory marker concentrations correlated with lung function. A) *Analysis of IL-6 concentrations present in CF sputum correlated with percentage predicted forced expiratory volume in one second ($ppFEV_1$) revealed no significant correlation.* ***B)*** *Analysis of TNF-α concentrations present in CF sputum correlated with $ppFEV_1$ showed no significant correlation.* ***C)*** *Analysis of IL-8 concentrations present in CF sputum correlated with $ppFEV_1$ demonstrated no significant correlation.* ***D)*** *Analysis of sputum calprotectin concentrations present in CF sputum revealed a statistically significant negative correlation ($r= -0.37$, $p=0.03$). Data represents individual data points and linear regression lines (solid black lines) with 95% confidence bands (dotted lines). All data analysed by Spearman rank correlation coefficient, asides from IL-8 data, which was analysed by Pearson correlation coefficient.*

Figure 3.17

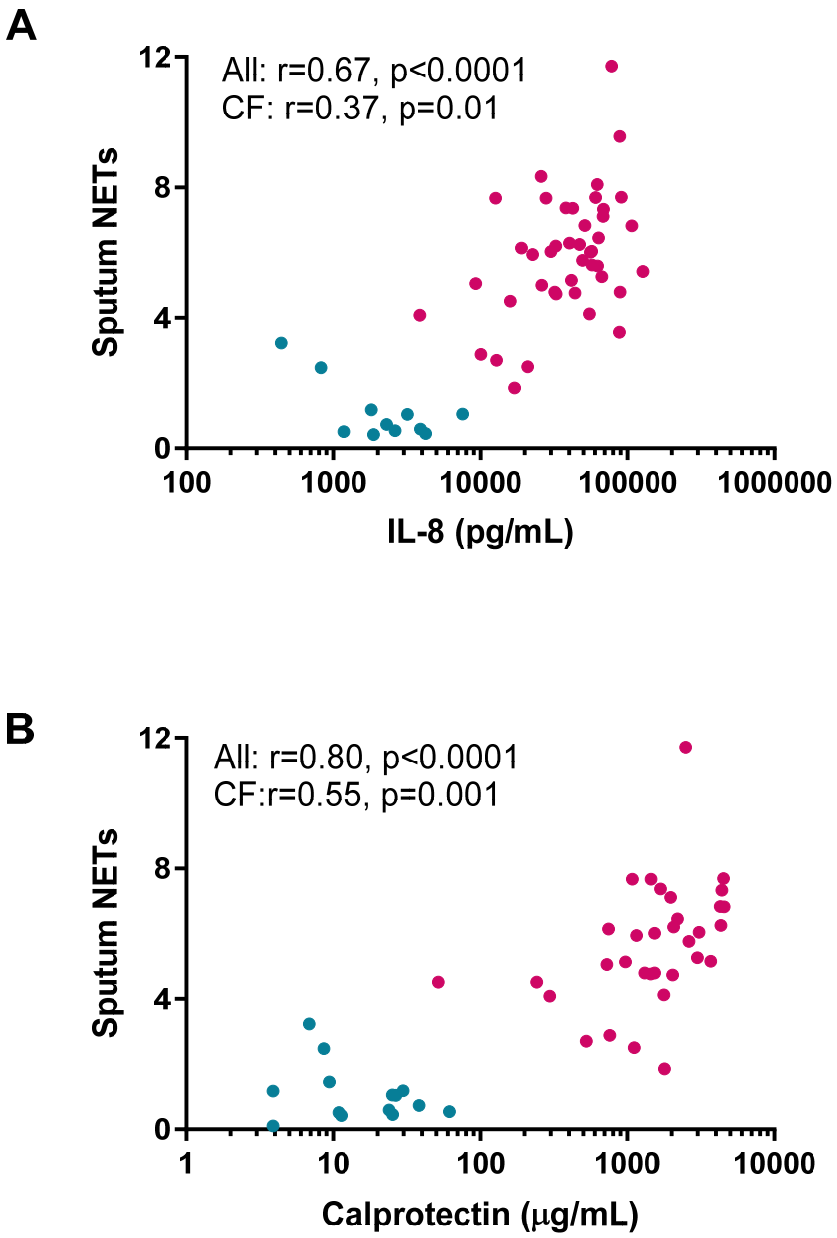

Figure 3.17: Sputum NETs correlated with sputum IL-8 and calprotectin concentrations. *Healthy control (HC) data represented in blue, Cystic Fibrosis (CF) data represented in pink.* ***A)*** *Analysis of sputum NETs correlated*

with sputum IL-8 concentrations by Spearman rank correlation coefficient revealed a significant positive correlation when HC and CF data were analysed together ($r=0.67$, $p<0.0001$) and when CF data were analysed alone ($r=0.37$, $p=0.01$). ***B)*** *Analysis of sputum NETs correlated with sputum calprotectin concentrations by Spearman rank correlation coefficient revealed a significant positive correlation when HC and CF data were analysed together ($r=0.80$, $p<0.0001$) and when CF data were analysed alone ($r=0.55$, $p=0.001$). Sputum NETs = fold change in optical density (OD) from mean HC OD.*

Figure 3.18

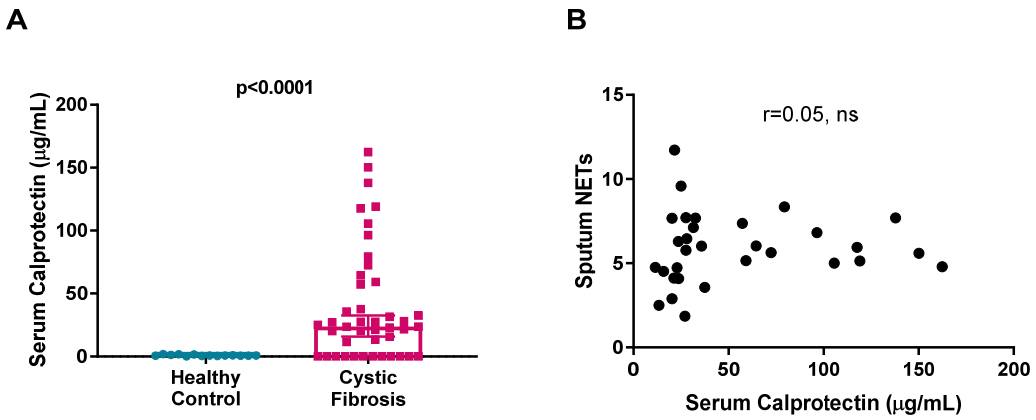

Figure 3.18: Serum calprotectin levels in Healthy Control (HC) and Cystic Fibrosis (CF) participants and correlation with sputum NETs in CF participants. ***A)*** *Analysis of calprotectin concentrations in CF versus HC serum by two-tailed Mann-Whitney test revealed significantly higher calprotectin concentrations in CF serum (p<0.0001). Data represents individual data points and median with 95% confidence intervals. HC n=15, CF n=31.* ***B)*** *Analysis of the correlation between sputum NET levels and serum calprotectin in CF participants by Pearson rank correlation coefficient revealed no significant correlation between these parameters (r=0.05, p=0.77). Sputum NETs = fold change in optical density (OD) from mean HC OD.*

Figure 3.19

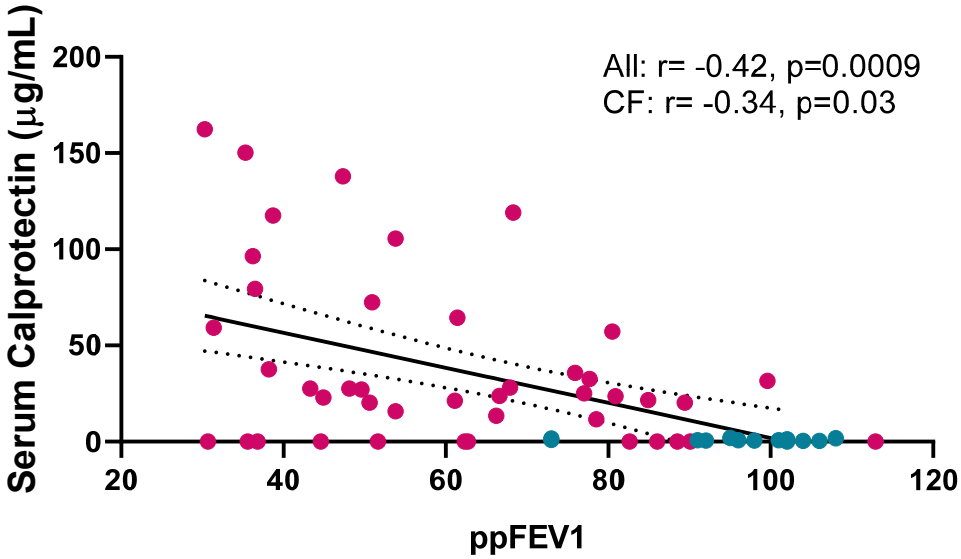

Figure 3.19: Serum calprotectin correlated with percentage predicated forced expiratory volume in one second (ppFEV$_1$). *When serum calprotectin concentrations were correlated with ppFEV$_1$, a measure of lung function, using Pearson rank correlation coefficient, there was a significant negative correlation. This was the case when Healthy Control (HC, shown in blue data points) data were combined with Cystic Fibrosis (CF, shown in pink data points) data (r=-0.42, p=0.0009), and when CF data were analysed alone (r= -0.34, p=0.03). Data represents individual data points and linear regression (solid black line) with 95% confidence interval bands (dotted lines).*

3.7 Establishing a model for co-culture of monocyte-derived macrophages with NETs

Having determined that sputum NETs were elevated in CF sputum and were positively associated with the levels of proinflammatory cytokines present in sputum, I sought to establish a cell culture model to investigate whether NETs exert proinflammatory effects, focussing on the interplay between neutrophils and macrophages.

Preliminary experiments were designed to determine which pharmacological agents should be used to stimulate and inhibit NET formation *in vitro*. PMA was chosen over ionomycin because it resulted in characteristic NET formation, with diffuse and spreading NETs evident and smaller standard deviations when quantified (Figure 3.20A and B, and Figure 3.21C). The concentration of PMA for optimal stimulation of NETs was then determined by quantification of NET formation using a fluorescence microscopy kinetic plate reader assay. 100nM PMA was the most effective stimulator of NET formation (Figure 3.20C and 3.21), whilst DNase (100U/mL) was the most effective inhibitor of NET formation (Figure 3.22). I next compared the extent of NET formation when neutrophils were exposed to PMA as either adherent cells (i.e. “plated culture”) or when cultured in suspension (i.e. “rolling culture”) (Figure 3.20D). This was done to quantify the percentage of cells which NETed in each condition to determine if they were comparable. There was a significant reduction in the percentage of neutrophils undergoing NET formation when

cells were cultured in suspension compared to adherent culture (20.3 ± 6.1% versus 53.7 ± 21.4%, respectively) (Figure 3.20D). In the control experiments (i.e. those without PMA) there was no significant difference in the percentage of neutrophils undergoing NET formation when comparing cells cultured either in suspension or as adherent cells (0.37 ± 0.4% versus 0.5 ± 0.4%, respectively). Despite there being fewer cells undergoing NET formation when cultured in suspension, this method allowed neutrophils to be washed, thus removing any residual PMA that might adversely affect MDM function prior to co-culture. The control experiment data revealed that the mechanical forces involved when cells were cultured in suspension did not stimulate NET formation.

Figure 3.20

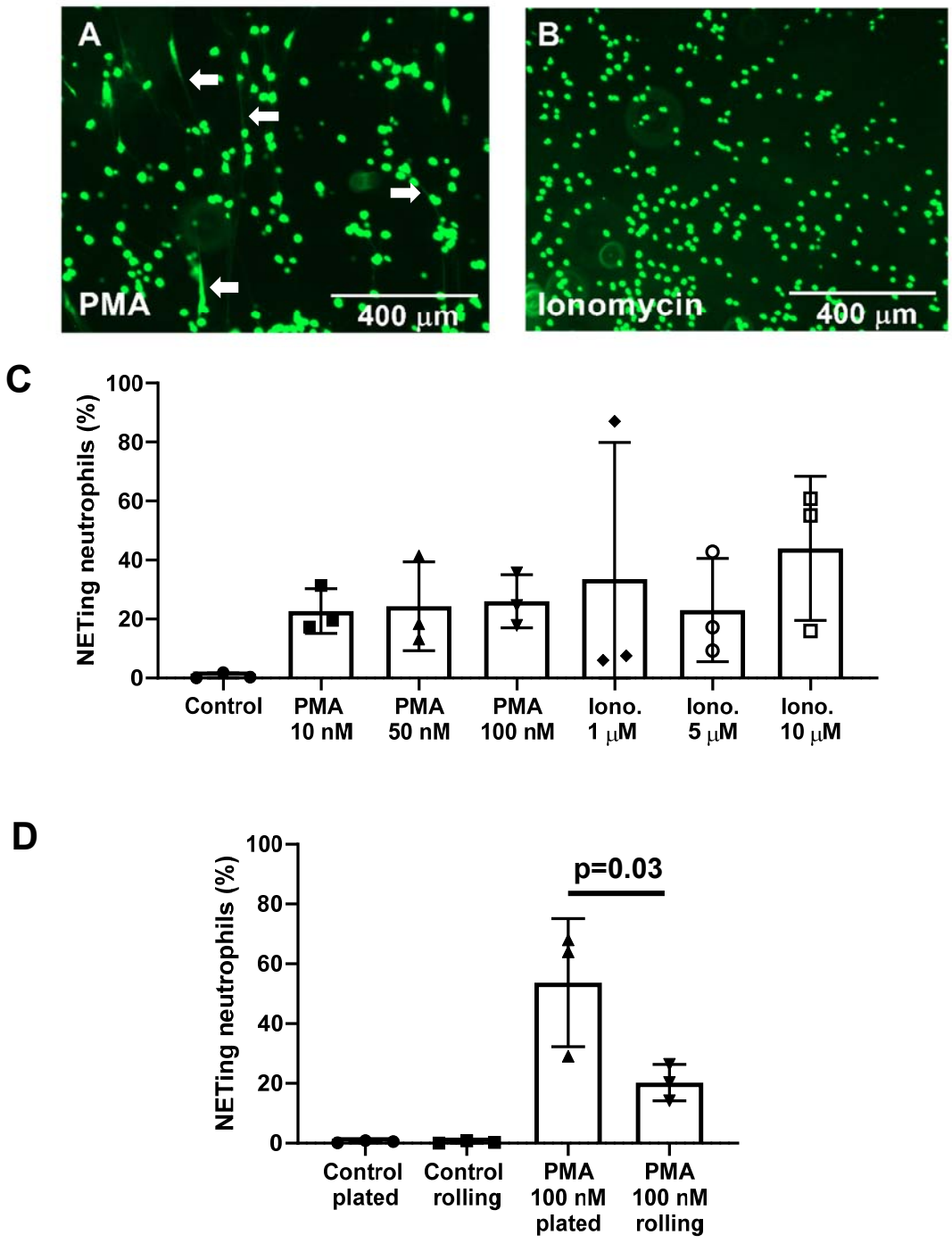

Figure 3.20: Quantification of* in vitro *neutrophil extracellular trap formation (NET formation) by fluorescence microscopy using SYTOX® green staining. ***A)*** *Representative photomicrograph image of fluorescence*

microscopy. When neutrophils were treated with PMA, this resulted in characteristic NET formation, with both diffuse and spreading NETs evident (white arrows). ***B)*** *Ionomycin-induced NETs were smaller and well-demarcated, with fewer spreading NETs, compared to those induced by PMA.* ***C)*** *Neutrophils were untreated (i.e. control) or treated with PMA (at 10, 50 and 100 nM) and Ionomycin (Iono.) (at 1, 5 and 10 μM). NET formation was then quantified using ImageJ software to count the percentage of neutrophils undergoing NET formation. The percentage of NETed neutrophils present in each condition were: control wells 0.73 ± 1.0, PMA 10 nM 22.7 ± 7.6, PMA 50 nM 24.4 ± 15, PMA 100 nM 26.1 ± 9, Ionomycin 1 μM 33.5 ± 46.3, Ionomycin 5 μM 23.7 ± 17.5, Ionomycin 10 μM 44 ± 24.4.* ***D)*** *Quantification of the extent of NET formation when neutrophils were exposed to PMA as either adherent cells (i.e. "plated") or when cultured in suspension (i.e. "rolling"). Control wells had no significant NET formation in either plated or rolling culture. Analysis of the percentage of neutrophils undergoing NET formation in plated versus rolling culture by one-way ANOVA with Tukey's multiple comparisons test revealed a significant decrease in NET formation with rolling culture (p=0.03). Data represents individual points and mean ± SD. n=3 for all experiments.*

Figure 3.21

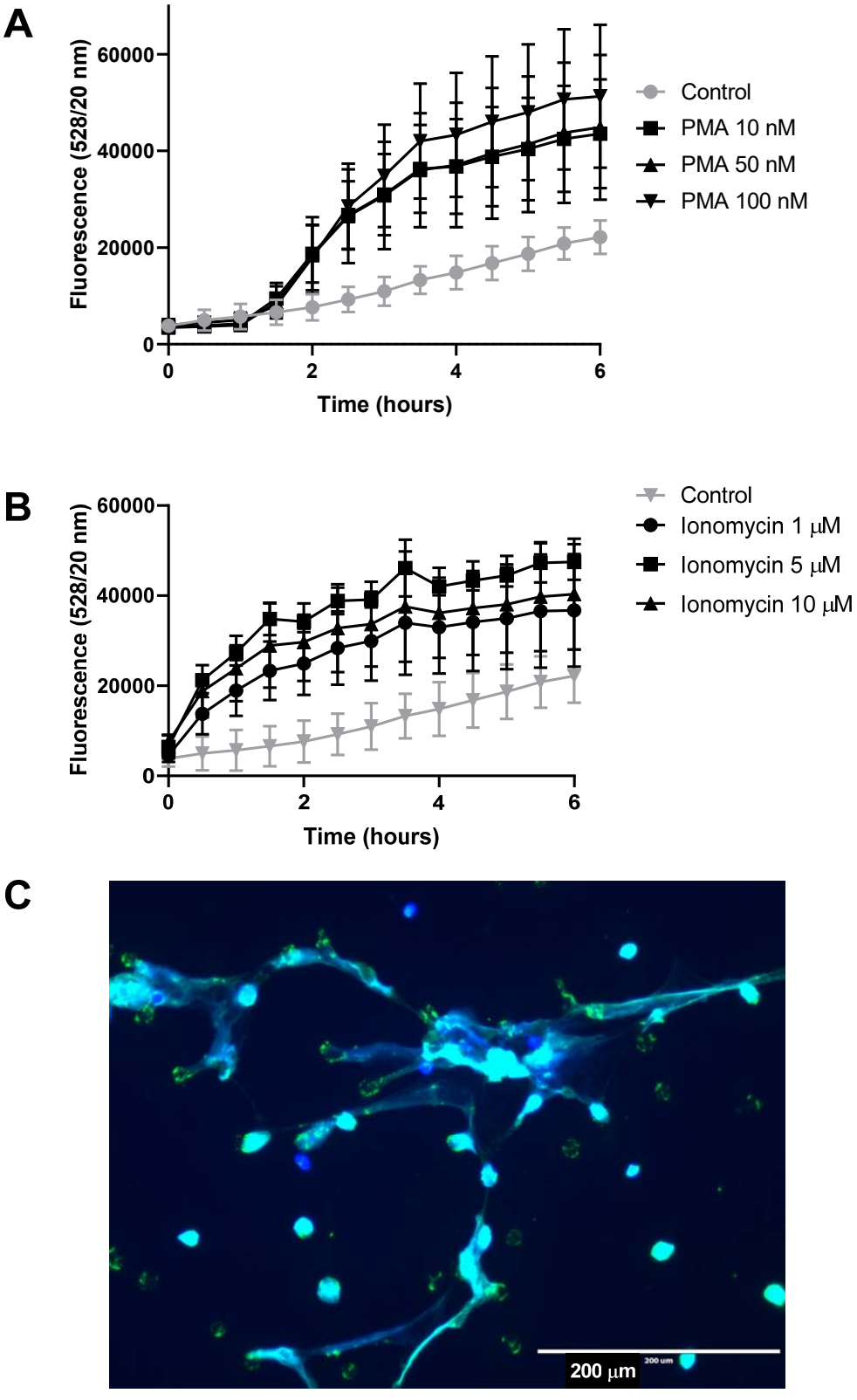
A
Fluorescence (528/20 nm)
60000
40000
20000
0
0
2
4
6
Time (hours)
Control
PMA 10 nM
PMA 50 nM
PMA 100 nM
B
Fluorescence (528/20 nm)
60000
40000
20000
0
0
2
4
6
Time (hours)
Control
Ionomycin 1 μM
Ionomycin 5 μM
Ionomycin 10 μM
C
200 μm

Figure 3.21: Quantification of DNA release by kinetic plate reader assay as a surrogate indicator of neutrophil extracellular trap (NET) formation. ***A)*** *Analysis of NET production in PMA treated cells versus control neutrophils by two-way ANOVA with Tukey's multiple comparisons test revealed significantly increased NET formation with PMA treatment (PMA 10 nM p=0.0006, PMA 50 nM p=0.0022, and PMA 100 nM p=0.0003).* ***B)*** *Analysis of NET production in ionomycin treated cells versus control neutrophils by two-way ANOVA with Tukey's multiple comparisons test showed significantly increased NET formation with ionomycin treatment (all concentrations, p<0.0001). Data represents mean ± SD.* ***C)*** *Neutrophils were stimulated with PMA 100 nM* in vitro *and NETs visualised using immunofluorescence. Co-localisation of Hoechst staining (blue) and antibodies against myeloperoxidase (green) implies NET formation.*

Figure 3.22

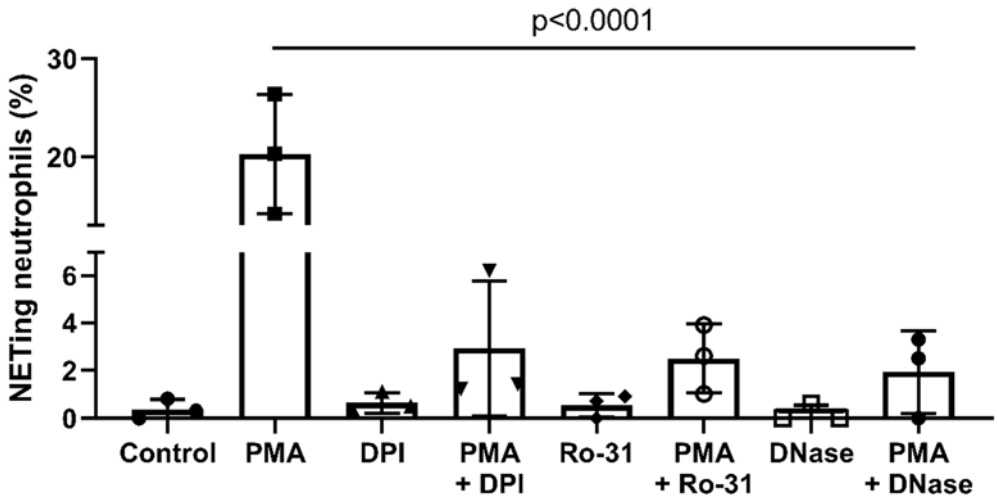

***Figure 3.22: Pharmacological inhibition of NET formation* in vitro.** *Neutrophils were cultured in suspension with PMA 100 nM and/or the inhibitors DPI, Ro-31-8220 and DNase, then plated and incubated for six hours. NET formation was visualised using SYTOX® green staining with fluorescence microscopy. ImageJ software was used to count the percentage of neutrophils undergoing NET formation. Analysis of the percentage of neutrophils undergoing NET formation by one-way ANOVA and Sidak's multiple comparisons test revealed that the most significant inhibition of NET formation was by DNase, p<0.0001. Data represents individual points and mean ± SD, n=3 for all experiments.*

3.8 Scanning electron microscopy revealed morphological differences between control and NETed neutrophils in co-culture with MDM

In order to investigate morphological differences between control neutrophils and NETing neutrophils, scanning electron microscopy was used alongside transmitted light microscopy during the co-culture experiments. Neutrophils were rolled in suspension for 15 min – half were control neutrophils and so were suspended in $HBSS^{-/-}$ only, whilst half were suspended in $HBSS^{-/-}$ and PMA to stimulate NET formation. These control/NETed neutrophils were subsequently co-cultured with MDM for 24 hours (in a ratio of 2:1 neutrophils to MDM). For the wells designated for scanning electron microscopy, cells were adhered to plastic Thermanox™ cover slips in wells of a 6-well plate, whilst those wells designated for investigation of supernatant cytokine levels simply had cells adhered to the base of the plastic wells. During the co-culture, cells were cultured in IMDM supplemented with 25mM HEPES and L-glutamine, 5% FCS and 1% Penicillin/Streptomycin. IMDM was selected because it is a highly enriched media suitable for rapidly proliferating, high-density cell cultures. The antibiotics were used to prevent bacterial infection of the MDM during their 7 days of culture. 5% FCS was used to maintain both neutrophils and MDM present and autologous serum was avoided for the co-culture because exposure to foreign autologous serum may have affected cell phenotypes, confounding results. Following co-culture of neutrophils/NETed neutrophils with MDM for 24 hours, in those cells destined for scanning electron microscopy experiments, Gluteraldehyde was applied as a fixative

then samples were processed ready for microscopy (see Chapter 2, section 2.3.11 for details of methodology).

Inspection of cell morphology using scanning electron microscopy revealed morphological differences between control neutrophils and NETing neutrophils and this was evident even using transmitted light microscopy at x20 magnification (Figure 3.23). Therefore, light microscopy was used after each co-culture experiment to confirm the NETs had been produced, where appropriate. Scanning electron microscopy revealed ultra-structures of the cell surfaces and NET-like extracellular strands were clearly visible (Figure 3.23C-E and Figure 3.24).

3.9 NETs were proinflammatory to MDM

Following the 24-hour co-culture between neutrophils/NETed neutrophils with MDM, supernatants were harvested and cytokine concentrations were quantified by ELISA. HC NETs were proinflammatory to CF MDM, causing an increase in IL-8 production after 24 hours of co-culture (Figure 3.25A). There was a similar trend in HC MDM but this failed to reach statistical significance (Figure 3.25B). Both HC and CF MDM had exaggerated IL-8 production in response to CF neutrophils/NETs, suggesting CF NETs are hyper-inflammatory relative to HC NETs (Figure 3.25). DNase treatment significantly

reduced IL-8 production from MDM in all co-culture combinations (Figure 3.25).

With regard to TNF-α production, CF MDM released more overall relative to HC MDM. However, sub-analysis of separate HC and CF MDM responses to co-culture with HC NETs revealed a trend for increased TNF-α production relative to those co-cultured with control neutrophils but this did not reach statistical significance (Figure 3.26A). DNase treatment significantly increased TNF-α production by CF MDM in response to HC NETs (Figures 3.26A). In the case of co-culturing with CF neutrophils/NETs, there was a trend for increased TNF-α production from MDM but this only reached statistical significance in the HC MDM group (Figure 3.26B).

IL-6 concentrations were low in all co-culture supernatants. However, a significant decrease in IL-6 production was noted when healthy MDM were co-cultured with CF control and NETed neutrophils (Figure 3.27B).

Finally, IL-10 was measured because it commonly functions as an anti-inflammatory cytokine. When HC and CF MDM were co-cultured with HC control neutrophils and NETs, there were significantly increased levels of IL-10 produced from CF MDM (Figure 3.28A). HC NETs were not, however, proinflammatory relative to control neutrophils (Figure 3.28A) to either HC or

CF MDM. Lastly, HC and CF MDM produced similar, albeit low levels, of IL-10 in response to CF neutrophils and NETs, with no significant differences between co-culture conditions (Figure 3.28B).

Figure 3.23

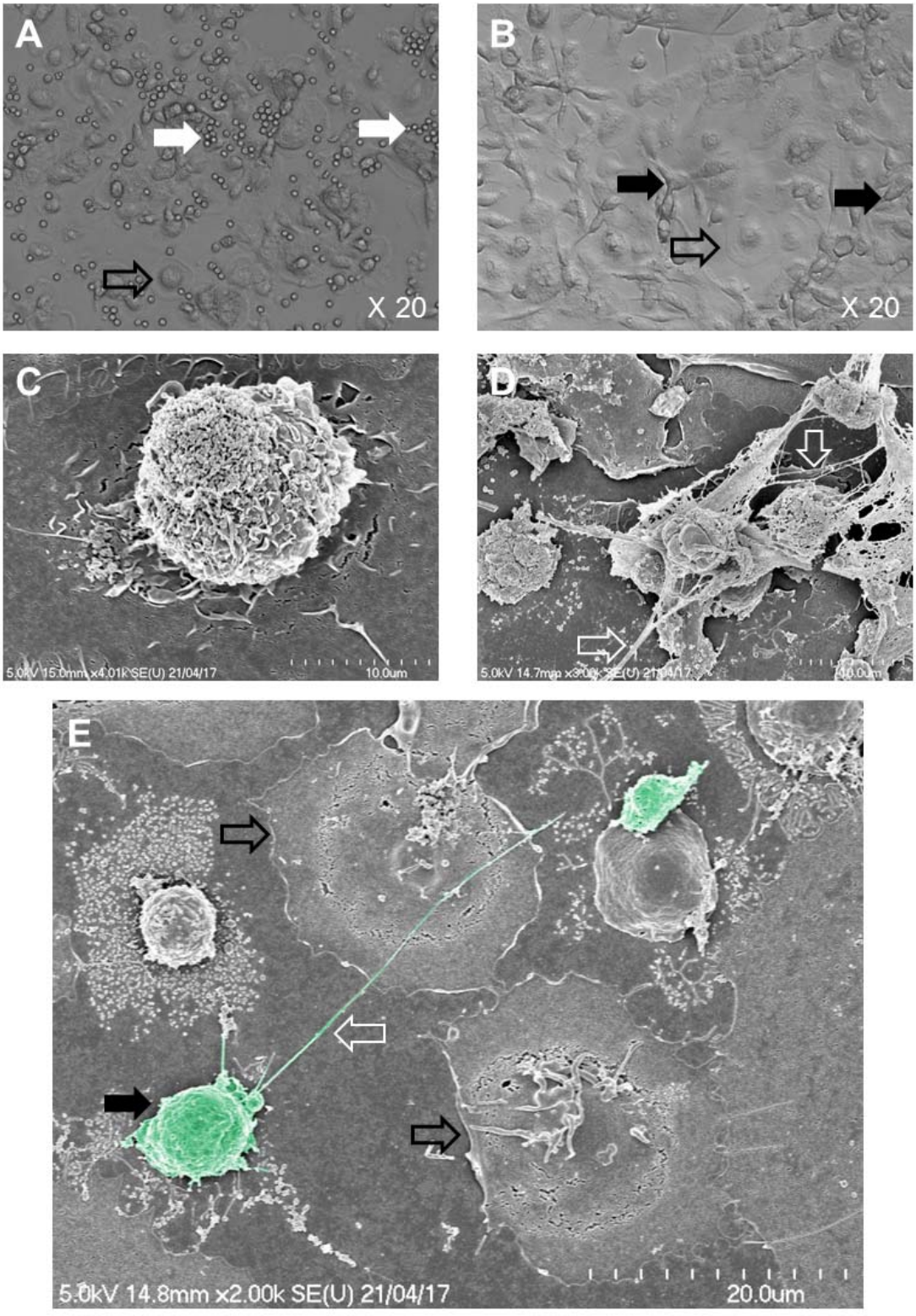

Figure 3.23: Scanning electron microscopy of the neutrophil/NETed neutrophil and monocyte-derived macrophage co-culture experiment. A) *Morphological differences exist between control and NETed neutrophils. Light microscopy showing control neutrophils (white arrows): small, round, well-demarcated cells, much smaller compared to adjacent MDM (clear black arrows).* ***B)*** *Light microscopy of NETed neutrophils (black arrows): larger and irregularly shaped in comparison to their control counterparts.* ***C)*** *scanning electron microscopy of a control neutrophil.* ***D)*** *scanning electron microscopy of NETed neutrophils with extracellular strands (clear white arrows), in-keeping with NETs.* ***E)*** *False-coloured image of the NET-MDM co-culture, showing a NETed neutrophil with an elongated extracellular strand.*

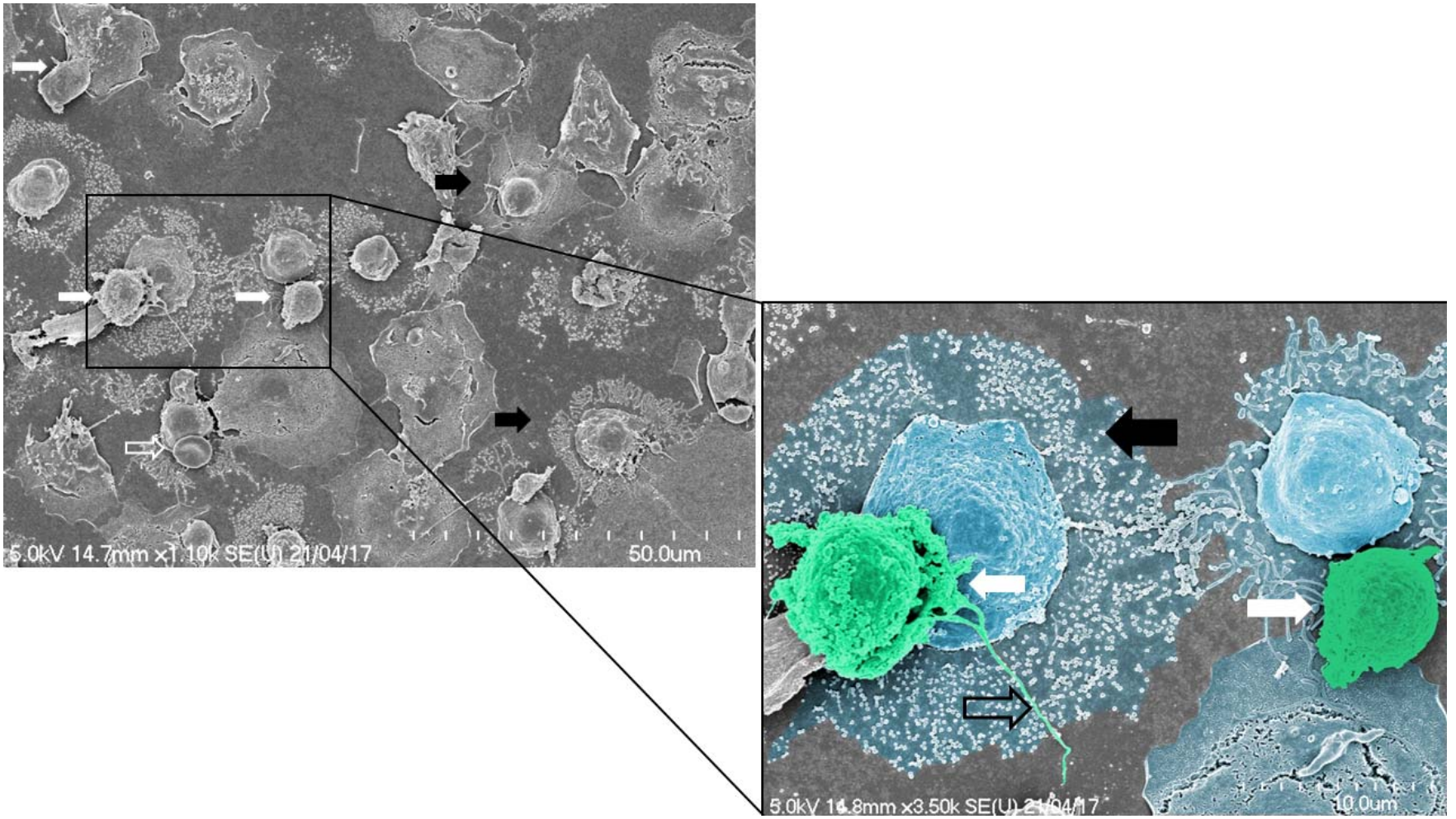
5.0kV 14.7mm x1.10k SE(U) 21/04/17
50.0um
5.0kV 14.8mm x3.50k SE(U) 21/04/17
10.0um

Figure 3.24

Figure 3.24: Scanning electron microscopy image of the co-culture between NETed neutrophils and monocyte-derived macrophages (MDM). *White arrows = NETed neutrophil; black arrows = MDM; clear white arrow = erythrocyte; clear black arrow = NET-like extracellular strand. In the false coloured image (right), the NETed neutrophils are shown in green whilst the MDM are shown in blue. Physical interactions between adjacent cells are evident and the cytoplasm of the MDM contains numerous, well demarcated rounded structures, which may be actin.*

Figure 3.25

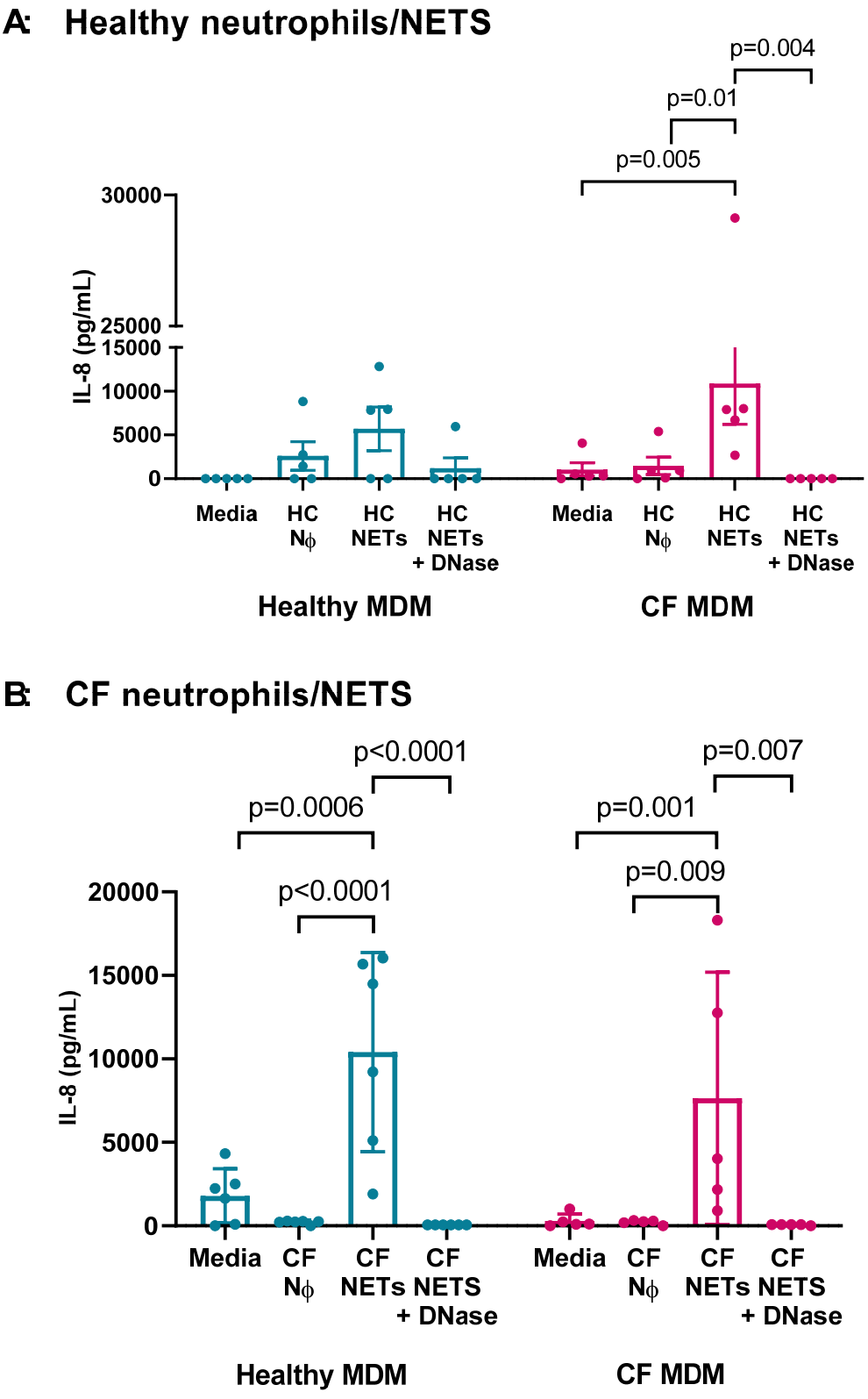
A: Healthy neutrophils/NETS
p=0.004
p=0.01
p=0.005
30000
25000
15000
10000
5000
0
IL-8 (pg/mL)
Media
HC Nϕ
HC NETs
HC NETs + DNase
Media
HC Nϕ
HC NETs
HC NETs + DNase
Healthy MDM
CF MDM
B: CF neutrophils/NETS
p<0.0001
p=0.0006
p<0.0001
p=0.007
p=0.001
p=0.009
20000
15000
10000
5000
0
IL-8 (pg/mL)
Media
CF Nϕ
CF NETs
CF NETS + DNase
Media
CF Nϕ
CF NETs
CF NETS + DNase
Healthy MDM
CF MDM

Figure 3.25: Quantification of supernatant IL-8 concentrations from the neutrophil/NETed neutrophil and monocyte-derived macrophage (MDM) co-culture experiments. *HC = healthy control (shown in blue), CF = cystic fibrosis (shown in pink), Nø = control neutrophil. Data represents individual data points and mean ± SD, n=5-6 per group. Neutrophil extracellular traps (NETs) increase IL-8 production by MDM and CF NETs exaggerate this effect.* ***A)*** *Analysis of supernatant IL-8 levels, when HC neutrophils/NETed neutrophils were co-cultured with either HC MDM or CF MDM, was performed using two-way ANOVA with Tukey's multiple comparisons test. This analysis revealed a significant increase in IL-8 levels when CF MDM are cultured with HC NETs, compared to CF MDM in media alone or cultured with control neutrophils ($p=0.005$ and $p=0.01$, respectively). Furthermore, DNase treatment caused a significant decrease in IL-8 levels where CF MDM were cultured with NETed neutrophils ($p=0.004$). Similar trends were seen for HC MDM but these failed to reach statistical significance.* ***B)*** *Analysis of supernatant IL-8 levels when CF neutrophils/NETed neutrophils were cultured with HC MDM, again by two-way ANOVA with Tukey's multiple comparisons test, revealed a significant increase in IL-8 levels when HC MDM were cultured with CF NETs versus those cultured in media alone or with control neutrophils. ($p=0.0006$ and $p<0.0001$, respectively). Similar, significant differences in supernatant IL-8 levels were found in CF neutrophil/NETed neutrophil and CF MDM co-culture. DNase treatment once again caused a significant decrease in IL-8 levels in HC and CF MDM ($p<0.0001$ and p-0.007, respectively).*

Figure 3.26

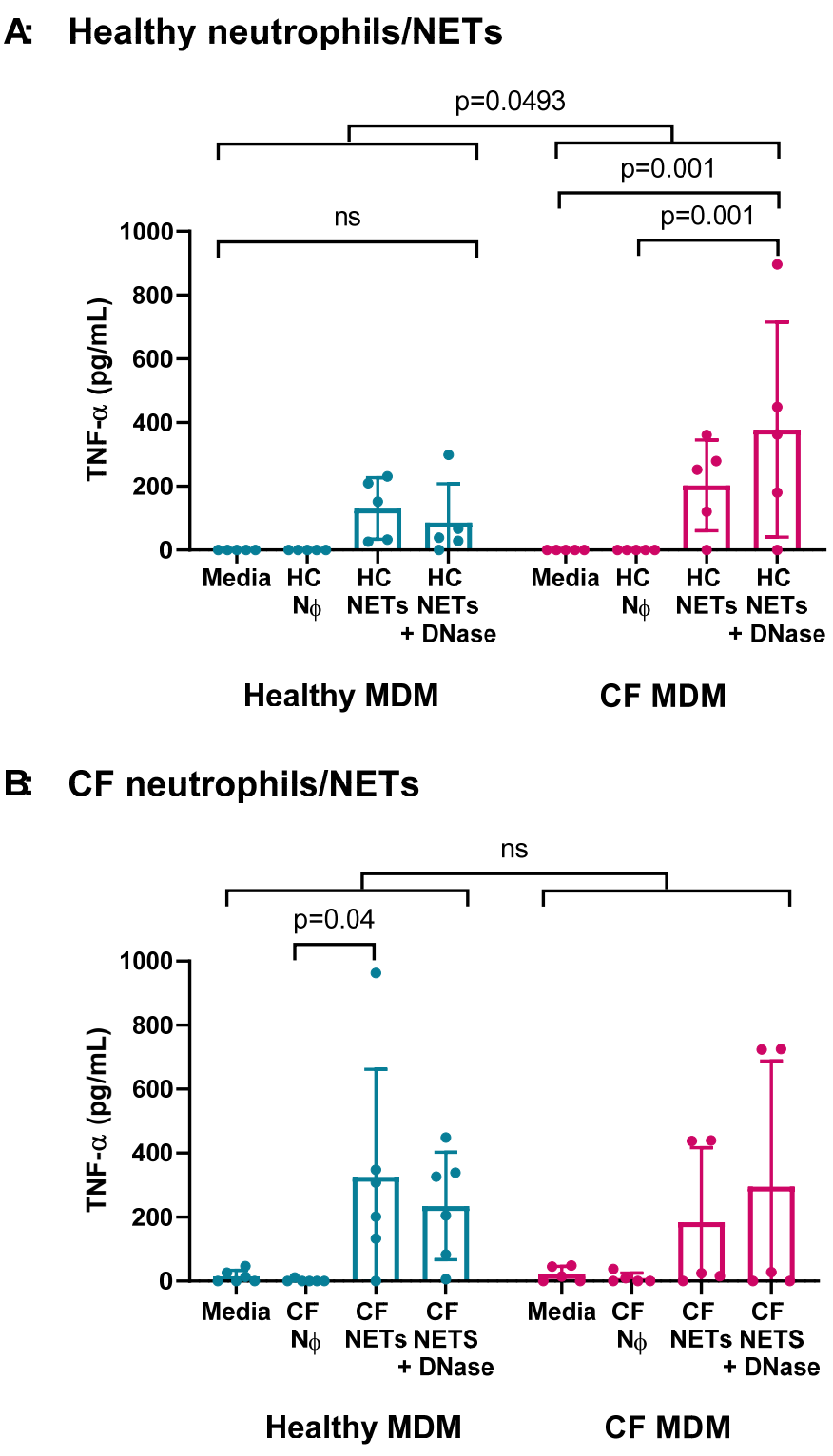
A: Healthy neutrophils/NETs
p=0.0493
p=0.001
ns
p=0.001
TNF-α (pg/mL)
1000
800
600
400
200
0
Media
HC Nϕ
HC NETs
HC NETs + DNase
Media
HC Nϕ
HC NETs
HC NETs + DNase
Healthy MDM
CF MDM
B: CF neutrophils/NETs
ns
p=0.04
TNF-α (pg/mL)
1000
800
600
400
200
0
Media
CF Nϕ
CF NETs
CF NETS + DNase
Media
CF Nϕ
CF NETs
CF NETS + DNase
Healthy MDM
CF MDM

Figure 3.26: Quantification of supernatant TNF-α concentrations from the neutrophil/NETed neutrophil and monocyte-derived macrophage (MDM) co-culture experiments. *HC = healthy control (shown in blue), CF = cystic fibrosis (shown in pink), Nø = control neutrophil. Data represents individual data points and mean ± SD, n=5-6 per group.* ***A)*** *Analysis of supernatant TNF-α levels produced by HC and CF MDM when co-cultured with HC neutrophils/NETed neutrophils by two-way ANOVA with Tukey's multiple comparisons test revealed that CF MDM produce significantly increased levels of TNF-α relative to HC MDM (p=0.0493). There were no significant differences in TNF-α levels from HC MDM between the different co-culture conditions. However, TNF-α levels were increased in CF MDM co-cultured with HC NETs in the presence of DNase, relative to CF MDM cultured alone or with HC control neutrophils (p=0.001 in both conditions).* ***B)*** *Analysis of supernatant TNF-α levels produced by HC and CF MDM when co-cultured with CF neutrophils/NETed neutrophils by two-way ANOVA with Tukey's multiple comparisons test revealed no significant difference in TNF-α production between genotypes. There were no significant differences in TNF-α levels from CF MDM when the different co-culture conditions were compared. With regard to TNF-α levels from HC MDM, statistical analysis revealed a significant increase in TNF-α levels when CF NETs were co-cultured with HC MDM versus control neutrophils (p=0.04). A similar trend was seen for CF MDM but this did not reach statistical significance.*

Figure 3.27

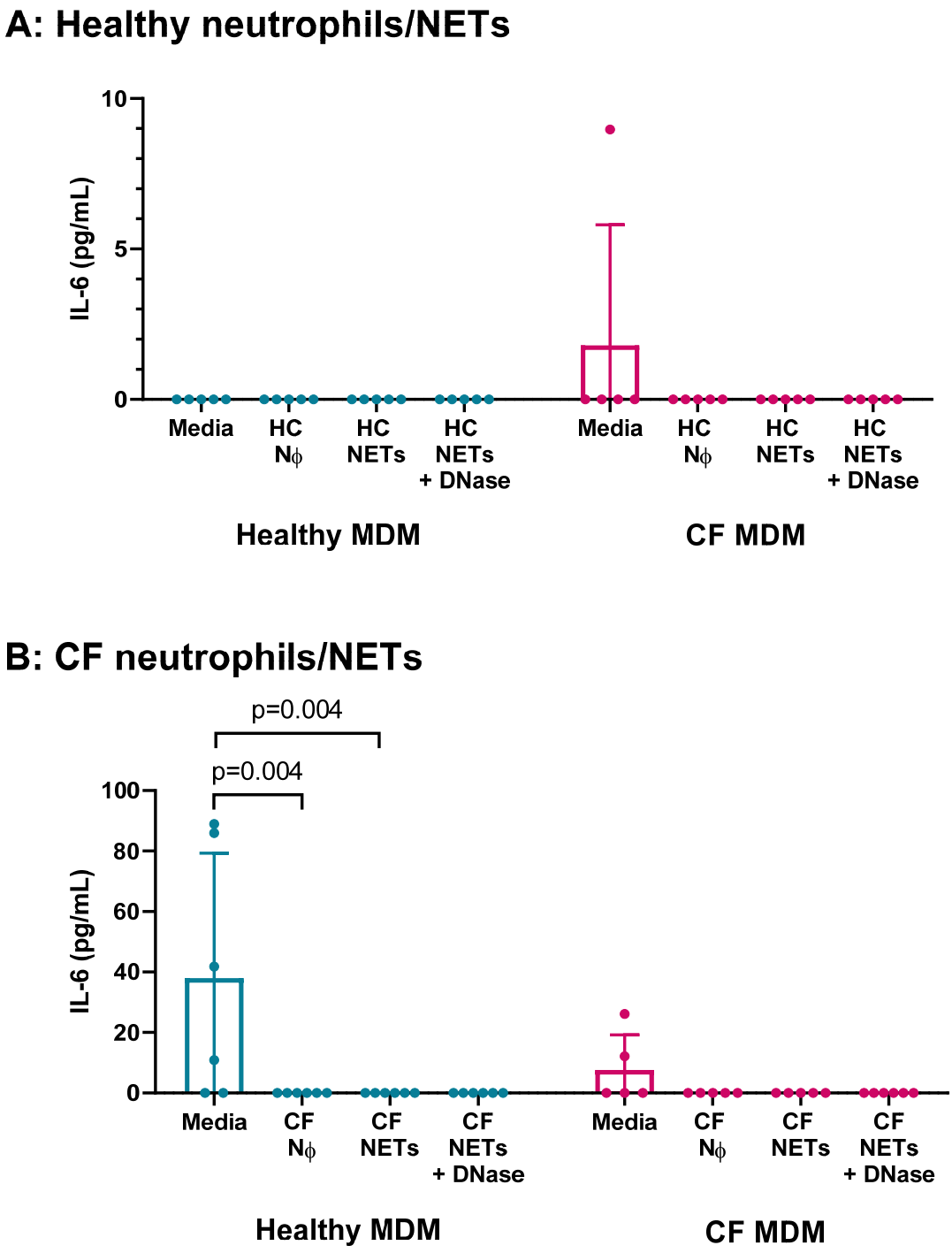
A: Healthy neutrophils/NETs
IL-6 (pg/mL)
10
5
0
Media
HC Nϕ
HC NETs
HC NETs + DNase
Media
HC Nϕ
HC NETs
HC NETs + DNase
Healthy MDM
CF MDM
B: CF neutrophils/NETs
p=0.004
p=0.004
IL-6 (pg/mL)
100
80
60
40
20
0
Media
CF Nϕ
CF NETs
CF NETs + DNase
Media
CF Nϕ
CF NETs
CF NETs + DNase
Healthy MDM
CF MDM

Figure 3.27: Quantification of supernatant IL-6 concentrations from the neutrophil/NETed neutrophil and monocyte-derived macrophage (MDM) co-culture experiments. *HC = healthy control (shown in blue), CF = cystic fibrosis (shown in pink), Nø = control neutrophil. Data represents individual data points and mean ± SD, n=5-6 per group. NETS do not induce an IL-6 response by either HC or CF MDM.* ***A)*** *There was no IL-6 production by HC MDM when co-cultured with HC neutrophils and NETs. The same was true for CF MDM, with the exception of one sample in which CF MDM were cultured in media alone.* ***B)*** *HC MDM cultured alone produce low levels of IL-6 (mean 37.9 pg/mL ± 41.3). Analysis of IL-6 levels by two-way ANOVA with Tukey's multiple comparisons test revealed a significant increase in IL-6 levels from HC MDM cultured alone versus those with CF control neutrophils or CF NETs (p=0.004 in both cases). No such difference existed in the co-culture conditions between CF neutrophils/NETs and CF MDM. DNase treatment did not affect IL-6 concentrations.*

Figure 3.28

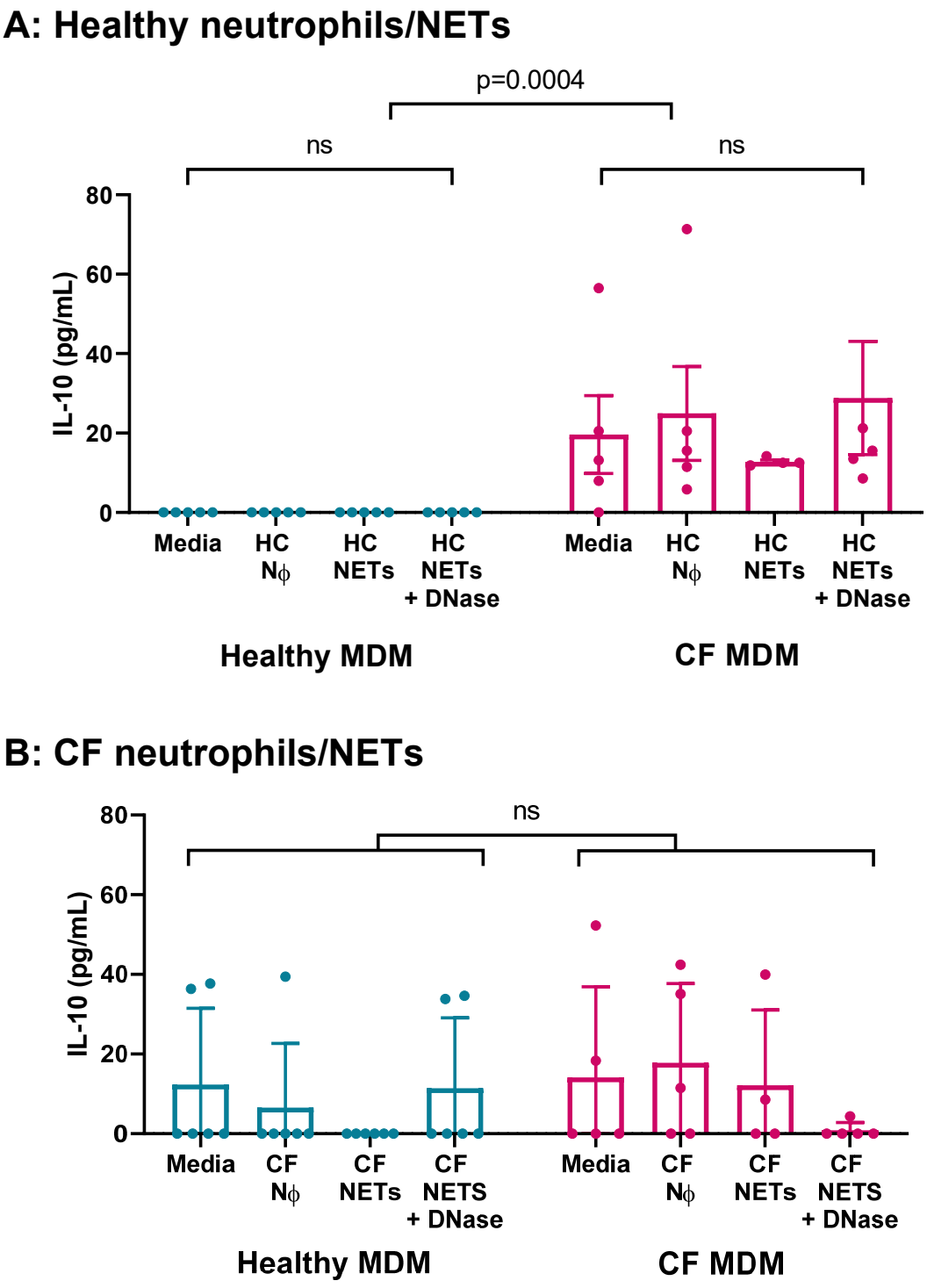
A: Healthy neutrophils/NETs
p=0.0004
ns
ns
IL-10 (pg/mL)
80
60
40
20
0
Media
HC Nϕ
HC NETs
HC NETs + DNase
Media
HC Nϕ
HC NETs
HC NETs + DNase
Healthy MDM
CF MDM
B: CF neutrophils/NETs
ns
IL-10 (pg/mL)
80
60
40
20
0
Media
CF Nϕ
CF NETs
CF NETS + DNase
Media
CF Nϕ
CF NETs
CF NETS + DNase
Healthy MDM
CF MDM

Figure 3.28: Quantification of supernatant IL-10 concentrations from the neutrophil/NETed neutrophil and monocyte-derived macrophage (MDM) co-culture experiments. *HC = healthy control (shown in blue), CF = cystic fibrosis (shown in pink), Nø = control neutrophil. Data represents individual data points and mean ± SD, n=5-6 per group.* ***A)*** *Analysis of IL-10 production by two-way ANOVA with Tukey's multiple comparisons test revealed an overall significant increase in IL-10 levels from CF MDM versus HC MDM (p=0.0004) but no differences between co-culture conditions when each genotype of MDM were analysed separately.* ***B)*** *There is no significant difference in IL-10 levels when HC and CF MDM were co-cultured with CF neutrophils/NETs. DNase does not affect IL-10 concentrations.*

Discussion

The data analysis in this chapter began with descriptive statistics of participant demographics. Although CF participants had poor lung function, they were systemically well, as indicated by their normal BMI. Indeed, the CF participants' median BMI was 22.5 kg/m^2 (where median male BMI was 23.2 kg/m^2 and female BMI was 21.4 kg/m^2). This suggests good practice by the participants' multi-disciplinary care team because for adults with CF, better lung function is associated with higher BMI(195); nutritional advice and interventions should be targeted at sustaining a BMI of 22 kg/m^2 in women and 23 kg/m^2 in men(196).

I next interrogated variations between HC and CF participants' sputum cell pellet differential cell counts. This was important to address the fundamental question of whether there might simply be more NETs in CF sputum than HC sputum because the former is characterised by neutrophilic infiltration of the airways. In agreement with the existing literature(192), it was found that CF sputum contained predominantly neutrophils whereas HC sputum had a variety of cell types present, the most numerous of which being the macrophage. Furthermore, light microscopy revealed that the CF sputum neutrophils differ morphologically when compared to HC counterparts, the former containing significantly more cytoplasmic vacuolations, many of which appeared to contain bacteria. This abnormality may reflect impaired phagocytosis in CF neutrophils. This would be in agreement with a previous

study by Morris *et al.* who showed that pulmonary neutrophils from patients with CF had a reduced phagocytic capacity for C3bi-opsonised Zymosan(197). They suggested that impaired phagocytic capacity was due to abnormal lung environment in CF or dysfunctional priming on neutrophil migration into the airway, rather than it being an intrinsic defect due to absent/dysfunctional CFTR(197). Investigation of whether phagocytosis is impaired in CF neutrophils was beyond the remit of this PhD but would be of interest for future research. Airway neutrophils could be isolated from BAL and cultured with an enhanced green fluorescent bacteria, such as *P.aeruginosa* or *S.aureus,* then both phagocytic capacity and subsequent bacterial degradation could be assessed by flow cytometry(198). Alternatively, or in addition to impaired phagocytosis, the vacuolations seen in CF neutrophils may be associated with abnormal autophagy. This is the process whereby aged portions of the cytosol are appropriated and broken down within double-membrane-bound vesicles termed autophagosomes, which also plays an important role in the killing of microorganisms by innate immune cells and is impaired in CF(199). Fluorescence microscopy could be used in CF and non-CF airway neutrophils to image autophagy markers such as microtubule-associated proteins 1A/1B light chain 3B (LC3) and lysosomal markers (e.g. LAMP-1/2 or LIMP-II).

In order to address the question of whether there are simply more NETs in CF sputum because it is a disease characterised by neutrophilic infiltration of the airways, I examined whether there was a correlation between neutrophils per

gram of sputum and sputum NETs. No significant correlation existed, which supports the suggestion that there is an intrinsic propensity for CF neutrophils to undergo NET formation, in agreement with recently-published data from our group(70).

Indeed, the data in this chapter confirm that CF sputum contains significantly higher levels of NETs than HC sputum and NETs are significantly associated with airway inflammation and decline in lung function in CF lung disease, in agreement with previous studies(94,180). Our ELISA was used to quantify NETs and it may be preferable to the PicoGreen® assay for two reasons. Firstly, because the ELISA detects histone-bound calprotectin it specifically enables measurement of NET-DNA as opposed to DNA from bacteria, which typically does not contain histones. Secondly, the ELISA demonstrates co-localisation between NET constituents, which is a key requirement of any *in vitro* assay measuring NETs(103). Using the ELISA, it was found that sputum NET levels were significantly lower in those CF participants treated with once daily DNase (Pulmozyme®) compared to those not on this therapy, which strengthens the conviction that the assay is a measure of NETs, since they should be cleared from the airways by DNase. Conversely, it is possible that DNase simply disrupts the association between histones and calprotectin.

To confirm that our NET ELISA results were in line with other indirect measures of NETs, MPO activity, dsDNA and NE assays were performed. Each of these

outputs were significantly higher in CF sputum relative to HC sputum and had significant positive correlations with NETs and significant negative correlations with lung function. Increased MPO and NE activity in the sputum implicates neutrophilic inflammation in the disease pathophysiology, as these can be released via degranulation and NET formation. When FEV_1 was predicted using the multivariate linear regression modelling, MPO activity, dsDNA levels and NE were not significant independent predictors of FEV_1, whereas sputum NET levels were and strengthened the model overall, as shown by an increase in its modified R^2 value. We conclude that our assay, which measured co-localisation between NET constituents, may be superior to these indirect measures of NETs.

CF sputum had increased levels of IL-8, TNF-α and calprotectin, relative to HC sputum. These cytokines are especially important for neutrophil chemotaxis and migration(109), which would occur during a CF exacerbation. However, all sputum samples were taken from non-exacerbating CF participants and so results are reflective of stable disease. These data suggest CF patients have chronic inflammation, even when not suffering infective exacerbations. IL-8 has previously been used as a biomarker for CF(200–202),but we found no significant negative correlation with $ppFEV_1$. This suggests sputum IL-8 is of limited use as a biomarker, in agreement with other studies which have shown that it does not always change during exacerbations(114,203). Interestingly, IL-6 was significantly lower in CF sputum compared to HC sputum, which has

been reported elsewhere(204); this altered regulation of IL-6 may contribute to the impaired resolution of the acute phase response and neutrophilia that typifies CF lung disease. It also lends support to the hypothesis that in certain contexts, IL-6 functions as an anti-inflammatory cytokine(186). When correlating these cytokines with sputum NETs, it was found that only IL-8 had a significant positive correlation with NETs, perhaps unsurprising since it plays a key role in neutrophil recruitment. Calprotectin, a protein which is highly abundant in neutrophils and activates macrophages via TLR-4(205), has been proposed as a biomarker for CF by our group(114). The data in this chapter support that viewpoint because calprotectin most strongly correlated with sputum NETs (more so than sputum IL-8 levels) and was the only proinflammatory protein measured which had a significant negative correlation with lung function. Multi-variate linear regression was finally used to determine the interplay between NETs and lung function; when FEV_1 was predicted, it was found that sputum NETs was an independent, significant predictor (alongside the number of exacerbations in 12 months, sputum neutrophils per gram, sex and age). To conclude, the data in this chapter have confirmed that NETs are associated with airway inflammation and predict FEV_1. However, the underlying mechanisms have not been fully resolved.

To investigate the antimicrobial association of sputum NETs, it was hypothesised that those CF participants colonised with *P.aeruginosa* would have higher levels of NETs in their sputum, since this organism is known to be

a potent activator of NET formation(89), but this was not the case when data was analysed. NETs are suited to degrading large microorganisms such as fungal hyphae which are too large to be phagocytosed and Marcos *et al.* found that airway NETs correlated with *A.fumigatus* colonisation(94). However, in our CF cohort sputum NET levels were unaffected by *A.fumigatus* colonisation. These findings support the view that NETs are proinflammatory and damaging in CF, rather than acting as effective antimicrobial mediators.

In order to try to elucidate mechanisms by which NETs were proinflammatory, an *in vitro* co-culture model was utilised, based on one previously used by our group(70). Preliminary experiments were carried out to stimulate and quantify NET formation, which found that PMA was more effective than ionomycin at inducing NET formation. Exposure of neutrophils to PMA resulted in NETs which were diffuse and spreading in appearance, characteristic features of *in vitro* NETs(61). Ionomycin on the other hand produced small, well-demarcated cells when visualised using SYTOX® Green, more characteristic of apoptotic cells. We did not assess neutrophil apoptosis rates; however, this could be addressed in future NET assay experiments by flow cytometry using annexin-V in combination with propidium iodide (PI) and morphological assessment of apoptotic changes by light microscopy of H&E stained cytocentrifuged neutrophils. Approximately 50% neutrophils NETed in response to culture with 100 nM PMA and this dropped to ~20% after rolling culture. However, the latter method was selected because it permitted washing of neutrophils to

remove any residual PMA, which may have adversely affected the MDM in the co-culture model. I did not investigate the potential effects PMA has on MDM. This is a question which could be addressed in future experiments by culturing them in IMDM supplemented with varying concentrations of PMA then assessing cell morphology and ability to secrete IL-8 in response to NETs and another inflammatory stimulus (e.g. LPS).

HC and CF control neutrophils and NETed neutrophils were co-cultured with HC and CF MDM for 24 hours in various combinations (see Figures 3.23 – 3.28). HC NETs stimulated IL-8 production by CF MDM, in agreement with previous experiments(70) and CF NETs exaggerated this effect; indeed when CF NETs were used, HC MDM also produced significantly increased levels of IL-8. This implies firstly that NETs produced by CF neutrophils are hyper-inflammatory relative to HC NETs and secondly that CF MDM are hyper-responsive relative to HC MDM. The underlying reasons for this are unclear. Intrinsic abnormalities in $CFTR^{-/-}$ neutrophils and macrophages do exist, but none directly pertaining to NET formation(66), although the Gray group has previously shown that CF neutrophils form more NETs over time(70). CF macrophages have significantly higher levels of TLR-4 on their plasma membranes(132) and so it may be that the calprotectin present on NETs activates macrophages to produce higher amounts of proinflammatory cytokines. To address this suggestion, measurement of TLR-4 protein and RNA expression from co-culture cell lysates would be of interest for future

research. DNase treatment rescued the proinflammatory MDM phenotype, significantly reducing IL-8 production in all co-culture combinations and this might contribute to the drug's anti-inflammatory properties(37). It may be that degradation of NETs by DNase facilitated their uptake by MDM into phagolysosomes. Phagocytosis of NETs is one mechanism by which NETs are cleared from the airways and does not result in proinflammatory cytokine secretion(206).

Regarding TNF-α, CF MDM produced more of this proinflammatory cytokine compared to HC MDM overall and sub-analysis revealed increased levels in response to CF NETs versus control neutrophils in the HC MDM group. However, TNF-α concentration did not differ between co-culture conditions to the same extent as IL-8, suggesting different cell signalling pathways govern the production of these two cytokines in response to NETs. DNase treatment increases TNF-α production by CF MDM, perhaps because fragmentation of the DNA increases the release of the NET constituent proinflammatory proteins.

In agreement with the sputum cytokine data, MDM did not produce IL-6 in response to NETs, suggesting it does not play a key role in the mechanism by which NETs are proinflammatory in CF lung disease.

Finally, IL-10 is a cytokine which has been described as anti-inflammatory in the context of CF(207,208). CF MDM produced higher baseline IL-10 levels than HC MDM, but this effect was not increased due to co-culture with NETs.

During the co-culture experiments, I only investigated the 24 hour time point. It may be that if supernatants had been harvested over a time course, the levels of proinflammatory cytokines would vary. In addition, the model studied only the co-culture between neutrophils/NETs and MDM. To mimic better the CF lung, in which inflammation is driven by infection with Gram-negative bacteria such as *P.aeruginosa,* the co-culture model could have a second stimulus added, such as LPS or live bacteria. I hypothesise this would result in a further exaggeration of proinflammatory cytokine release by the MDM. Given that the macrophages used were monocyte-derived macrophages, it is unlikely that they had any exposure to bacteria (unlike alveolar macrophages) and so the hyper-activation of the CF macrophage is likely to be due to an intrinsic defect.

The data in this chapter supports our hypothesis that NETs accumulate in CF airways and are associated with inflammation and increased severity of lung disease. Furthermore, we have shown that NETs are proinflammatory to MDM and this response is exaggerated in CF MDM.

Chapter 4: Examination of the acute inflammatory response in CFTR$^{-/-}$ mice

Background

The data discussed in the previous chapter suggest that the presence of NETs in the airways is associated with airways inflammation and increased severity of CF lung disease in our patient cohort. These findings led to the question of whether a mouse model of CF could be utilised to elucidate further the mechanisms by which NETs cause inflammation in CF lung disease and assess whether clearing NETs from the airways reduces inflammation.

The *Cftr*^{tm1Unc}Tg(FABPCFTR)1Jaw/J mice (Charles River Laboratories Ltd., UK) were used in the CF mouse models in this chapter. The characterisation of the mice have been described previously(172). In brief, these bi-transgenic mice have both the FABP-hCFTR transgene (human fatty acid binding protein 1 liver (*FABP1*) promoter directing expression of a human cystic fibrosis transmembrane conductance regulator (ATP-binding cassette sub-family C, member 7) (*CFTR*) gene) *and* a targeted mutation of the cystic fibrosis transmembrane conductance regulator homolog gene (*Cftr*^{tm1Unc}). The first transgene corrects the lethal gut phenotype typical of CFTR knockout mice (i.e. they usually die within 40 days due to intestinal obstruction, with or without perforation and resultant peritonitis(209)). This bi-transgenic model allows

mice to have normal gut function whilst ensuring little or no CFTR expression in the airways. Various other CF mouse models have been used previously to investigate the pathophysiology of CF lung disease(210). Of relevance to this thesis, previous studies by other groups have demonstrated that CF mice have an exaggerated response to both sterile and bacterial-induced inflammation. For example, Su *et al.* exposed CD1 wild-type (WT) and F508del-CF mice (the latter back-crossed into a CD1 genetic background (>eight generations)) to intratracheal LPS and culled the animals at 24 hours then performed BAL. Neutrophils within the BAL were positively stained by anti-CFTR antibody (showing that these activated neutrophils express CFTR). The *CFTR* knockout mice had increased production of proinflammatory cytokines by activation of NF-κB, and worsened LPS-induced acute lung inflammation and damage 24 hours following LPS(211). Similarly, Bonfield *et al.* subjected WT, whole body *CFTR* KO and myeloid-specific *CFTR* KO mice to infection using *P.aeruginosa*-laden agarose beads instilled into their right main bronchi with culls performed at three and 10 days. Myeloid-specific *CFTR* KO was achieved crossing a LysM promoter-driven Cre recombinase transgene into a "floxed" *CFTR* line carrying a *CFTR* allele with LoxP sites flanking exon 10(19). Both whole-body and myeloid-specific *CFTR* KO resulted in increased lung damage at day 10 as demonstrated by increased erythema and nodularity on macroscopic examination, BAL neutrophilia, elevated BAL proinflammatory cytokines (including IL-1β, IL-6 and monocyte chemoattractant protein-1 (MCP-1) at both days three and 10) and reduced survival(19). The myeloid-specific *CFTR* KO mice had an intermediate severity phenotype, indicating that

myeloid-derived innate immune cells play a crucial role in the pathophysiology of CF lung disease.

Existing literature therefore shows that CF mouse models are important tools with which to study dysfunctional innate immunity in the context of CF. I chose to examine LPS-mediated acute lung injury throughout the animal experiments of this thesis. Mice were nebulised with LPS from *P.aeruginosa* (serotype *10*). LPS is a principal constituent of the outer membrane of gram-negative bacteria, it is an established TLR-4 agonist, induces neutrophil-driven inflammation and some groups report that it stimulates NET formation both *in vitro* and *in vivo*(108,212–214). LPS is comprised of three principal structural parts: lipid A, a core domain containing an oligosaccharide component, and a repetitive polysaccharide, known as the O-antigen(215). Pieterse *et al*. demonstrated that LPS induces NET formation and the type of NETs produced *in vitro* in response to LPS depends upon culture conditions and the bacterial source of LPS – in serum- and platelet-free culture, only LPS from *E.coli O128:B12 and P.aeruginosa 10* induced "suicidal" NETs in an autophagy and ROS-dependent but TLR-4-independent manner(212). The authors speculated that this was because these two bacteria are able to evade killing by phagocytosis, *P.aeruginosa* through the formation of biofilms and *E.coli O128:B12* due to the sugar composition of its O-antigen(212) and therefore NET formation provided neutrophils with an alternative bactericidal mechanism. Conversely, in the presence of platelets *in vitro* and in whole

blood cultures *ex vivo*, all LPS serotypes stimulated "vital" NETosis, independent from ROS formation and autophagy but requiring platelet-TLR4 and CD62P-dependent platelet–neutrophil interactions(212). In agreement with Pieterse *et al.'s* findings, Clark *et al.* found that *in vitro*, NETs only formed in the presence of both LPS and platelets(216). However, the molecular mechanisms responsible for CD62P-induced NET formation remain unknown. It follows that for our *in vivo* model, the use of LPS from *P.aeruginosa (*serotype *10)* should be appropriate to induce NET formation. I chose to induce inflammation using LPS as opposed to an infection model because it allowed elucidation of any NET-associated phenotype, without the confounding factors of possible defects in bacterial killing caused by absence of CFTR in innate immune cells. This model produces consistent and reproducible neutrophil-dominated lung inflammation and so mimics the inflammation seen in early CF lung disease, prior to bacterial colonisation.

Previous murine, pig and human CF models have implicated macrophages in the production of damaging proinflammatory cytokines in response to LPS. Bruscia *et al.* demonstrated that CFTR$^{-/-}$ murine macrophages have higher basal levels of macrophages in their BAL compared to WT mice at 0 hours following a nebulised LPS challenge(217). CF murine macrophages also produced increased levels of IL-6, IL-1α, G-CSF and MCP-1 over 24 hours following stimulation with LPS *in vitro* whilst cytokine levels in heterozygote animals were intermediate between CF and WT values(217). Furthermore,

Paemka *et al.* used an *ex vivo* CF pig model to demonstrate that macrophages from newborn CF pigs have an absence of functional CFTR and exhibit an increased inflammatory response to an LPS challenge(21). In this study, PBMC were isolated from whole blood then adherent cells were differentiated in IMDM supplemented with foetal bovine serum, Pen/Strep and M-CSF for 6 days. Resultant CF pig MDM produced significantly more IL-8 and TNF-α in response to 200 ng/mL LPS relative to non-CF pigs(21). The authors suggested that an intrinsic defect in the CF macrophage was responsible for the hyper-responsive phenotype, since it occurred in newborn animals, which were yet to develop inflammatory lung disease(21). They speculated that M1 macrophage polarisation might cause this intrinsic defect(21) but did not investigate this at a mechanistic level. With regard to possible mechanisms underlying development of human disease, addition of NETs to HC and CF human MDM resulted in the induction of IL-8 and TNF-α production after 24 hours' co-culture and this cytokine response was heightened in CF MDM compared to HC MDM, although the method of control of cytokine production was not defined(70). Data presented in Chapter 3, which details a co-culture experiment between HC and CF control/NETed neutrophils and MDM in various combinations, corroborates and builds upon these findings. Therefore, to assess innate immune cell function (by which we infer this to be macrophage function) proinflammatory cytokine levels within BALF were measured at 24 and 72 hours post-LPS challenge as the output for the CF mouse model experiments. To investigate whether clearing NETs would reduce inflammation seen in the CF mouse, nebulised DNase therapy was

administered at 12 hours' post-LPS nebulisation to half of the animals of each genotype. DNase was selected for two reasons: firstly, data from Chapter 3 show that DNase was the most effective inhibitor of NET formation *in vitro* (see Figure 3.17). Secondly, DNase is an established treatment for CF patients (see Chapter 1 and 3). Experiments designed to assess the impact of DNase treatment on proinflammatory cytokine production would provide insight into potential anti-inflammatory mechanisms of actions.

Hypotheses and Aims

It was hypothesised that there would be increased levels of NETs in the CF mouse lung and consequently more severe inflammation compared to WT littermates. Furthermore, DNase treatment would be predicted to normalise levels of NETs, BALF proinflammatory cytokine levels and lung inflammation scores in CF mice in line with levels seen in WT littermates. The aims of these experiments were:

1) To determine whether NET formation and associated inflammation are increased in *Cftr*^{tm1Unc}Tg(FABPCFTR)1Jaw/J mice in comparison to WT littermates following a sterile inflammatory challenge using nebulised lipopolysaccharide from *P.aeruginosa* (serotype *10*).

2) To investigate whether nebulised DNase treatment clears NETs and reduces inflammatory indices in the *Cftr*^{tm1Unc}Tg(FABPCFTR)1Jaw/J mice and WT littermates.

Results

4.1 Characterisation of LPS-induced acute lung inflammation in mice

Preliminary experiments in C57BL/6 mice nebulised with PBS or LPS were used to determine when peak and resolution of inflammation occurred. Peak inflammation was defined as the time point at which BAL neutrophil counts, BAL IL-6 levels (because it is a key cytokine in the acute phase response) and semi-quantitative scoring of acute lung injury (including inflammatory cell infiltration of the alveoli) on histology sections were at their maximum. Resolution of inflammation was defined as the time point at which these parameters returned to baseline levels (i.e. the levels observed in the zero hour time point mice). These experiments revealed that peak inflammation occurs at 24 hours following LPS-mediated acute lung injury, with subsequent resolution after 72 hours. This was assessed using three parameters: BALF differential cell counts, semi-quantitative scoring of acute lung inflammation on H&E stained lung sections, and quantification of BALF supernatant IL-6 levels. With regard to the semi-quantitative scoring of H&E stained lung sections, four parameters were scored: vascular congestion, thickness of the interalveolar septa (indicative of oedema), inflammatory cell infiltration, and haemorrhage. There was a significant increase in total cell count and neutrophil counts in BALF at 24, 48 and 72 hours post-LPS (Figure 4.1A and B). Macrophage numbers did not differ between groups until 72 hours post-LPS (Figure 4.1C), which accounted for the differences seen in total cell count at that time-point, suggesting that macrophages play a key role in resolution of inflammation. In

agreement with these data, a semi-quantitative score of acute lung inflammation demonstrated peak damage at 24 hours post-LPS, largely resolved by 72 hours (Figures 4.2 and 4.3). This may imply that damage is neutrophil dependent, since BALF neutrophils also peak at 24 hours post-LPS. Resolution of this neutrophil-driven inflammation begins by 48 hours post-LPS because neutrophil numbers and lung inflammation scores are falling by this time point. In addition to the histological changes seen, analysis of the BALF supernatant revealed significantly elevated levels of IL-6 24 hours post-LPS, which had returned to baseline by 72 hours (Figure 4.4). These data informed the CF mouse model experiments – samples were collected at 24 and 72 hours post-LPS in order to quantify levels of NETs and inflammatory parameters at peak and resolution of inflammation.

Figure 4.1

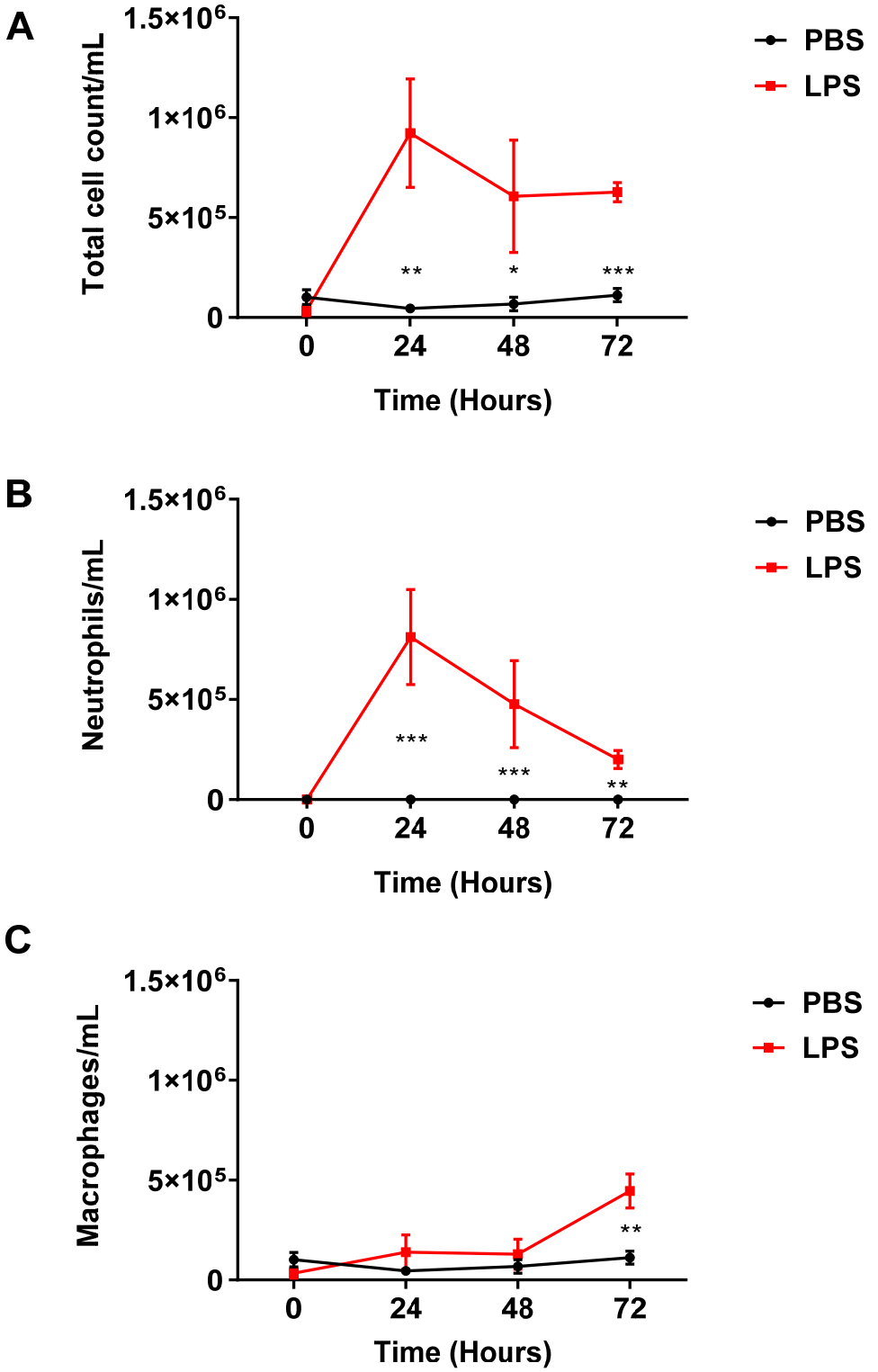
A
Total cell count/mL
1.5×10⁶
1×10⁶
5×10⁵
0
**
*
***
0
24
48
72
Time (Hours)
PBS
LPS
B
Neutrophils/mL
1.5×10⁶
1×10⁶
5×10⁵
0
***
***
**
0
24
48
72
Time (Hours)
PBS
LPS
C
Macrophages/mL
1.5×10⁶
1×10⁶
5×10⁵
0
**
0
24
48
72
Time (Hours)
PBS
LPS

Figure 4.1: Neutrophilic inflammation peaks 24 hours after lipopolysaccharide (LPS)-mediated lung injury. *C57BL/6 mice were treated with nebulised LPS or PBS. Bronchoalveolar lavage samples were analysed for total cell counts and macrophage and neutrophil counts. Data represents mean ± SD. Data analysed by multiple* t-*tests with the Holm-Sidak adjustment for multiple comparisons to compare cell counts between PBS and LPS treated groups. n=4 per group per time point. *** p<0.001. ** p<0.01, * p<0.05.* ***A)*** *Total cell count/mL peaks 24 hours post-LPS and remains elevated even at 72 hours.* ***B)*** *Neutrophils/mL also peaks at 24 hours post-LPS and has almost normalised by 72 hours.* ***C)*** *Macrophages/mL does not significantly differ between groups until 72 hours post-LPS. PBS did not affect BALF cell counts (**A-C**).*

In order to compare cell counts obtained at the different time points, two-way ANOVA with Sidak's multiple comparisons test was used. There were no significant differences in the PBS group BALF total cell counts across the time course. The LPS treated group had significantly higher total cell counts at 24, 48 and 72 hours post-LPS vs. zero hours (p>0.0001, p=0.0002 and p=0.0001), and at 48 and 72 hours vs. 24 hours (p=0.02 and p=0.04, respectively). There was no significant difference in total cell count in the LPS treated group at 72 vs. 48 hours (p=0.997). BALF neutrophils per mL did not significantly differ over time in the PBS treated group. The LPS treated group had significantly increased neutrophils per mL at 24 vs. 0 hours (p<0.0001) 48 vs. 0 hours (p<0.0001) but not at 72 hours (p=0.12). The LPS treated group had significantly increased neutrophils per mL at 48 vs. 24 hours (p=0.002), 72 vs. 24 hours (p<0.0001) and 72 vs. 48 hours (p=0.01). BALF macrophages per mL did not significantly differ over time in the PBS treated group. The LPS treated group had significantly increased macrophages per mL at 72 vs. zero hours, 72 vs. 24 hours, and 72 vs. 48 hours (all p<0.0001). There was no significant difference in the LPS treated group BALF macrophages per mL at 24 and 48 hours vs. zero hours (p=0.13 and p=0.21, respectively) or at 48 vs. 24 hours (p>0.99).

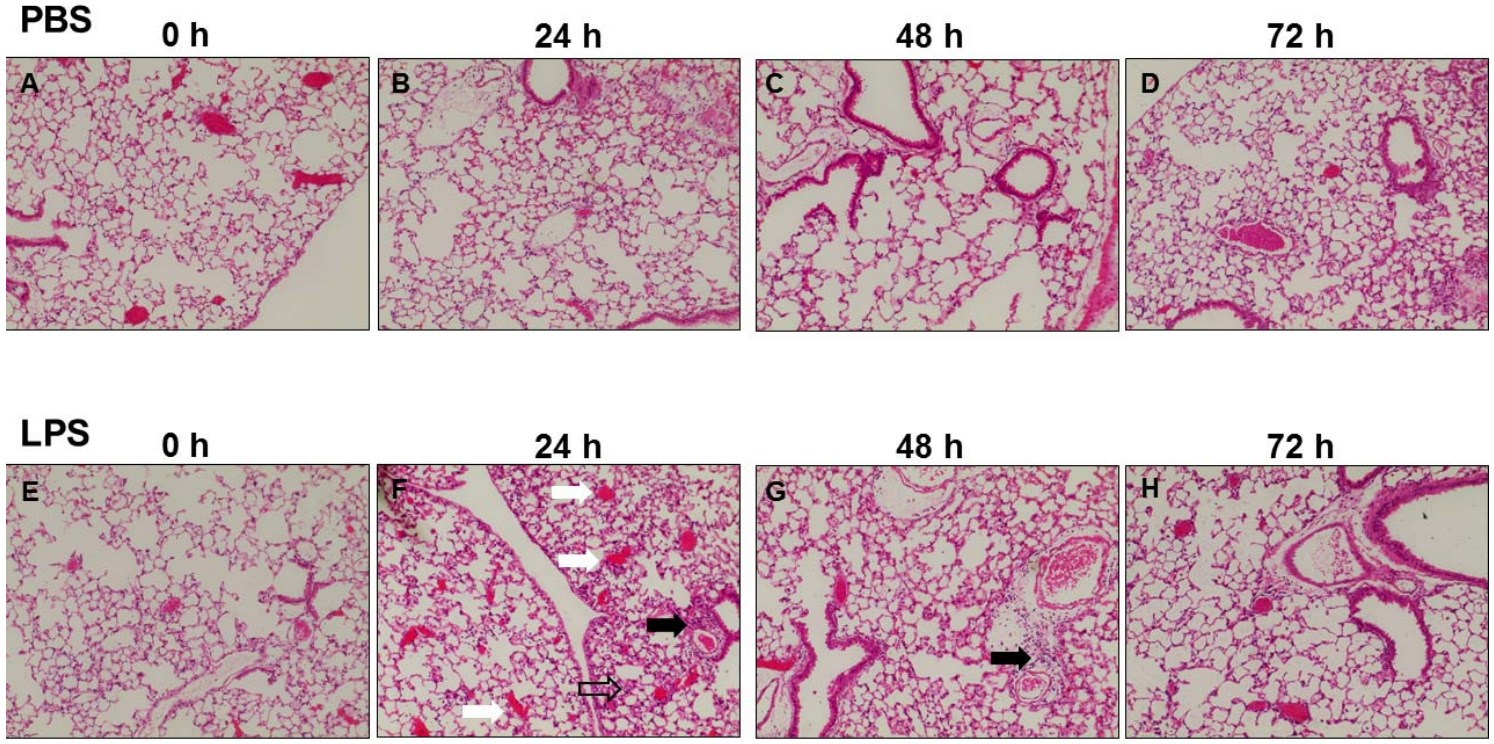

Figure 4.2: Temporal changes in lung histopathology following LPS administration. A-D *) PBS-treated mice had no increase in vascular congestion (white arrows), thickening of the interalveolar septa (clear black arrow), inflammatory cell infiltration (solid black arrow) or haemorrhage (too small to see at this scale) over the time course experiment.* ***E-F)*** *In contrast, lipopolysaccharide (LPS)-treated mice had inflammation peaking at 24 hours and mainly resolving by 72 hours. All images at X 20 magnification.*

Figure 4.3

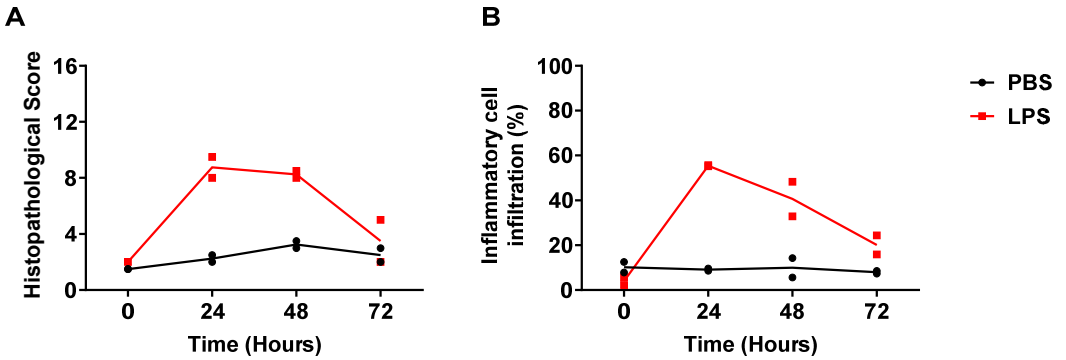

Figure 4.3: Inflammation peaks at 24 hours and has resolved by 72 hours. *The lungs of C57BL/6 mice were harvested at 0, 24, 48 and 72 hours following nebulised PBS or lipopolysaccharide (LPS) treatment.* ***A)*** *Haematoxylin & Eosin stained sections were scored using a semi-quantitative score for acute lung inflammation.* ***B)*** *Inflammatory cell infiltration (percentage of lung parenchyma (i.e. excluding blood vessels) within which inflammatory cells were evident) was also quantified. Data reveals peak inflammation at 24 hours and resolution by 72 hours in the LPS-treated group. n=2 per group per time point.*

Figure 4.4

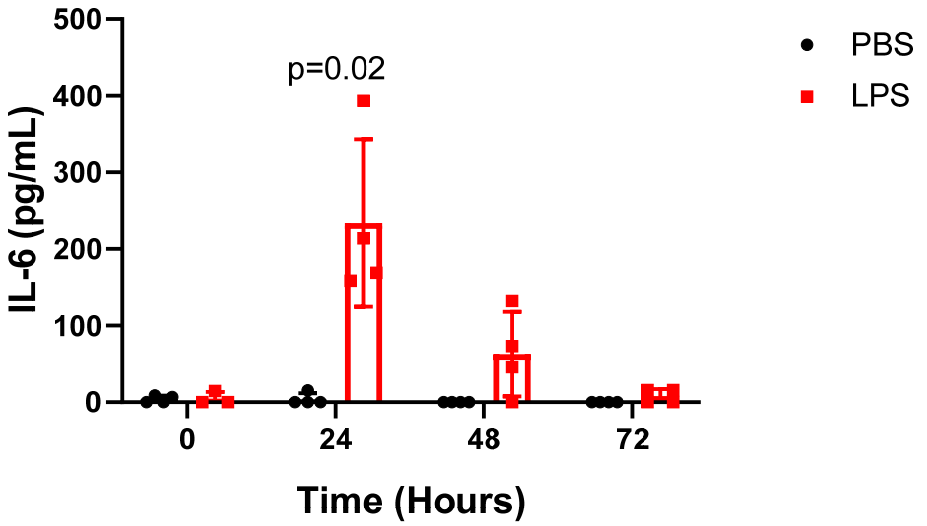

Figure 4.4: Bronchoalveolar lavage (BAL) IL-6 levels peak at 24 hours following lipopolysaccharide (LPS)-mediated acute lung injury. *C57BL/6 mice were treated with nebulised PBS or LPS then BAL fluid was collected at 0, 24, 48 and 72 hours. There was a significant increase in IL-6 concentration with LPS treatment (standardised for BAL volume) compared to PBS at 24 hours (p=0.02). Data represents individual values, mean ± SD. Data analysed using multiple* t*-tests with the Holm-Sidak adjustment for multiple comparisons. n=4 per group per time point.*

4.2 CFTR$^{-/-}$ mice have an exaggerated acute inflammatory response to LPS-mediated lung injury

Based on the preliminary results of LPS-induced acute lung inflammation in C57BL/6 mice, I next examined the development and resolution of acute lung inflammation in *Cftr*^{tm1Unc}Tg(FABPCFTR)1Jaw/J mice (CFTR$^{-/-}$) and C57BL/6 WT littermate mice, examining samples taken at 24 and 72 hours following LPS administration. These time points were selected in order to investigate potential differences in the time of peak inflammation and subsequent resolution of inflammation. Analysis of BALF cell differential counts revealed that following LPS challenge, the cell composition changed from alveolar macrophages at baseline (i.e. within the time course experiment) to predominantly neutrophils at 24 hours, but neither genotype nor DNase treatment had a significant impact on cell counts (Figure 4.5). However, CFTR$^{-/-}$ mice had a statistically significant increase in acute inflammation (characterised histologically by the presence of pulmonary oedema, inflammatory cell infiltration, vascular congestion and haemorrhage) relative to their WT littermates at 24 hours post-LPS (Figures 4.6 and 4.7). Of note, the histopathological semi-quantitative scores at 72 hours were not as low as that seen at baseline in the time course experiment, suggesting a degree of inflammation was still present at 72 hours in both genotypes. With regard to BAL cell counts and histology scores, inflammation had decreased to the same extent in both genotypes by 72 hours post-LPS, suggesting there was no problem with resolution of inflammation in CFTR$^{-/-}$ mice (Figures 4.5 and 4.7). Given the difference in estimation of inflammation based on BAL cell count and

histology at 24 hours' post-LPS, it was hypothesised that inflammatory cells present in the BALF of CFTR$^{-/-}$ mice may exhibit exaggerated proinflammatory responses to give rise to increased inflammation. This hypothesis was further examined by measuring cytokine levels in BALF supernatants using a multiplex array. CFTR$^{-/-}$ mice were noted to have significantly increased levels of IL-6, TNF-α, IL-17 and IL-10 at the 24 hour time point relative to their WT littermates (Figure 4.8). In contrast, levels of IFN-ɣ, IL-23, KC, IL-1β, MIP-2 and MCP-1 did not significantly differ with genotype or DNase treatment (see Appendix 8). By 72 hours, all cytokine levels had decreased to almost undetectable levels, with no significant differences between genotype and treatment groups (see Appendix 8).

Finally, to provide a potential quantitative method for scoring lung inflammation 24 hours' post-LPS, a [3H]-PK11195 radiotracer, which binds TSPO (mitochondrial translocator protein, a protein demonstrating increased expression in immune cells during inflammatory responses), was used together with autoradiography (work performed in collaboration with Dr Adriana Tavares, who directly supervised my experiments). Unfortunately, a common problem with PK11195 is high non-specific binding *in vivo* and this was also the case in this *ex vivo* experiment, as shown by the high uptake in "non-specific binding" radiotracer control lung sections (Figure 4.9B). This meant that when the "non-specific binding" ROI mean pixel intensity was subtracted from "total binding" ROI mean pixel intensity, resultant values sat

too low on the calibration curve and so extrapolation of nCi/mg (i.e. the non-SI unit of radioactivity) would have been inaccurate. Therefore, results were expressed in terms of percentage specific binding. These data failed to reveal a significant difference in lung PK11195 levels between groups (Figure 4.9C). The data also exhibited a wide standard deviation and it may be that in these assays the PK11195 was too non-specific to discriminate reliably inflammatory cells (since TSPO is expressed on haematopoietic and lymphatic cells). Future studies should therefore have increased sample sizes and/or utilise a more specific, second generation TSPO radiotracer – such as 18F-LW223, currently under development by Dr Adriana Tavares' group.

Figure 4.5

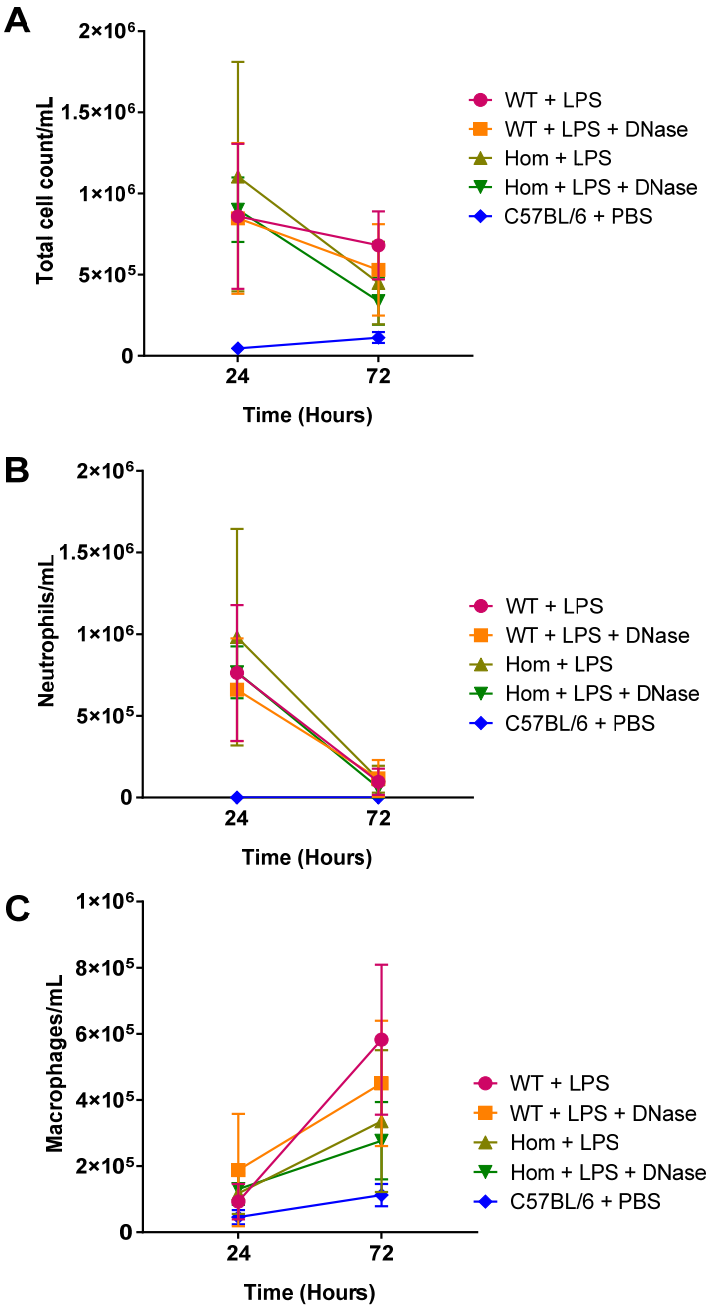

Figure 4.5: Genotype and DNase treatment did not affect BALF cell counts at 24 or 72 hours post-LPS. *BALF differential cell counts from CFTR$^{-/-}$ (Hom) and WT mice, at 24 and 72 hours post-LPS were analysed for* ***A)*** *total cell count,* ***B)*** *neutrophil count and* ***C)*** *macrophage count. Data represent mean ± SD. Data analysed by two-way ANOVA with Sidak's multiple comparisons test. n=4-7 per group.*

Figure 4.6

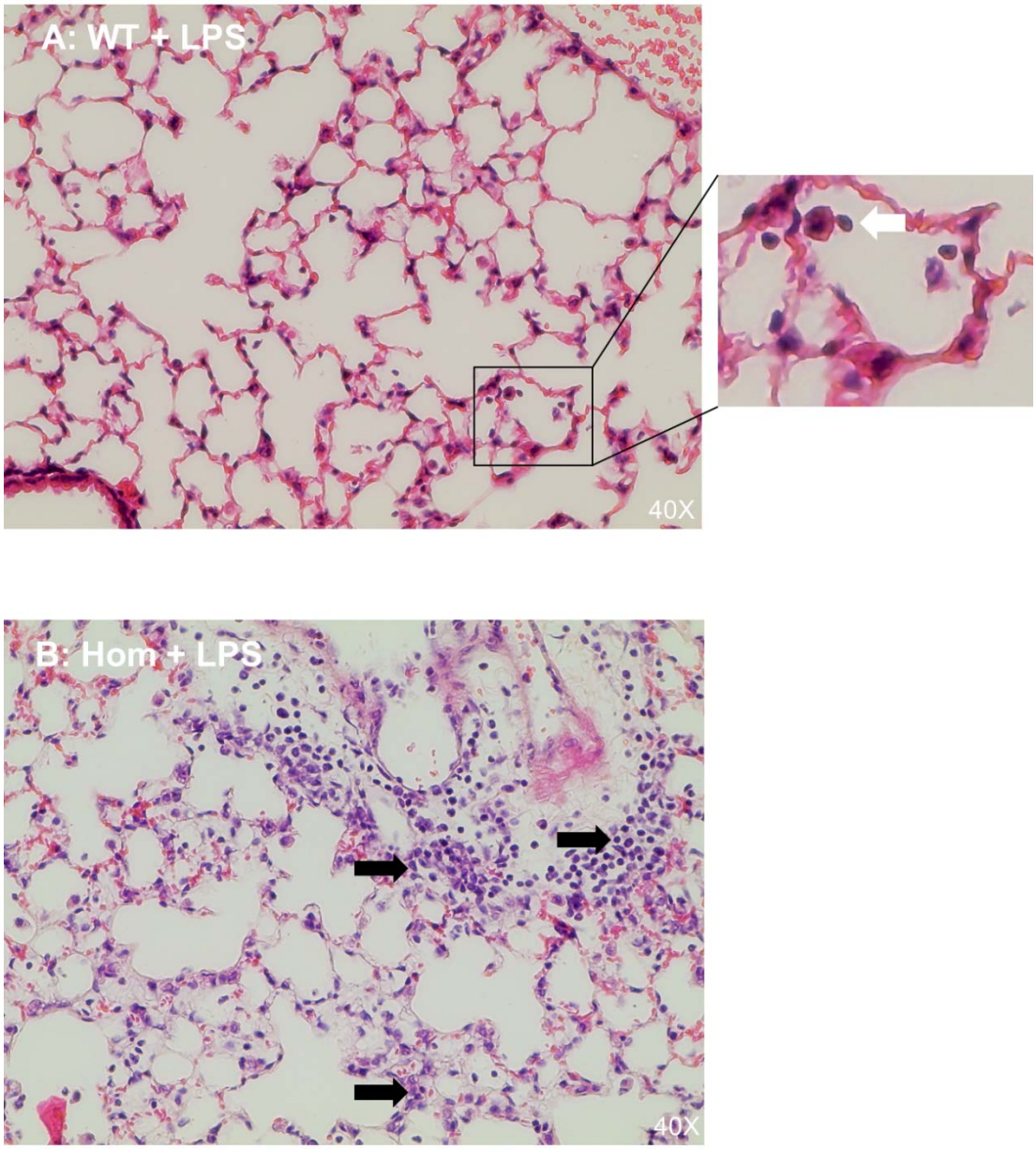

Figure 4.6: Histology sections of WT and CFTR$^{-/-}$ (Hom) murine lung sections at 24 hours post-LPS. *The semi-quantitative score measured the extent of pulmonary oedema (thickening of the alveolar interstitium), inflammatory cell infiltration (white arrow), vascular congestion and pulmonary haemorrhage. Inflammatory cell infiltrates are seen in* ***(B)*** *as purple, nucleated cells (black arrows).*

Figure 4.7

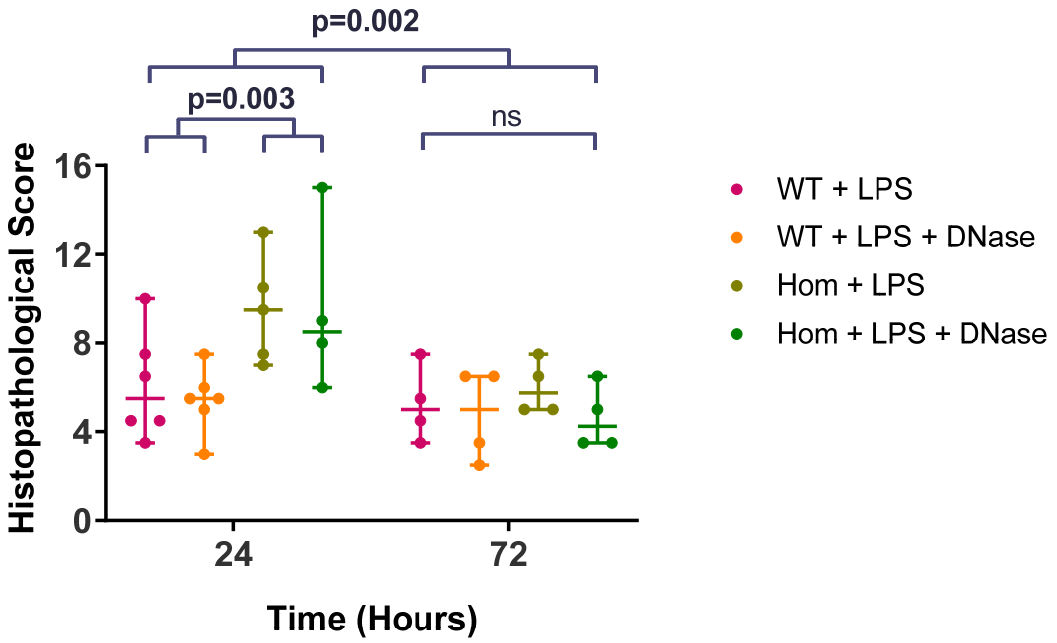

Figure 4.7: Histopathological scoring of acute lung inflammation following LPS-mediated acute lung injury. *CFTR$^{-/-}$ mice have excessive acute sterile lung inflammation relative to WT littermates 24 hours following LPS administration. By 72 hours, this inflammation has resolved to near baseline (mean scores of 2 were obtained in baseline samples in the time course experiments) in both genotypes. H&E stained lung sections were analysed using a semi-quantitative score for acute lung inflammation. Data represents individual points and mean ± SD. 24-hour and 72-hour data analysed separately using two-way ANOVA, then combined data analysed using two-way ANOVA to compare time points. n=4-6 per group.*

Figure 4.8

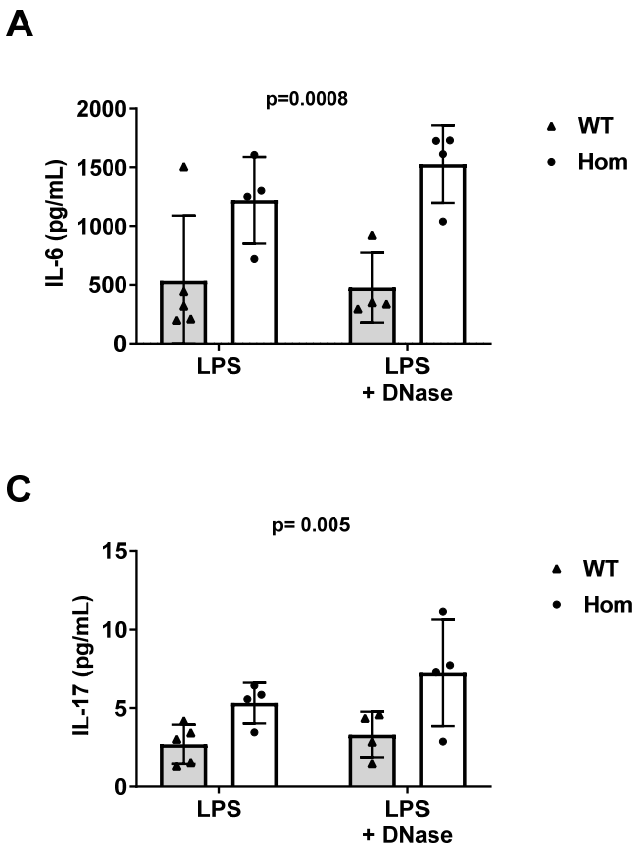

Figure 4.8: Murine bronchoalveolar lavage fluid (BALF) cytokine levels 24 hours post-LPS in WT and CFTR$^{-/-}$ mice. *Filled bars = WT, non-filled = CFTR$^{-/-}$. CFTR$^{-/-}$ mice have significantly higher levels of IL-6* ***(A),*** *TNF-α* ***(B),*** *IL-17* ***(C)*** *and IL-10* ***(D)*** *in their BALF at 24 hours post-LPS relative to C57BL/6 WT littermates. DNase does not affect cytokine levels. Data analysed by two-way ANOVA with Tukey's multiple comparisons test. Data represents individual points and mean ± SD. n=4-5 per group. p-values refer to two-way ANOVA analysis determining whether there was a statistically significant difference in cytokine levels between genotypes.*

Figure 4.9

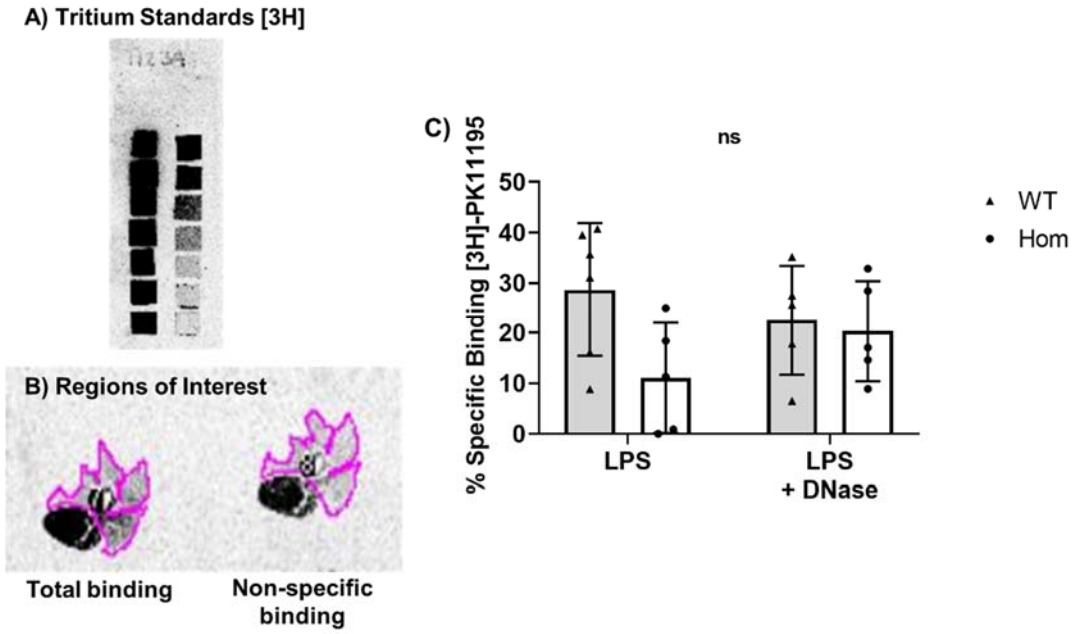

Figure 4.9: Autoradiography of* ex vivo *murine lung sections for translocator protein (TSPO) quantification. ***A)*** *Regions of interest (ROI) were drawn round Tritium standards [3H] to generate a calibration curve.* ***B)*** *ROI were then drawn round consecutive lung sections (see purple outlines) for total and non-specific binding, mean pixel intensities extracted and calibrated against the standard curve generated from* ***(A).*** ***C)*** *WT = filled bars, CFTR$^{-/-}$ = non-filled bars. There were no significant differences between groups for percentage specific binding of [3H]-PK11195 to TSPO. In addition, possible differences in TSPO binding may have been obscured by large SD values. The translocator protein (TSPO) [3H]-PK11195 radiotracer assay is too insensitive to measure murine lung inflammation* ex vivo *24 hours post-LPS. Data represent individual points and mean ± SD. Data analysed using two-way ANOVA. n=5 per group.*

4.3 Airway NETs do not differ between genotypes but significantly reduce on resolution of inflammation

Having determined that CFTR$^{-/-}$ mice have heightened inflammation at 24 hours in response to LPS, the role that NETs play in this phenomenon was interrogated. NETs were quantified in BALF supernatants using an in-house ELISA using an anti-histone primary antibody from a cell death detection kit, followed by a mouse S100A9 ELISA kit for the detection antibody. Data show that no significant differences in the level of BALF NETs were present in WT or CFTR$^{-/-}$ mice either at peak inflammation (24 hours) or during subsequent resolution (72 hours) (Figure 4.10). However, there was a statistically significant decrease in BALF NETs at 72 hours post-LPS relative to 24 hours post-LPS for both genotypes (Figure 4.10). Furthermore, there was a trend for reduced levels of NETs with DNase treatment, although this failed to reach statistical significance. It may be that more mouse numbers would make the data significant. Alternatively, one possible explanation for the lack of difference between levels of NETs between WT and CFTR$^{-/-}$ would be that the BAL fails to sample airway NETs effectively. I therefore used immunohistochemistry to image neutrophils and NETed neutrophils within *ex vivo* murine lung sections (Figure 4.11). Whilst total neutrophil count did not differ between groups, the CFTR$^{-/-}$ mice had a significant increase in neutrophil recruitment into the alveolar compartments, relative to their WT littermates (Figure 4.12B). Neutrophils were deemed NETing if 1) they were triple positive for Hoechst DNA staining and antibodies against MPO and S100A9 with co-localisation of MPO and S100A9 revealed by the presence of yellow pixelation

(Figure 4.11). Quantification of NETs by counting triple-positive cells support the BALF NET ELISA results. There were no significant differences in NETs between genotype or treatment groups at 24 hours post-LPS. Similar to the ELISA-based findings, there was a trend for decreased NETs with DNase treatment (Figure 4.12B & C). It is likely that additional experiments (to increase the sample size) would be required to confirm or refute the trends seen in the data with regard to DNase treatment. The 72 hour time point was not examined using immunohistochemistry because it was predicted that numbers of NETing neutrophils would be too low to provide a reliable estimate of NETing cells. C57BL/6 mice treated with nebulised PBS served as a negative control for this experiment (Figure 4.12A-C). Since only a few studies have been published which describe how to image murine NETs in lung sections *ex vivo* using immunohistochemistry(108,214), the approach used here could be added to the repertoire of methods for quantification of the presence of NETs *in vivo*.

Figure 4.10

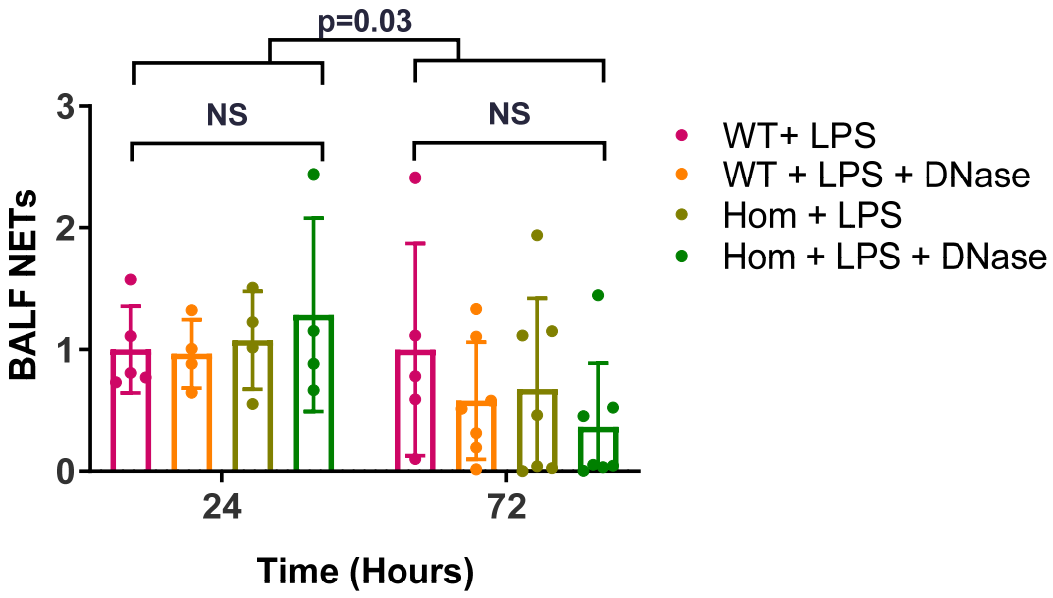

Figure 4.10: Quantification of bronchoalveolar lavage fluid (BALF) NET levels by ELISA. *BALF NETs significantly decrease on resolution of inflammation but do not differ between genotypes at individual time points. At 24 hours' post-LPS, there is no significant difference in BALF NETs between groups. At 72 hours' post-LPS, there is a trend for decreased NETs with DNase treatment in both genotypes, but this did not reach statistical significance. BALF NETs significantly decrease at 72 hours relative to 24 hours (p=0.03). NETs quantified using fold-change in optical density from WT + LPS readouts. Data represents individual points and mean ± SD. 24 hour and 72 hour data analysed separately using two-way ANOVA with Sidak's multiple comparisons test, then time points compared using two-way ANOVA. n=4-7 per group.*

Figure 4.11

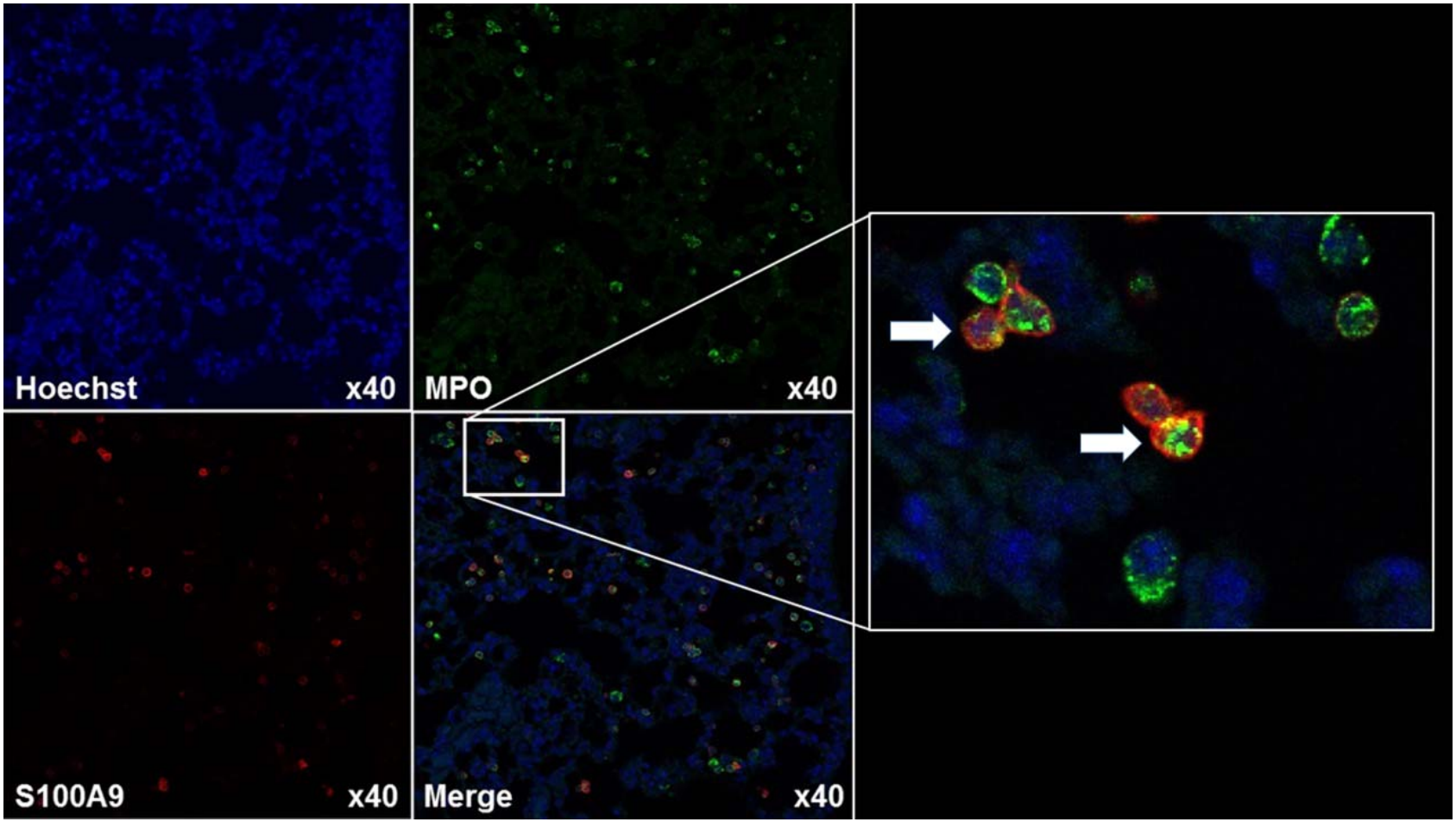

Figure 4.11: Immunohistochemistry of NETs in* ex vivo *murine lung sections following LPS-mediated acute lung injury. *NETs can be imaged using immunohistochemistry and quantified through detection of co-localisation of constituent proteins. Representative confocal microscopy images of lung sections from a C57BL/6 WT mouse 24 hours following LPS-mediated acute lung injury. The zoomed-in image (right) shows co-localisation of MPO (green) and S100A9 (red), i.e. yellow pixelation. The number of cells triple positive for Hoechst (blue), MPO and S100A9 and with yellow pixels, were deemed NETed neutrophils (white arrows).*

Figure 4.12

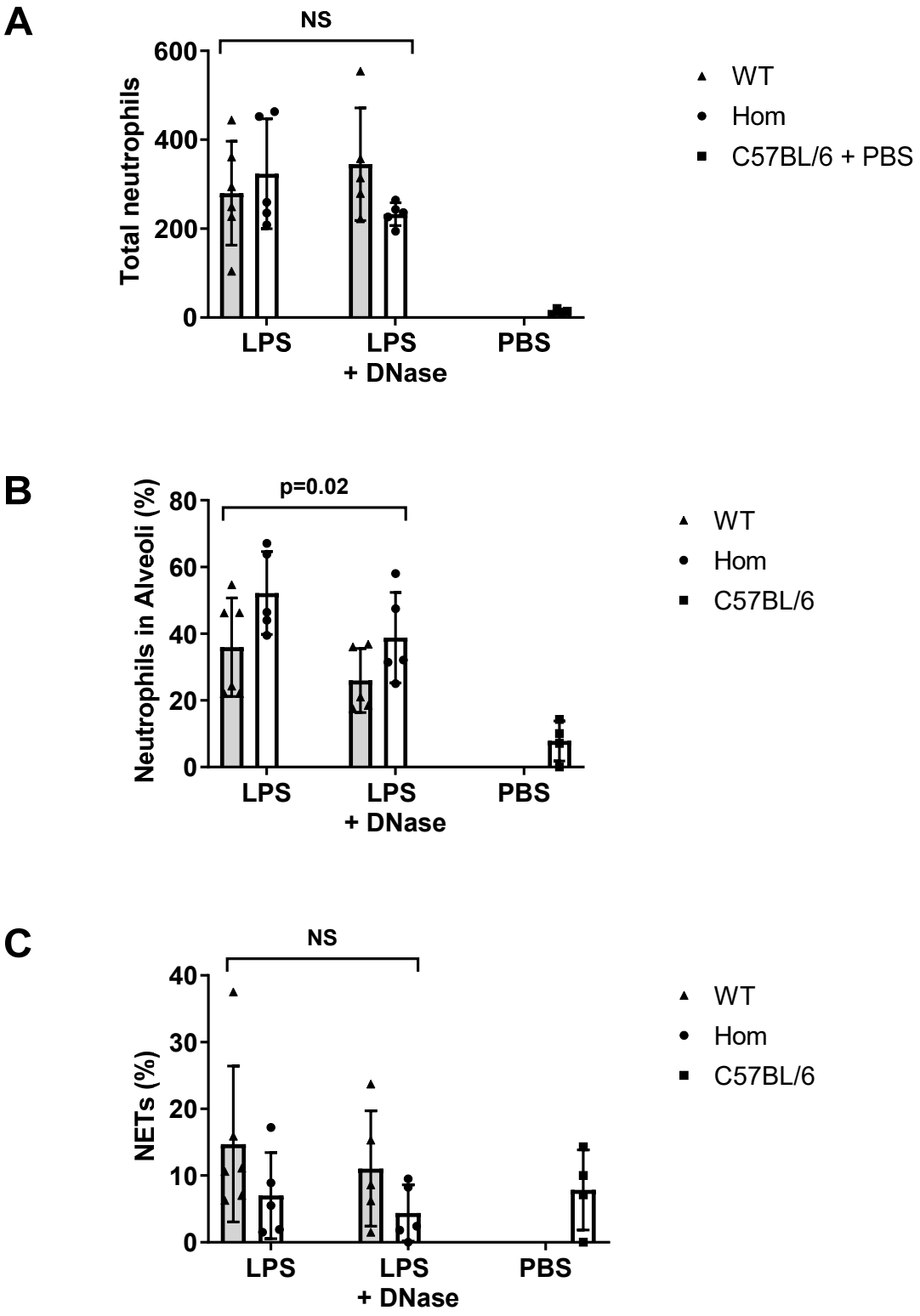
A
NS
Total neutrophils
600
400
200
0
LPS
LPS + DNase
PBS
WT
Hom
C57BL/6 + PBS
B
p=0.02
Neutrophils in Alveoli (%)
80
60
40
20
0
LPS
LPS + DNase
PBS
WT
Hom
C57BL/6
C
NS
NETs (%)
40
30
20
10
0
LPS
LPS + DNase
PBS
WT
Hom
C57BL/6

Figure 4.12: Quantification of* ex vivo *murine lung neutrophil numbers and NETs by examination of immunohistochemistry images. *WT littermates = filled bars with triangle symbols, CFTR$^{-/-}$ =clear bars with round symbols, C57BL/6 controls = clear bars with square symbols. CFTR$^{-/-}$ mice have higher numbers of neutrophils in the alveolar compartment compared to WT littermates 24 hours following LPS.* ***A)*** *The total number of neutrophils in lung sections per six fields-of-view on CLSM did not differ between genotype groups or with DNase treatment.* ***B)*** *CFTR$^{-/-}$ mice have increased recruitment of neutrophils into the alveolar compartments compared to WT littermates (p=0.02).* ***C)*** *The percentage of neutrophils deemed NETing (see Figure 4.11 for criteria) did not differ between genotypes but there was a trend for reduction in NETs with DNase treatment. Parameters were compared to PBS-treated control C57BL/6 mice lung sections (**A-C**). Data represents individual points and mean ± SD. Data for LPS-treated mice analysed by two-way ANOVA with Sidak's multiple comparisons test. n=4-6 per group.*

4.4 Surrogate markers of NETs corroborated the NET ELISA results

As a comparison to ELISA-based NET quantification, BALF supernatant was collected from mice at 24 and 72 hours' post-LPS induced acute lung injury and MPO activity, PicoGreen® and Pierce® BCA assays were assessed. There were significant reductions in both protein and dsDNA concentrations at resolution of inflammation (72 h) compared to peak inflammation (24 h) (Figure 4.13C-F). At 24 hours post-LPS, there was no significant difference in MPO activity within BALF of WT and CFTR$^{-/-}$ mice and DNase treatment did not affect MPO activity (Figure 4.13A). At 72 hours' post-LPS, however, CFTR$^{-/-}$ mice had higher MPO activity when treated with DNase, relative to WT littermates (Figure 4.13B). BALF supernatant protein concentrations were significantly elevated in CFTR$^{-/-}$ mice relative to WT littermates at peak inflammation (Figure 4.13C). There was no significant difference in BALF dsDNA concentrations between genotypes and treatment groups at either peak or resolution of inflammation (Figure 4.13E&F). Taken together alongside the NET results, these findings suggest that in the CF mouse model of LPS-induced acute lung inflammation, NETs are not the main cause of the exaggerated inflammatory response seen in CFTR$^{-/-}$ mice. Alternatively, repeated challenge would be needed to replicate human CF lung disease where there is no resolution, as was the case in this mouse model.

Figure 4.13

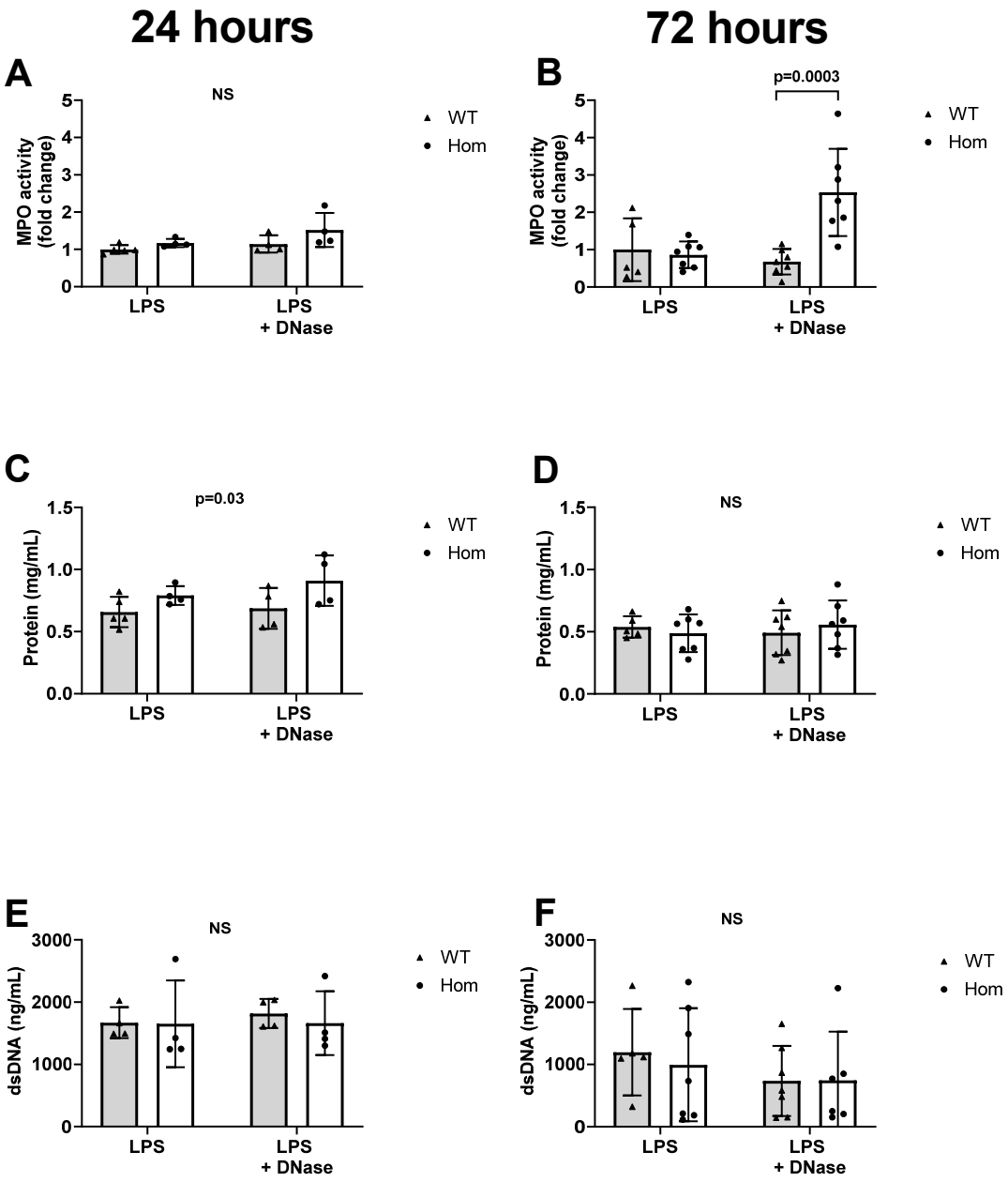

Figure 4.13: MPO activity, Pierce® BCA, and PicoGreen® assays on murine bronchoalveolar lavage fluid 24 and 72 hours following LPS-induced acute lung inflammation. *WT = filled bars. CFTR$^{-/-}$ = non-filled bars. LPS-induced acute lung injury causes significant increases in airway protein and dsDNA concentrations at peak inflammation. BALF supernatant was collected from mice 24 and 72 hours post-LPS and analysed for* ***A&B)***

MPO activity, ***C&D)*** *protein concentration and* ***E&F)*** *dsDNA concentration.* ***B)*** *There was a significant increase in MPO activity in CFTR$^{-/-}$ mice treated with LPS + DNase relative to WT littermates at 72 hours. MPO activity was expressed as fold-change from mean WT+ LPS optical density.* ***C)*** *CFTR$^{-/-}$ mice have significant elevation in BALF protein concentration at 24 hours post-LPS relative to WT.* ***C&D)*** *Protein concentrations fall significantly with resolution of inflammation.* ***E&F)*** *There was no significant difference in BALF dsDNA concentrations between genotypes and treatment groups but levels significantly fall upon resolution of inflammation. Data represent individual points and mean ± SD. The 24 and 72 hour data were analysed separately using two-way ANOVA with Sidak's multiple comparisons tests. Thereafter, time points were compared to one another using two-way ANOVA. n=4-7 per group.*

4.5 DNase is effectively delivered to the lung via nebulisation

Two experiments were carried out to demonstrate that DNase is active, even when administered by nebulisation to the mice. Firstly, *in vitro* DNA digestion was shown using DNA gel electrophoresis experiments, in which calf thymus DNA was loaded onto the gels alone or in combination with increasing concentrations of DNase (625 U – 2500 U). These experiments revealed that DNase fragmented calf thymus DNA at all of the concentrations (Figure 4.14A). Having confirmed that the drug was active *in vitro,* I designed an experiment to demonstrate effective delivery of DNase to the airways via nebulisation. I treated heterozygote mice (CFTR$^{-/+)}$ with 2.5mL DPBS or DNase 2500 U (they did not receive LPS) for ~ 10 min, prior to animals being culled and BALF harvested. BALF was then incubated with 1μg/mL calf thymus DNA then dsDNA concentrations quantified using the PicoGreen® assay. Incubation with BALF from DNase-treated mice resulted in a significant decrease in dsDNA levels relative to PBS control BALF (Figure 4.14B). These two experiments confirmed that DNase was active and nebulisation effectively delivered the drug to the airways sampled by BAL.

With regard to the CF mouse model of LPS-induced acute lung inflammation, I decided to treat CFTR$^{-/-}$ mice and WT littermates with 2500 U DNase 12 hours after the administration of LPS, and once daily thereafter in the case of the mice culled at 72 hours post-LPS. The maximum DNase dose was selected so that it increased the likelihood of active drug being in the airways when NETs were formed. With regard to the assays measuring murine airway NETs, a trend was noted for decreased levels of NETs when mice were treated with

DNase (Figures 4.10 and 4.12C). Moreover, MPO activity in BALF supernatant was increased with DNase treatment (Figure 4.13A&B). Conversely, DNase did not significantly affect other parameters such as semi-quantitative scoring of lung damage (Figure 4.7) and BALF proinflammatory cytokine concentrations (Figure 4.8). It is likely that further experiments to increase the sample sizes would be required to confirm or refute the trends seen in the NET quantification data. Moreover, it may be that DNase administered at the same time as LPS, as well as once daily thereafter, would have been more effective.

Figure 4.14

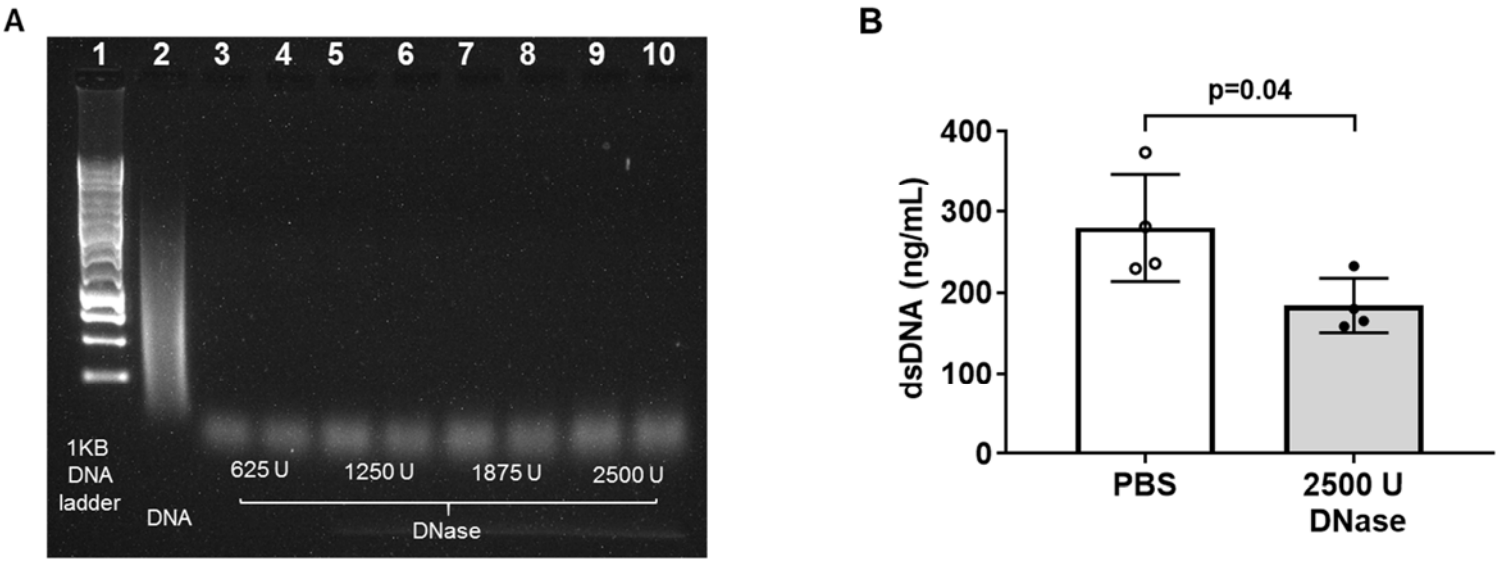

Figure 4.14: Nebulisation delivers active DNase to murine airways. ***A)*** *DNA gel electrophoresis with 1kb DNA ladder (lane 1), calf thymus DNA 1µg/mL only (lane 2) and calf thymus DNA 1µg/mL incubated with increasing doses of DNase (625 U – 2500 U in lanes 3 - 10, each dose in duplicate). The drug actively fragments DNA at all doses. Representative gel of n=3 experiments.* ***B)*** *CFTR$^{+/-}$ mice were nebulised with 2.5 mL 2500U DNase or PBS control then BALF harvested. Resultant supernatant was incubated with calf thymus DNA then dsDNA was quantified using a PicoGreen® assay kit. There is a significant decrease in dsDNA when calf thymus DNA was incubated with BALF supernatant from mice treated with DNase in comparison to PBS control. Data represents individual points and mean ± SD. Data analysed by two-tailed student's* t*-test. n=4 per group over two separate experiments.*

4.6 The exaggerated acute inflammatory response of CFTR$^{-/-}$ mice is associated with increased expression of RAGE

Data in this chapter thus far have shown that CFTR$^{-/-}$ mice have a heightened inflammatory response to acute LPS-induced lung injury. To investigate whether NET constituents are critical players in the causative mechanisms, RT-PCR and western blot techniques were performed on whole lung lysates from mice culled 24 hours following LPS. The 24 hour time point was selected to assess parameters when inflammation was at its peak. Whole lung lysates were used instead of BALF because the latter would also sample anything produced by AEC (which may confound results) and because lysates permit sampling of the lung interstitium, which may also contain immune cells. Gene expression for PRR and receptors which have NET constituents as ligands were assessed by RT-PCR, namely TLR-2, -4, -9 and RAGE. This revealed no alteration in TLR-2, -4 or -9 mRNA expression between genotypes and treatment groups (Figure 4.15A-C). However, RAGE mRNA expression was significantly upregulated in CFTR$^{-/-}$ mice (Figure 4.15D). Western blot analysis revealed no difference in whole lung RAGE protein expression in CFTR$^{-/-}$ mice relative to WT littermates (Figure 4.16). These data suggest that RAGE may have altered intracellular processing or location between genotypes, a suggestion that requires further detailed examination.

Figure 4.15

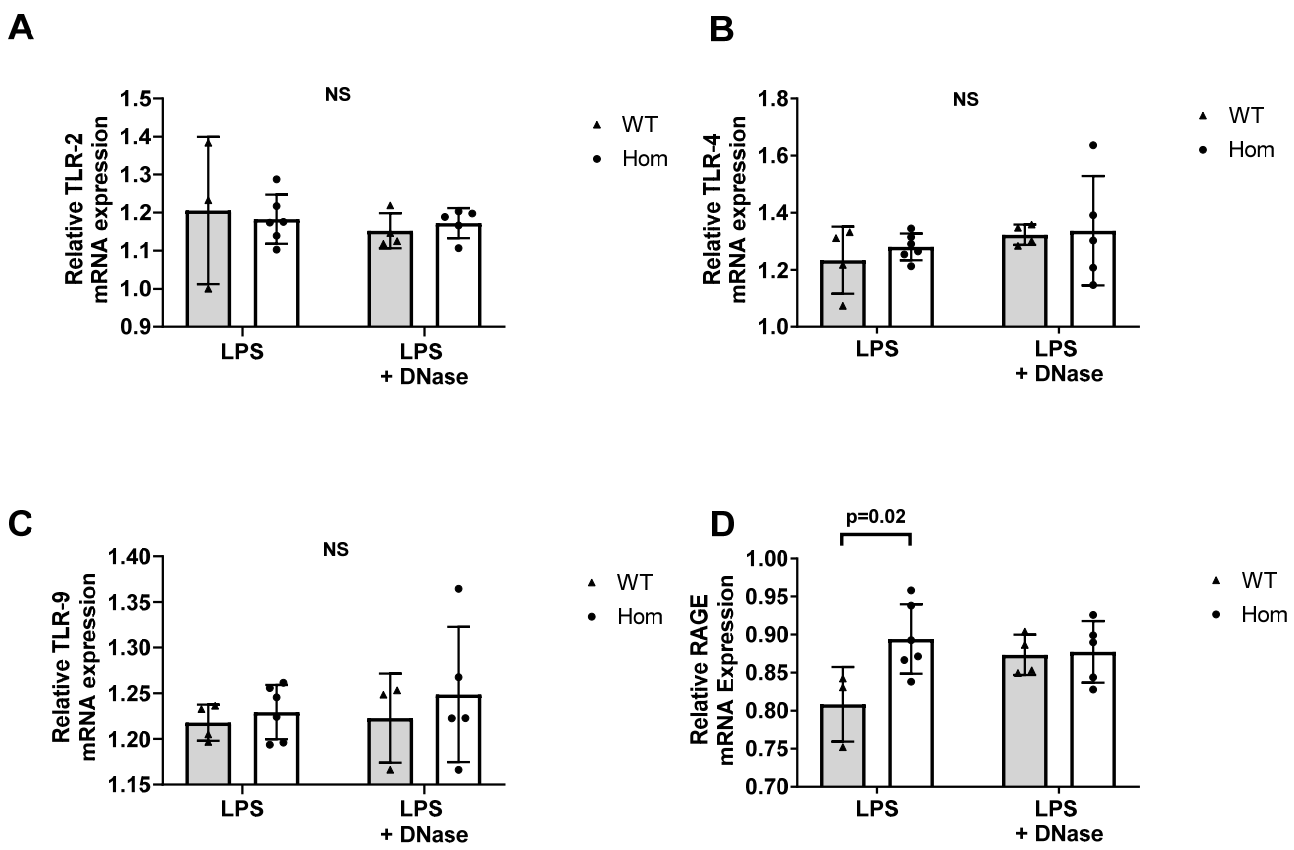

Figure 4.15: Relative RAGE mRNA expression is upregulated in CFTR$^{-/-}$ mice relative to WT littermates 24 hours post-LPS (D). *Expression of innate immune cells' pattern recognition receptor genes was analysed by RT-PCR analysis of murine whole lung lysates. Data is expression relative to β-actin gene expression. Data represents individual values and mean ± SD. n=3-6.* ***A–C)*** *Relative expression of TLR-2, -4 and -9 mRNA is unaffected by genotype or DNase treatment.* ***D)*** *Relative RAGE mRNA expression is affected significantly by genotype (p=0.04) (with significant elevation in expression in Hom + LPS compared to WT + LPS (p=0.02)) but unaffected by DNase. Data analysed by two-way ANOVA with Sidak's multiple comparisons test.*

Figure 4.16

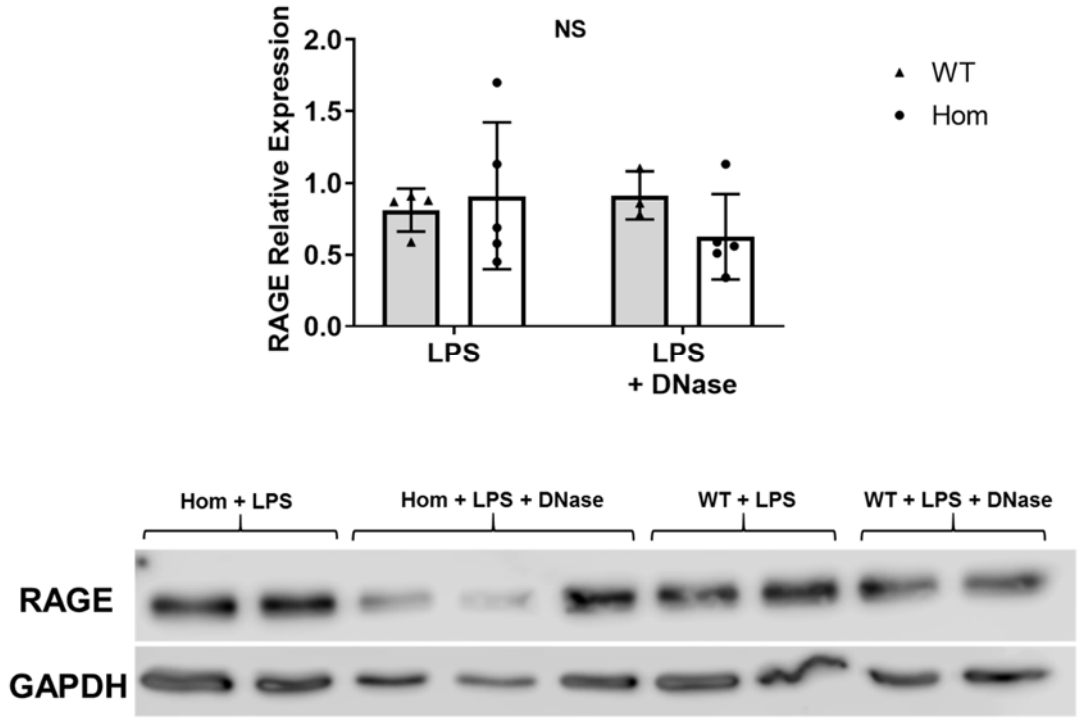

Figure 4.16: Expression of RAGE protein in lung lysates from WT and CFTR$^{-/-}$ (Hom) mice at 24 hours following LPS administration as assessed by western blot analysis*. WT = filled bars. CFTR$^{-/-}$ = non-filled bars. n=3-5. Representative immunoblot shown for RAGE with expression of GAPDH used as a protein loading control. Data in graph represents individual values for expression of RAGE relative to GAPDH shown as mean ± SD. Data were analysed by two-way ANOVA.*

Discussion

Previous studies have demonstrated that innate immune cells including neutrophils and macrophages express CFTR mRNA at low levels(19) and express functional CFTR protein both intracellularly(218) and at the cell membrane(21,124,219). In human and murine neutrophils, the protein is present in secretory vesicles and phagolysosomes, inferring that CFTR is a critical regulator of neutrophil phagocytosis(83,211). Specifically, Painter *et al.* suggest that CFTR-containing secretory vesicles merge with phagosomes during the formation of phagolysosomes(83). Furthermore, using immunofluorescent staining of murine neutrophils they found that CFTR was associated with phagocytic vacuoles containing green fluorescent protein-expressing *P.aeruginosa* and lack of CFTR on phagolysosomes resulted in defective chlorination (and therefore degradation) of bacterial proteins within this organelle(83). The role of CFTR in macrophage function will be discussed fully in Chapter 5.

Data presented in this chapter confirm that CFTR$^{-/-}$ mice have an abnormal acute inflammatory response to LPS in their lungs, in agreement with findings by Su *et al.*(211). The CFTR$^{-/-}$ mice used in this study did not have an increase in BAL neutrophil counts at 24 hours post-LPS administration when compared with WT littermates. One possibility is that the lavage method used did not dislodge all of the cells present within the lower airway compartments, which had yet to migrate up into the airways for clearance following migration into the

alveoli. Moreover, the 24 hour time point may have been too late to see any difference in BAL neutrophil counts, since Su *et al.* demonstrated higher neutrophil counts at 4 hours post-LPS(211). In spite of this, the CFTR$^{-/-}$ mice used in our experiments had increased levels of the proinflammatory cytokines IL-6, TNF-α and IL-17 in their BAL at 24 hours post-LPS. TNF-α is a prolific inflammatory cytokine made by activated macrophages and signals to both macrophages and neutrophils in the acute phase response and throughout the inflammation time course. It can prime neutrophil effector function (which augments their response to secondary stimuli such as LPS), induces oxygen radical generation and degranulation(220), and acts upon the endothelium to increase expression of adhesion molecules such as ICAM-1 and VCAM-1 to aid neutrophil adhesion(221). It is likely that elevated levels of BAL TNF-α contribute to the acute lung injury seen in the CFTR$^{-/-}$ mice. Elevated TNF-α levels were also found in the sputum of non-exacerbating CF participants when compared to healthy controls (Chapter 3, Figure 3.15). Conversely, IL-6 levels were significantly elevated in the CFTR$^{-/-}$ mice but significantly reduced in CF participants' sputum relative to HC. These data raise the possibility that IL-6 may have pleiotropic effects which are context-dependent – it may be proinflammatory by driving macrophage proinflammatory cytokine production, or anti-inflammatory to aid resolution of inflammation(186). IL-17 was increased in CFTR$^{-/-}$ mice BAL 24 hours post-LPS compared to WT littermates. IL-17 is a proinflammatory cytokine produced by Th17 cells, neutrophils, gamma-delta T cells and natural killer cells(222) that regulates granulopoiesis(41) and neutrophil recruitment(223). IL-17 levels are elevated

in the sputum of adult CF patients during exacerbations and decrease with antibiotic therapy(222). Finally, increased levels of IL-10 in murine BAL at 24 hours post-LPS mirrored data from the human MDM-neutrophil/NET co-culture experiment in Chapter 3.7, in which CF human MDM produced significantly increased levels of IL-10 at 24 hours relative to HC MDM. Other studies have shown IL-10 to be reduced in the context of CF(207,208), suggesting an imbalance which drives inflammation. It may be that the chronic inflammation and infection of CF lung disease is not fully represented by the CF mouse model of LPS-induced acute lung but we would suggest that it is nevertheless useful for the study of dysfunctional innate immune cell responses to inflammation in CF and the acute lung injury setting.

Elevated levels of proinflammatory cytokines may have contributed to the significant increase in neutrophil recruitment to the alveolar compartments seen on IHC of CFTR$^{-/-}$ murine lung sections. Histological scoring of acute lung inflammation using a modified, validated score(173,174,224) also supported these results: CFTR$^{-/-}$ mice had evidence of exaggerated lung damage in response to LPS, in agreement with Su *et al.*(211). BAL protein levels were also significantly higher in CFTR$^{-/-}$ mice 24 hours post-LPS, which could be due to increased albumin due to endothelial damage and pulmonary oedema. To test the hypothesis that elevated proinflammatory cytokines contribute to increased neutrophil recruitment, the experiments could be repeated with CFTR$^{-/-}$ mice being treated with commercially available

antibodies, e.g. tocilizumab (anti-IL-6 receptor(225)), infliximab (anti-TNF(226)) and secukinumab (anti-IL-17A(227)). Alternatively, double knockout mouse models could be set up (i.e. IL-6, TNF-α, or IL-17a/IL17ra knockout mice could be crossed with CFTR knockout mice) and animals challenged with LPS, although the time it would take to breed such animals may make such models impractical and whether or not such double knockouts would be viable is uncertain.

Data in this chapter support the suggestion that NETs, airway proteins and dsDNA all accumulate at peak inflammation and clear at subsequent resolution in both genotypes. One might have expected delayed resolution or persistence of NETs in the CFTR$^{-/-}$ mice given the fact NETs accumulate in CF participants' airways (see Chapter 3) but the acute nature of the experiment likely accounts for this discrepancy. It appears that airway NETs are not solely responsible for the heightened inflammation seen in the CFTR$^{-/-}$ mice because there was no increase in BAL NETs in these mice relative to WT littermates at 24 hours post-LPS. However, sample sizes were small (owing to the slow breeding of CF mice) and SD large and so inferences drawn from these findings are limited. It could be that there is a difference between genotypes undetected due to insufficient group size; additional experimentation is required to confirm or refute our conclusions regarding airway NETs in the CF mouse model. Other intrinsic defects of the CF neutrophil, such as enhanced

recruitment to the alveoli and a propensity to degranulate and produce reactive oxygen species, may account for the lung damage demonstrated(109).

When ELISA and IHC quantified NETs, there was a trend for decreased NETs in mice treated with DNase. Whilst further experiments (to increase the sample size) are likely needed to confirm or refute these results, they may suggest that DNase was active and targets NETs. This is in agreement with the human data, which show that CF participants taking DNase had significantly lower levels of sputum NETs compared to those not on the medication. Overall, DNase treatment did not significantly affect LPS-mediated inflammation. In contrast, Liu *et al*. report that DNase I treatment significantly reduced NET-DNA levels in BALF and reduced LPS-induced lung injury (as assessed by histological lung injury scores, pulmonary wet/dry weights and total proteins in BALF)(108). In their experiment, mice were treated with DNase I at 0 hours and 10 hours post-LPS administration and so with regard to our experiments, it is possible that inflammation would have been reduced if DNase had been given at the time of LPS administration, instead of at 12 hours following LPS treatment. Furthermore, the DNase doses may not have been comparable as they were delivered by different routes (i.e. nebulised vs. intratracheal instillation).

Our data does suggest that DNase releases NET-bound MPO from the inhibitory effect of interactions with negatively charged DNA; BAL MPO activity was significantly higher in CFTR$^{-/-}$ mice treated with the DNase once daily for 72 hours. Extrapolating this result to human patients with CF, the implication is that DNase treatment might result in increased MPO activity in the airways. Given that this peroxidase is a principal contributor to CF lung damage(228,229), it may be that some patients clinically deteriorate when taking DNase because MPO activity is increased. Further studies – including *in vitro* study of NETs and clinical studies of CF patient airway samples would be required to investigate this hypothesis. These data are in line with results from Dubois *et al.* regarding human NE, which shows increased activity *in vitro* in the presence of DNase(102). However, the same pattern was not seen in WT mice and so future work should re-examine this finding.

To investigate potential mechanisms by which NET constituents could contribute to heightened LPS-mediated inflammation in CFTR$^{-/-}$ mice, expression of RAGE and three key TLR were studied using RT-PCR. The TLRs are transmembrane PRR, which recognise and bind PAMPs or DAMPs (see Table 4.1). The former are microbial-derived whilst the latter are host-derived factors. The interaction between these ligands and the TLRs induce proinflammatory gene expression via activation of NF-κB, AP1 and interferon-regulatory factors(230). NET constituents (see Introduction for full descriptions of each) may function as DAMP ligands upon TLR:

TLR	Classic Ligands	NET constituent
TLR-2	Lipid-containing PAMPs, e.g. glycoproteins of viruses, porins of bacteria such as *H.influenzae*, Zymosan of fungi, as well as endogenous ligands such as hyaluronan.	Histones and HMGB1
TLR-4	LPS, viral polysaccharides, low-density lipoprotein, beta-defensin, heat shock proteins	Histones, S100 proteins, HMGB1
TLR-9	unmethylated CpG sequences in DNA molecules, dsDNA	Self-nucleic acids, HMGB1, LL37

Table 4.1: Toll-like receptors (TLR), their classic ligands(230) **and NET constituents that activate respective TLR.**

LPS was used to induce lung inflammation in mice and it is a well-known PAMP ligand for TLR-4. The intracellular processing of TLR4 is abnormal in CFTR$^{-/-}$ mice, with retention of TLR4 within the early endosome and reduced translocation to lysosomes(132). This ultimately leads to increased LPS-induced inflammation by inhibiting the downregulation of proinflammatory gene transcription. RAGE is a PRR for glycoproteins, HMGB1 and S100 proteins(231). Both serum and sputum HMBG1 are strong risk markers for lung function decline in CF patients(232) and so it is possible NETs drive inflammation via HMGB1 and calprotectin interactions with RAGE.

The RT-PCR data did not reveal any differences in TLR-2, -4, and -9 mRNA expression in our murine whole lung lysates. This technique has limitations however because it does not specifically study the airway innate immune cells. Future experiments could isolate these cells from BAL by flow sorting (using Ly6G for neutrophils and Siglec-F for macrophages) prior to cell pellet RNA extraction and RT-PCR. However, this would require higher numbers of animals (which should be avoided where possible when designing such experiments) and so *in vitro* models could be designed instead. For example, CFTR$^{-/-}$ and WT littermate mice could be culled then isolation of bone marrow-derived neutrophils and differentiation of bone marrow-derived macrophages performed (i.e. bone marrow cells would be differentiated into macrophages using macrophage colony-stimulating factor). These cells would then be challenged with LPS prior to cell pellet RNA extraction and RT-PCR. Alternatively, single cell RNA sequencing could be performed on isolated airway innate immune cells and so cell numbers obtained might not be so critical.

My data suggest that CFTR$^{-/-}$ mice had increased RAGE mRNA expression but normal protein expression in lung lysates in response to LPS-induced lung inflammation. This observation raises the possibility that CFTR mutation causes RAGE up-regulation and/or intracellular trafficking perturbations, which may contribute to increased ligand binding and subsequent proinflammatory gene expression in CF lung disease. There is evidence that RAGE signalling

is involved in autophagy: activation of adenosine 5′-monophosphate-activated protein kinase (AMPK) is RAGE-dependent(231) and could therefore regulate autophagosome formation. Thus, if CF cells have upregulation of RAGE, this may lead to enhanced activation of AMPK and increased autophagosome formation, which would account for the increased vacuolations seen in human CF neutrophils in Chapter 3. That said I did not see evidence for vacuolation in the mouse BAL neutrophils. The study of RAGE-dependent AMPK activation and subsequent autophagosome formation was beyond the scope of this thesis but could provide another avenue of future research.

Chapter 5: Exploring Macrophage Acidification in Cystic Fibrosis using Optical Nanosensors

Background

"Macrophage" is derived from the Greek μακρός (makrós) = large and φαγείν (phageín) = to eat, and so macrophages are literally the "big eaters" of the innate immune system. They have been shown to express CFTR mRNA at low levels(19) and express functional CFTR protein intracellularly(20) and at the cell membrane(21,124,219). In a process called phagocytosis (see Chapter 1: Introduction), macrophages engulf microbes, cellular debris and foreign material into phagosomes, which are plasma membrane-derived vacuoles within the cytoplasm. These in turn fuse with lysosomes, which are organelles containing numerous enzymes that break down biological polymers including proteins, carbohydrate and nucleic acids(233). When a phagosome fuses with a lysosome they form a membrane-bound organelle called a phagolysosome (see Figure 5.2). The resultant phagolysosome has an acidic pH, which facilitates bacterial killing(126,234). Mature phagolysosomes reach pH 4.5 - 5.0(8,9), principally regulated by the vacuolar proton ATPase(236). However, CFTR has been suggested as an extra and important mediator of organelle pH(237) and faulty macrophage phagolysosomal acidification has been incriminated in pathophysiology of bacterial infectious diseases by organisms such as *Mycobacterium tuberculosis and S.aureus* (13,14).

Previous studies investigating the role of CFTR in regulating changes to organelle pH have had conflicting results. A seminal paper by Di *et al.* reported that alveolar macrophages from CFTR-deficient mice had defective phagolysosomal acidification and therefore sub-optimal killing of internalised *P.aeruginosa*(20). Furthermore, it has been shown that these cells have alkalinised pH of intracellular vesicles (presumed to be lysosomes) relative to WT macrophages(240). It has been proposed that this pH change affects the action of enzymes involved in ceramide metabolism, ultimately resulting in defective acute response of alveolar macrophages to *P.aeruginosa*. On the other hand, some authors suggest CFTR-deficient macrophage cell lines and primary mouse and human alveolar macrophages have no change in the pH of phagosomes (241–243).

Such discrepancies in reported phagolysosomal pH may be due to different methods used to measure pH. To date, pH quantification has been limited to the use of pH-sensitive fluorescence spectroscopy. If single wavelength or dual-dye pseudo-ratiometric protocols are followed, insensitive quantification may result. This is due to issues such as laser drift, shifts in focus, irregular labelling and photobleaching of the fluorophores(244). In addition to these issues is the problem encountered with the use of non-ratiometric fluorescence spectroscopy - fluorescence changes depending upon fluorophore concentration. Hence, results may be insensitive due to simple differences in the quantity of dye molecules taken up by the cells, rather than there being actual differences in pH. However, fluorescence spectroscopy quantification

of phagolysosomal pH, with careful and appropriate experimental design, could produce accurate pH readouts.

Surface-enhanced Raman spectroscopy (SERS)-based nanosensors are a potentially superior alternative to analyse pH within living systems. The scientific theory behind Raman spectroscopy is eloquently summarised elsewhere(245) but shall be described here in brief because in order to understand the results of this chapter, a basic understanding of the underpinning physics is required. Raman spectroscopy is a technique that uses an inelastic scattering interaction between light and matter to obtain chemical information. Monochromatic light – the incident light – strikes a surface and excites briefly a molecule within that surface into its "virtual" state (i.e. above the vibrational state but not reaching the electronic state, see Figure 5.1). Following this, several light scattering possibilities may occur. Elastic scattering is where scattered light has the same frequency as the incident light (Rayleigh scattering). Alternatively, inelastic scattering – where the scattered light has either a lower (Stokes Raman) or higher (Anti-Stokes Raman) frequency than the incident light – may occur. Raman scattering is named after the Indian scientist Sir Chandrashekhara Venkata Raman, who first observed the phenomenon in 1928(246). He received the Nobel Prize for Physics for his work on the Raman effect (i.e. inelastic scattering) in 1930 and in the same year, received an LL.D. from the University of Glasgow(246). However, it was not until the 1960s, after the invention of the laser, that Raman spectroscopes were widely developed for use in analytical chemistry.

Using Raman spectroscopy, Raman scattered light is collected by a spectrometer and the energy difference of scattered light relative to the incident light (i.e. Raman shift) is calculated. This energy difference equates to the energy of the bond vibrations of the molecule. When the energy of the bond vibrations are plotted against the intensity, a unique fingerprint spectrum is acquired for the molecule. This spectrum may change in appearance if factors such as molecular structure and confirmation and chemical environment are altered, as these affect the vibrational energy of each bond within the molecule. Hence, chemists have designed molecules that reliably and predictably change structure in response to an analyte in order to measure the amount of analyte present in a system (by detecting changes in the fingerprint spectra). That said the interaction between incident light and a molecule normally results in Rayleigh scattering rather than Raman (by a factor of 10^7). To overcome this problem and increase the propensity with which light Raman scatters, surface-enhancing techniques are employed, usually functionalising the molecules to high conductivity metals like silver and gold. In doing so, the molecule interacts with surface plasmons (i.e. rapid oscillations of the electron density) on the nanoparticle surface, which creates an electromagnetic field to enhance Raman scattering(247). Furthermore, functionalisation to nanoparticles results in charge transfer between the substrate and the probed molecules. These effects result in significantly stronger Raman scattering(247), which can be detected on a spectrometer. Chemists have engineered nanoparticles to provide optimal surface enhancement of the Raman signal when excited by the relevant incident light, coining the term SERS.

In this proof-of-concept study, which was a collaboration between Samuel J Stanfield (a Chemistry PhD student, Supervisor Professor Colin Campbell) and me, the Raman spectrum of *para*-mercaptobenzoic acid (*p*-MBA) was used to provide information about the pH of the macrophage phagolysosome. *p*MBA - illustrated in Figure 5.2 - contains a carboxylic acid moiety that can be deprotonated to yield the carboxylate anion, resulting in anticipated and dependable changes to the Raman spectrum. Hence, a relationship between pH and Raman signal was established and calibrated. The specifically designed nanosensors (MBA-NP) therefore comprise 150 nm gold nanoparticles functionalised using *p*-MBA. When excited at their plasmon resonance frequency using a 785 nm laser, the gold nanoparticles enhance the spectroscopic response of *p*-MBA molecules. MBA-NP has been shown to accurately quantify pH within the physiological range(178,248–250).

Hypothesis and Aims

It was hypothesised that MBA-NP could be used to measure phagolysosomal pH in macrophages and would be more sensitive than non-ratiometric fluorescence spectroscopy. The aims of the chapter were:

1) Demonstrate nanoparticle uptake into MDM phagolysosomes using transmission electron microscopy.

2) Develop a new *in vitro* experimental technique using optical nanosensors to quantify macrophage phagolysosomal pH.

Figure 5.1

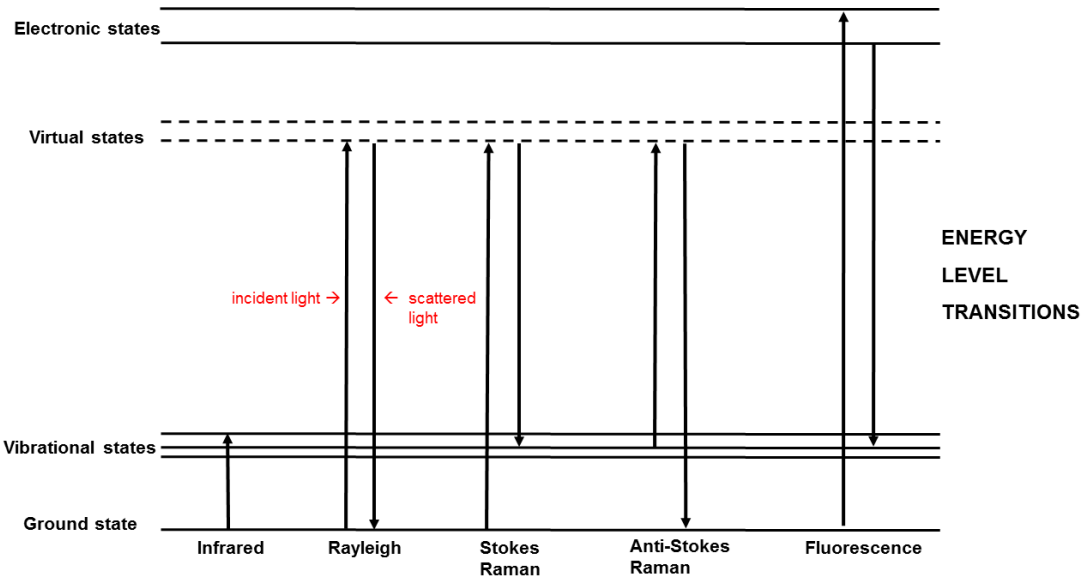

Figure 5.1: Jablonski diagram illustrating infrared, Rayleigh, Raman and fluorescence energy level transitions, modified from(251). *Within this diagram, the absorbance of a photon of a particular energy (i.e. the incident light) by a molecule of interest is indicated by the arrows pointing up. Absorbance is the method by which an electron is excited from a lower energy level to a higher energy level using the energy transferred from the photon. Incident light strikes a surface and excites briefly a molecule within that surface into its "virtual" state (a very short-lived, unobservable quantum state*(251)*). Following this, several scattering possibilities may occur. Elastic scattering is where light has the same frequency as the incident light (Rayleigh scattering) and so returns to the ground state. Alternatively, inelastic scattering – where the scattered light has either a lower (Stokes Raman) or higher (Anti-Stokes Raman) frequency than the incident light – may occur. In contrast, fluorescence involves the emission of a photon by a molecule as a means of dealing with the energy received from the incident light. The energy of the fluorescent photon is always less than that of the incident photon.*

Figure 5.2

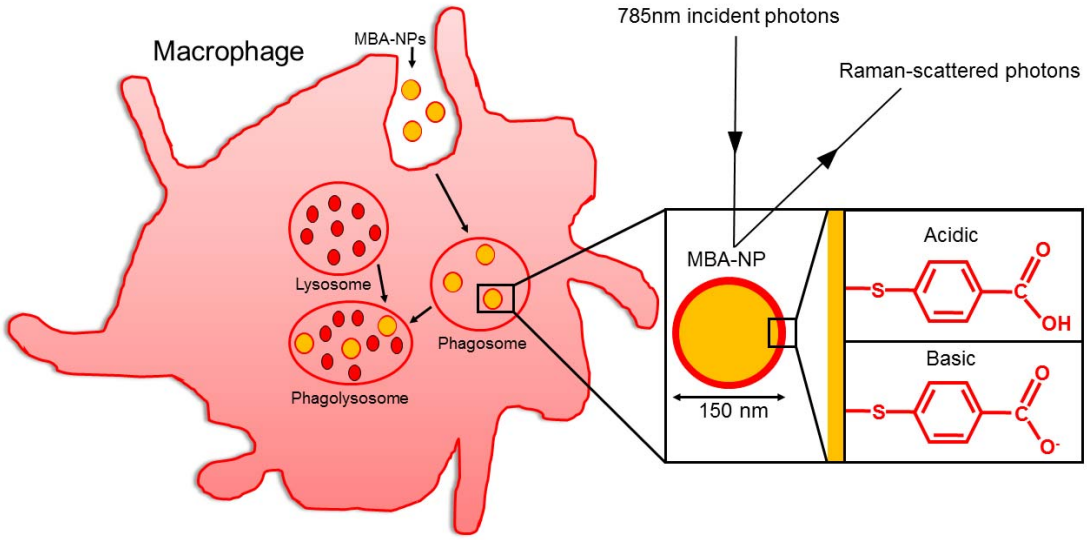

Figure 5.2: Phagocytosis of functionalised gold nanoparticles by a macrophage. *Gold nanoparticles are functionalised with* para-*mercaptobenzoic acid to form our pH-sensitive nanoparticles, MBA-NP. They are engulfed by the cell's plasma membrane, forming an intracellular phagosome. The phagosome fuses with a lysosome, containing proteolytic enzymes, to form an acidic phagolysosome. The right-hand-side demonstrates the structure of MBA-NP (not to scale). Note the alteration of the carboxyl group in response to hydrogen ion concentration within the environment. This structural change gives rise to changes in the Raman spectrum acquired when excited with monochromatic light at 785 nm.*

Results

5.1 Participant demographics reveal no significant differences between groups

Demographic data were analysed and showed that age and sex demographics did not differ between groups (see Table 5.1). This is important because macrophage functions, including phagocytosis, are impaired with increasing age(252,253). CF participant demographics included genotype and $ppFEV_1$ (as detailed in Table 5.2). Experiments were performed on cells from CF participants with F508del mutation (heterozygous and homozygous) to ensure maximal impairment of CFTR function within the CF groups. Lung function varied in the CF participants, with $ppFEV_1$ ranging from 34.1 – 102.1% (mean 65.6%).

Table 5.1

Participant Group Demographics						
	HC (n=6)	**CF (n=6)**	**HC (treated with $CFTR_{inh}$-172) (n=6)**	**HC (treated with Bafilomycin A1) (n=5)**	**CF (treated with Bafilomycin A1) (n=5)**	**Group Comparisons, p-value for one-way ANOVA**
Age range	25-56	18-38	24-43	24-43	18-29	n/a
Mean age (± SD)	36.7 (± 11.7)	27.5 (± 8.19)	31.7 (± 7.9)	33.4 (± 7.77)	24 (± 4.3)	p=0.146 F=0.189 DF=27
Sex	F=3 M=3	F=3 M=3	F = 3 M = 3	F=1 M=4	F=3 M=2	n/a

Table 5.1: Participant group demographics, specifically age and sex*. There are no significant differences in participant demographics, analysed using one-way analysis of variance (ANOVA). SD, standard deviation; F, female; M, male; n/a, not applicable. Sample sizes in parentheses. Data summarised as mean ± SD where appropriate.*

Table 5.2

Cystic Fibrosis Participant Demographics, Genotypes and Spirometry				
Cystic Fibrosis Participant	**Age**	**Sex**	**Genotype**	**Percentage predicted FEV_1**
1	29	F	DF508/1717-1G>A	74.1
2	28	F	DF508/G493x	68.3
3	38	M	DF508/DF508	50.1
4	18	M	DF508/DF508	70.7
5	34	M	DF508/DF508	41.5
6	18	F	DF508/G493x	55.0
7	24	F	DF508/DF508	102.1
8	29	M	DF508/DF508	34.1
9	22	M	DF508/G542x	57.3
10	27	F	DF508/G542x	71.6
11	23	F	DF508/p67L	82.9
12	19	M	DF508/G551d	79.9
Mean ± SD	**25.8 (± 6.3)**	n/a	n/a	**65.6 (± 19)**

Table 5.2: CF participant demographics, including age, sex, genotype and spirometry *with data summarised as mean ± SD where appropriate.* F, female; M, male; % predicted FEV_1 = Percentage Predicted Forced Expiratory Volume in one second; n/a, not applicable; SD, standard deviation.

5.2 Transmission electron microscopy confirmed localisation of MBA-NP to phagolysosomes

Firstly, TEM confirmed that following one-hour co-incubation of MDM and MBA-NP, MBA-NP were present within the cellular organelle of interest (see Figure 5.3). Figure 5.3D demonstrates a 150 nm diameter MBA-NP within an electron-dense, single-membrane endosome, which is characteristic of a phagolysosome(193). Due to the nature of TEM, it was difficult to find phagolysosomes containing MBA-NP and so in some experiments, MDM were pre-treated with LPS to prime them for phagocytosis. Figure 5.4 shows several MBA-NP within a phagolysosome following LPS pre-treatment of MDM. This LPS pre-treatment was not used for the experiments in which Raman spectra were acquired from samples, because the clumping of MBA-NP gave signal intensities too strong to be interpreted.

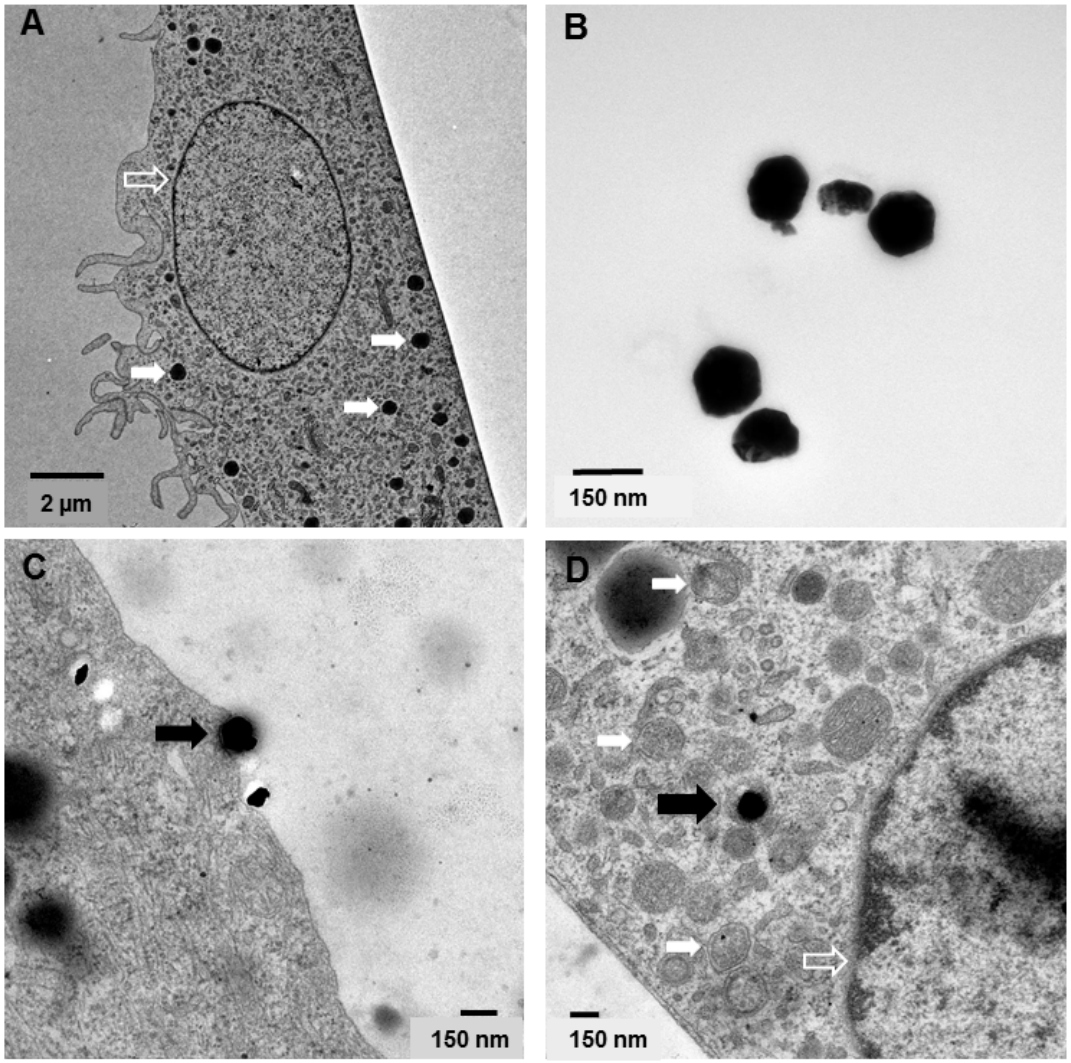

Figure 5.3: Transmission electron microscopy images of monocyte-derived macrophages (MDM) and functionalised nanoparticles (MBA-NP). *Note the difference in scale between* ***A (****2 µm scale bar) and* ***B-D*** *(150 nm scale bar).* ***A)*** *MDM without any MBA-NP. Note the characteristic features: it is a large, irregular cell with an eccentrically placed nucleus (clear white arrow), numerous vesicles and vacuoles, and ruffled surface*(31)*. There are electron-dense, membrane-bound endosomes throughout the cytoplasm (solid white arrows).* ***B)*** *MBA-NP: note their characteristic well-circumscribed, electron-dense appearance and 150 nm diameter.* ***C)*** *MBA-NP being engulfed by the MDM cell membrane (black arrow).* ***D)*** *MBA-NP within a phagolysosome, an electron-dense, membrane-bound organelle (solid black arrow). Note endosomes throughout the cytoplasm (solid white arrows) and the nucleus (clear white arrow). Representative images of n=3 experiments.*

Figure 5.4

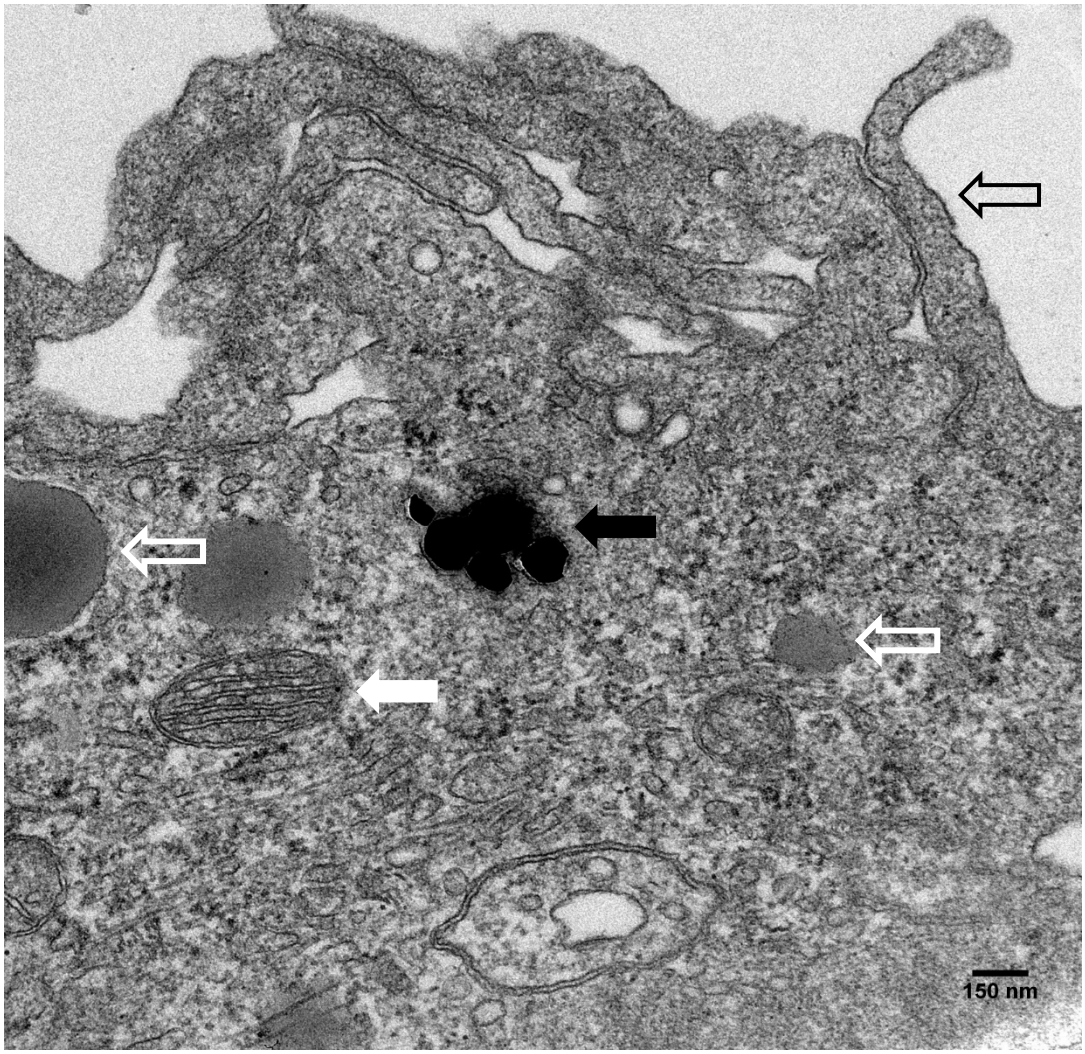

Figure 5.4: Transmission electron microscopy image of a lipopolysaccharide-treated monocyte-derived macrophage (MDM) containing several functionalised nanoparticles (MBA-NP) clumped together in a membrane-bound organelle*, taken to be a phagolysosome (solid black arrow). Also visible is the ruffled surface of the cell membrane (clear black arrow), electron-dense lysosomes (clear white arrows) and a mitochondrion (solid white arrow). The scale bar is set to 150 nm, which is the diameter of a MBA-NP.*

5.3 The percentage of MDM performing MBA-NP phagocytosis in healthy and CF MDM are the same and equally inhibited by cytochalasin D.

Next, the study sought to evaluate whether both CF and HC MDM were capable of efficient phagocytosis of MBA-NP. Whilst there is evidence that bacterial phagocytosis is impaired in CF macrophages(124), it was found that the percentage of MDM that had taken up MBA-NP by phagocytosis did not differ between HC and CF (see Figure 5.5A). Phagocytosis is dependent upon actin polymerisation and so to provide evidence that MBA-NP were being taken up via phagocytosis, MDM were pre-treated with cytochalasin D, an actin polymerisation inhibitor (see Figure 5.5). The percentage of MDM that had taken up MBA-NP decreased significantly by cytochalasin D treatment equally in both genotypes. These results suggest that MBA-NP uptake is unaffected by loss of CFTR function.

Cytochalasin D treatment also affected MDM morphology with treated cells displaying decreased diameter, rounding up and loss of pseudopods (Figure 5.6). These changes occurred consistently in both genotypes.

Figure 5.5

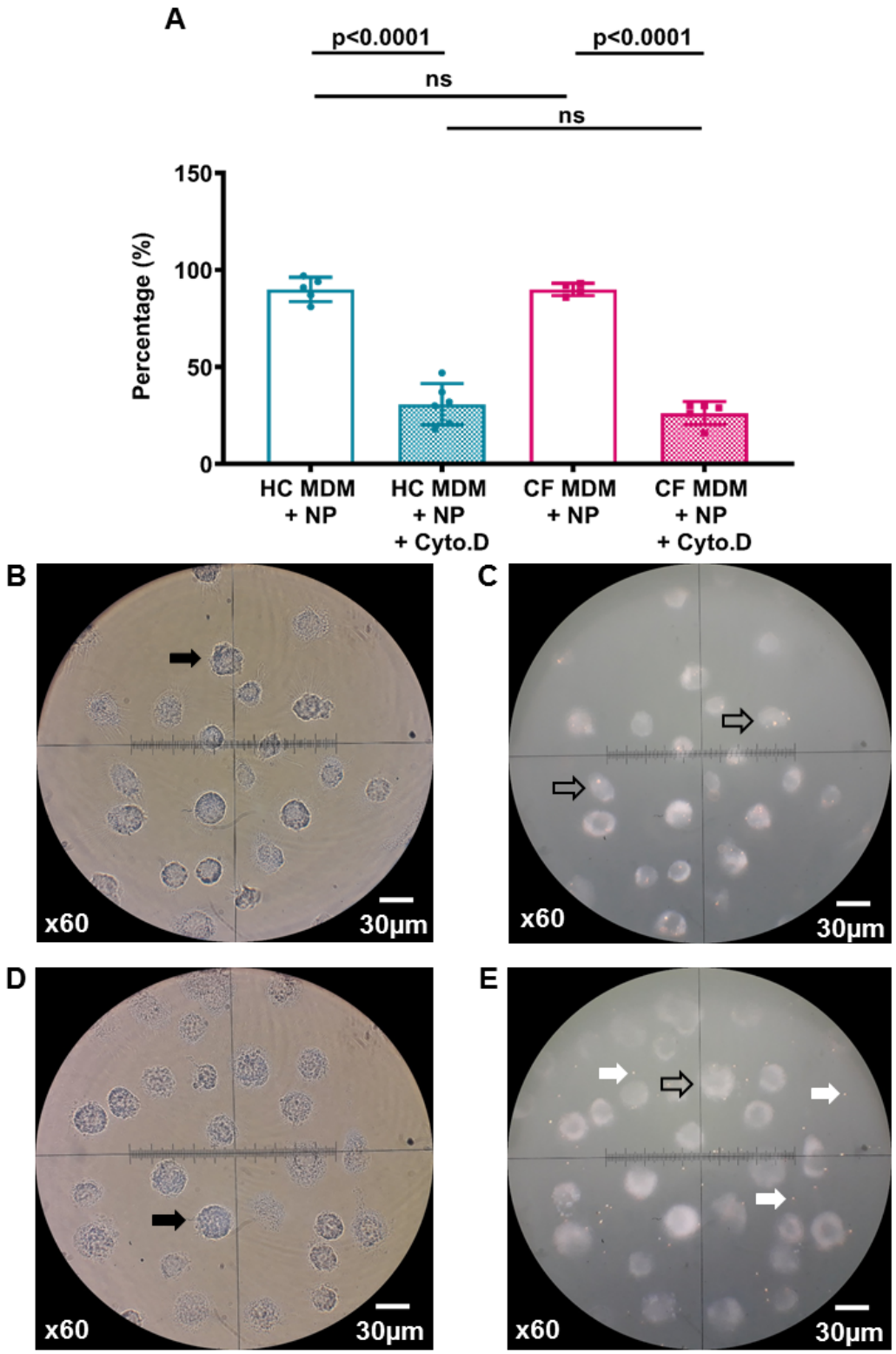
A
p<0.0001
p<0.0001
ns
ns
Percentage (%)
150
100
50
0
HC MDM + NP
HC MDM + NP + Cyto.D
CF MDM + NP
CF MDM + NP + Cyto.D
B
C
D
E
x60
30µm

Figure 5.5: Photomicrograph images used to quantify phagocytosis of functionalised nanoparticles (MBA-NP) by monocyte-derived macrophages (MDM), with and without cytochalasin D (Cyto.D) treatment. *Representative photomicrograph images of MDM from healthy control (HC) and Cystic Fibrosis (CF) donors (all images were photographed using a x60 magnification lens).* ***A)*** *No significant difference in MBA-NP phagocytosis was found between genotypes when quantified by light microscopy: HC 90 ± 6% vs. CF 90 ± 3%, p>0.9999. Cytochalasin D treatment (10 µg/mL) was found to significantly inhibit phagocytosis in both genotypes (HC 30.8 ± 10.6% and CF 26.2 ± 5.93%), p<0.0001. Data analysed using one-way ANOVA with Tukey's multiple comparisons test. Summary data expressed as mean ± SD (n=6 HC and n=5 CF).* ***B-E*** *are representative photomicrograph images used to quantify phagocytosis (scale bar = 30µm):* ***B)*** *MDM (solid black arrows);* ***C)*** *MDM with intracellular MBA-NP (clear black arrows);* ***D)*** *Light microscopy of MDM treated with cytochalasin D; and* ***E)*** *MDM with mostly extracellular MBA-NP (solid white arrows) when treated with cytochalasin D.*

Figure 5.6

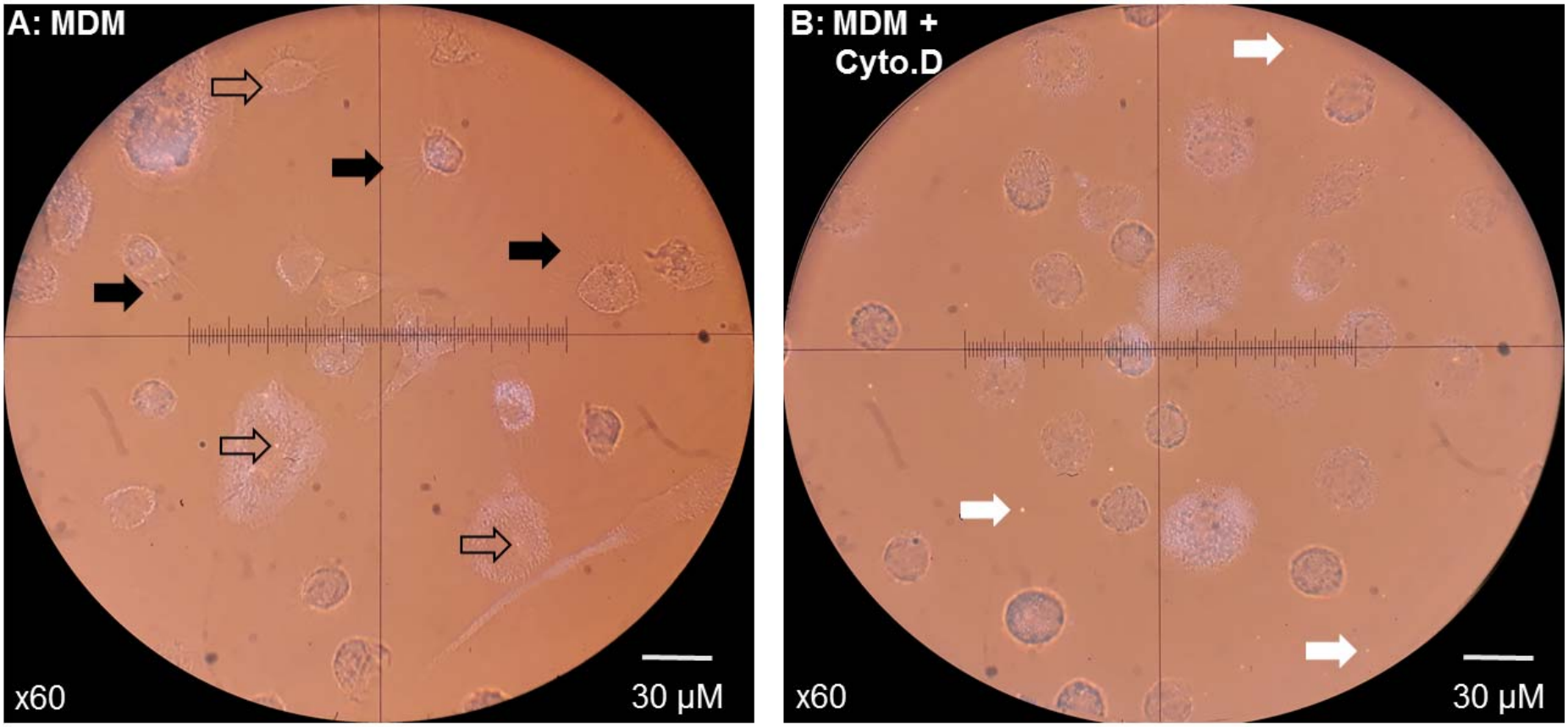

Figure 5.6: Photomicrograph images illustrate Cystic Fibrosis (CF) monocyte-derived macrophage (MDM) morphology in the presence and absence of cytochalasin D (Cyto. D) *(all images were photographed using a x60 magnification lens). MDM were differentiated from peripheral blood mononuclear cells over seven days then incubated with functionalised nanoparticles (MBA-NP) for one hour. Where MDM were treated with cytochalasin D, this actin polymerisation inhibitor was present during a one hour pre-treatment and during MDM-MBA-NP incubation. MDM morphology changes in the presence of cytochalasin D. CF MDM* ***(A)*** *were spread out on the glass coverslip and numerous pseudopods were present (solid black arrows). Intracellular MBA-NP are evident (clear black arrows). In contrast, with cytochalasin D* ***(B)****, MDM have decreased diameter and have rounded up, with loss of pseudopods. As in Figure 5.5, cytochalasin D inhibits MBA-NP uptake, with the majority remaining extracellularly (white arrows). This was a consistent finding in all experiments and was present in both genotypes. Representative images of n = 10 experiments.*

5.4 SERS-based nanosensors accurately quantify pH

Preceding data demonstrated that MBA-NP uptake rates do not differ between HC and CF MDM. We next determined whether the Raman shift resulting from inelastic scattering of 785 nm photons off internalised MBA-NP could be measured to quantify accurately the pH of the phagolysosome. A calibration curve was formulated from data collected by my collaborator Samuel J Stanfield (Figure 5.7C) by plotting pH measurements of IMDM titrated with NaOH/HCl using a Mettler-Toledo InLab Ultra-Micro-ISM pH electrode and against spectra from the MBA-NP collected on a Raman spectrometer (Figure 5.7A&B). The calibration curve R^2 = 0.9895 (see Materials and Methods, section 2.5.3 for details of the line equation) and permits accurate measurement of pH ranging from 4.0 – 9.0.

Figure 5.7

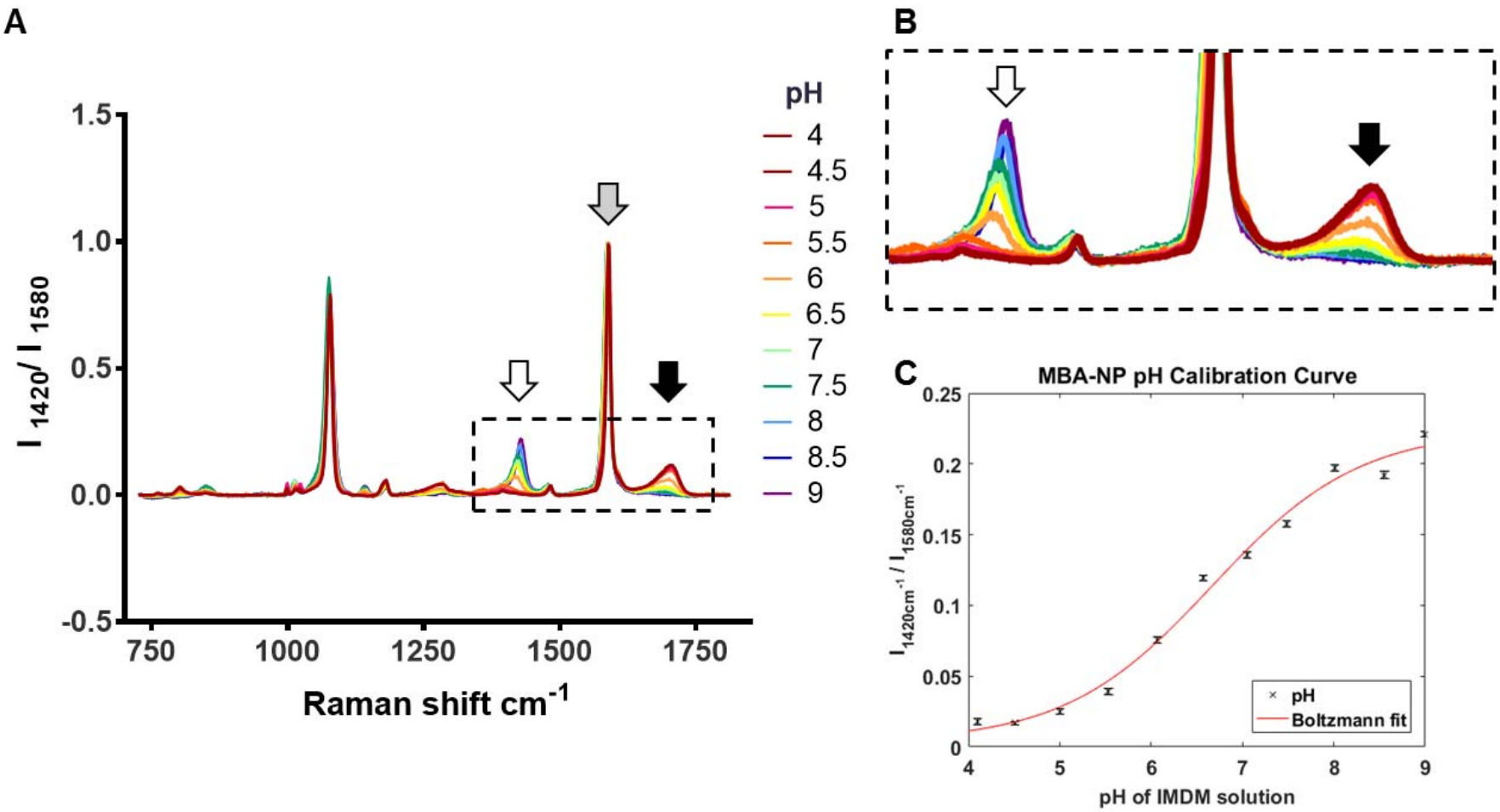
A
B
C
pH
4
4.5
5
5.5
6
6.5
7
7.5
8
8.5
9
1.5
1.0
0.5
0.0
-0.5
750
1000
1250
1500
1750
Raman shift cm-1
I 1420/ I 1580
MBA-NP pH Calibration Curve
0.25
0.2
0.15
0.1
0.05
0
4
5
6
7
8
9
pH of IMDM solution
I1420cm-1 / I1580cm-1
pH
Boltzmann fit

Figure 5.7: Surface enhanced Raman spectroscopy (SERS) spectra obtained from gold nanoparticles functionalised with* para-*mercaptobenzoic acid (MBA-NP) at pH values 4.0 – 9.0 and subsequent generation of a pH calibration curve. ***A)*** *SERS spectra of* para-*mercaptobenzoic acid (*p-*MBA) at pH values 4 to 9. The spectra were baseline corrected and normalised to a reference Raman-shift position (1580 cm^{-1}) (grey arrow), the intensity of which was invariant to pH.* ***With*** *increasing acidity, there was a decrease in the COO^- peak at ~1420 cm^{-1}(white arrow) and a corresponding increase in the CO peak at ~1700 cm^{-1} (black arrow) - see panel* ***B)*** *for close-up image of relevant spectra.* ***C)*** *Nanosensor pH calibration curve, formulated by plotting pH measurements of IMDM titrated with NaOH/HCl using a Mettler-Toledo InLab Ultra-Micro-ISM pH electrode against band ratios of spectra from the MBA-NP collected on a Raman spectrometer (Intensity1420cm^{-1}/Intensity1580cm^{-1} ($I_{1420}cm^{-1}/I_{1580}cm^{-1}$).*

5.5 Preliminary experiments generated Raman heat maps from extracellular and intracellular MBA-NP

Preliminary experiments were conducted in which MDM and MBA-NP were incubated together for 60 min before acquisition of spectra. Raman heat maps were collected with a Renishaw streamline 785 nm laser at 0.875 mW and a 30 s acquisition time. Raman heat map acquisition was possible because the microscope had a motorised XY stage and the software enabled us to acquire a complete spectrum at each pixel of the image. The software interrogates these spectra to generate false colour images to highlight where Raman peak intensity occurs. In effect, this permits visualisation of where the MBA-NP are within the field-of-view. Specifically, the data were processed using WIRE™ 2.0 software, to produce heat maps of Raman intensity based on the peak at 1580 cm^{-1}, in which any pixels with a relative Raman intensity at 1580 cm^{-1} are highlighted in green. The SERS spectra obtained at those areas clearly demonstrate alkaline conditions extracellularly and acidic conditions intracellularly after 60 min MDM-MBA-NP incubation (Figure 5.8).

Figure 5.8

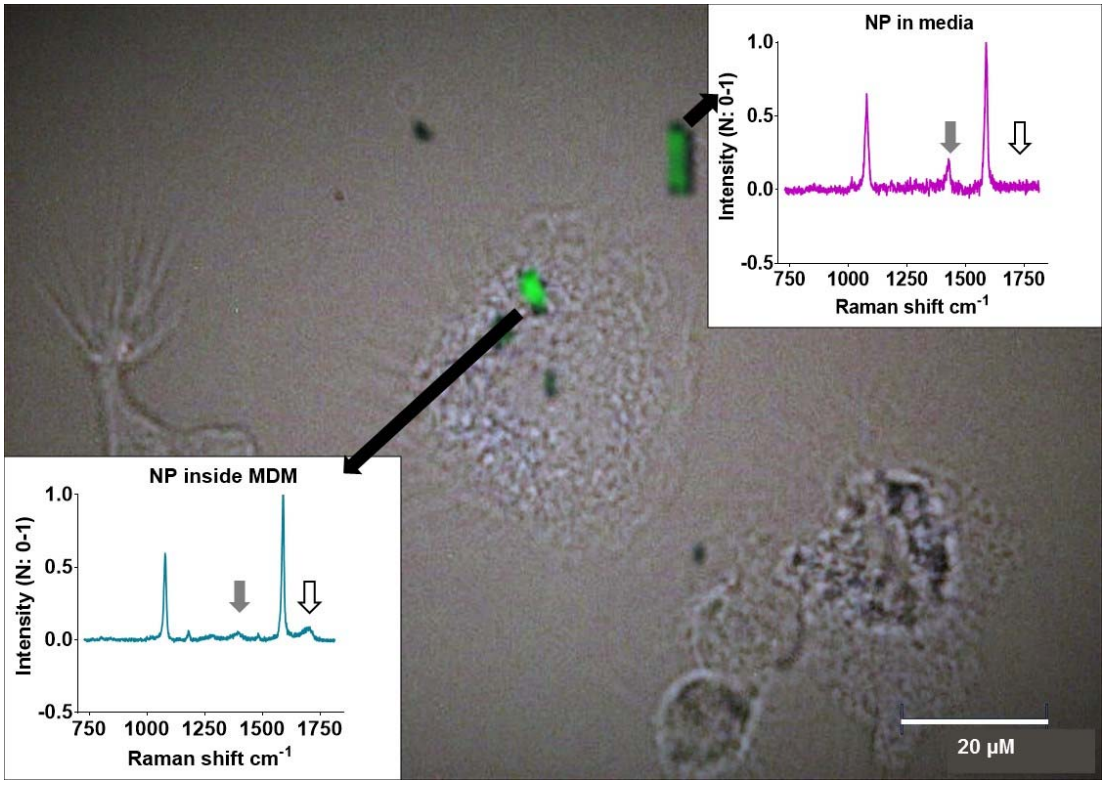

Figure 5.8: Acquisition of Raman heat maps. *Representative photomicrograph image showing functionalised nanoparticles (MBA-NP) both inside and outside of a healthy control MDM, imaged following 60 min co-incubation. Superimposed green areas (false-coloured using WIRE™ 2.0 software) show relative Raman intensity at 1580 cm^{-1} and therefore the position of MBA-NP within the field-of-view. Focussed SERS spectra were acquired from both of these MBA-NP. The resultant inset spectra show alkaline conditions extracellularly (purple spectra), with a clear increase in the COO- peak at ~ 1420 cm^{-1} (solid grey arrow) and acidic conditions intracellularly (blue spectra), with an increase in the CO peak at ~ 1700 cm^{-1} (clear black arrow). Representative image of n=3 experiments.*

5.6 Sequential SERS measurements demonstrate the rate of phagolysosome acidification is equal between HC and CF MDM

Having optimised the spectral acquisition technique, subsequent live cell Raman microscopy enabled targeting of a single MBA-NP for acquisition of spectra, allowing spatially defined ratiometric measurement. To obtain temporally resolved pH measurements, Raman spectra were acquired from the same MBA-NP at least every five min from 10 min of incubation with MDM through to two hours from n=3 from each genotype (see Figure 5.9). To do this, light microscopy was used to identify an extracellular MBA-NP in contact with the cell membrane, which was then followed it as it was taken up by the cell and processed through the phagocytosis apparatus. Raman spectra were acquired over time, which demonstrated spectral change from basic to acidic appearances (see Figure 5.7) as the MBA-NP was processed into acidic compartments. To avoid possible laser damage to the cells and MBA-NP during these two hour-long experiments, the laser power was reduced to 0.0875 mW (from 0.875 mW for the other acquisitions, which gave optimal spectra in terms of signal/noise ratio). This laser power of 0.0875mW is far below that which has been shown to be safe to use within living cells(254) but still gave satisfactory spectra. Visual inspection of the macrophage morphology, as well as of the Raman spectra, confirmed that the laser damaged neither the cells nor the nanosensors during our experiments.

The results confirm that as the individual MBA-NP were internalised and processed through the cells' phagocytosis apparatus, the pH progressively decreases at a similar rate in both genotypes, with most if not all pH decrease

occurring over ~15-20 minutes and stabilising after 60 min incubation (see Figure 5.9) to between pH 4.5-5.5. These data are consistent with previous studies, which suggest maximal acidification is reached within 5-15 min of particle ingestion(241,242,255) and our monitoring of pH over time revealed that pH had stabilised within 60 min incubation of MBA-NP with MDM (Figure 5.9), suggesting full maturation of the phagolysosome. Hence, the 60-minute time point was selected to acquire spectra from MBA-NP within multiple cells, to provide accurate comparison of mature phagolysosomal pH between CF and HC MDM.

Figure 5.9

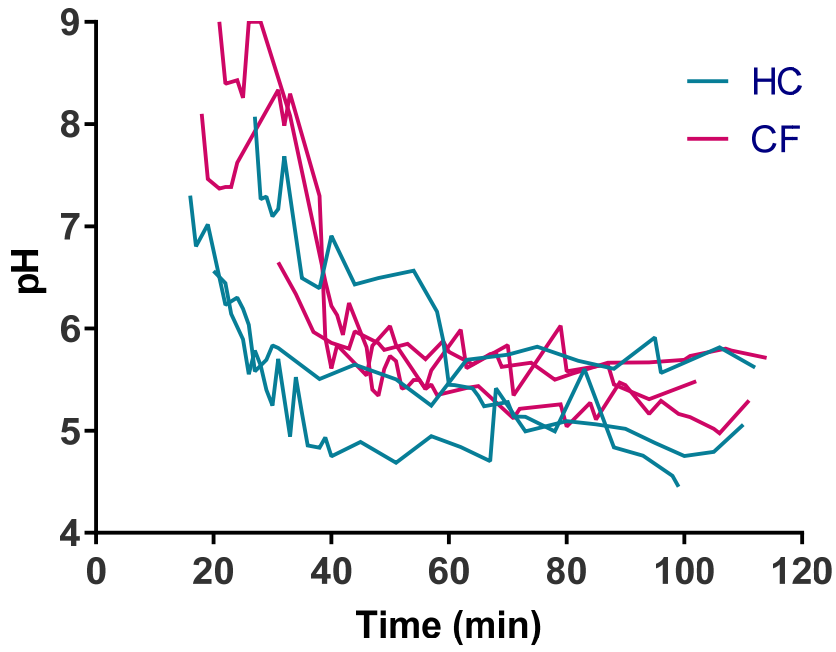

Figure 5.9: Sequential SERS measurements from individual functionalised nanoparticles (MBA-NP) quantify pH as the MBA-NP are phagocytosed by monocyte-derived macrophages. *Healthy control (HC) data shown in blue and Cystic Fibrosis (CF) in pink. SERS measurements quantify the pH of MDM phagocytosis organelles as MBA-NP were processed from the extracellular environment into a mature phagolysosome. MDM were incubated with MBA-NP for 10 min prior to acquisition of Raman spectra from an MBA-NP, which was taken up by the MDM and processed through the phagocytosis apparatus over two hours. MDM phagolysosomal acidification occurs at a similar rate in both genotypes with most of the pH decrease occurring in ~15-20 minutes and pH was stable at ~4.5-5.5 by 60 min. n=3 for each genotype.*

5.7 SERS measurements reveal no difference in phagolysosomal pH between CF and HC MDM

We finally went on to address whether there was an acidification defect in CF MDM phagolysosomes. All these experiments had spectral acquisition performed following 60 minutes' incubation of MDM with MBA-NP. To confirm that MBA-NP were sensitive to pH changes, phagolysosomal pH was measured following incubation of MDM with Bafilomycin A1, a vacuolar ATPase inhibitor required for macrophage phagosomal acidification(256). We anticipated alkaline SERS spectra from MBA-NP in Bafilomycin A1-treated cells, which would strengthen our conviction that the MBA-NP were within phagolysosomes. In addition, we interrogated the role of CFTR protein in phagolysosomal acidification by treating HC MDM with $CFTR_{inh}$-172 in some experiments. We hypothesised that pharmacological inhibition of the CFTR protein would result in pH readouts similar to those obtained from MBA-NP within CF MDM.

As shown in Figure 5.10A, there was no statistically significant difference between phagolysosomal pH of HC and CF MDM. Furthermore, pharmacological inhibition of CFTR by $CFTR_{inh}$-172 treatment did not alter phagolysosomal pH in HC MDM (Figure 5.10A). As hypothesised, when both HC and CF MDM were treated with Bafilomycin A1, phagolysosomes failed to acidify, reaching pH of 7.74 and 7.48 for HC and CF MDM, respectively, in agreement with existing literature(242).

Figure 5.10

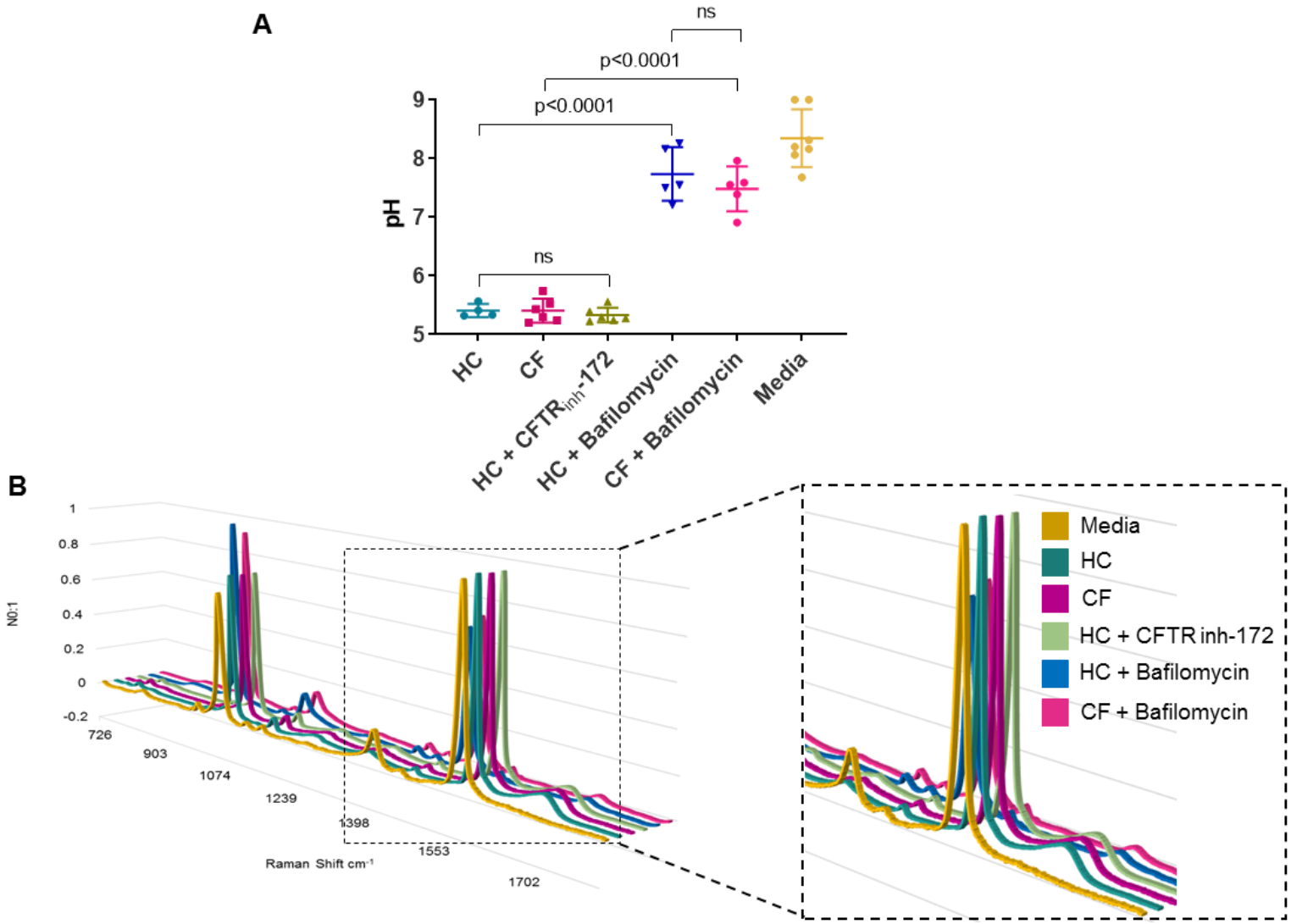
A
ns
p<0.0001
p<0.0001
ns
pH
9
8
7
6
5
HC
CF
HC + CFTRinh-172
HC + Bafilomycin
CF + Bafilomycin
Media
B
1
0.8
0.6
0.4
0.2
0
-0.2
NO:1
726
903
1074
1239
1398
1553
1702
Raman Shift cm-1
Media
HC
CF
HC + CFTR inh-172
HC + Bafilomycin
CF + Bafilomycin

Figure 5.10: Quantification of monocyte-derived macrophage (MDM) phagolysosomal pH using surface enhanced Raman spectroscopy (SERS)-based nanosensors. ***A)*** *MBA-NP quantify pH of MDM phagolysosomes. There was no statistically significant difference between phagolysosomal pH of HC and CF MDM: 5.41 ± 0.11 vs. 5.41 ± 0.20, p>0.9999. Pharmacological inhibition of Cystic Fibrosis Transmembrane conductance Regulator (CFTR) by $CFTR_{inh}$-172 treatment did not alter phagolysosomal pH in HC MDM, which measured 5.33 ± 0.13, p=0.999. There was a statistically significant increase in pH from nanosensors within the media compared to within MDM phagolysosomes, media pH measuring 8.34 ± 0.49, p<0.0001. Bafilomycin A1 treatment equally inhibits phagolysosomal acidification in both genotypes (p<0.0001); pH measured 7.74 ± 0.46 and 7.48 ± 0.38 for HC and CF, respectively.* ***B)*** *Averaged spectra from each group showing a clear difference spectra from intracellular MBA-NP vs. those within media and those treated with Bafilomycin A1. Summary data expressed as mean ± SD and analysed using one-way ANOVA with Sidak's multiple comparisons test. Sample sizes: HC, n=4 (comprising 13 technical replicates from different cells); CF, n=6 (comprising 18 technical replicates); $CFTR_{inh}$-172, n=6 (comprising 18 technical replicates); media, n=7 (comprising 10 technical replicates); HC + Bafilomycin A1 n=5 (comprising 18 technical replicates); and CF + Bafilomycin A1 n=5 (comprising 20 technical replicates).*

5.8 Comparison between SERS-based nanosensors and pHrodo™ Green Zymosan Bioparticles® Conjugates revealed MBA-NP were superior in quantification of MDM phagolysosomal pH

As a comparison to our novel technique, we also measured MDM phagolysosomal acidification using pHrodo™ Green Zymosan Bioparticles® Conjugates. pHrodo™ is a fluorogenic dye that significantly increases its fluorescence emission with decreasing environmental pH. There was no statistically significant difference in mean fluorescence intensity (MFI) between genotypes (see Figure 5.11), in agreement with our nanosensor data.

In addition, both cytochalasin D and Bafilomycin A1 treatment significantly decreased fold change in MFI. The reduced fluorescence in the presence of cytochalasin D was likely due to less Zymosan Bioparticles® being trafficked into the phagolysosomes. Bafilomycin A1 on the other hand functions to inhibit vacuolar ATPase and so it is likely that the Bioparticles® reached an alkaline phagolysosome.

These data also demonstrate pHrodo™ measurement is highly variable with a high coefficient of variation (CV) in both HC and CF (15.6% and 13.5% respectively) when compared with MBA-NP (2 and 4% respectively), underlining the superior accuracy of measuring pH with nanosensors.

Figure 5.11

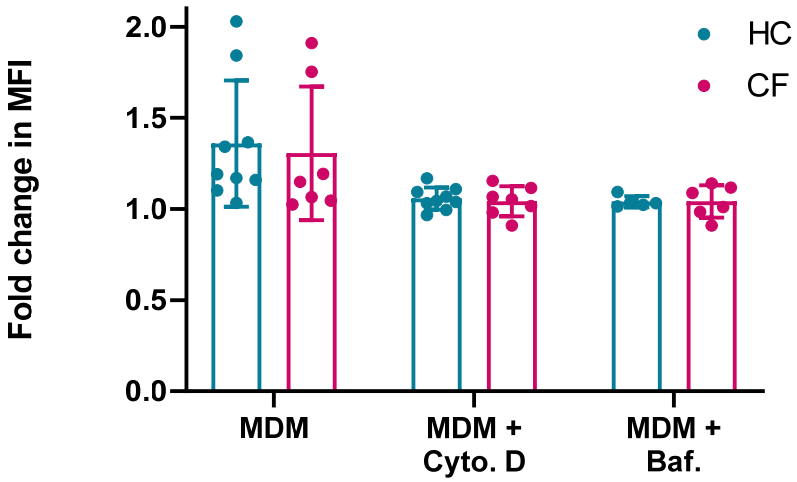

Figure 5.11: Measurement of monocyte-derived macrophage (MDM) phagolysosomal acidification using pHrodo™ Green Zymosan Bioparticles® Conjugates fluorescence spectroscopy. *MDM were incubated with pHrodo™ Green Zymosan Bioparticles® Conjugates for one hour. In some experiments, cells were treated with the actin polymerisation inhibitor, cytochalasin D (Cyto. D) or the vacuolar ATPase inhibitor, Bafilomycin A1 (Baf.) as a pre-treatment and during incubation with the Zymosan. Fluorescence was then measured using a digital plate reader. Mean Fluorescence Intensity (MFI) increases with increasing acidification and was expressed as a fold change from Zymosan-only control wells. There are statistically significant decreases in fold-change in MFI from MDM treated with cytochalasin D and Bafilomycin A1, p=0.003 and p=0.006, respectively. Genotype did not significantly affect fold change in MFI. Summary data expressed as mean ± SD and analysed using two-way ANOVA and Tukey's multiple comparisons test. Sample sizes: HC n=9, CF n=7, HC + Cyto.D n=8, CF + Cyto.D n=7, HC + Bafilomycin A1 n=5, CF = Bafilomycin A1 n=6.*

Discussion

This chapter aimed to examine whether SERS-based nanosensors could be used to measure the pH of macrophage phagolysosomes with greater accuracy than fluorescence spectroscopy techniques. This is an important question because a debate exists in the literature around whether defective phagolysosomal acidification contributes to bacterial colonisation and infection and therefore the pathogenesis of CF lung disease.

The first step in addressing this question was to provide evidence that the MBA-NP are trafficked into the phagolysosome. Phagocytosis has been defined as "*the uptake of large particles (>0.5 μm) into cells*" and "*occurs by an actin-dependent mechanism and is usually independent of clathrin"*(257). Professional phagocytes such as macrophages, neutrophils and dendritic cells internalise particulate matter with high efficiency. However, as described in this review article by Aderem and Underhill(257), phagocytosis has had to evolve into an extremely complex process, so as to deal with the wide array of microbes and self-debris requiring clearance. Importantly, there are diverse receptor structures that play a role in phagocytosis, including receptors for immunoglobulin (FcR), complement (CR1 and CR3), lipids (phosphatidylserine and oxidised lipids), and scavenger receptors. Indeed, scavenger receptors have been directly implicated in the uptake of gold nanoparticles with diameters < 100 nm(258) and nanoparticles of various sizes, including those ≤ 0.5 μM, have been taken up by macrophages via size-

independent phagocytosis(259). In agreement, we used TEM to demonstrate that 150 nm diameter MBA-NP are taken up into membrane-bound, electron-dense organelles, the appearance of which were in keeping with phagolysosomes(193). Our images are remarkably similar to those published by Chithrani *et al.*(260) and support our assertion that MBA-NP are phagocytosed. Furthermore, the measured pH falls as low as pH 4.4 - 5.0 when spectra were acquired over two hours, suggesting that MBA-NP are in a phagolysosome, as late endosomes usually do not acidify to that extent(127).

Having established that MBA-NP nanosensors were indeed transported into the organelle of interest, we then asked whether uptake was affected by CFTR function. Previous studies have suggested that CF macrophage phagocytosis is impaired. This may be due to numerous factors, for example the high levels of NE present in CF airways may result in cleavage of CR1(261) and so bacterial recognition will be impaired. Furthermore, in a study of human macrophages from HC and CF participants, macrophages from the CF sputum had significantly reduced expression of scavenger receptors and CD206 at both the mRNA and protein levels, the former was shown to impair phagocytosis of non-opsonised particles as well as microbes(262). Analysis of photomicrograph images (Figure 5.5) taken using the Raman microscope permitted effective quantification of nanosensor uptake in our model. There was no difference in nanosensor uptake between genotypes, indicating MBA-NP uptake is CFTR independent.

MDM were treated with cytochalasin D as a pharmacological means by which to interrogate underlying endocytic pathways. Cytochalasin D inhibits nanosensor uptake equally in both genotypes, demonstrating an active involvement of the actin cytoskeleton in uptake of nanosensors. Reassuringly, photomicrograph images such as those represented in Figure 5.6 reveal that cytochalasin D modulates MDM morphology, in agreement with published literature(263,264) and provide further evidence that the inhibitor was pharmacologically active in our model. Whilst these results do not answer whether uptake was via phagocytosis or macropinocytosis, both of which are actin-dependent endocytic pathways, this question has been addressed in other studies: França *et al.* used pharmacological inhibitors of mediators of macropinocytosis and clathrin-mediated endocytosis to confirm that 150 nm gold NP uptake was likely via phagocytosis(258). Regardless of the endocytic pathway used by MDM, the TEM images of MBA-NP within membrane-bound organelles coupled with SERS pH readouts of 4.0 - 5.0 strongly suggest that MBA-NP end up in a phagolysosome.

After establishing that MBA-NP were located in the phagolysosome after 60 minutes of incubation with MDM, we next measured the organelle's pH. SERS-based nanosensors are a novel means of quantifying the phagolysosomal pH environment of macrophages and this data suggests they are superior to conventional fluorescence spectroscopy for several reasons. Firstly, a general limitation of fluorescence-based pH measurements is the

concentration range the sensor covers. This range is dependent upon the acid dissociation constant (K_a) of the fluorophore, which gives a sigmoidal calibration curve with a non-linear association between fluorescence and pH, meaning that pH quantification may be insensitive at the sensor's range limit(235). It is therefore important to have a sensor with a wide range, especially when interrogating the endosomal-lysosomal system in which the pH can alter by at least 2.5 units from baseline(235). In contrast to pH-sensitive fluorophores, MBA-NP are excited using a single wavelength and use the ratio of vibrational modes from a single reporter molecule to measure pH in a range that is determined by the reporter's pK_a. Thus, MBA-NP are concentration independent, i.e. pH measurement is independent of the number of particles phagocytosed. Whilst ratiometric, dual-dye fluorescence spectroscopy protocols such as that performed by Haggie and Verkman(242) may address this problem to an extent, there remains the limitations of differential bleaching and laser drift, to which nanosensors are insensitive. Hence, MBA-NP nanosensors exhibit superiority over fluorescence spectroscopy in terms of sensitivity, ratiometric quantification, and both spatial and temporal resolution.

Raman spectroscopy also enabled real-time monitoring of reductions in pH as the MBA-NP were processed through the phagocytosis apparatus with excellent spatial resolution. Numerous other studies have investigated the kinetics of phagolysosomal acidification and suggest acidification begins within

two to three minutes of fluorescent probe binding and is completed within 5-15 min(20,241,242,255,265–267). In contrast, the data in this chapter demonstrates that it took up to 60 min for phagolysosomal maturation to occur, potentially because our MBA-NP are processed differently to Zymosan or bacteria.

The key question addressed in this chapter was whether macrophage phagolysosomal acidification was CFTR dependent. Using SERS-based nanosensors we found no significant difference in phagolysosomal acidification between human CF and HC MDM; this observation was further confirmed by pharmacological inhibition of CFTR using $CFTR_{inh}$-172. Taken together, these findings suggest CFTR has no direct role in phagolysosomal acidification. Our comparative analysis of phagolysosomal pH measurement using conventional fluorescence spectroscopy also demonstrated no difference between HC and CF macrophages, but with a higher degree of uncertainty. Phagolysosomal acidification was found to be sensitive to the vacuolar ATPase inhibitor, Bafilomycin A1, suggesting that the phagosome formed around MBA-NP both contains and is acidified by this crucial regulator of acidification, similar to the phagosomes formed around bacteria(256,265). The data in this chapter imply that the well-established bacterial killing defect of CF macrophages(20,268–270) may not be solely due to failure of phagolysosomal acidification. We suggest that future experiments utilising a SERS-based approach would permit the measurement of other sub-cellular

processes, such as intracellular redox potential(271), which may contribute to the impaired bacterial killing noted in CF macrophages.

Earlier studies of CF macrophage phagolysosomal acidification used murine macrophages in which *CFTR* has been deleted (20,242,243,272). In spite of this, and in contrast to humans, CF mice do not develop spontaneous lung disease and thus the relevance of these studies' observations to human disease remains questionable. Conversely, a strength of this study is that it investigated acidification of phagolysosomes in primary human HC and CF MDM and our data underline the importance of undertaking such studies in humans.

There were two key limitations to our experimental model. The first was the use of MDM because we were unable to obtain HC and CF alveolar macrophages (from bronchoalveolar lavage or sputum). We acknowledge that MDM are unlikely to function identically to alveolar macrophages, which acquire an activated phenotype in the context of the CF lung, which has an inflammatory milieu(273,274). Measurement of the phagolysosomal pH of alveolar macrophages, ideally from human participants, using SERS-based nanosensors would be an important goal for further research. The second key limitation of our model is that macrophage endocytosis and phagolysosomal acidification are adaptive processes and so there may be differences in macrophage phagolysosomal maturation for MBA-NP compared to bacteria.

Future experiments, in which alveolar macrophages uptake bacteria such as *H.influenzae, S.aureus and P.aeruginosa* alongside MBA-NP would be of interest to address this limitation and to mimic more accurately the CF lung environment.

With regard to additional directions for future work, it would be interesting and important to investigate the precise mechanisms by which MBA-NP were endocytosed by macrophages, perhaps through antibody-mediated inhibition of the various cell surface receptors that may be responsible, or through use of a cell line in which receptor expression has been inhibited using small interfering RNA(258). Confocal microscopy could potentially be used to show co-localisation of nanosensors with phagolysosomal markers such as lysosomal-associated membrane proteins 1 and 2 (LAMP-1, -2) and lysosomal integral membrane protein (LIMP-II)(239). Furthermore, probes of this general design (i.e. a sensing molecule attached to a metal nanoparticle) have the potential to be utilised in other areas of innate immune cell study. For example, nanosensors could be used to measure the pH of the neutrophil phagosome, which does not acidify(275). Whilst the focus of these proof-of-concept experiments was on CF, our technique could have widespread application to a wide range of respiratory diseases associated with airway infection and inflammation such as pneumonia, Tuberculosis, Chronic Obstructive Pulmonary Disease and non-CF bronchiectasis.

In conclusion, we have developed a novel and highly accurate technique with which to measure phagolysosomal acidification, compatible with real-time analysis of phagocytosis. Using SERS-based nanosensors, we demonstrate that MDM phagolysosomal acidification is CFTR-independent and may not be critical in the pathophysiology of CF.

Chapter 6: General Discussion, Therapeutic Implications and Future Directions

Summary of Key Findings

The absence of functional CFTR protein in neutrophils and macrophages from CF patients causes impaired innate immune responses and contributes to the pathophysiology of CF lung disease.

There were two main aims of this project: firstly, to determine whether increased production of NETs was associated with airways inflammation and lung function decline in CF and secondly, to determine whether CF macrophages display impaired phagolysosomal acidification using nanosensor-based measurements.

NETs are associated with airways inflammation and increased severity of CF lung disease

In Chapter 3, I confirmed that NETs, defined based on histone-associated calprotectin, accumulate in CF airways. CF participants were free of recent respiratory tract infection (i.e. >two weeks), demonstrating that NETs are abundant in CF airways even with stable disease. Furthermore, sub-analysis

of the CF cohort showed no difference in levels of sputum NETs in patients with or without colonisation with *P.aeruginosa* or *A.fumigatus,* suggesting that NETs do not play a significant antimicrobial role in CF lung disease. However, sputum NETs were associated with airways inflammation as measured by levels of proinflammatory cytokines and represent a significant independent predictor of lung function.

CF participants treated with once daily nebulised rhDNase (recombinant human deoxyribonuclease; dornase alfa) had a significant reduction in sputum NETs compared to CF participants not taking the drug, suggesting that DNase eithers inhibits NET formation or facilitates lysis of NETs and their removal via the mucociliary clearance escalator.

There are two therapeutic implications of our findings. Firstly, disrupting NETs likely represents an important therapeutic target in the treatment of CF lung disease. Dornase alfa (rhDNase) is a mucolytic treatment that breaks down polymerised DNA and is indicated in CF patients over five years of age with an FVC of greater than 40% predicted to improve lung function(144,276,277). This nebulised therapy has been shown to reduce neutrophilic inflammation, possibly due to improved mucociliary clearance of fragmented DNA(149,278). Our data implies that rhDNase also functions to inhibit NET formation or clear NETs once they are formed, suggesting that early use of rhDNase therapy represents a prophylactic measure against airways inflammation. I therefore

suggest that future longitudinal clinical studies should investigate whether the introduction of rhDNase in patients younger than five years of age would protect patients from lung function decline. Furthermore, proinflammatory NET-associated proteins, including NE, MPO and calprotectin, may represent therapeutic targets to counter the unrelenting neutrophilic inflammation of CF lung disease.

NETs are proinflammatory to MDM and this effect is enhanced in CF

The *in vitro* co-culture model used in Chapter 3 demonstrated that NETs were proinflammatory via stimulation of proinflammatory cytokine release from MDM. This effect was enhanced in CF MDM and when the NETs were CF neutrophil-derived. Using blood-derived innate immune cells instead of airway samples meant that intrinsic defects could be delineated, without confounding effects from microbial colonisation in the lung environment. These observations suggest that blood-derived neutrophils and MDM have intrinsic defects in function due to *CFTR* mutation. Furthermore, DNase treatment abrogated MDM IL-8 production, hinting at an anti-inflammatory mechanism of action.

CF mice have an exaggerated acute inflammatory response to LPS

In chapter 4, a mouse model of acute sterile lung inflammation was used to determine that CF mice have an exaggerated inflammatory response to LPS

relative to WT littermates, both in terms of BALF proinflammatory cytokine concentrations and histological acute lung injury scores. RT-PCR experiments revealed that CF mice have increased RAGE mRNA expression. This observation requires further research to determine whether RAGE upregulation is linked to the chronic inflammation characterising CF lung disease. BALF NETs increase at peak inflammation and fall during resolution of inflammation. Going against our hypothesis and human study data, however, the CF mice did not produce more NETs in comparison to WT littermates. In addition, although there were consistent trends suggesting DNase was targeting NETs, the difference between groups did not reach statistical significance. We conclude that the CF mouse model is useful in investigating dysfunctional innate immune cells but does not fully mimic NET formation of human disease.

SERS-based nanosensors accurately quantify MDM phagolysosomal pH

Chapter 5 demonstrated that SERS-based nanosensors are a sensitive tool with which to quantify MDM phagolysosomal pH using *ex vivo* live cell imaging of HC and CF cells. To our knowledge, this is the first time these nanosensors have been used in this context. TEM confirmed nanosensor localisation to the phagolysosomes. We revealed that SERS-based nanosensors are superior to non-ratiometric fluorescence spectroscopy in pH quantification and that phagolysosomal acidification is CFTR-independent, which agrees with previous studies(135,241,243).

The therapeutic implications of these results are limited because the experiment was a proof-of-concept study to confirm a new utility of nanosensor technology. If future experiments confirm that human alveolar macrophage phagolysosomal acidification is similarly CFTR-independent, this would suggest that pharmacological manipulation of phagolysosomal pH might not be an important therapeutic strategy for CF drug development.

Future Directions

The most striking and unexplored finding of Chapter 3 was that CF sputum neutrophils contain numerous cytoplasmic vacuolations, not present in HC sputum neutrophils. One might expect these vacuolations to represent phagosomes or phagolysosomes, given the microbial colonisation of the lungs from which the cells originated, and yet the majority of these vacuolations did not contain bacteria. At the time of literature review, this increase in sputum neutrophil vacuolation in CF relative to HC is a previously unpublished finding.

There is one paper by Mihalache *et al.* investigating autophagy-related necrotic cell death of neutrophils in the context of several inflammatory conditions(279). *Ex vivo* lung tissue sections from cystic fibrosis patients (n=3) were fixed then stained with H&E and light microscopy examination to reveal cytoplasmic vacuolation of neutrophils (presumed to be within the alveolar compartments, although this is not specified)(279). The authors did not

expand upon this finding in the context of CF airway neutrophils but concluded that inflammatory neutrophils have a propensity for autophagy-related necrotic cell death(279).

In a study by Luciani *et al.,* mechanisms linking CFTR and autophagy have been interrogated using mouse and human epithelial cell culture and *in vivo* mouse experiments(280,281). Defective CFTR up-regulates ROS and transglutaminase 2 (TG2), the latter an enzyme which catalyses calcium-dependent post-translational modifications of proteins(280). TG2 drives the sequestration of the beclin 1 interactome (a complex of proteins critical for autophagosome formation), into aggresomes. Intervention by overexpression of beclin 1, inhibition of TG2 using cystamine, and treatment with anti-oxidants rescued autophagy and restored CFTR trafficking to the plasma membrane in mouse and human CF epithelial cells. IP anti-oxidant treatment of mice similarly restored autophagy and decreased lung inflammation (shown by an increase in LC3-positive vesicles and decreased macrophage infiltration and MPO activity in the lungs, respectively) of mice homozygous for F508del mutation in CFTR(281).

Data in Chapter 3 shows increased cytoplasmic vacuolation in CF neutrophils when compared to HC neutrophils, suggesting defective CFTR in these innate immune cells is associated with abnormal autophagy. We hypothesise autophagy is increased in CF and may contribute to the increased airway NET

formation seen in our CF cohort(14,76)(76)(76). Hence, it may be beneficial to inhibit autophagy in CF. This hypothesis would be in-keeping with a recent study by Tang *et al.* who investigated associations between autophagy and NET formation in the context of anti-neutrophil cytoplasmic antibody (ANCA)-associated vasculitis(76). In this study, they show that LAMP-2 (the receptor for chaperone-mediated autophagy, which directly translocates cytosolic proteins across the lysosomal membrane for degradation within the lysosomes(282)) is an antigen for auto-antibodies and is incorporated into NETs during NET formation(76). Additionally, anti-LAMP-2 antibody-stimulated neutrophils displayed increased NET formation and autophagosome formation and decreased apoptosis(76). They showed that the non-specific autophagy inhibitors 3MA and LY294002 significantly inhibited this NET formation(76) via impaired chromatin decondensation, although underlying signalling pathways remain unknown. Additionally, Junkins *et al.* compared bacterial clearance of *P.aeruginosa* in normal human16HBE14o$^-$ bronchial epithelial cells, and CFTR DF508 homozygous CFBE41o$^-$ epithelial cells(283). The CFBE41o$^-$ cells had defective killing of internalised bacteria, which was abrogated by rapamycin, which induces autophagy(283).

Considering these studies' conclusions alongside my findings in Chapter 3, which show CF sputum neutrophils to have increased cytoplasmic vacuolations, I hypothesise that CF sputum neutrophils have abnormalities in autophagy regulation, causing increased autophagy, which in turn contributes

to excessive NET formation. This should be investigated using a combination of TEM and immunofluorescence microscopy to a) look for double membrane vesicles and b) identify the presence of autolysosomes within both HC and CF neutrophils. Autolysosomes could be identified by co-localisation of microtubule-associated proteins 1A/1B light chain 3B (LC3) and lysosomal markers (e.g. LAMP-1/2 or LIMP-II) by fluorescence microscopy. Possible associations between NET formation and autophagy in HC and CF blood neutrophils would be further interrogated by quantification of PMA-induced NET formation in the presence or absence of autophagy inhibitors (e.g. using one of the selective Vps34 inhibitors(284))(285)(285)(284)(284)(283)(283)(282)(282)(282)(18)(18).

Vps34 (*v*acuolar *p*rotein *s*orting) is a Class III phosphatidylinositol 3-kinase (PI3K). The PI3K family of enzymes are a family of lipid kinases capable of phosphorylating the 3rd hydroxyl on phosphoinositides in cell membranes(284). Vps34 signalling plays a role in membrane trafficking and protein sorting pathways. It is therefore critical for autophagosome formation and so pharmacological inhibitors of Vps34 would be permit more specific for study of autophagy than other non-specific PI3K inhibitors such as Wortmannin and LY294002, which have been used in previous autophagy studies but may cause abnormalities in NET formation through the induction of apoptosis, rather than by direct affecting autophagy(76,285,286). Fluorescence microscopy will also be utilised to image autophagy markers in this model. I hypothesise CF neutrophils will undergo NET formation more readily and have increased autophagy, relative to HC neutrophils, and that

autophagy inhibitors will inhibit NET formation. If this hypothesis was confirmed, subsequent studies could investigate the potential role of Vps34 inhibitors in the treatment of the chronic inflammation contributing to CF lung disease pathogenesis. Ultimately, this may lead to a new class of anti-inflammatory drugs for CF patients.

With regard to the *in vitro* MDM-neutrophil co-culture model described in Chapter 3, there are several ways in which the experimental model could be improved. I only sampled supernatants at 24 hours' post-co-culture and it may be that proinflammatory cytokine production peaks earlier than this(211) and so supernatants could be harvested at 0, 6, 12, 18 and 24 hours post co-culture. Furthermore, I used a neutrophil:MDM ratio of 2:1 based on our group's previous work(70). This may not mimic *in vivo* conditions and so the ratio of cells within sputum sample differential cell counts could be calculated to inform future experiments. It might also be worth introducing human bronchial epithelial cells into the model, again to better mimic the airway environment. TRIzol-treated co-culture samples could be interrogated using RNA sequencing in an attempt to discover which cell signalling pathways are responsible for the NET-induced exaggerated inflammatory response seen in CF. I hypothesise that these experiments would reveal upregulation of genes involved in the proinflammatory pathways such as NF-κB and MAPK. This would be in agreement with the recently published, elegant study by Carmona-Rivera *et al.*, who investigated adenosine-induced NET formation and NET-

macrophage interactions in the context of a genetic, systemic vasculitis called Deficiency of adenosine deaminase 2 (DADA2)(287). The authors carried out *in vitro* co-culture experiments, similar to those performed in Chapter 3, between NETs and macrophages; contact of NETs with macrophages activated NF-κB translocation to nuclei of the macrophages and led to their production and release of proinflammatory cytokines, including TNF-α(287). Given that NETs have at least 24 associated proteins incorporated onto their chromatin backbone, it is probable that numerous pathways will be implicated in the CF MDM hyper-inflammatory phenotype. To determine which of these NET proteins are the most inflammatory to MDM, experiments in which the major protein constituents of NETs (e.g. histones, NE, MPO, calprotectin, and LL37) were blocked with neutralising antibodies in the NETs/MDM co-culture model would be informative, measuring proinflammatory cytokine production to characterise responses.

Regarding the CF mouse model used in Chapter 4, the LPS-mediated acute lung injury (ALI) experiments require a PBS control experiment in which BAL fluid NETs are quantified using our in-house ELISA. I would hypothesise that the airway neutrophils from PBS-treated animals would not undergo NET formation, which when contrasted to results from the LPS-mediated ALI experiments, would confirm or refute our hypothesis that LPS induces *in vivo* NET formation in a murine CF model. Admittedly, the CF mouse model has its limitations because the mice do not develop spontaneous post-natal lung

disease and so do not closely model the human disease. However, such experiments remain an important adjunct to clinical studies, in which drug treatments, in particular, can be tested prior to being introduced to human participants.

Going forward, a chronic inflammation model could be established, using $CFTR^{-/-}$ and WT mice, to better represent human CF lung disease. In view of my findings, the focus will likely shift away from NET formation and towards whether RAGE-dependent AMPK activation and subsequent autophagosome formation is the driving mechanism underlying the exaggerated inflammatory response seen in CF mice. Western blot and RT-PCR could be used to study the protein and gene expression of relevant proteins (e.g. RAGE, AMPK, Vps34, and LC3) in *in vitro* mouse and human bronchial epithelial cell lines, as well as *ex vivo* mouse airway innate immune cells from $CFTR^{-/-}$ and WT mice. Such studies could also be performed on *ex vivo* human lung tissue to provide further evidence that autophagy is implicated in the inflammation characterising CF lung disease(199).

Murine alveolar macrophages from WT and CF murine BAL fluid could also be used to extend the SERS-based nanosensor experiments in the future. Alveolar macrophages could be isolated by flow sorting (using Siglec-F as a macrophage marker) from BAL samples. The isolated alveolar macrophages would be incubated with MBA-NP as described in Chapter 5 to permit

quantification of their phagolysosomal pH using Raman spectroscopy. We hypothesise that, in line with the data from human MDM phagolysosomal pH experiments, there will be no acidification defect in CF murine alveolar macrophages. This would have implications for CF patients because it might highlight that macrophage phagolysosomal acidification should not be a target for new therapies in CF.

Ultimately, to permit extrapolation of results to our CF population, we need to perform the SERS-based nanosensor experiments using human alveolar macrophages from HC and CF participants obtained via BAL. With regard to the CF cohort, this would permit the study of cells that are likely to have ingested bacteria, which may have an effect upon phagolysosomal maturation. In addition to this, HC alveolar macrophages could be cultured with SERS-based nanosensors alone or in combination with nanosensors in addition to bacteria that which commonly colonise/infect the lungs of CF patients (e.g. *P.aeruginosa, H.influenzae, S.aureus, B.cepacia)* then Raman spectroscopy used to quantify pH. It may be that the presence of bacteria affects phagolysosomal pH. It has been shown that bacteria have numerous mechanisms by which to evade phagocytosis-mediated degradation via inhibition of acidification (e.g. *Mycobacterium tuberculosis* prevents accumulation of vacuolar ATPase on phagolysosomal membranes(239,288)). Thus, I hypothesise that in the presence of internalised bacteria, the alveolar macrophage phagolysosomes will not fully acidify or will do so more slowly.

It would also be important to confirm whether CFTR is present in these human alveolar macrophages and expressed on their phagolysosomal membranes; we cannot surmise that acidification is CFTR-dependent/-independent if we have not shown the protein to be present within the system. CFTR identification could be done by total cellular protein extraction from alveolar macrophages then using an anti-CFTR antibody for subsequent western blot analysis. Fluorescence microscopy using anti-CFTR antibodies, as used by Su *et al.*(211), would also permit imaging of CFTR localisation to the phagolysosomal membrane. I would predict that CFTR is present within macrophages, in line with previous reports(19–21,124,219) and located to the phagolysosomal and plasma membranes. These future experiments would provide further evidence that SERS-based nanosensors represent a new tool with which to investigate phagolysosomal acidification in live cell systems.

Conclusions

The data presented in this thesis show that neutrophils and NETs are key regulators of airways inflammation in CF lung disease. Within the CF airways, neutrophils accumulate and undergo NET formation, which is associated with inflammation and subsequent lung function decline. These data suggest that DNase either inhibits NET formation or aids in the clearance of NETs through their fragmentation and thus could represent a prophylactic therapy for paediatric patients, rather than being introduced only once lung disease is

established. Furthermore, the data suggests that macrophage phagolysosomal acidification is CFTR independent and so other factors must be responsible for the bacterial killing defect of CF macrophages. Future research will focus on 1) whether there is enhanced autophagy in CF neutrophils and whether this affects NET formation, and 2) whether SERS-based nanosensors can be used to measure alveolar macrophage phagolysosomal pH, in both the presence and absence of bacteria. Ultimately, we hope our research will contribute to the discovery of new drug targets in CF lung disease, with the overall aim of improving the quality of life and increasing the life expectancy of our patients.

References

1. UK CF Registry at-a-glance report 2017 [Internet]. Cystic Fibrosis Trust.; 2017 [cited 2019 Oct 6]. Available from: https://www.cysticfibrosis.org.uk/the-work-we-do/uk-cf-registry/reporting-and-resources/at-a-glance-report-2017

2. Kelly J. Environmental scan of cystic fibrosis research worldwide. Journal of Cystic Fibrosis. 2017 May;16(3):367–70.

3. Quinton PM. Physiological Basis of Cystic Fibrosis: A Historical Perspective. Physiological Reviews. 1999 Jan;79(1):S3–22.

4. Nick JA. Cystic Fibrosis: History [Internet]. National Jewish Health; 2012 [cited 2019 Oct 6]. Available from: https://www.nationaljewish.org/conditions/cystic-fibrosis-cf/history

5. Fanconi G, Uehlinger E, Knauer C. Das Coeliakie-syndrom bei angeborener zystischer Pankreasfibromatose und Bronchiektasien. Wien Med Wchnschr. 1936;86:753–6.

6. Image:Dorothy Hansine Andersen.jpg [Internet]. 2006 [cited 2019 Oct 6]. Available from: http://www.nlm.nih.gov/changingthefaceofmedicine/physicians/bio

7. Andersen DH. CYSTIC FIBROSIS OF THE PANCREAS AND ITS RELATION TO CELIAC DISEASE: A CLINICAL AND PATHOLOGIC STUDY. Am J Dis Child. 1938 Aug 1;56(2):344.

8. Andersen DH. CELIAC SYNDROME: V. Genetics of Cystic Fibrosis of the Pancreas With a Consideration of Etiology. Am J Dis Child. 1946 Jul 1;72(1):62.

9. Kessler WR, Andersen DH. Heat prostration in fibrocystic disease of the pancreas and other conditions. Pediatrics. 1951 Nov;8(5):648–56.

10. Di Sant'agnese P, Darling RC, Perara GA, Shea E. Abnormal electrolyte composition of sweat in cystic fibrosis of the pancreas. AMA Am J Dis Child. 1953 Nov;86(5):618–9; discussion, 619.

11. Collie JTB, Massie RJ, Jones OAH, LeGrys VA, Greaves RF. Sixty-five years since the New York heat wave: Advances in sweat testing for cystic fibrosis: Advances in Cystic Fibrosis Sweat Chloride Testing. Pediatr Pulmonol. 2014 Feb;49(2):106–17.

12. Kerem B, Rommens JM, Buchanan JA, Markiewicz D, Cox TK, Chakravarti A, et al. Identification of the cystic fibrosis gene: genetic analysis. Science. 1989 Sep 8;245(4922):1073–80.

13. Farrell P, Férec C, Macek M, Frischer T, Renner S, Riss K, et al. Estimating the age of p.(Phe508del) with family studies of geographically distinct European populations and the early spread of cystic fibrosis. Eur J Hum Genet. 2018 Dec;26(12):1832–9.

14. Price TD, Knipper C, Grupe G, Smrcka V. Strontium Isotopes and Prehistoric Human Migration: The Bell Beaker Period in Central Europe. Eur j archaeol. 2004;7(1):9–40.

15. Riordan JR, Rommens JM, Kerem B, Alon N, Rozmahel R, Grzelczak Z, et al. Identification of the cystic fibrosis gene: cloning and characterization of complementary DNA. Science. 1989 Sep 8;245(4922):1066–73.

16. Elborn S, Vallieres E. Cystic fibrosis gene mutations: evaluation and assessment of disease severity. AGG. 2014 Oct;161.

17. Livraghi-Butrico A, Kelly EJ, Wilkinson KJ, Rogers TD, Gilmore RC, Harkema JR, et al. Loss of *Cftr* function exacerbates the phenotype of Na^+ hyperabsorption in murine airways. American Journal of Physiology-Lung Cellular and Molecular Physiology. 2013 Apr;304(7):L469–80.

18. Stoltz DA, Meyerholz DK, Welsh MJ. Origins of Cystic Fibrosis Lung Disease. Longo DL, editor. N Engl J Med. 2015 Jan 22;372(4):351–62.

19. Bonfield TL, Hodges CA, Cotton CU, Drumm ML. Absence of the cystic fibrosis transmembrane regulator (Cftr) from myeloid-derived cells slows resolution of inflammation and infection. Journal of Leukocyte Biology. 2012 Nov 1;92(5):1111–22.

20. Di A, Brown ME, Deriy LV, Li C, Szeto FL, Chen Y, et al. CFTR regulates phagosome acidification in macrophages and alters bactericidal activity. Nature Cell Biology. 2006 Sep;8(9):933–44.

21. Paemka L, McCullagh BN, Abou Alaiwa MH, Stoltz DA, Dong Q, Randak CO, et al. Monocyte derived macrophages from CF pigs exhibit increased inflammatory responses at birth. Journal of Cystic Fibrosis. 2017 Jul;16(4):471–4.

22. Plasschaert LW, Žilionis R, Choo-Wing R, Savova V, Knehr J, Roma G, et al. A single-cell atlas of the airway epithelium reveals the CFTR-rich pulmonary ionocyte. Nature. 2018 Aug;560(7718):377–81.

23. CFTR protein [Internet]. [cited 2019 Jun 29]. Available from: http://massgenomics.org/2011/02/a-promising-new-drug-for-cystic-fibrosis.html

24. Morgan WJ, Butler SM, Johnson CA, Colin AA, FitzSimmons SC, Geller DE, et al. Epidemiologic study of cystic fibrosis: design and implementation of a prospective, multicenter, observational study of patients with cystic fibrosis in the U.S. and Canada. Pediatr Pulmonol. 1999 Oct;28(4):231–41.

25. Gray R, McCullagh B, McCray P. NETs and CF Lung Disease: Current Status and Future Prospects. Antibiotics. 2015 Jan 15;4(1):62–75.

26. Meyerholz DK, Stoltz DA, Gansemer ND, Ernst SE, Cook DP, Strub MD, et al. Lack of cystic fibrosis transmembrane conductance regulator disrupts fetal airway development in pigs. Lab Invest. 2018 Jun;98(6):825–38.

27. Xie Y, Ostedgaard L, Abou Alaiwa MH, Lu L, Fischer AJ, Stoltz DA. Mucociliary Transport in Healthy and Cystic Fibrosis Pig Airways. Annals ATS. 2018 Nov;15(Supplement_3):S171–6.

28. Esther CR, Muhlebach MS, Ehre C, Hill DB, Wolfgang MC, Kesimer M, et al. Mucus accumulation in the lungs precedes structural changes and infection in children with cystic fibrosis. Sci Transl Med. 2019 Apr 3;11(486):eaav3488.

29. De Rose V, Molloy K, Gohy S, Pilette C, Greene CM. Airway Epithelium Dysfunction in Cystic Fibrosis and COPD. Mediators of Inflammation. 2018;2018:1–20.

30. Tabary O, Zahm JM, Hinnrasky J, Couetil JP, Cornillet P, Guenounou M, et al. Selective Up-Regulation of Chemokine IL-8 Expression in Cystic Fibrosis Bronchial Gland Cells in Vivo and in Vitro. The American Journal of Pathology. 1998 Sep;153(3):921–30.

31. Haq IJ, Gray MA, Garnett JP, Ward C, Brodlie M. Airway surface liquid homeostasis in cystic fibrosis: pathophysiology and therapeutic targets. Thorax. 2016 Mar;71(3):284–7.

32. Shah VS, Meyerholz DK, Tang XX, Reznikov L, Abou Alaiwa M, Ernst SE, et al. Airway acidification initiates host defense abnormalities in cystic fibrosis mice. Science. 2016 Jan 29;351(6272):503–7.

33. Smith JJ, Welsh MJ. cAMP stimulates bicarbonate secretion across normal, but not cystic fibrosis airway epithelia. J Clin Invest. 1992 Apr 1;89(4):1148–53.

34. Pezzulo AA, Tang XX, Hoegger MJ, Abou Alaiwa MH, Ramachandran S, Moninger TO, et al. Reduced airway surface pH impairs bacterial killing in the porcine cystic fibrosis lung. Nature. 2012 Jul;487(7405):109–13.

35. Abou Alaiwa MH, Beer AM, Pezzulo AA, Launspach JL, Horan RA, Stoltz DA, et al. Neonates with cystic fibrosis have a reduced nasal liquid pH; A small pilot study. Journal of Cystic Fibrosis. 2014 Jul;13(4):373–7.

36. Khan TZ, Wagener JS, Bost T, Martinez J, Accurso FJ, Riches DW. Early pulmonary inflammation in infants with cystic fibrosis. Am J Respir Crit Care Med. 1995 Apr;151(4):1075–82.

37. Konstan MW, Ratjen F. Effect of dornase alfa on inflammation and lung function: Potential role in the early treatment of cystic fibrosis. Journal of Cystic Fibrosis. 2012 Mar;11(2):78–83.

38. Sly PD, Gangell CL, Chen L, Ware RS, Ranganathan S, Mott LS, et al. Risk Factors for bronchiectasis in Children with Cystic Fibrosis. New England Journal of Medicine. 2013 May 23;368(21):1963–70.

39. Regamey N, Tsartsali L, Hilliard TN, Fuchs O, Tan H-L, Zhu J, et al. Distinct patterns of inflammation in the airway lumen and bronchial mucosa of children with cystic fibrosis. Thorax. 2012 Feb;67(2):164–70.

40. Hartl D, Gaggar A, Bruscia E, Hector A, Marcos V, Jung A, et al. Innate immunity in cystic fibrosis lung disease. Journal of Cystic Fibrosis. 2012 Sep;11(5):363–82.

41. Aujla SJ, Dubin PJ, Kolls JK. INTERLEUKIN-17 IN PULMONARY HOST DEFENSE. Experimental Lung Research. 2007 Jan;33(10):507–18.

42. Henig NR. Sputum induction as a research tool for sampling the airways of subjects with cystic fibrosis. Thorax. 2001 Apr 1;56(4):306–11.

43. Summers C, Rankin SM, Condliffe AM, Singh N, Peters AM, Chilvers ER. Neutrophil kinetics in health and disease. Trends in Immunology. 2010 Aug;31(8):318–24.

44. Pillay J, den Braber I, Vrisekoop N, Kwast LM, de Boer RJ, Borghans JAM, et al. In vivo labeling with 2H2O reveals a human neutrophil lifespan of 5.4 days. Blood. 2010 Jul 29;116(4):625–7.

45. Teng T-S, Ji A, Ji X-Y, Li Y-Z. Neutrophils and Immunity: From Bactericidal Action to Being Conquered. Journal of Immunology Research. 2017;2017:1–14.

46. Rigby KM, DeLeo FR. Neutrophils in innate host defense against Staphylococcus aureus infections. Semin Immunopathol. 2012 Mar;34(2):237–59.

47. Hoth JJ, Wells JD, Hiltbold EM, McCall CE, Yoza BK. Mechanism of Neutrophil Recruitment to the Lung After Pulmonary Contusion: Shock. 2011 Jun;35(6):604–9.

48. Miralda I, Uriarte SM, McLeish KR. Multiple Phenotypic Changes Define Neutrophil Priming. Front Cell Infect Microbiol. 2017;7:217.

49. Worthen GS, Haslett C, Rees AJ, Gumbay RS, Henson JE, Henson PM. Neutrophil-mediated Pulmonary Vascular Injury: Synergistic Effect of Trace Amounts of Lipopolysaccharide and Neutrophil Stimuli on Vascular Permeability and Neutrophil Sequestration in the Lung. Am Rev Respir Dis. 1987 Jul;136(1):19–28.

50. Amulic B, Cazalet C, Hayes GL, Metzler KD, Zychlinsky A. Neutrophil Function: From Mechanisms to Disease. Annu Rev Immunol. 2012 Apr 23;30(1):459–89.

51. Winterbourn CC, Kettle AJ, Hampton MB. Reactive Oxygen Species and Neutrophil Function. Annu Rev Biochem. 2016 Jun 2;85(1):765–92.

52. Nijhawan D, Honarpour N, Wang X. Apoptosis in neural development and disease. Annu Rev Neurosci. 2000;23:73–87.

53. Savill JS, Wyllie AH, Henson JE, Walport MJ, Henson PM, Haslett C. Macrophage phagocytosis of aging neutrophils in inflammation. Programmed cell death in the neutrophil leads to its recognition by macrophages. J Clin Invest. 1989 Mar 1;83(3):865–75.

54. Jones HR, Robb CT, Perretti M, Rossi AG. The role of neutrophils in inflammation resolution. Seminars in Immunology. 2016 Apr;28(2):137–45.

55. Yasuhara S, Asai A, Sahani ND, Martyn JAJ. Mitochondria, endoplasmic reticulum, and alternative pathways of cell death in critical illness: Critical Care Medicine. 2007 Sep;35(Suppl):S488–95.

56. Kaczmarek A, Vandenabeele P, Krysko DV. Necroptosis: The Release of Damage-Associated Molecular Patterns and Its Physiological Relevance. Immunity. 2013 Feb;38(2):209–23.

57. Iba T, Hashiguchi N, Nagaoka I, Tabe Y, Murai M. Neutrophil cell death in response to infection and its relation to coagulation. j intensive care. 2013 Dec;1(1):13.

58. Labbé K, Saleh M. Cell death in the host response to infection. Cell Death Differ. 2008 Sep;15(9):1339–49.

59. Cheng OZ, Palaniyar N. NET balancing: a problem in inflammatory lung diseases. Frontiers in Immunology [Internet]. 2013 [cited 2017 Dec 12];4. Available from: http://journal.frontiersin.org/article/10.3389/fimmu.2013.00001/abstract

60. Rahman S, Gadjeva M. Does NETosis Contribute to the Bacterial Pathoadaptation in Cystic Fibrosis? Frontiers in Immunology [Internet]. 2014 Aug 11 [cited 2017 Dec 12];5. Available from: http://journal.frontiersin.org/article/10.3389/fimmu.2014.00378/abstract

61. Robb CT, Dyrynda EA, Gray RD, Rossi AG, Smith VJ. Invertebrate extracellular phagocyte traps show that chromatin is an ancient defence weapon. Nature Communications [Internet]. 2014 Dec [cited 2018 Jul 26];5(1). Available from: http://www.nature.com/articles/ncomms5627

62. Palić D, Ostojić J, Andreasen CB, Roth JA. Fish cast NETs: Neutrophil extracellular traps are released from fish neutrophils. Developmental & Comparative Immunology. 2007;31(8):805–16.

63. Chuammitri P, Ostojić J, Andreasen CB, Redmond SB, Lamont SJ, Palić D. Chicken heterophil extracellular traps (HETs): Novel defense mechanism of chicken heterophils. Veterinary Immunology and Immunopathology. 2009 May;129(1–2):126–31.

64. Jeffery U, Kimura K, Gray R, Lueth P, Bellaire B, LeVine D. Dogs cast NETs too: Canine neutrophil extracellular traps in health and immune-mediated hemolytic anemia. Veterinary Immunology and Immunopathology. 2015 Dec;168(3–4):262–8.

65. Brinkmann V. Neutrophil Extracellular Traps Kill Bacteria. Science. 2004 Mar 5;303(5663):1532–5.

66. Law SM, Gray RD. Neutrophil extracellular traps and the dysfunctional innate immune response of cystic fibrosis lung disease: a review. Journal of Inflammation [Internet]. 2017 Dec [cited 2018 Feb 2];14(1). Available from: https://journal-inflammation.biomedcentral.com/articles/10.1186/s12950-017-0176-1

67. Papayannopoulos V. Neutrophil extracellular traps in immunity and disease. Nature Reviews Immunology [Internet]. 2017 Oct 9 [cited 2017 Dec 12]; Available from: http://www.nature.com/doifinder/10.1038/nri.2017.105

68. Kenny EF, Herzig A, Krüger R, Muth A, Mondal S, Thompson PR, et al. Diverse stimuli engage different neutrophil extracellular trap pathways. Elife. 2017 Jun 2;6.

69. G Nel J, Theron AJ, Durandt C, Tintinger GR, Pool R, Mitchell TJ, et al. Pneumolysin activates neutrophil extracellular trap formation. Clin Exp Immunol. 2016 Jun;184(3):358–67.

70. Gray RD, Hardisty G, Regan KH, Smith M, Robb CT, Duffin R, et al. Delayed neutrophil apoptosis enhances NET formation in cystic fibrosis. Thorax. 2017 Sep 15;thoraxjnl-2017-210134.

71. Boeltz S, Amini P, Anders H-J, Andrade F, Bilyy R, Chatfield S, et al. To NET or not to NET:current opinions and state of the science regarding the formation of neutrophil extracellular traps. Cell Death Differ. 2019 Mar;26(3):395–408.

72. Gordon RA, Herter JM, Rosetti F, Campbell AM, Nishi H, Kashgarian M, et al. Lupus and proliferative nephritis are PAD4 independent in murine models. JCI Insight. 2017 May 18;2(10):e92926.

73. Lewis HD, Liddle J, Coote JE, Atkinson SJ, Barker MD, Bax BD, et al. Inhibition of PAD4 activity is sufficient to disrupt mouse and human NET formation. Nat Chem Biol. 2015 Mar;11(3):189–91.

74. Wang Y, Li M, Stadler S, Correll S, Li P, Wang D, et al. Histone hypercitrullination mediates chromatin decondensation and neutrophil extracellular trap formation. The Journal of Cell Biology. 2009 Jan 26;184(2):205–13.

75. Remijsen Q, Vanden Berghe T, Wirawan E, Asselbergh B, Parthoens E, De Rycke R, et al. Neutrophil extracellular trap cell death requires both autophagy and superoxide generation. Cell Res. 2011 Feb;21(2):290–304.

76. Tang S, Zhang Y, Yin S-W, Gao X-J, Shi W-W, Wang Y, et al. Neutrophil extracellular trap formation is associated with autophagy-related signalling in ANCA-associated

vasculitis: NET formation involves autophagy in AAV. Clin Exp Immunol. 2015 Jun;180(3):408–18.

77. Mitroulis I, Kambas K, Chrysanthopoulou A, Skendros P, Apostolidou E, Kourtzelis I, et al. Neutrophil Extracellular Trap Formation Is Associated with IL-1β and Autophagy-Related Signaling in Gout. Fritz JH, editor. PLoS ONE. 2011 Dec 16;6(12):e29318.

78. Germic N, Stojkov D, Oberson K, Yousefi S, Simon H-U. Neither eosinophils nor neutrophils require ATG5-dependent autophagy for extracellular DNA trap formation. Immunology. 2017 Nov;152(3):517–25.

79. Moriceau S, Lenoir G, Witko-Sarsat V. In Cystic Fibrosis Homozygotes and Heterozygotes, Neutrophil Apoptosis Is Delayed and Modulated by Diamide or Roscovitine: Evidence for an Innate Neutrophil Disturbance. Journal of Innate Immunity. 2010;2(3):260–6.

80. Dibbert B, Weber M, Nikolaizik WH, Vogt P, Schoni MH, Blaser K, et al. Cytokine-mediated Bax deficiency and consequent delayed neutrophil apoptosis: A general mechanism to accumulate effector cells in inflammation. Proceedings of the National Academy of Sciences. 1999 Nov 9;96(23):13330–5.

81. Ranganathan SC, Parsons F, Gangell C, Brennan S, Stick SM, Sly PD, et al. Evolution of pulmonary inflammation and nutritional status in infants and young children with cystic fibrosis. Thorax. 2011 May 1;66(5):408–13.

82. Elizur A, Cannon CL, Ferkol TW. Airway Inflammation in Cystic Fibrosis. Chest. 2008 Feb;133(2):489–95.

83. Painter RG, Valentine VG, Lanson, NA, Leidal K, Zhang Q, Lombard G, et al. CFTR Expression in Human Neutrophils and the Phagolysosomal Chlorination Defect in Cystic Fibrosis †. Biochemistry. 2006 Aug;45(34):10260–9.

84. Hampton MB, Kettle AJ, Winterbourn CC. Inside the neutrophil phagosome: oxidants, myeloperoxidase, and bacterial killing. Blood. 1998 Nov 1;92(9):3007–17.

85. Sagel SD, Sontag MK, Accurso FJ. Relationship between antimicrobial proteins and airway inflammation and infection in cystic fibrosis. Pediatr Pulmonol. 2009 Apr;44(4):402–9.

86. Stockley RA. Neutrophils and protease/antiprotease imbalance. Am J Respir Crit Care Med. 1999 Nov;160(5 Pt 2):S49-52.

87. Pohl K, Hayes E, Keenan J, Henry M, Meleady P, Molloy K, et al. A neutrophil intrinsic impairment affecting Rab27a and degranulation in cystic fibrosis is corrected by CFTR potentiator therapy. Blood. 2014 Aug 14;124(7):999–1009.

88. Akong-Moore K, Chow OA, von Köckritz-Blickwede M, Nizet V. Influences of Chloride and Hypochlorite on Neutrophil Extracellular Trap Formation. Wehkamp J, editor. PLoS ONE. 2012 Aug 13;7(8):e42984.

89. Rada B. Neutrophil extracellular trap release driven by bacterial motility: Relevance to cystic fibrosis lung disease. Communicative & Integrative Biology. 2017 Mar 4;10(2):e1296610.

90. Martínez-Alemán SR, Campos-García L, Palma-Nicolas JP, Hernández-Bello R, González GM, Sánchez-González A. Understanding the Entanglement: Neutrophil Extracellular Traps (NETs) in Cystic Fibrosis. Frontiers in Cellular and Infection

Microbiology [Internet]. 2017 Apr 6 [cited 2017 Apr 25];7. Available from: http://journal.frontiersin.org/article/10.3389/fcimb.2017.00104/full

91. Young RL, Malcolm KC, Kret JE, Caceres SM, Poch KR, Nichols DP, et al. Neutrophil Extracellular Trap (NET)-Mediated Killing of Pseudomonas aeruginosa: Evidence of Acquired Resistance within the CF Airway, Independent of CFTR. Jeyaseelan S, editor. PLoS ONE. 2011 Sep 1;6(9):e23637.

92. Fuchs TA, Abed U, Goosmann C, Hurwitz R, Schulze I, Wahn V, et al. Novel cell death program leads to neutrophil extracellular traps. The Journal of Cell Biology. 2007 Jan 15;176(2):231–41.

93. Branzk N, Lubojemska A, Hardison SE, Wang Q, Gutierrez MG, Brown GD, et al. Neutrophils sense microbe size and selectively release neutrophil extracellular traps in response to large pathogens. Nature Immunology. 2014 Sep 14;15(11):1017–25.

94. Marcos V, Zhou-Suckow Z, Önder Yildirim A, Bohla A, Hector A, Vitkov L, et al. Free DNA in Cystic Fibrosis Airway Fluids Correlates with Airflow Obstruction. Mediators of Inflammation. 2015;2015:1–11.

95. Thanabalasuriar A, Scott BNV, Peiseler M, Willson ME, Zeng Z, Warrener P, et al. Neutrophil Extracellular Traps Confine Pseudomonas aeruginosa Ocular Biofilms and Restrict Brain Invasion. Cell Host & Microbe. 2019 Apr;25(4):526-536.e4.

96. Kaplan MJ, Radic M. Neutrophil Extracellular Traps: Double-Edged Swords of Innate Immunity. The Journal of Immunology. 2012 Sep 15;189(6):2689–95.

97. Hakkim A, Fürnrohr BG, Amann K, Laube B, Abed UA, Brinkmann V, et al. Impairment of neutrophil extracellular trap degradation is associated with lupus nephritis. Proc Natl Acad Sci USA. 2010 May 25;107(21):9813–8.

98. Hu SC-S, Yu H-S, Yen F-L, Lin C-L, Chen G-S, Lan C-CE. Neutrophil extracellular trap formation is increased in psoriasis and induces human β-defensin-2 production in epidermal keratinocytes. Sci Rep. 2016 Aug 5;6:31119.

99. Fuchs TA, Brill A, Wagner DD. Neutrophil Extracellular Trap (NET) Impact on Deep Vein Thrombosis. Arteriosclerosis, Thrombosis, and Vascular Biology. 2012 Aug 1;32(8):1777–83.

100. Warnatsch A, Ioannou M, Wang Q, Papayannopoulos V. Neutrophil extracellular traps license macrophages for cytokine production in atherosclerosis. Science. 2015 Jul 17;349(6245):316–20.

101. Kirchner KK, Wagener JS, Khan TZ, Copenhaver SC, Accurso FJ. Increased DNA levels in bronchoalveolar lavage fluid obtained from infants with cystic fibrosis. American Journal of Respiratory and Critical Care Medicine. 1996 Nov;154(5):1426–9.

102. Dubois AV, Gauthier A, Bréa D, Varaigne F, Diot P, Gauthier F, et al. Influence of DNA on the Activities and Inhibition of Neutrophil Serine Proteases in Cystic Fibrosis Sputum. American Journal of Respiratory Cell and Molecular Biology. 2012 Jul;47(1):80–6.

103. Nauseef WM, Kubes P. Pondering neutrophil extracellular traps with healthy skepticism: Skepticism about neutrophil extracellular traps. Cellular Microbiology. 2016 Oct;18(10):1349–57.

104. Urban CF, Ermert D, Schmid M, Abu-Abed U, Goosmann C, Nacken W, et al. Neutrophil Extracellular Traps Contain Calprotectin, a Cytosolic Protein Complex Involved in Host Defense against Candida albicans. Levitz SM, editor. PLoS Pathog. 2009 Oct 30;5(10):e1000639.

105. Abrams ST, Zhang N, Manson J, Liu T, Dart C, Baluwa F, et al. Circulating Histones Are Mediators of Trauma-associated Lung Injury. American Journal of Respiratory and Critical Care Medicine. 2013 Jan 15;187(2):160–9.

106. Bosmann M, Grailer JJ, Ruemmler R, Russkamp NF, Zetoune FS, Sarma JV, et al. Extracellular histones are essential effectors of C5aR- and C5L2-mediated tissue damage and inflammation in acute lung injury. The FASEB Journal. 2013 Dec 1;27(12):5010–21.

107. Fattahi F, Grailer JJ, Lu H, Dick RS, Parlett M, Zetoune FS, et al. Selective Biological Responses of Phagocytes and Lungs to Purified Histones. J Innate Immun. 2017;9(3):300–17.

108. Liu S, Su X, Pan P, Zhang L, Hu Y, Tan H, et al. Neutrophil extracellular traps are indirectly triggered by lipopolysaccharide and contribute to acute lung injury. Sci Rep. 2016 Nov 16;6:37252.

109. Downey DG, Bell SC, Elborn JS. Neutrophils in cystic fibrosis. Thorax. 2008 Oct 3;64(1):81–8.

110. Metzler KD, Fuchs TA, Nauseef WM, Reumaux D, Roesler J, Schulze I, et al. Myeloperoxidase is required for neutrophil extracellular trap formation: implications for innate immunity. Blood. 2011 Jan 20;117(3):953–9.

111. Niggemann B, Stiller T, Magdorf K, Wahn U. Myeloperoxidase and eosinophil cationic protein in serum and sputum during antibiotic treatment in cystic fibrosis patients with *Pseudomonas aeruginosa* infection. Mediators of Inflammation. 1995;4(4):282–8.

112. Downey DG, Martin SL, Dempster M, Moore JE, Keogan MT, Starcher B, et al. The relationship of clinical and inflammatory markers to outcome in stable patients with cystic fibrosis. Pediatr Pulmonol. 2007 Mar;42(3):216–20.

113. Regelmann WE, Siefferman CM, Herron JM, Elliott GR, Clawson CC, Gray BH. Sputum peroxidase activity correlates with the severity of lung disease in cystic fibrosis. Pediatr Pulmonol. 1995 Jan;19(1):1–9.

114. Gray RD, Imrie M, Boyd AC, Porteous D, Innes JA, Greening AP. Sputum and serum calprotectin are useful biomarkers during CF exacerbation. Journal of Cystic Fibrosis. 2010 May;9(3):193–8.

115. Hessian PA, Edgeworth J, Hogg N. MRP-8 and MRP-14, two abundant Ca(2+)-binding proteins of neutrophils and monocytes. J Leukoc Biol. 1993 Feb;53(2):197–204.

116. Yui S, Nakatani Y, Mikami M. Calprotectin (S100A8/S100A9), an inflammatory protein complex from neutrophils with a broad apoptosis-inducing activity. Biol Pharm Bull. 2003 Jun;26(6):753–60.

117. Bullock S, Hayward C, Manson J, Brock DJ, Raeburn JA. Quantitative immunoassays for diagnosis and carrier detection in cystic fibrosis. Clin Genet. 1982 May;21(5):336–41.

118. Dorin JR, Novak M, Hill RE, Brock DJH, Secher DS, van Heyningen V. A clue to the basic defect in cystic fibrosis from cloning the CF antigen gene. Nature. 1987 Apr;326(6113):614–7.

119. Liu JZ, Jellbauer S, Poe AJ, Ton V, Pesciaroli M, Kehl-Fie TE, et al. Zinc Sequestration by the Neutrophil Protein Calprotectin Enhances Salmonella Growth in the Inflamed Gut. Cell Host & Microbe. 2012 Mar;11(3):227–39.

120. Yui S, Nakatani Y, Mikami M. Calprotectin (S100A8/S100A9), an inflammatory protein complex from neutrophils with a broad apoptosis-inducing activity. Biol Pharm Bull. 2003 Jun;26(6):753–60.

121. Passey RJ, Xu K, Hume DA, Geczy CL. S100A8: emerging functions and regulation. J Leukoc Biol. 1999 Oct;66(4):549–56.

122. Riva M, Källberg E, Björk P, Hancz D, Vogl T, Roth J, et al. Induction of nuclear factor-κB responses by the S100A9 protein is Toll-like receptor-4-dependent. Immunology. 2012 Oct;137(2):172–82.

123. Reid PA, McAllister DA, Boyd AC, Innes JA, Porteous D, Greening AP, et al. Measurement of Serum Calprotectin in Stable Patients Predicts Exacerbation and Lung Function Decline in Cystic Fibrosis. American Journal of Respiratory and Critical Care Medicine. 2015 Jan 15;191(2):233–6.

124. Bruscia EM, Bonfield TL. Cystic Fibrosis Lung Immunity: The Role of the Macrophage. Journal of Innate Immunity. 2016;8(6):550–63.

125. Botelho RJ, Teruel M, Dierckman R, Anderson R, Wells A, York JD, et al. Localized Biphasic Changes in Phosphatidylinositol-4,5-Bisphosphate at Sites of Phagocytosis. J Cell Biol. 2000 Dec 25;151(7):1353–68.

126. Flannagan RS, Cosío G, Grinstein S. Antimicrobial mechanisms of phagocytes and bacterial evasion strategies. Nature Reviews Microbiology. 2009 May;7(5):355–66.

127. Russell DG, Vanderven BC, Glennie S, Mwandumba H, Heyderman RS. The macrophage marches on its phagosome: dynamic assays of phagosome function. Nat Rev Immunol. 2009;9(8):594–600.

128. Bonfield TL, Panuska JR, Konstan MW, Hilliard KA, Hilliard JB, Ghnaim H, et al. Inflammatory cytokines in cystic fibrosis lungs. Am J Respir Crit Care Med. 1995 Dec;152(6):2111–8.

129. Meyer M, Huaux F, Gavilanes X, van den Brûle S, Lebecque P, Lo Re S, et al. Azithromycin Reduces Exaggerated Cytokine Production by M1 Alveolar Macrophages in Cystic Fibrosis. American Journal of Respiratory Cell and Molecular Biology. 2009 Nov;41(5):590–602.

130. Bosnar M, Bosnjak B, Cuzic S, Hrvacic B, Marjanovic N, Glojnaric I, et al. Azithromycin and Clarithromycin Inhibit Lipopolysaccharide-Induced Murine Pulmonary Neutrophilia Mainly through Effects on Macrophage-Derived Granulocyte-Macrophage Colony-Stimulating Factor and Interleukin-1. Journal of Pharmacology and Experimental Therapeutics. 2009 Oct 1;331(1):104–13.

131. Rogers CS, Stoltz DA, Meyerholz DK, Ostedgaard LS, Rokhlina T, Taft PJ, et al. Disruption of the CFTR Gene Produces a Model of Cystic Fibrosis in Newborn Pigs. Science. 2008 Sep 26;321(5897):1837–41.

132. Bruscia EM, Zhang P-X, Satoh A, Caputo C, Medzhitov R, Shenoy A, et al. Abnormal Trafficking and Degradation of TLR4 Underlie the Elevated Inflammatory Response in Cystic Fibrosis. The Journal of Immunology. 2011 Jun 15;186(12):6990–8.

133. Van de Weert–van Leeuwen PB, Van Meegen MA, Speirs JJ, Pals DJ, Rooijakkers SHM, Van der Ent CK, et al. Optimal Complement-Mediated Phagocytosis of *Pseudomonas aeruginosa* by Monocytes Is Cystic Fibrosis Transmembrane Conductance Regulator–Dependent. Am J Respir Cell Mol Biol. 2013 Sep;49(3):463–70.

134. Barnaby R, Koeppen K, Nymon A, Hampton TH, Berwin B, Ashare A, et al. Lumacaftor (VX-809) restores the ability of CF macrophages to phagocytose and kill Pseudomonas aeruginosa. Am J Physiol Lung Cell Mol Physiol. 2018 Mar 1;314(3):L432–8.

135. Haggie PM, Verkman AS. Cystic Fibrosis Transmembrane Conductance Regulator-independent Phagosomal Acidification in Macrophages. Journal of Biological Chemistry. 2007 Oct 26;282(43):31422–8.

136. Sorio C, Montresor A, Bolomini-Vittori M, Caldrer S, Rossi B, Dusi S, et al. Mutations of Cystic Fibrosis Transmembrane Conductance Regulator Gene Cause a Monocyte-Selective Adhesion Deficiency. Am J Respir Crit Care Med. 2016 May 15;193(10):1123–33.

137. Hisert KB, Schoenfelt KQ, Cooke G, Grogan B, Launspach JL, Gallagher CG, et al. Ivacaftor-Induced Proteomic Changes Suggest Monocyte Defects May Contribute to the Pathogenesis of Cystic Fibrosis. Am J Respir Cell Mol Biol. 2016 Apr;54(4):594–7.

138. Konstan MW, Döring G, Heltshe SL, Lands LC, Hilliard KA, Koker P, et al. A randomized double blind, placebo controlled phase 2 trial of BIIL 284 BS (an LTB4 receptor antagonist) for the treatment of lung disease in children and adults with cystic fibrosis. Journal of Cystic Fibrosis. 2014 Mar;13(2):148–55.

139. Ford-Hutchinson AW, Bray MA, Doig MV, Shipley ME, Smith MJH. Leukotriene B, a potent chemokinetic and aggregating substance released from polymorphonuclear leukocytes. Nature. 1980 Jul;286(5770):264–5.

140. Flume PA, O'Sullivan BP, Robinson KA, Goss CH, Mogayzel PJ, Willey-Courand DB, et al. Cystic Fibrosis Pulmonary Guidelines: Chronic Medications for Maintenance of Lung Health. Am J Respir Crit Care Med. 2007 Nov 15;176(10):957–69.

141. Lands LC, Stanojevic S. Oral non-steroidal anti-inflammatory drug therapy for lung disease in cystic fibrosis. Cochrane Cystic Fibrosis and Genetic Disorders Group, editor. Cochrane Database of Systematic Reviews [Internet]. 2016 Apr 7 [cited 2019 Jun 17]; Available from: http://doi.wiley.com/10.1002/14651858.CD001505.pub4

142. Konstan MW, Byard PJ, Hoppel CL, Davis PB. Effect of High-Dose ibuprofen in Patients with Cystic Fibrosis. N Engl J Med. 1995 Mar 30;332(13):848–54.

143. Liao TH, Salnikow J, Moore S, Stein WH. Bovine pancreatic deoxyribonuclease A. Isolation of cyanogen bromide peptides; complete covalent structure of the polypeptide chain. J Biol Chem. 1973 Feb 25;248(4):1489–95.

144. Cystic fibrosis: diagnosis and management. National Institute for Health and Care Excellence. NICE guideline 78. [Internet]. 2017 [cited 2019 Jun 6]. Available from: https://bnf.nice.org.uk/drug/dornase-alfa.html

145. McCoy K, Hamilton S, Johnson C. Effects of 12-Week Administration of Dornase Alfa in Patients with Advanced Cystic Fibrosis Lung Disease. Chest. 1996 Oct;110(4):889–95.

146. Fuchs HJ, Borowitz DS, Christiansen DH, Morris EM, Nash ML, Ramsey BW, et al. Effect of Aerosolized Recombinant Human DNase on Exacerbations of Respiratory Symptoms and on Pulmonary Function in Patients with Cystic Fibrosis. New England Journal of Medicine. 1994 Sep 8;331(10):637–42.

147. Quan JM, Tiddens HA, Sy JP, McKenzie SG, Montgomery MD, Robinson PJ, et al. A two-year randomized, placebo-controlled trial of dornase alfa in young patients with cystic fibrosis with mild lung function abnormalities. J Pediatr. 2001 Dec;139(6):813–20.

148. Konstan MW, Wagener JS, Pasta DJ, Millar SJ, Jacobs JR, Yegin A, et al. Clinical use of dornase alfa is associated with a slower rate of FEV_1 decline in cystic fibrosis. Pediatr Pulmonol. 2011 Jun;46(6):545–53.

149. Paul K, Rietschel E, Ballmann M, Griese M, Worlitzsch D, Shute J, et al. Effect of Treatment with Dornase Alpha on Airway Inflammation in Patients with Cystic Fibrosis. Am J Respir Crit Care Med. 2004 Mar 15;169(6):719–25.

150. Ratjen F. Matrix metalloproteases in BAL fluid of patients with cystic fibrosis and their modulation by treatment with dornase alpha. Thorax. 2002 Nov 1;57(11):930–4.

151. Donaldson SH, Bennett WD, Zeman KL, Knowles MR, Tarran R, Boucher RC. Mucus Clearance and Lung Function in Cystic Fibrosis with Hypertonic Saline. N Engl J Med. 2006 Jan 19;354(3):241–50.

152. Mingeot-Leclercq M-P, Glupczynski Y, Tulkens PM. Aminoglycosides: Activity and Resistance. Antimicrob Agents Chemother. 1999 Apr 1;43(4):727–37.

153. MacLusky IB, Gold R, Corey M, Levison H. Long-term effects of inhaled tobramycin in patients with cystic fibrosis colonized with Pseudomonas aeruginosa. Pediatr Pulmonol. 1989;7(1):42–8.

154. Ramsey BW, Dorkin HL, Eisenberg JD, Gibson RL, Harwood IR, Kravitz RM, et al. Efficacy of Aerosolized Tobramycin in Patients with Cystic Fibrosis. N Engl J Med. 1993 Jun 17;328(24):1740–6.

155. Ramsey BW, Pepe MS, Quan JM, Otto KL, Montgomery AB, Williams-Warren J, et al. Intermittent Administration of Inhaled Tobramycin in Patients with Cystic Fibrosis. N Engl J Med. 1999 Jan 7;340(1):23–30.

156. Principi N, Blasi F, Esposito S. Azithromycin use in patients with cystic fibrosis. Eur J Clin Microbiol Infect Dis. 2015 Jun;34(6):1071–9.

157. Cramer CL, Patterson A, Alchakaki A, Soubani AO. Immunomodulatory indications of azithromycin in respiratory disease: a concise review for the clinician. Postgraduate Medicine. 2017 Jul 4;129(5):493–9.

158. Parnham MJ, Haber VE, Giamarellos-Bourboulis EJ, Perletti G, Verleden GM, Vos R. Azithromycin: Mechanisms of action and their relevance for clinical applications. Pharmacology & Therapeutics. 2014 Aug;143(2):225–45.

159. Murphy DM, Forrest IA, Corris PA, Johnson GE, Small T, Jones D, et al. Azithromycin Attenuates Effects of Lipopolysaccharide on Lung Allograft Bronchial Epithelial Cells. The Journal of Heart and Lung Transplantation. 2008 Nov;27(11):1210–6.

160. Culić O, Eraković V, Cepelak I, Barisić K, Brajsa K, Ferencić Z, et al. Azithromycin modulates neutrophil function and circulating inflammatory mediators in healthy human subjects. Eur J Pharmacol. 2002 Aug 30;450(3):277–89.

161. Condren ME, Bradshaw MD. Ivacaftor: a novel gene-based therapeutic approach for cystic fibrosis. J Pediatr Pharmacol Ther. 2013 Jan;18(1):8–13.

162. Hisert KB, Heltshe SL, Pope C, Jorth P, Wu X, Edwards RM, et al. Restoring Cystic Fibrosis Transmembrane Conductance Regulator Function Reduces Airway Bacteria and Inflammation in People with Cystic Fibrosis and Chronic Lung Infections. Am J Respir Crit Care Med. 2017 Jun 15;195(12):1617–28.

163. Wainwright CE, Elborn JS, Ramsey BW, Marigowda G, Huang X, Cipolli M, et al. Lumacaftor–Ivacaftor in Patients with Cystic Fibrosis Homozygous for Phe508del *CFTR*. N Engl J Med. 2015 Jul 16;373(3):220–31.

164. Taylor-Cousar JL, Munck A, McKone EF, van der Ent CK, Moeller A, Simard C, et al. Tezacaftor–Ivacaftor in Patients with Cystic Fibrosis Homozygous for Phe508del. N Engl J Med. 2017 Nov 23;377(21):2013–23.

165. Rowe SM, Daines C, Ringshausen FC, Kerem E, Wilson J, Tullis E, et al. Tezacaftor–Ivacaftor in Residual-Function Heterozygotes with Cystic Fibrosis. N Engl J Med. 2017 Nov 23;377(21):2024–35.

166. Davies JC, Moskowitz SM, Brown C, Horsley A, Mall MA, McKone EF, et al. VX-659–Tezacaftor–Ivacaftor in Patients with Cystic Fibrosis and One or Two Phe508del Alleles. N Engl J Med. 2018 Oct 25;379(17):1599–611.

167. Alton EWFW, Armstrong DK, Ashby D, Bayfield KJ, Bilton D, Bloomfield EV, et al. Repeated nebulisation of non-viral CFTR gene therapy in patients with cystic fibrosis: a randomised, double-blind, placebo-controlled, phase 2b trial. The Lancet Respiratory Medicine. 2015 Sep;3(9):684–91.

168. Miller MR. Standardisation of spirometry. European Respiratory Journal. 2005 Aug 1;26(2):319–38.

169. Pizzichini E, Pizzichini MMM, Efthimiadis A, Hargreave FE, Dolovich J. Measurement of inflammatory indices in induced sputum: effects of selection of sputum to minimize salivary contamination. European Respiratory Journal. 1996 Jun 1;9(6):1174–80.

170. Gray RD, Lucas CD, MacKellar A, Li F, Hiersemenzel K, Haslett C, et al. Activation of conventional protein kinase C (PKC) is critical in the generation of human neutrophil extracellular traps. Journal of Inflammation. 2013;10(1):12.

171. Zhou L, Dey CR, Wert SE, DuVall MD, Frizzell RA, Whitsett JA. Correction of lethal intestinal defect in a mouse model of cystic fibrosis by human CFTR. Science. 1994 Dec 9;266(5191):1705–8.

172. McCutcheon JC, Hart SP, Canning M, Ross K, Humphries MJ, Dransfield I. Regulation of macrophage phagocytosis of apoptotic neutrophils by adhesion to fibronectin. J Leukoc Biol. 1998 Nov;64(5):600–7.

173. Heasman SJ, Giles KM, Rossi AG, Allen JE, Haslett C, Dransfield I. Interferonγ suppresses glucocorticoid augmentation of macrophage clearance of apoptotic cells. European Journal of Immunology. 2004 Jun;34(6):1752–61.

174. Choudhury D, Tanner MG, McAughtrie S, Yu F, Mills B, Choudhary TR, et al. Endoscopic sensing of alveolar pH. Biomed Opt Express. 2017 Jan 1;8(1):243–59.

175. Urban CF, Ermert D, Schmid M, Abu-Abed U, Goosmann C, Nacken W, et al. Neutrophil Extracellular Traps Contain Calprotectin, a Cytosolic Protein Complex Involved in Host Defense against Candida albicans. Levitz SM, editor. PLoS Pathog. 2009 Oct 30;5(10):e1000639.

176. Dwyer M, Shan Q, D'Ortona S, Maurer R, Mitchell R, Olesen H, et al. Cystic Fibrosis Sputum DNA Has NETosis Characteristics and Neutrophil Extracellular Trap Release Is Regulated by Macrophage Migration-Inhibitory Factor. Journal of Innate Immunity. 2014;6(6):765–79.

177. Sagel SD, Wagner BD, Anthony MM, Emmett P, Zemanick ET. Sputum Biomarkers of Inflammation and Lung Function Decline in Children with Cystic Fibrosis. American Journal of Respiratory and Critical Care Medicine. 2012 Nov;186(9):857–65.

178. Dittrich AS, Kühbandner I, Gehrig S, Rickert-Zacharias V, Twigg M, Wege S, et al. Elastase activity on sputum neutrophils correlates with severity of lung disease in cystic fibrosis. European Respiratory Journal. 2018 Mar;51(3):1701910.

179. Lieberman J. Dornase aerosol effect on sputum viscosity in cases of cystic fibrosis. JAMA. 1968 Jul 29;205(5):312–3.

180. Hubbard RC, McElvaney NG, Birrer P, Shak S, Robinson WW, Jolley C, et al. A preliminary study of aerosolized recombinant human deoxyribonuclease I in the treatment of cystic fibrosis. N Engl J Med. 1992 Mar 19;326(12):812–5.

181. Blikstad I, Markey F, Carlsson L, Persson T, Lindberg U. Selective assay of monomeric and filamentous actin in cell extracts, using inhibition of deoxyribonuclease I. Cell. 1978 Nov;15(3):935–43.

182. Hunter CA, Jones SA. IL-6 as a keystone cytokine in health and disease. Nat Immunol. 2015 May;16(5):448–57.

183. Chen G. TNF-R1 Signaling: A Beautiful Pathway. Science. 2002 May 31;296(5573):1634–5.

184. Wajant H, Pfizenmaier K, Scheurich P. Tumor necrosis factor signaling. Cell Death Differ. 2003 Jan;10(1):45–65.

185. Arango Duque G, Descoteaux A. Macrophage Cytokines: Involvement in Immunity and Infectious Diseases. Front Immunol [Internet]. 2014 Oct 7 [cited 2019 Jul 25];5. Available from: http://journal.frontiersin.org/article/10.3389/fimmu.2014.00491/abstract

186. Ruffin M, Roussel L, Maillé É, Rousseau S, Brochiero E. Vx-809/Vx-770 treatment reduces inflammatory response to *Pseudomonas aeruginosa* in primary differentiated cystic fibrosis bronchial epithelial cells. American Journal of Physiology-Lung Cellular and Molecular Physiology. 2018 Apr;314(4):L635–41.

187. Konstan MW, Hilliard KA, Norvell TM, Berger M. Bronchoalveolar lavage findings in cystic fibrosis patients with stable, clinically mild lung disease suggest ongoing infection and inflammation. Am J Respir Crit Care Med. 1994 Aug;150(2):448–54.

188. Henig NR, Tonelli MR, Pier MV, Burns JL, Aitken ML. Sputum induction as a research tool for sampling the airways of subjects with cystic fibrosis. Thorax. 2001 Apr;56(4):306–11.

189. Auger MJ, Ross JA. The Biology of the Macrophage. Oxford: Oxford University Press; 1993. 1–74 p.

190. Lowe JS, Anderson PG, Stevens A. Stevens & Lowe's human histology. Fourth edition. Philadelphia, PA: Elsevier/Mosby; 2015. 429 p.

191. Stallings VA, Stark LJ, Robinson KA, Feranchak AP, Quinton H. Evidence-Based Practice Recommendations for Nutrition-Related Management of Children and Adults with Cystic Fibrosis and Pancreatic Insufficiency: Results of a Systematic Review. Journal of the American Dietetic Association. 2008 May;108(5):832–9.

192. Nutritional Management of Cystic Fibrosis [Internet]. CF Trust; 2016 [cited 2019 Apr 22]. Available from: https://www.cysticfibrosis.org.uk/the-work-we-do/clinical-care/consensus-documents

193. Morris MR, Doull IJM, Dewitt S, Hallett MB. Reduced iC3b-mediated phagocytotic capacity of pulmonary neutrophils in cystic fibrosis. Clin Exp Immunol. 2005 Oct;142(1):68–75.

194. Bicker H, Hoflich C, Wolk K, Vogt K, Volk H-D, Sabat R. A Simple Assay to Measure Phagocytosis of Live Bacteria. Clinical Chemistry. 2008 May 1;54(5):911–5.

195. Junkins RD, McCormick C, Lin T-J. The emerging potential of autophagy-based therapies in the treatment of cystic fibrosis lung infections. Autophagy. 2014 Mar 3;10(3):538–47.

196. Ordoñez CL, Henig NR, Mayer-Hamblett N, Accurso FJ, Burns JL, Chmiel JF, et al. Inflammatory and Microbiologic Markers in Induced Sputum after Intravenous Antibiotics in Cystic Fibrosis. Am J Respir Crit Care Med. 2003 Dec 15;168(12):1471–5.

197. Colombo C, Costantini D, Rocchi A, Cariani L, Garlaschi ML, Tirelli S, et al. Cytokine levels in sputum of cystic fibrosis patients before and after antibiotic therapy. Pediatr Pulmonol. 2005 Jul;40(1):15–21.

198. Mayer-Hamblett N, Aitken ML, Accurso FJ, Kronmal RA, Konstan MW, Burns JL, et al. Association between Pulmonary Function and Sputum Biomarkers in Cystic Fibrosis. Am J Respir Crit Care Med. 2007 Apr 15;175(8):822–8.

199. Horsley AR, Davies JC, Gray RD, Macleod KA, Donovan J, Aziz ZA, et al. Changes in physiological, functional and structural markers of cystic fibrosis lung disease with treatment of a pulmonary exacerbation. Thorax. 2013 Jun;68(6):532–9.

200. Vogl T, Tenbrock K, Ludwig S, Leukert N, Ehrhardt C, van Zoelen MAD, et al. Mrp8 and Mrp14 are endogenous activators of Toll-like receptor 4, promoting lethal, endotoxin-induced shock. Nat Med. 2007 Sep 2;13(9):1042–9.

201. Farrera C, Fadeel B. Macrophage clearance of neutrophil extracellular traps is a silent process. J Immunol. 2013 Sep 1;191(5):2647–56.

202. Dhooghe B, Noël S, Huaux F, Leal T. Lung inflammation in cystic fibrosis: Pathogenesis and novel therapies. Clinical Biochemistry. 2014 May;47(7–8):539–46.

203. Bonfield TL, Konstan MW, Berger M. Altered respiratory epithelial cell cytokine production in cystic fibrosis☆☆☆★. Journal of Allergy and Clinical Immunology. 1999 Jul;104(1):72–8.

204. Snouwaert JN, Brigman KK, Latour AM, Malouf NN, Boucher RC, Smithies O, et al. An Animal Model for Cystic Fibrosis Made by Gene Targeting. Science. 1992 Aug 21;257(5073):1083–8.

205. Semaniakou A, Croll RP, Chappe V. Animal Models in the Pathophysiology of Cystic Fibrosis. Front Pharmacol. 2019 Jan 4;9:1475.

206. Su X, Looney MR, Su H, Lee JW, Song Y, Matthay MA. Role of CFTR expressed by neutrophils in modulating acute lung inflammation and injury in mice. Inflammation Research. 2011 Jul;60(7):619–32.

207. Pieterse E, Rother N, Yanginlar C, Hilbrands LB, van der Vlag J. Neutrophils Discriminate between Lipopolysaccharides of Different Bacterial Sources and Selectively Release Neutrophil Extracellular Traps. Front Immunol [Internet]. 2016 Nov 4 [cited 2019 May 7];7. Available from: http://journal.frontiersin.org/article/10.3389/fimmu.2016.00484/full

208. Zou Y, Chen X, Xiao J, Zhou DB, Lu XX, Li W, et al. Neutrophil extracellular traps promote lipopolysaccharide-induced airway inflammation and mucus hypersecretion in mice. Oncotarget [Internet]. 2018 Mar 2 [cited 2018 May 31];9(17). Available from: http://www.oncotarget.com/fulltext/24022

209. da Cunha AA, Nuñez NK, de Souza RG, Moraes Vargas MH, Silveira JS, Antunes GL, et al. Recombinant human deoxyribonuclease therapy improves airway resistance and reduces DNA extracellular traps in a murine acute asthma model. Experimental Lung Research. 2016 Feb 7;42(2):66–74.

210. Raetz CRH, Whitfield C. Lipopolysaccharide Endotoxins. Annu Rev Biochem. 2002 Jun;71(1):635–700.

211. Clark SR, Ma AC, Tavener SA, McDonald B, Goodarzi Z, Kelly MM, et al. Platelet TLR4 activates neutrophil extracellular traps to ensnare bacteria in septic blood. Nat Med. 2007 Apr;13(4):463–9.

212. Bruscia EM, Zhang P-X, Ferreira E, Caputo C, Emerson JW, Tuck D, et al. Macrophages Directly Contribute to the Exaggerated Inflammatory Response in Cystic Fibrosis Transmembrane Conductance Regulator $^{-/-}$ Mice. Am J Respir Cell Mol Biol. 2009 Mar;40(3):295–304.

213. Di A, Brown ME, Deriy LV, Li C, Szeto FL, Chen Y, et al. CFTR regulates phagosome acidification in macrophages and alters bactericidal activity. Nature Cell Biology. 2006 Aug 20;8:933.

214. Lévêque M, Le Trionnaire S, Del Porto P, Martin-Chouly C. The impact of impaired macrophage functions in cystic fibrosis disease progression. Journal of Cystic Fibrosis. 2017 Jul;16(4):443–53.

215. McLeish KR, Merchant ML, Creed TM, Tandon S, Barati MT, Uriarte SM, et al. Frontline Science: Tumor necrosis factor-α stimulation and priming of human neutrophil granule exocytosis. J Leukoc Biol. 2017 Jul;102(1):19–29.

216. Goldblum SE, Hennig B, Jay M, Yoneda K, McClain CJ. Tumor necrosis factor alpha-induced pulmonary vascular endothelial injury. Infect Immun. 1989 Apr;57(4):1218–26.

217. Tan H-L, Regamey N, Brown S, Bush A, Lloyd CM, Davies JC. The Th17 Pathway in Cystic Fibrosis Lung Disease. Am J Respir Crit Care Med. 2011 Jul 15;184(2):252–8.

218. Brodlie M, McKean MC, Johnson GE, Anderson AE, Hilkens CMU, Fisher AJ, et al. Raised interleukin-17 is immunolocalised to neutrophils in cystic fibrosis lung disease. European Respiratory Journal. 2011 Jun 1;37(6):1378–85.

219. Murakami K, McGuire R, Cox RA, Jodoin JM, Bjertnaes LJ, Katahira J, et al. Heparin nebulization attenuates acute lung injury in sepsis following smoke inhalation in sheep. Shock. 2002 Sep;18(3):236–41.

220. Kusano T, Chiang K-C, Inomata M, Shimada Y, Ohmori N, Goto T, et al. A novel anti-histone H1 monoclonal antibody, SSV monoclonal antibody, improves lung injury and survival in a mouse model of lipopolysaccharide-induced sepsis-like syndrome. Biomed Res Int. 2015;2015:491649.

221. Gibson-Corley KN, Olivier AK, Meyerholz DK. Principles for valid histopathologic scoring in research. Vet Pathol. 2013 Nov;50(6):1007–15.

222. Schoels MM, van der Heijde D, Breedveld FC, Burmester GR, Dougados M, Emery P, et al. Blocking the effects of interleukin-6 in rheumatoid arthritis and other inflammatory rheumatic diseases: systematic literature review and meta-analysis informing a consensus statement. Ann Rheum Dis. 2013 Apr;72(4):583–9.

223. Scheinfeld N. A comprehensive review and evaluation of the side effects of the tumor necrosis factor alpha blockers etanercept, infliximab and adalimumab. J Dermatolog Treat. 2004 Sep;15(5):280–94.

224. Beringer A, Noack M, Miossec P. IL-17 in Chronic Inflammation: From Discovery to Targeting. Trends Mol Med. 2016 Mar;22(3):230–41.

225. Witko-Sarsat V, Delacourt C, Rabier D, Bardet J, Nguyen AT, Descamps-Latscha B. Neutrophil-derived long-lived oxidants in cystic fibrosis sputum. Am J Respir Crit Care Med. 1995 Dec;152(6 Pt 1):1910–6.

226. Kim J-S, Okamoto K, Rubin BK. Pulmonary Function Is Negatively Correlated With Sputum Inflammatory Markers and Cough Clearability in Subjects With Cystic Fibrosis But Not Those With Chronic Bronchitis. Chest. 2006 May;129(5):1148–54.

227. Vencken SF, Greene CM. Toll-Like Receptors in Cystic Fibrosis: Impact of Dysfunctional microRNA on Innate Immune Responses in the Cystic Fibrosis Lung. J Innate Immun. 2016;8(6):541–9.

228. Xie J, Méndez JD, Méndez-Valenzuela V, Aguilar-Hernández MM. Cellular signalling of the receptor for advanced glycation end products (RAGE). Cellular Signalling. 2013 Nov;25(11):2185–97.

229. Chirico V, Lacquaniti A, Leonardi S, Grasso L, Rotolo N, Romano C, et al. Acute pulmonary exacerbation and lung function decline in patients with cystic fibrosis: high-mobility group box 1 (HMGB1) between inflammation and infection. Clinical Microbiology and Infection. 2015 Apr;21(4):368.e1-368.e9.

230. Cooper G. The Cell: A Molecular Approach. 2nd edition. Sunderland (MA): Sinauer Associates Inc.; 2000.

231. Aderem A. Phagocytosis and the Inflammatory Response. The Journal of Infectious Diseases. 2003 Jun 15;187(s2):S340–5.

232. Benjaminsen RV, Sun H, Henriksen JR, Christensen NM, Almdal K, Andresen TL. Evaluating nanoparticle sensor design for intracellular pH measurements. ACS Nano. 2011 Jul 26;5(7):5864–73.

233. Forgac M. Structure, mechanism and regulation of the clathrin-coated vesicle and yeast vacuolar H(+)-ATPases. J Exp Biol. 2000 Jan;203(Pt 1):71–80.

234. Barasch J, Kiss B, Prince A, Saiman L, Gruenert D, al-Awqati Q. Defective acidification of intracellular organelles in cystic fibrosis. Nature. 1991 Jul 4;352(6330):70–3.

235. Queval CJ, Song O-R, Carralot J-P, Saliou J-M, Bongiovanni A, Deloison G, et al. Mycobacterium tuberculosis Controls Phagosomal Acidification by Targeting CISH-Mediated Signaling. Cell Reports. 2017 Sep;20(13):3188–98.

236. Jubrail J, Morris P, Bewley MA, Stoneham S, Johnston SA, Foster SJ, et al. Inability to sustain intraphagolysosomal killing of *Staphylococcus aureus* predisposes to bacterial persistence in macrophages: *S. aureus* killing by macrophages. Cellular Microbiology. 2016 Jan;18(1):80–96.

237. Zhang Y, Li X, Grassme H, Doring G, Gulbins E. Alterations in Ceramide Concentration and pH Determine the Release of Reactive Oxygen Species by Cftr-Deficient Macrophages on Infection. The Journal of Immunology. 2010 May 1;184(9):5104–11.

238. Steinberg BE, Touret N, Vargas-Caballero M, Grinstein S. In situ measurement of the electrical potential across the phagosomal membrane using FRET and its contribution to the proton-motive force. Proc Natl Acad Sci USA. 2007 May 29;104(22):9523–8.

239. Haggie PM, Verkman AS. Cystic Fibrosis Transmembrane Conductance Regulator-independent Phagosomal Acidification in Macrophages. J Biol Chem. 2007 Oct 26;282(43):31422–8.

240. Barriere H, Bagdany M, Bossard F, Okiyoneda T, Wojewodka G, Gruenert D, et al. Revisiting the role of cystic fibrosis transmembrane conductance regulator and counterion permeability in the pH regulation of endocytic organelles. Mol Biol Cell. 2009 Jul;20(13):3125–41.

241. Nunes P, Guido D, Demaurex N. Measuring Phagosome pH by Ratiometric Fluorescence Microscopy. J Vis Exp. 2015 Dec 7;(106):e53402.

242. Stiles PL, Dieringer JA, Shah NC, Van Duyne RP. Surface-Enhanced Raman Spectroscopy. Annual Rev Anal Chem. 2008 Jul;1(1):601–26.

243. Chandrasekhara Venkata Raman, 1888-1970. Biogr Mems Fell R Soc. 1971 Nov;17:564–92.

244. Wu D, Chen Y, Hou S, Fang W, Duan H. Intracellular and Cellular Detection by SERS-Active Plasmonic Nanostructures. ChemBioChem. 2019 Apr 8;cbic.201900191.

245. Bishnoi SW, Rozell CJ, Levin CS, Gheith MK, Johnson BR, Johnson DH, et al. All-Optical Nanoscale pH Meter. Nano Letters. 2006 Aug;6(8):1687–92.

246. Fisher KM, Campbell CJ. Ratiometric biological nanosensors. Biochemical Society Transactions. 2014 Aug 1;42(4):899–904.

247. Jamieson LE, Jaworska A, Jiang J, Baranska M, Harrison DJ, Campbell CJ. Simultaneous intracellular redox potential and pH measurements in live cells using SERS nanosensors. The Analyst. 2015;140(7):2330–5.

248. Bunaciu AA, Aboul-Enein HY, Fleschin Ş. Vibrational Spectroscopy in Clinical Analysis. Applied Spectroscopy Reviews. 2015 Feb 7;50(2):176–91.

249. Fei F, Lee KM, McCarry BE, Bowdish DME. Age-associated metabolic dysregulation in bone marrow-derived macrophages stimulated with lipopolysaccharide. Sci Rep. 2016 Sep;6(1):22637.

250. Plowden J, Renshaw-Hoelscher M, Engleman C, Katz J, Sambhara S. Innate immunity in aging: impact on macrophage function: Innate immunity in aging, J. Plowden et al. Aging Cell. 2004 Jul 9;3(4):161–7.

251. Notingher I, Verrier S, Romanska H, Bishop AE, Polak JM, Hench LL. *In situ* Characterisation of Living Cells by Raman Spectroscopy. Spectroscopy. 2002;16(2):43–51.

252. Yates RM, Russell DG. Phagosome maturation proceeds independently of stimulation of toll-like receptors 2 and 4. Immunity. 2005 Oct;23(4):409–17.

253. Lukacs GL, Rotstein OD, Grinstein S. Phagosomal acidification is mediated by a vacuolar-type H(+)-ATPase in murine macrophages. J Biol Chem. 1990 Dec 5;265(34):21099–107.

254. Aderem A, Underhill DM. Mechanisms of phagocytosis in macrophages. Annu Rev Immunol. 1999;17:593–623.

255. França A, Aggarwal P, Barsov EV, Kozlov SV, Dobrovolskaia MA, González-Fernández Á. Macrophage scavenger receptor A mediates the uptake of gold colloids by macrophages *in vitro*. Nanomedicine. 2011 Sep;6(7):1175–88.

256. Park JH, Oh N. Endocytosis and exocytosis of nanoparticles in mammalian cells. International Journal of Nanomedicine. 2014 May;51.

257. Chithrani BD, Ghazani AA, Chan WCW. Determining the Size and Shape Dependence of Gold Nanoparticle Uptake into Mammalian Cells. Nano Letters. 2006 Apr;6(4):662–8.

258. Döring G. The role of neutrophil elastase in chronic inflammation. Am J Respir Crit Care Med. 1994 Dec;150(6 Pt 2):S114-117.

259. Wright AKA, Rao S, Range S, Eder C, Hofer TPJ, Frankenberger M, et al. Pivotal Advance: Expansion of small sputum macrophages in CF: failure to express MARCO and mannose receptors. Journal of Leukocyte Biology. 2009 Sep;86(3):479–89.

260. Haberzettl P, Duffin R, Krämer U, Höhr D, Schins RPF, Borm PJA, et al. Actin plays a crucial role in the phagocytosis and biological response to respirable quartz particles in macrophages. Arch Toxicol. 2007 Jun 26;81(7):459–70.

261. McWhorter FY, Wang T, Nguyen P, Chung T, Liu WF. Modulation of macrophage phenotype by cell shape. Proceedings of the National Academy of Sciences. 2013 Oct 22;110(43):17253–8.

262. Lukacs GL, Rotstein OD, Grinstein S. Determinants of the phagosomal pH in macrophages. In situ assessment of vacuolar H(+)-ATPase activity, counterion conductance, and H+ ‘leak’. J Biol Chem. 1991 Dec 25;266(36):24540–8.

263. Yates RM, Hermetter A, Taylor GA, Russell DG. Macrophage Activation Downregulates the Degradative Capacity of the Phagosome. Traffic. 2007 Mar;8(3):241–50.

264. Hackam DJ, Rotstein OD, Zhang W-J, Demaurex N, Woodside M, Tsai O, et al. Regulation of Phagosomal Acidification: DIFFERENTIAL TARGETING OF Na^+/H^+ EXCHANGERS, Na^+/K^+-ATPases, AND VACUOLAR-TYPE H^+-ATPases. J Biol Chem. 1997 Nov 21;272(47):29810–20.

265. Li C, Wu Y, Riehle A, Ma J, Kamler M, Gulbins E, et al. Staphylococcus aureus Survives in Cystic Fibrosis Macrophages, Forming a Reservoir for Chronic Pneumonia. Infect Immun. 2017;85(5).

266. Del Porto P, Cifani N, Guarnieri S, Di Domenico EG, Mariggiò MA, Spadaro F, et al. Dysfunctional CFTR alters the bactericidal activity of human macrophages against Pseudomonas aeruginosa. PLoS ONE. 2011;6(5):e19970.

267. Kopp BT, Abdulrahman BA, Khweek AA, Kumar SB, Akhter A, Montione R, et al. Exaggerated inflammatory responses mediated by Burkholderia cenocepacia in human macrophages derived from Cystic fibrosis patients. Biochem Biophys Res Commun. 2012 Jul 27;424(2):221–7.

268. Camus VL, Stewart G, Nailon WH, McLaren DB, Campbell CJ. Measuring the effects of fractionated radiation therapy in a 3D prostate cancer model system using SERS nanosensors. The Analyst. 2016;141(17):5056–61.

269. Deriy LV, Gomez EA, Zhang G, Beacham DW, Hopson JA, Gallan AJ, et al. Disease-causing mutations in the cystic fibrosis transmembrane conductance regulator determine the functional responses of alveolar macrophages. J Biol Chem. 2009 Dec 18;284(51):35926–38.

270. Murphy BS, Bush HM, Sundareshan V, Davis C, Hagadone J, Cory TJ, et al. Characterization of macrophage activation states in patients with cystic fibrosis. Journal of Cystic Fibrosis. 2010 Sep;9(5):314–22.

271. Trojanek JB, Cobos-Correa A, Diemer S, Kormann M, Schubert SC, Zhou-Suckow Z, et al. Airway Mucus Obstruction Triggers Macrophage Activation and Matrix Metalloproteinase 12–Dependent Emphysema. American Journal of Respiratory Cell and Molecular Biology. 2014 Nov;51(5):709–20.

272. Foote JR, Patel AA, Yona S, Segal AW. Variations in the Phagosomal Environment of Human Neutrophils and Mononuclear Phagocyte Subsets. Frontiers in Immunology [Internet]. 2019 Mar 1 [cited 2019 Apr 3];10. Available from: https://www.frontiersin.org/article/10.3389/fimmu.2019.00188/full

273. Shak S, Capon DJ, Hellmiss R, Marsters SA, Baker CL. Recombinant human DNase I reduces the viscosity of cystic fibrosis sputum. Proc Natl Acad Sci USA. 1990 Dec;87(23):9188–92.

274. Brandt T, Breitenstein S, von der Hardt H, Tümmler B. DNA concentration and length in sputum of patients with cystic fibrosis during inhalation with recombinant human DNase. Thorax. 1995 Aug;50(8):880–2.

275. Ratjen F, Paul K, van Koningsbruggen S, Breitenstein S, Rietschel E, Nikolaizik W, et al. DNA concentrations in BAL fluid of cystic fibrosis patients with early lung disease: Influence of treatment with dornase alpha. Pediatr Pulmonol. 2005 Jan;39(1):1–4.

276. Mihalache CC, Yousefi S, Conus S, Villiger PM, Schneider EM, Simon H-U. Inflammation-Associated Autophagy-Related Programmed Necrotic Death of Human Neutrophils Characterized by Organelle Fusion Events. JI. 2011 Jun 1;186(11):6532–42.

277. Maiuri L, Luciani A, Giardino I, Raia V, Villella VR, D'Apolito M, et al. Tissue Transglutaminase Activation Modulates Inflammation in Cystic Fibrosis via PPARγ Down-Regulation. J Immunol. 2008 Jun 1;180(11):7697–705.

278. Luciani A, Villella VR, Esposito S, Brunetti-Pierri N, Medina D, Settembre C, et al. Defective CFTR induces aggresome formation and lung inflammation in cystic fibrosis through ROS-mediated autophagy inhibition. Nat Cell Biol. 2010 Sep;12(9):863–75.

279. Kaushik S, Cuervo AM. Chaperone-mediated autophagy: a unique way to enter the lysosome world. Trends Cell Biol. 2012 Aug;22(8):407–17.

280. Junkins RD, Shen A, Rosen K, McCormick C, Lin T-J. Autophagy Enhances Bacterial Clearance during P. aeruginosa Lung Infection. Jeyaseelan S, editor. PLoS ONE. 2013 Aug 28;8(8):e72263.

281. Stark A-K, Sriskantharajah S, Hessel EM, Okkenhaug K. PI3K inhibitors in inflammation, autoimmunity and cancer. Curr Opin Pharmacol. 2015 Aug;23:82–91.

282. Pasquier B. Autophagy inhibitors. Cell Mol Life Sci. 2016 Mar;73(5):985–1001.

283. Blommaart EFC, Krause U, Schellens JPM, Vreeling-Sindelarova H, Meijer AJ. The Phosphatidylinositol 3-Kinase Inhibitors Wortmannin and LY294002 Inhibit Autophagy in Isolated Rat Hepatocytes. Eur J Biochem. 1997 Jan;243(1–2):240–6.

284. Carmona-Rivera C, Khaznadar SS, Shwin KW, Irizarry-Caro JA, O'Neil LJ, Liu Y, et al. Deficiency of adenosine deaminase 2 triggers adenosine-mediated NETosis and TNF production in patients with DADA2. Blood. 2019 Jul 25;134(4):395–406.

285. Uribe-Querol E, Rosales C. Control of Phagocytosis by Microbial Pathogens. Front Immunol. 2017 Oct 24;8:1368.

Appendices

Appendix 1: Genotyping of Murine Ear Clippings by qPCR for *Cftr^{tm1Unc}Tg(FABPCFTR)1Jaw/J.*

Reagent	Concentration	Volume per reaction (µL)
ddH_20	-	4.00
PCR buffer	6.00 x	1.00
dNTP	0.20 mM	0.96
Primer CF common (E00246F11 (F11))	100 µM	0.25
Primer CF Mutant (E00246F12 (F12))	100 µM	0.25
Primer Transgene (FABPCFTR) Forward (E00246G02 (G02))	100 µM	0.25
Primer Transgene (FABPCFTR) Reverse (E00246G03 (G03))	100 µM	0.25
gDNA	-	1
Taq polymerase	-	6.25

Table A1: PCR screening reagents for murine Cftr^{tm1Unc}Tg(FABPCFTR)1Jaw/J genotyping. Primers (Invitrogen (USA), PCR buffer (Life technologies, USA), dNTRP and Taq polymerase (Promega, USA).

Step	Temperature (˚C)	Time
1	95	2 min
2	95	30 sec
3	52	45 sec
4	72	45 sec
5	Repeat steps 2-4 for 30 cycles – more for backcrossed animals as transgene is lost at ~ 50	-
6	72	10 min

Table A2: PCR reaction conditions for murine Cftr^{tm1Unc}Tg(FABPCFTR)1Jaw/J genotyping. Lauren Melrose conducted PCRs. They were conducted using a C1000 Touch™ cycler (Bio Rad, UK). Products were subsequently run on a 1.0% agarose (SLS, UK) gel. Expected weights using the above primers: CF Mutant 357 bp; CF Het 357 bp and 562 bp; WT 562 bp; and Tg(FABPCFTR)1Jaw/J 413 bp.

Appendix 2: U-PLEX® Biomarker Group 1 (Mouse) Analyte concentrations

Analyte Description	Amount of Analyte in Calibrator (pg)	Stock Concentration of Reconstituted Calibrator (vol. = 250 µL) (pg/mL)	Concentration of Standard (after five-fold dilution) (pg/mL)
IFN-ɣ	3600	14 400	2880
IL-1β	16 250	65 000	13 000
IL-17A	2 650	10 600	2120
IL-23	23 875	95 500	19 100
MCP-1	1625	6500	1300
MIP-2	2550	10 200	2040
IL-6	20 000	80 000	16 000
IL-10	28 500	114 000	2 800
TNF-α	7688	30 750	3150
KC	2800	11 200	2240

All Meso Scale Diagnostics.

Appendix 3: Murine Lung NET Immunohistochemistry

Sodium Citrate Buffer for Murine Lung Immunohistochemistry Antigen Retrieval

10 mM Sodium Citrate Buffer and 0.05% Tween, pH 6	
Tri-sodium citrate dehydrate	2.94 g
dH_2O	1000 mL
HCl	add until pH 6
Tween-20	0.5 mL

Primary Antibodies

Target	Description	Dilution	Manufacturer
S100A9	Rat anti-mouse monoclonal (MAB2065)	1:100	R&D Systems
MPO	Rabbit anti-human polyclonal (A0398)	1:200	Dako

Secondary Antibodies

Target	Description	Dilution	Manufacturer
Rat anti-mouse 1° against S100A9	Alexa Fluor 568 Goat anti-rat IgG (A11077)	1:300	Molecular Probes
Rabbit anti-human 1° against MPO	Alexa Fluor 488 Goat anti-rabbit IgG (A11034)	1:300	Invitrogen, Thermo Fisher Scientific

Goat Serum Dilutions

25% goat serum for blocking slides: made by mixing 500 µL goat serum with 1500 µL DPBS. 10% goat serum for antibody dilution: made by mixing 1700 µL 25% goat serum with 2550 µL DPBS.

Appendix 4: [3H]-PK11195 Autoradiography Reagents

50 mM Tris-Base buffer (pH 7.4)

1) MW Trizma Base = 121.14
2) Volume H_2O: 5L
3) Weight of compound: 30.285g
4) Adjusted pH (HCl): ~17.6 mL

10μM PK11195 Displacer preparation

1) MW PK11195 = 352.86
2) Stock 15mM = 2.65 mg + 500 μL 100% Ethanol
3) Stock 800μM = 53.3μL of 15mM stock + 946.7 μL 100% Ethanol
4) 10μM PK11195 = 625μL of 800μM stock + ~50mL Tris-Base Buffer (→ 1.25% total Ethanol content)

[3H]-PK11195 solution:

5mL stock [3H]PK (PerkinElmer) added to 300 mL buffer and mixed well then 20 μL of this diluted stock was further diluted in 2.5 mL Scintillation Cocktail in a PicoPrias glass vial to check concentration using a Hidex Scintillation Counter machine. A concentration of 1.87 nM was given.

Appendix 5: cDNA generation and RT-PCR Analysis

2X Reverse Transcription Master Mix

Reagent	Volume per sample (µL)
Buffer	2
dNTP Mix (100 mM)	0.8
10X random primers	2
Multiscribe™ Reverse transcriptase	1
RNase inhibitor	1
Nuclease-free water	3.2

Primer Probes – PrimeTime® qPCR Assays

Target	Product Reference
TLR-2	Mm.PT.58.45820113
TLR-4	Mm.PT.58.41643680
TLR-9	Mm.PT.58.5114450
RAGE	Mm.PT.58.32442175
Actb	Mm.PT.39a.22214843.g

All from Integrated DNA Technologies, Leuven.

Appendix 6: Murine Lung Lysis Buffers

Laemmli Buffer		
0.5 M Tris HCl pH 6.8	250 µL	1.25 mL
100% Glycerol	200 µL	1 mL
10% SDS	400 µL	2 mL
Complete inhibitors (Roche 04693159001) 1 tablet in 2mL	400 µL	2 mL
Phosphatase inhibitors (Roche 04906845001) 1 tablet in 500 µL	100 µL	500 µL
H_2O	650 µL	3.25 mL
Final volume	2 mL	10 mL

The additional protease inhibitor Phenylmethylsulfonyl fluoride (PMSF) was added to complete Laemmli buffer to a final concentration of 1 mM.

SDS Lysis Buffer			
Stock Concentration	**Target Concentration**		**To Add**
	Molarity	%	
DTT 1 M	0.2		308.5 mg
SDS 20%		4	2 mL
Glycerol 100%		20	2 mL
Tris-HCl pH 6.8	0.1		2 mL
Bromophenol Blue 2%		0.04	0.1 mL
Protease inhibitor cocktail			0.2 mL
H_2O			3.7 mL
Final volume			**10 mL**

Appendix 7: Immunoblot for Protein Expression: Gels, Buffers and Primary Antibody Dilutions

SDS-PAGE gels: for 1.5 mm gel plates

Stacking Gel	Volume to be added for two gels
Water	6 mL
40% Acrylamide	1240 µL
0.5 M Tris pH 6.8	2520 µL
20% SDS	50 µL
20% APS	100 µL
TEMED	10 µL

Resolving Gel	Volume to be added for 10% gel
Water	7.2 mL
40% Acrylamide	3.8 mL
1.5 M Tris pH 6.8	3.8 mL
20% SDS	75 µL
20% APS	150 µL
TEMED	6 µL

Running Buffer

10X Running Buffer	
Glycine	190 g
Tris Base	30.3 g
20% SDS	50 mL
dH_2O	to final volume of one litre

1X Running Buffer made with 100 mL 10X running buffer and 900 mL dH_2O.

Transfer Buffer

10X Transfer Buffer	
Glycine	145 g
Tris Base	29 g
dH_2O	to a final volume of 800 mL

1X Transfer Buffer made with 100 mL of 10X Transfer Buffer, 200mL methanol and 700 mL dH_2O.

TBST

10X TBS-Tween	
Tris-HCl 1M pH 8.0	100 mL
NaCl	97.3 g
dH_2O	to a final volume of 1000 mL
Tween-20	5 mL

1X TBST (0.05%) made with 100 mL 10X TBS-Tween and 900 mL dH_2O.

Primary Antibodies

Target	Predicted Molecular Weight (kDa)	Description	Dilution	Manufacturer
RAGE	43	Rabbit monoclonal (ab181293)	1:5000	Abcam
GAPDH	36	Rabbit monoclonal (ab181602)	1:10000	Abcam

Appendix 8: Supplementary murine BALF cytokine results

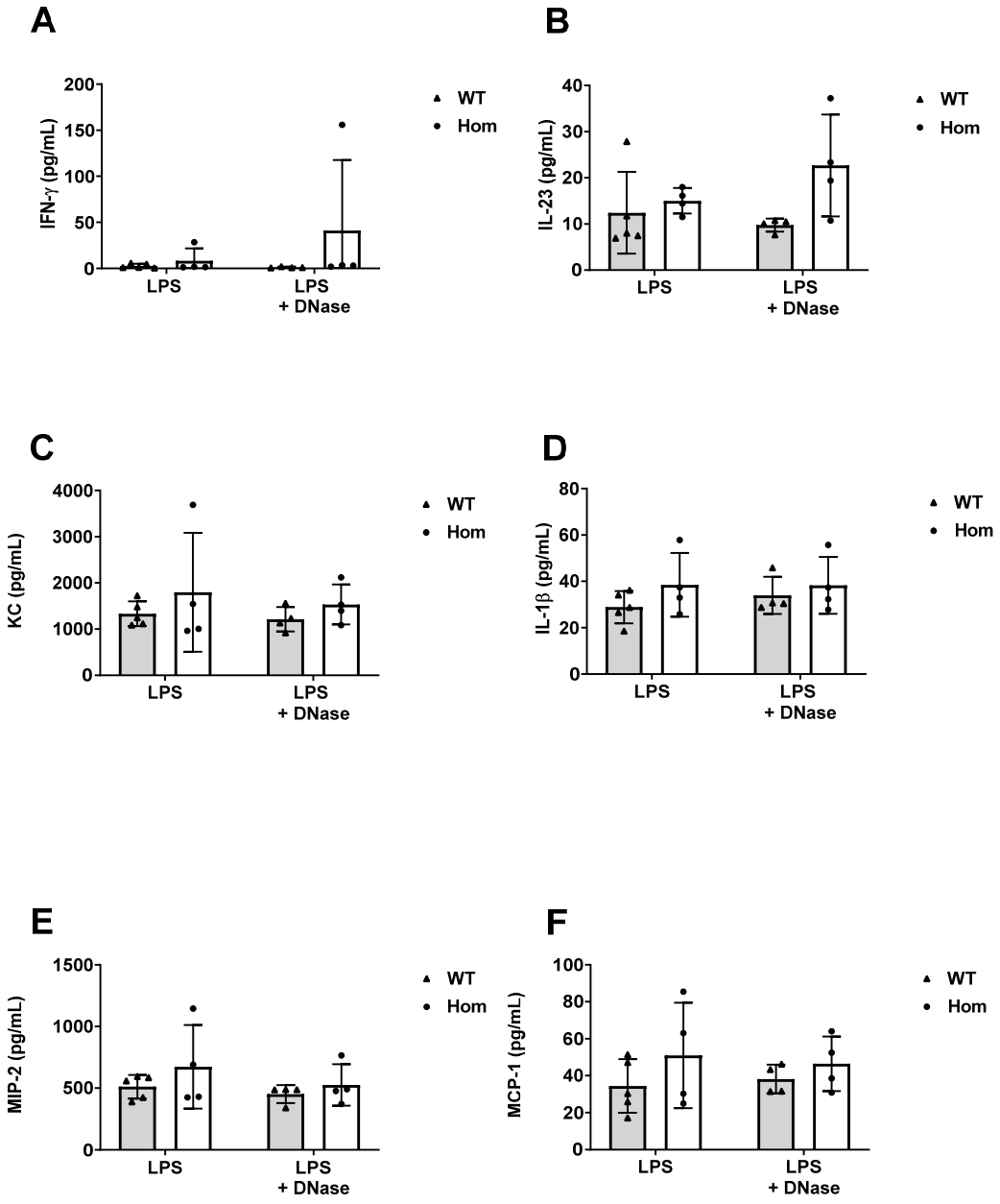

Figure A8a: Murine BALF cytokine concentrations 24 hours' post-LPS in WT and CFTR$^{-/-}$ mice. *Filled bars = WT, non-filled = CFTR$^{-/-}$. There were no significant differences in either genotype or treatment group in the levels of IFN-ɣ* ***(A)****, IL-23* ***(B)****, KC* ***(C)****, IL-1β* ***(D)****, MIP-2* ***(E)*** *and MCP-1* ***(F).*** *Data analysed by two-way ANOVA with Tukey's multiple comparisons test. Data represents individual points and mean ± SD. n=4-5 per group.*

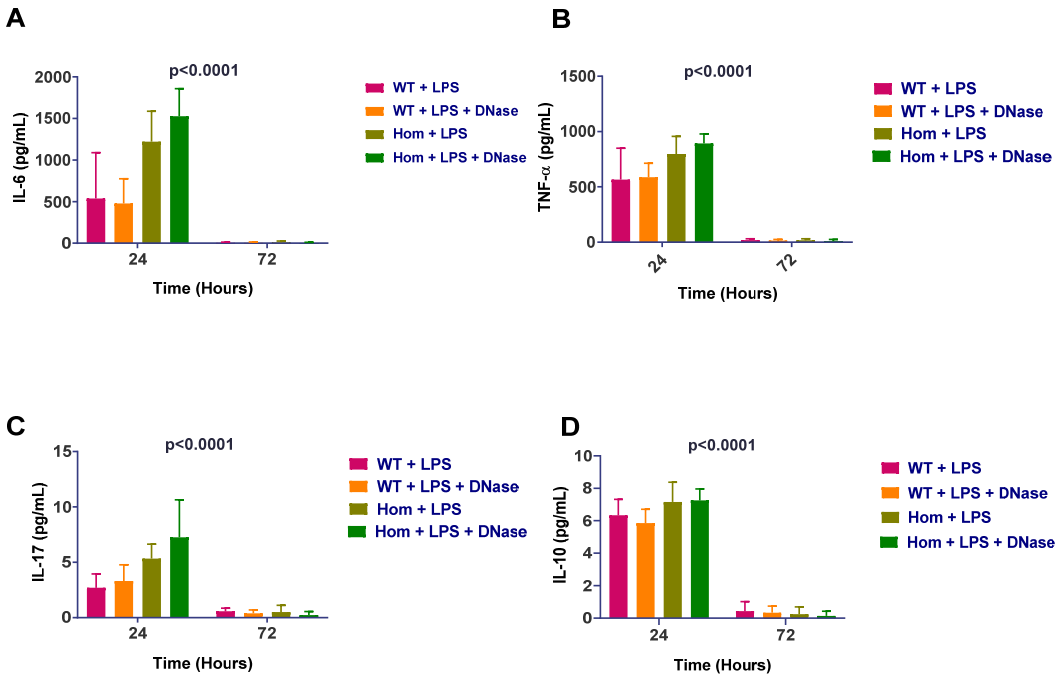

Figure A8b: Murine BALF cytokine levels at 24 and 72 hours' post-LPS in WT and CFTR$^{-/-}$ mice. (A-D) *IL-6, TNF-α, IL-17 and IL-10 concentrations were all significantly higher in CF mice compared to WT littermates at 24 hours' post LPS. DNase did not affect cytokine levels. However, by 72 hours' post-LPS, all of these cytokines had fallen to near undetectable levels. P-values shown are for time point differences analysed by two-way ANOVA with Tukey's multiple comparisons test. Data represents mean ± SD. n=4-5 per group.*

Appendix 9: Presentations and Publications arising from this thesis

Presentations

Presentation Type	Abstract Title	Meeting	Month/Year
Poster discussion	Optical Nanosensors Illuminate the pH Debate: Surface-enhanced Raman Spectroscopy-based Nanosensors demonstrate no acidification defect in Cystic Fibrosis Macrophage Phagolysosomes.	North American Cystic Fibrosis Conference, Denver, CO, USA	October 2018
Oral presentation	Neutrophil extracellular traps accumulate in Cystic Fibrosis sputum and are associated with inflammation and lung function decline. DOI: 10.1111/eci.13108	European Society for Clinical Investigation, Coimbra, Portugal	May 2019
Poster*	P221 Neutrophil extracellular traps are elevated in cystic fibrosis sputum and associated with neutrophilic inflammation and lung function decline June 2019, Journal of Cystic Fibrosis 18:S119 DOI: 10.1016/S1569-1993(19)30514-4	European Cystic Fibrosis Conference, Liverpool, UK	June 2019

*presented by Dr Gareth Hardisty on my behalf

Publications

Law SM, Gray RD. Neutrophil extracellular traps and the dysfunctional innate immune response of cystic fibrosis lung disease: a review. J Inflamm (Lond). 2017 Dec 28;14:29. doi: 10.1186/s12950-017-0176-1. eCollection 2017.

Law SM, Stanfield SJ, Hardisty GR, Dransfield I, Campbell CJ, Gray RD. Human cystic fibrosis monocyte derived macrophages display no defect in acidification of phagolysosomes when measured by optical nanosensors. J Cyst Fibros. 2019 Sep 6. pii: S1569-1993(18)30792-6. doi: 10.1016/j.jcf.2019.09.003